HELENA MARIA RODRIGUES GONÇALVES

Analytical Applications of Fluorescent Carbon Dots

DEPARTAMENTO DE QUÍMICA E BIOQUÍMICA

FACULDADE DE CIÊNCIAS DA UNIVERSIDADE DO PORTO

MAIO/2013

HELENA MARIA RODRIGUES GONÇALVES

Analytical Applications of Fluorescent Carbon Dots

Dissertação submetida à Faculdade de Ciências da Universidade do Porto para a obtenção do grau de Doutor em Química

DEPARTAMENTO DE QUÍMICA E BIOQUÍMICA

FACULDADE DE CIÊNCIAS DA UNIVERSIDADE DO PORTO

MAIO/2013

“Research is the immersion into the unknown. (...)

The “stupidity” is an existential fact, inherent in our efforts to push our way into unfamiliar knowledge’s. The more comfortable we become with being “stupid”, the deeper we will wade into the unknown and the more likely we are to make big discoveries”.

Martin A. Schwartz, 2008.

Agradecimentos

Antes de mais gostaria de agradecer às pessoas sem as quais jamais teria realizado um percurso académico, nomeadamente: à minha mãe, ao meu irmão, ao Pedro, à D. Marieta e ao Sr. Manuel, por todo o seu amor e apoio incondicional que me permitiu ultrapassar todos os obstáculos inerentes a este percurso.

Não poderia deixar de agradecer ao INESC-Porto, em particular ao Dr. Pedro Jorge e ao Dr. Ramiro Fernandes pela participação na produção das nanopartículas.

Gostaria ainda de agradecer a todos os meus amigos e amigas pelo apoio e amizade ao longo de todos estes anos. O seu apoio e capacidade de discussão foi fundamental. De todos os que foram e são especiais para mim, não poderia deixar de mencionar: Abel Duarte, Diana Crista, Emanuel Ferreira, Isabel Tavares, Natércia Teixeira, Simone Marques e Sónia Salomé.

Agradeço ainda a todos os que de uma forma directa ou indirecta participaram neste meu percurso. A todos o meu muito obrigada.

Não poderia ainda deixar de agradecer à FCT pela atribuição da bolsa de doutoramento concedida, com a referência: SFRH/BD/46406/2008.

FCT
Fundação para a Ciência e a Tecnologia
MINISTÉRIO DA CIÊNCIA, TECNOLOGIA E ENSINO SUPERIOR

Abstract

The development in the nanochemistry over the past few years is overwhelming. Indeed, what was considered somewhat futuristic a few years ago is now a common reality in this area.

The work that will be presented is focused on a new type of carbon-based nanoparticles – Carbon Dots (Cdots). This new class of nanomaterials are being pointed out as the solution to overcome the toxicity issues inherent to the traditional Cadmium-based Quantum Dots (QDs). Traditional QDs posses outstanding fluorescence properties that are quite helpful in the nanosensor area, however their core is based on heavy metals, which limits its applicability for *in vivo* sensing. Cdots posses the same interesting features of their counterparts QDs, with the great advantage of non-toxicity. This is one of the main reasons why Cdots are so interesting for bioimaging and sensing applications. In this sense several synthesis strategies are now being developed in an area where it is easy to become obsolete.

In this work Cdots were produced by direct laser ablation [UV pulsed laser irradiation (248 nm, KrF)] of a carbon target immersed in water. The Cdots produced this way were functionalized initially with PEG_{200}, since it has been proven that the presence of this polymer on the nanoparticles surface helps prevent cytotoxicity responses. Additionally they were further functionalized with different molecules, in order to render the Cdots a given specificity towards an analyte. As such they were functionalized with N-acetyl-L-cysteine and mercaptosuccinic acid, for Hg(II) and iodine sensing, respectively.

The results showed that the Cdots functionalized with N-acetyl-L-cysteine are sensitive to Hg(II) in a micromolar range and suffer from Cu(II) interference in the same concentration. Additionally these Cdots are also quite sensitive to the media pH. This can be viewed as an advantage, indeed this sensor can be used for these three analytes, provided that adequate precautions are taken to guarantee that only one analyte is present at each time.

On the other hand the Cdots functionalized with mercaptosuccinic acid are quite sensitive to milimolar concentrations of iodine. This sensitivity was measured as a decrease in the fluorescence intensity at the maximum emission wavelength.

Furthermore this Cdots are also sensitive to the pH media thereby presenting the double usage advantage.

Additionally it was determined that the Hg(II) sensing Cdots could be immobilized in adequate matrixes, as such they were immobilized in the tip of an optical fiber using the sol-gel technique. The immobilization of the Cdots is quite difficult since the objective is to maintain the photophysical properties and sensitivity and the same time that the nanoparticles are now part of another solid system. In a common scenario the Cdots tend to be less fluorescent and less sensitive since not all the nanoparticles are able to interact with the analyte due to its unavailability related with the characteristics of the solid matrix. Indeed, when the synthesized Cdots were immobilized in the sol-gel matrix there was a decrease in the quenching effect by 10%, which was expectable. Nonetheless the Cdots remained sensitive to Hg(II), Cu(II) and the solution pH. Furthermore, the sensing system responded in less than a second and it was completely reversible. The film was quite homogenous and had a thickness of about 700 nm. As such, the immobilization was successful and provided interesting results.

In an attempt to improve this sensing system in both time response and sensitivity, a new immobilization technique was applied to the same nanoparticles: the layer-by-layer immobilization. This technique allows the deposition of discrete layers of nanoparticles onto an adequate surface. In this sense, the Cdots were again immobilized in the tip of an optical fiber, that suffered the same pre-treatment as for the sol-gel immobilization, in order to establish a comparison between the two methods. The results obtained for this new sensing system were quite promising for the development of new lab-on-a-chip system based on Cdots. Indeed, it was determined that the quenching effect was more pronounced as the number of layers increased, reaching the best result at 6 mono-layers. Moreover, even with just one layer, the quenching effect was superior to the one observed using the sol-gel technique. This sensitivity with the number of layers is probably due to two main effects: the etching of the fiber leaves its surface quite irregular so as the number of layers increases the roughness of the fiber decreases and the Cdots deposition is more homogenous. On the other hand, this technique does not immobilized the Cdots in a solid matrix where its porosity needs to be adapted for both analyte and nanoparticles. In the solid matrix, the reaction is limited by the diffusion of the analyte through the matrix, on the contrary to the layer-by-layer deposition, where the Cdots are on the surface ready to interact. As such, it is easy to understand that by using the layer-by-layer technique the system response is only limited by the capacity of the acquisition equipment.

In all the sensing system described not all the obtained data are totally explored. Indeed, it is possible to use the Cdots Excitation Emission Matrixes (EEM) and chemometrics analysis to establish a different size population interaction with the analyte. As such, by using the Cdots functionalized with PEG_{200} and N-acetyl-L-cysteine it was possible to distinguish between two different size populations that were responding to both pH and Hg(II).

Up until now the Cdots have been used as sensors for different analytes by taking advantage of the quenching effect on its fluorescence intensity. However this sensing system is limited by the capacity of the equipment to distinguish between the background noise and the quenching effect. In this sense the use of fluorescence enhancement is quite advantageous, however it is not easy to develop nanoparticles that will respond this way in the presence of an analyte. In an attempt to create such a system the Cdots were located near a Plasmon supporting material – silver islands, and the enhancement effect obtained is quite remarkable. This effect can be used for example when the immobilization of the Cdots results in a dramatic decrease in the fluorescence signal that will ultimately inhibit their further application.

There is an entire new world of applications were it is possible to use Cdots to improve numerous systems and create new ones. Since their discovery the interest in these nanoparticles has been growing and it is my believe that they will be a part of our daily life.

Resumo

O desenvolvimento da nanoquímica ao longo dos últimos anos é impressionante. Na verdade, o que foi considerado futurista há alguns anos, agora é uma realidade comum.

Este trabalho focar-se-á num novo tipo de nanopartículas à base de carbono – *Carbon Dots* (Cdots). Esta nova classe de nanomateriais está a ser apontada como a possibilidade para a superação dos problemas de toxicidade inerentes aos tradicionais *Quantum Dots* (QDs). Os QDs possuem excelentes propriedades de fluorescência, sendo portanto bastante úteis na área dos nanosensores, no entanto o seu núcleo é constituído por metais pesados, o que limita a sua aplicabilidade para a detecção *in vivo*. Os Cdots possuem as mesmas características interessantes dos seus homólogos QDs, com a grande vantagem de não-toxicidade. Esta é uma das principais razões pelas quais os Cdots são tão interessantes para aplicações em bioimagem. Neste sentido, estão a ser desenvolvidas várias estratégias de síntese numa área onde é fácil tornar-se obsoleto.

Neste trabalho os Cdots foram produzidos por ablação laser directa [irradiação com laser pulsado de UV (248 nm, KrF)], de um alvo de carbono imerso em água. Os Cdots produzido desta forma foram inicialmente funcionalizados com PEG_{200}, uma vez que tenha sido provado que a presença deste polímero sobre a superfície das nanopartículas ajuda a evitar respostas de citotoxicidade. Adicionalmente, os Cdots foram funcionalizadas com outras moléculas, de forma a torna-los sensores específicos para um determinado analito. Deste modo, os Cdots foram funcionalizados com a N-acetil-L-cisteína e o ácido mercaptossuccínico, para detecção do Hg (II) e do iodo, respectivamente.

Os resultados mostraram que os Cdots funcionalizados com N-acetil-L-cisteína são sensíveis a Hg (II) numa gama micromolar e sofrem a interferência de Cu (II) na mesma gama de concentrações. Estes Cdots são muito sensíveis ao pH do meio, sendo por isso possível utilizá-los como sensor de pH. Isto pode ser visto como uma vantagem, na verdade, este sensor pode ser utilizado para os três analitos, desde que sejam tomadas as devidas precauções para garantir que apenas um analito está presente em cada momento.

Por outro lado, os Cdots funcionalizados com o ácido mercaptossuccínico são bastante sensíveis a concentrações milimolar de iodo. Esta sensibilidade foi medida

como uma redução na intensidade de fluorescência no comprimento de onda de emissão máxima. Adicionalmente, os Cdots são também sensíveis ao pH do meio, apresentando assim a vantagem da dupla aplicação.

Os Cdots funcionalizados com PEG_{200} e N-acetil-L-cisteína foram imobilizados na ponta de uma fibra óptica usando a técnica de sol-gel. A imobilização dos Cdots é bastante difícil, pois o objetivo é manter as propriedades fotofísicas e sensibilidade ao mesmo tempo que as nanopartículas são agora parte de um outro sistema sólido. Num cenário comum os Cdots tendem a ser menos fluorescentes e menos sensíveis, uma vez que nem todas as nanopartículas são capazes de interagir com o analito, alguns. estão indisponíveis devido às características da matriz sólida. Com efeito, quando os Cdots sintetizados foram imobilizados na matriz de sol-gel, ocorreu uma diminuição no efeito de *quenching* de 10%, o que era expectável. No entanto, os Cdots permaneceram sensíveis ao Hg (II), Cu (II) e o pH da solução. Adicionalmente, o sistema de detecção respondeu em menos de um segundo e foi completamente reversível. A película era completamente homogénea e tinha uma espessura de cerca de 700 nm.

Numa tentativa de melhorar este sistema de sistema de detecção tanto no tempo de resposta como na sensibilidade, foi aplicada uma nova técnica de imobilização: imobilização camada por camada. Esta técnica permite a deposição de camadas distintas de nanopartículas sobre uma superfície adequada. Neste sentido, os Cdots foram novamente imobilizadas na ponta de uma fibra óptica, que sofreu o mesmo pré-tratamento usado na imobilização de sol-gel, de modo a ser possível estabelecer uma comparação. Os resultados obtidos para este novo sistema de detecção foram bastante promissores para o desenvolvimento de um sistema *lab-on-a-chip* novo baseado em Cdots. De facto, determinou-se que o efeito de *quenching* foi mais pronunciado à medida que o número de camadas aumentava, atingindo o melhor resultado com 6 monocamadas. Além disso, mesmo com apenas uma camada, o efeito de *quenching* foi superior ao observado usando a técnica de sol-gel. Esta sensibilidade com o número de camadas é provavelmente devido a dois efeitos: o pré-tratamento da fibra deixa a sua superfície bastante irregular, deste modo, à medida que o número de camadas aumenta a rugosidade das fibras diminui o que leva a uma deposição mais homogénea dos Cdots. Por outro lado, esta técnica não imobiliza os Cdots numa matriz sólida em que a sua porosidade deve ser adaptada tanto para o analito como para as nanopartículas. Na matriz sólida, a reacção é limitada pela difusão do analito através da matriz, ao contrário do que acontece na deposição de camada por camada, em que os Cdots estão na superfície prontos para interagir.

Como tal, é fácil compreender que, usando a técnica de deposição de camada por camada, a resposta do sistema é limitada apenas pela capacidade de aquisição do equipamento.

Em todos os sistema de detecção descritos até agora, não são utilizados todos os dados disponíveis. Com efeito, é possível utilizar as Matrizes de Excitação Emissão (EEM) dos Cdots para estabelecer uma correlação entre as diferentes populações (em tamanho) com as substâncias a analisar. Deste modo, usando os Cdots funcionalizados com PEG_{200} e N-acetil-L-cisteína, foi possível distinguir entre duas populações de tamanhos diferentes que respondiam ao pH e Hg (II).

Até agora os Cdots foram usados como sensores para diferentes analitos, usando como propriedade aproveitando o efeito de *quenching*. No entanto, este sistema de detecção é limitado pela capacidade do equipamento de distinguir entre o ruído de fundo e o efeito de *quenching*. Neste sentido, o uso do aumento de fluorescência em vez da diminuição é muito vantajoso, no entanto, não é fácil desenvolver nanopartículas que respondam dessa forma. Numa tentativa de criar um sistema deste tipo os Cdots foram localizados perto um material com efeito Plasmónico - ilhas de prata, e o aumento da fluorescência obtido é bastante notável. Este efeito pode ser usado, por exemplo, quando a imobilização das Cdots leva a uma diminuição da fluorescência e este facto é limitativo na aplicação desejada.

Há todo um mundo de novas aplicações onde é possível usar os Cdots para melhorar sistemas já existentes, bem como criar novos sistemas. Desde a sua descoberta o interesse por essas nanopartículas tem crescido e é minha convicção que eles serão uma parte integrante da nossa vida diária.

Contents

Figure Contents

Abbreviations and Acronyms

A

Abs. - Absorption.

C

Cdots – Carbon Dots.

H

HOMO - Highest Occupied Molecular Orbital.

L

LUMO - Lowest Unoccupied Molecular Orbital.

M

MWCNT – Multi-walled Carbon Nanotubes

N

NAC – N-acetyl-L-cysteine

Q

QDs - Quantum Dots.

P

PAGE – Polyacrylamide gel electrophoresis

PEG - Polyethyleneglycol

PBS - Phosphate Buffered Saline.

R

ROS – Reactive Oxygen Species.

S

Sidots – Silicon Dots

T

TEPA - tetraethylenepentamine pentahydrochloride

TEOS - Tetraethyl ortosilicate.

U

UV – Ultravioleta.

Preface

Nanoparticles are the theme of the century. Their application has expanded to almost all fields of research and the results are visible in daily life. In fact, nanoparticles are being used to change the properties of a given material, as advanced drug delivery systems, in therapeutics, electronics, environmental sensors, among others. As such, a question arises: What makes this nanoparticles so special? One can say that the main difference lies in the size. Indeed as the size decreases the properties of the material becomes different. It is possible to see changes in colour, reactivity, strength, thermal properties, electronical properties, magnetic properties, optical properties, among others.

The appearance of the semiconductor Quantum Dots (QDs) can be viewed as a changing point in the nanochemistry. These nanoparticles present outstanding properties, has led their application in fields, such as, environment, pharmaceutical, solar energy conversion, optoelectronic devices, molecular and cellular imaging and ultrasensitive detection. Despite the numerous QDs applications a problem arisen from their inherent toxicity. In fact, the traditional QDs, are heavy metal core-based, which for in vivo applications represents a toxicity problem. Some studies have been performed to evaluate their toxicity in biological media and it has been described an increase in Reactive Oxygen Species (ROS) due to their interaction with organelles. Other studies have concluded that part of the toxicity is due to bioaccumulation of the nanoparticles which lead to toxicity due to their heavy metal nature. Therefore the search for nanoparticles, that have the outstanding properties of QDs and at the same time do not represent a toxicological issue in biological media, began. As a solution to this problem silicon and carbon dots where found.

Silicon Dots (Sidots) and Carbon Dots (Cdots) are fluorescent nanoparticles that possess unique light emitting properties, such as, biocompatibility, high photoluminescence quantum efficiency, stability against photobleaching, and the non-blinking. Additionally the emission wavelength of these nanoparticles can be adjusted by size selection and/or functionalization with several molecules. In a similar manner of the traditional cadmium based QDs the functionalization can be performed, in theory, with any molecule, and this molecule can be chosen in such a way that it turns the nanoparticle into a sensor for a given analyte. Furthermore, both Sidots as Cdots can be use in Single Photon Excitation (UV: 330-400 nm), as well as, Two Photon Excitation (near infrared: 720-850 nm) that is considered biologically friendly.

Thesis Layout

Throughout the three years of the PhD numerous experiments were performed, some gave rise to interesting results and some definitely did not work. The interesting results were published in international, peer review, journals and the bad results were considered a platform for the achievement of better ones.

This thesis results from an organized compilation of the main papers produced during these three years. In this sense the thesis layout is as follow:

Chapter 1 is an Introduction to the nanoparticles theme that is mainly focused on the Carbon Dots and the fluorescence mechanism by which these nanoparticles interact with the analyte.

Chapter 2 is a review on Silicon Dots that was published in the Current Analytical Chemistry with the reference: Vol. 8, 2012, page 67.

Chapter 3 is a compilation of results obtained for Cdots that were adequately functionalized for Hg(II) and pH sensing. These functionalized nanoparticles were extensively tested over more than three months and the results were published in Sensors and Actuators B with the reference: Vol. 145, 2010, page 702.

Chapter 4 represents a system developed for iodine sensing based on Carbon Dots. This system resulted from the selection of the most interesting fluorescence nanoparticles obtained from direct laser ablation. These results were published in the Journal of Fluorescence with the reference: Vol. 20, 2010, page 1023.

Chapter 5 is the follow up of the results obtained in Chapter 3. The nanoparticles functionalized obtained and tested in Chapter 4 were immobilized in the tip of an optical fiber using the sol-gel technique. The results were published in Biosensors and Bioelectronics with the reference: Vol. 26, 2010, page 1302.

The results obtained in Chapter 5 were consistent with the current immobilization procedures, where there is a decrease in the fluorescence intensity due to the nanoparticles entrapment. Chapter 6 represents a new immobilization method was tested and the objective was achieved. The results were published in Analytica Chimica Acta with the reference: Vol. 26, 2010, page 1302.

Chapter 7 represent a compilation of the results obtained through chemometrics for the Cdots functionalized for Hg(II) and pH sensing. The results were published in the Journal of Chemometrics with the reference: Vol. 24, 2010, page 655.

Chapter 8 represents the enhancement of the fluorescence intensity due to the plamonic effect of silver islands that were put in contact to the Cdots produced by laser ablation. The results were published in Chemical Communications with the reference: Vol. 47, 2011, page 5313.

Chapter 9 is a general conclusion of all the data obtained and discussed throughout the thesis.

Finally the thesis finishes with some final remarks on the work developed in the three years of PhD.

Chapter 1 – Introduction

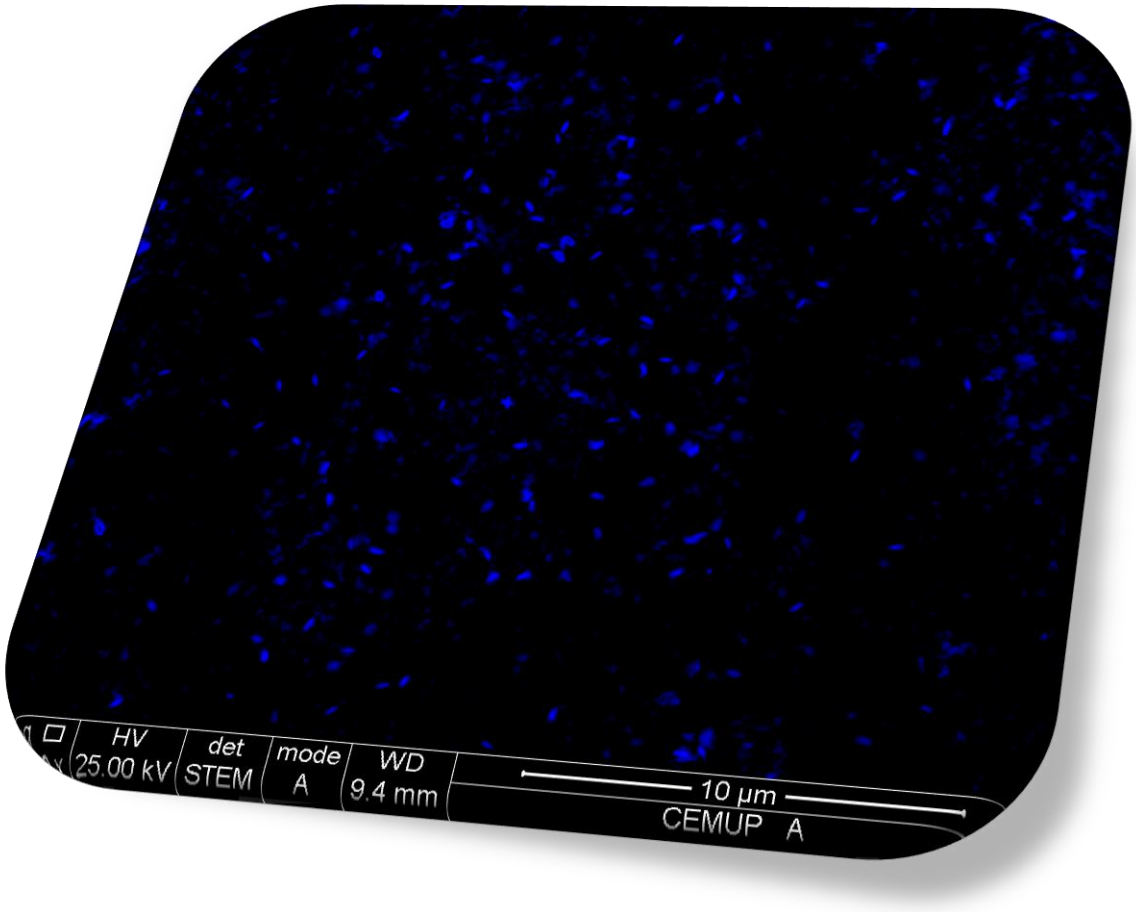

1.1. Overview

Carbon Dots (Cdots) are the newest class of fluorescent nanoparticles. Ever since it appearance the number of papers on the theme has been rapidly increasing. These fluorescent nanoparticles present some outstanding properties, such as, high photostability, tuneable emission and excitation wavelength, ability to be functionalized with different molecules according to their desired application, high stability over time, among others. These properties have made them quite interesting in numerous areas, for example, biosensing, bioimaging, pharmaceuticals and fuel cells [1-4].

Cdots are viewed as the new member of the Quantum Dots (QDs) family. Indeed, they share some of the physical properties that have made QDs one of the most relevant propellant in the nanochemistry area, however the traditional QDs have a heavy metal core, that prevents its application for *in vivo* assays [5]. In this sense some authors have mentioned that Cdots are the most promising alternative to these traditional QDs. In fact, some studies have showed that Cdots are competitive agents for bioimaging studies [6].

Ever since their serendipitously discovery in 2004 there has been a great interest in this new carbon-based material. Cdots present themselves as a non-toxic alternative to the traditional Cadmium-based QDs and, as such, the synthetic pathways for their production are increasing rapidly. Nowadays there are several top-down and bottom-up approaches [7-17] for the Cdots synthesis. Nonetheless they can be grouped into nine main production methods. All the synthetic methods have advantages and disadvantages that need to be taken into account before starting their production. This methods differ mainly in the starting material, as such, for top-down approaches (Fig.1.1) it is possible to use: Multi-walled Carbon Nanotubes (MWCNT), Graphite and candle soot.

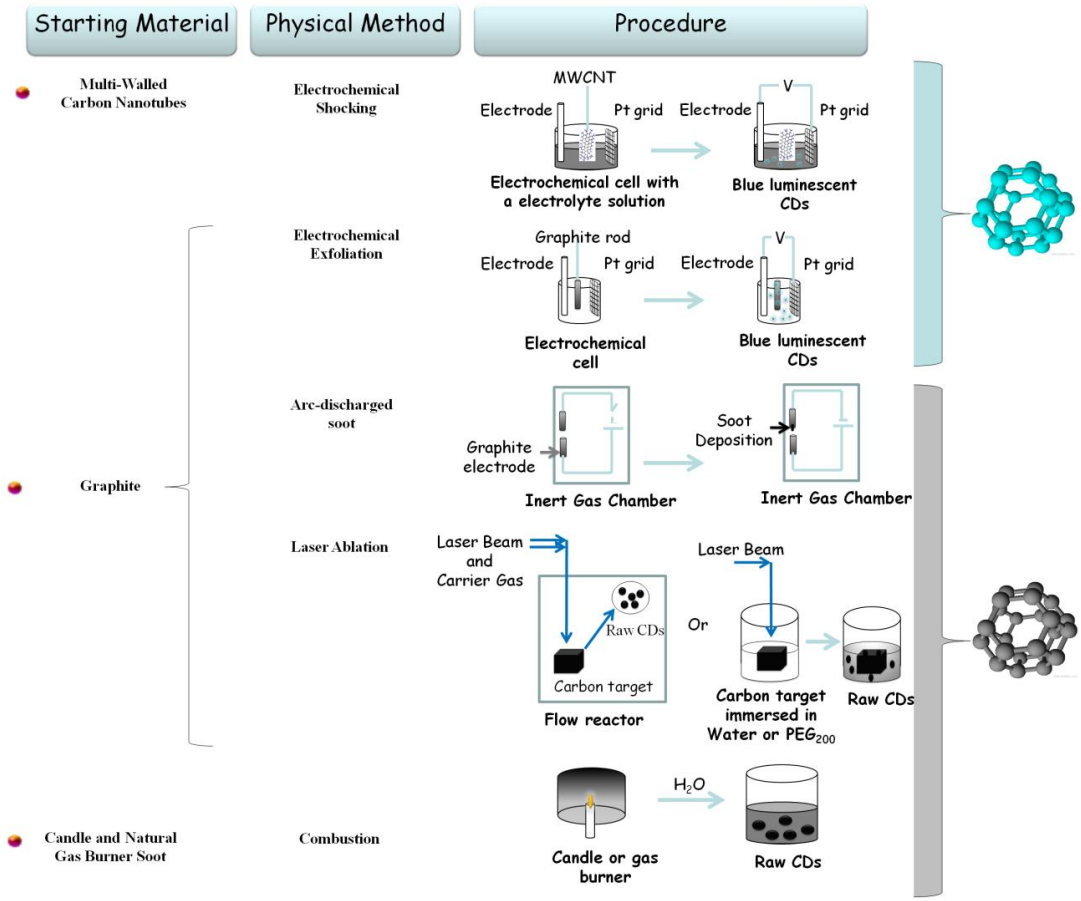

Fig.1.1. – Synthetic pathways for Cdots production using Top-Down approaches, adapted from [18].

1.1.1. Electrochemical Shocking of Multi-Walled Carbon Nanotubes

The electrochemical methods are becoming popular since it allows the production of blue luminescent Cdots in a simple path, on the contrary of the other Top-Down methods that requires an activation procedure for the Cdots to become fluorescent. This method uses as a starting material MWCNT, that are insoluble in water and it allows the production of highly luminescent, water stable, Cdots [11].

Zheng L. *et al.,* (2009) [12] reported the production of well-defined spherical Cdots with an average size of ~20 nm where the smallest population has an average size of ~2 nm. In order to obtain such results they used MWCNT immersed in acetonitrile and realized despite the solvent used there were no change into the effective area of the working electrode (graphite rod). This led them to the discovery that the Cdots produced where initially immobilized into the porous graphite electrode and when exposed to Phosphate Buffered Saline (PBS) and electrochemically

oxidized, they became water soluble and released into the water phase. The main disadvantage of this method is the size dispersion of the nanoparticles, however it has the advantage of producing blue luminescent Cdots in a single step, which allows the method to be faster than others and, therefore most cost effective.

1.1.2. Electrochemical Exfoliation of Graphite

The electrochemical exfoliation of graphite can be viewed as a process where small particles are removed from a graphite electrode by using an adequate current. Li H. *et al.,* (2010) [17] reported the synthesis Cdots with sizes ranging from 1.2 to 3.8 nm. This was performed using graphite rods as both anode and cathode, and NaOH/EtOH as electrolyte. Additionally they evaluated the necessity of having a alkali vs. acid media (NaOH:EtOH/H_2SO_4:EtOH) as an electrolyte solution for the Cdots production. Their results led to the discovered that for the electrochemical oxidation of graphite to result in Cdots it is necessary to have an alkali media.

1.1.3. Arch-Discharge Soot

This can be considered the original method. In fact, the discovery of Cdots were made by chance upon the purification of Single-Walled Carbon Nanotubes (SWCNT) obtained by this method [8]. The production of Cdots from this method presents a great challenge in the separation step. Indeed this is one of the methods that generates more impurities, which makes it more difficult to remove. Common techniques of separation, such as, dialysis, fails since the impurities rapidly bock the pores of the membranes. In this sense the technique that has prove to be quite good for separating Cdots from impurities produced upon their production is electrophoresis. In fact the use of Polyacrylamide gel electrophoresis (PAGE) or agarose worked quite well in two senses: it allowed the separation of Cdots from the impurities, as well as, the separation of the different size populations of Cdots.

1.1.4. Laser Ablation

Laser ablation of carbon targets to obtain surface controlled Cdots is one of the most popular methods of production. However it is necessary to have specialized personnel operating the laser and the equipment itself is rather expensive. Nonetheless this method, since it allows to have a gas controlled atmosphere upon the Cdots production, it promotes a higher control over the chemical surface of the nanoparticles. Additionally it is possible to perform the laser ablation with the target immersed in an appropriate solvent. This has the advantage of dispersing the nanoparticles in the solvent of interest. When using this immersion technique is it necessary to have into account the absorption wavelength of the solvent, since it will be responsible for decreasing the energy for extracting nanoparticles from the carbon target. Moreover if the solvent used is not water it is probable that it will decompose and that the surface groups of the Cdots will affected by it. This also can be viewed as an advantage, since the surface groups are partially responsible for the fluorescence properties of these nanoparticles. One of the main disadvantages of the laser ablation is the high size dispersion of the Cdots, however this can be overcome using separation methods like dialysis and electrophoresis that allows the separation of the different size Cdots populations.

1.1.5. Candle and Natural Gas Burner Soot

Many research groups have been using this method, mainly due to the simplicity of acquiring the starting material [13]. In fact, this method provides a new use for a complicated by-product. However it has its disadvantages, namely the broad size dispersion, the uncontrolled chemical surface and the production of many products that can be dangerous to the human health. Nonetheless it is possible to separate the different nanoparticles using, for example, electrophoresis, but this still leaves the problem of dealing with the other by-products that can be dangerous to the researchers health.

On the other hand for bottom-up methods the starting material can simply be suitable carbon-based molecules (Fig.1.2). It is on this method that the researchers have been focusing lately, where the biggest innovation is the possibility of using

biomass for the Cdots production [19]. This is in fact quite remarkable since it allows the possibility of using, for example, industrial waste/by-products.

When using bottom-up approaches for producing Cdots it is possible to use three different physical methods: Ultrasonic treatment, Acid dehydration and Thermal carbonization of adequate carbon-based molecules. In this sense it is possible to use both acidic and alkali media, as well as, high temperatures to obtain either raw Cdots (that require an activation step in HNO_3 reflux for them to become luminescent) or blue luminescent Cdots, as it is possible to observe in Fig.1.2.

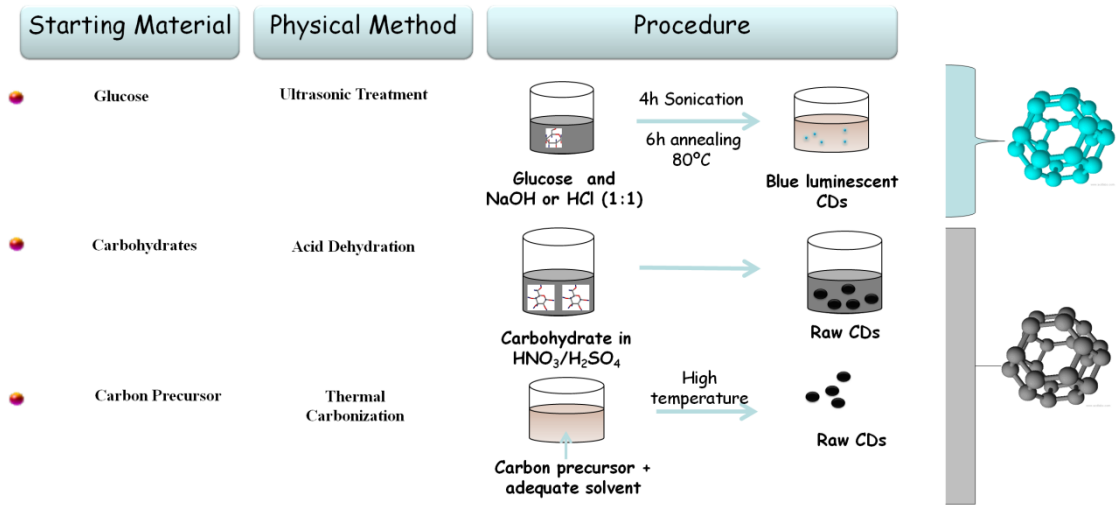

Fig.1.2. – Synthetic pathways for Cdots production using Bottom-Up approaches, adapted from [18].

Despite of the Cdots production method it is possible to cover their surface with adequate molecules according to their intended application, this step is called functionalization. For this step to elapse in the best way it is of the outmost importance to have a well characterized Cdots surface. As long as the functional groups in the surface are well known, it is possible to use soft chemistry to attach different molecules onto the nanoparticles exterior. These procedures have consequences into the luminescent properties of the Cdots. In fact, any operation that results into a change into the nanoparticles will have an influence on its optical properties. This can be used as an advantage by the researcher, since by knowing the effect that the surface change will produce into the nanoparticle optical properties it is possible to tune them just by introducing such changes. Sun Y-P. *et al.,* 2008 [20], for example, introduced a ZnS and a ZnO shell onto the Cdots surface in order to enhance its Quantum Yield. This operation is usually called doping and is quite common for the traditional

Cadmium-based QDs. With this procedure it is possible to overcome one of the major drawbacks of the Cdots, that is a relative low Quantum Yield, when compared to the traditional QDs. In fact their work proved that Cdots doped with ZnS and ZnO are competitive with the common CdSe/ZnO QDs.

Since these surface changes have an influence on both Sidots and Cdots optical properties, it is safe to say that they represent a significant part in the fluorescence mechanism.

1.2. Fluorescence Mechanism of Cdots

There has been several attempts over the years to explain the fluorescence mechanism of the nanoparticles [21]. The most common theory is related to the Quantum Confinement. This theory states that all particles are confined in size between the band gap formed by the Highest Occupied Molecular Orbital (HOMO) and the Lowest Unoccupied Molecular Orbital (LUMO) [22]. In fact, as the particles get smaller the energy gap between these two orbitals becomes larger, hence the electrons in the HOMO orbital need more energy to be excited into the LUMO orbital. Upon excitation the electron relaxes and returns to the ground state with emission of light. As such, it is possible to say that the energy gap determines the emission wavelength of the nanoparticle [23].

The fluorescence mechanism of these new nanoparticles is not clearly defined, however it seems to be dependent of two main factors: the surface state defects and the quantum confinement. Indeed as mentioned before, almost all modifications onto the surface of these nanoparticles are followed by a change in their optical properties (fluorescence intensity, radiative lifetime and excitation/emission wavelength). This seems easy to understand since the nanoparticles are constituted by only a small amount of atoms that are mainly on the surface, therefore any change in these atoms results into a modification in the nanoparticle properties.

Since this is a quite interesting and important topic many researchers have attempt to prove these theories. Initially the theory was developed for Silicon Dots (Sidots), that are silicon-based nanoparticles. These nanoparticles were discovered long before Cdots, and since both nanoparticles are not intrinsic semiconductors, the theory for the fluorescence mechanism developed for Sidots is now accepted for Cdots. Some authors have concluded that the most important factor in quantum

confinement [22] (as their family counterparts - QDs). However these nanoparticles are not intrinsic semiconductors and, since this theory mainly applies to semiconductors, some researchers believe that the fluorescence mechanism of Sidots and Cdots is determined by the surface state defects [7]. In this sense there has been some experimental proves, as well as, theoretical calculations [24]. An example is the work of Yang *et al.* in 1999 [23], on Sidots with different surface groups. Their results led them to conclude that the optical differences between the Sidots are consistent with the quantum confinement theory, however it was not taken into account that the method of producing larger nanoparticles was by annealing smaller nanoparticles at different temperatures. The temperature itself can be responsible for changing the surface of the Sidots, as they proved by FT-IR, nevertheless this factor was not taken into account on their conclusions about the fluorescence mechanism.

The fluorescence mechanism of these nanoparticles needs to take into account two main factors: surface state defects and quantum confinement. This theory of the two factors influencing the fluorescence mechanism was proposed, for the Sidots, by Putzer A. *et al.,* in 2003 [25]. They based the theory in computational studies where they evaluated the difference in ionic rearrangements and electronic relaxations upon absorption and emission, as well as, the resulting Stokes shift, with different surface molecules. From this study it became clear that all these factors were extremely sensitive to the surface groups, thereby supporting the surface state defects influence on the fluorescence mechanism. In fact, a 1 nm cluster can change ± 0.9 eV depending on the surface oxygen configuration – double bonded or bridged. Additionally they studied different clusters size with the same surface groups, and again there was a different in the mentioned parameters, even though the surface groups were the same, hence supporting the quantum size dependence of the fluorescence mechanism of Sidots. These results can carefully be extrapolated to Cdots, even though up to know there are no studies performed in this sense. Nevertheless and, since they share luminescent properties and there are experimental data that support this two factors theory for the fluorescence mechanism, it seems easy to accept that Cdots and Sidots share the same fluorescence mechanism dependence.

Common fluorescence sensors are based on the decrease of the fluorescence intensity in the presence of the analyte, this process is called *quenching*. The *quenching* phenomenon was first observed and its relation to fluorescence sensing determined in 1919 by Stern and Volmer [26]. This process occurs through a bimolecular reaction between an excited luminescent molecule, M^*, and an external molecule *quencher*, *Q*. The fluorescent molecule absorbs light and passes to an

excited state. When this two molecules interact, the fluorescent molecule decays by non-radiative mechanisms (e.g.: electronic transfer, molecular rearrangements and others.), with a rate of k_q (Fig.1.3). The passage of M^* to the ground-state also happens in the absence of a *quencher* but when this molecule is present and interacts with M^*, the fluorescence intensity decreases more rapidly.

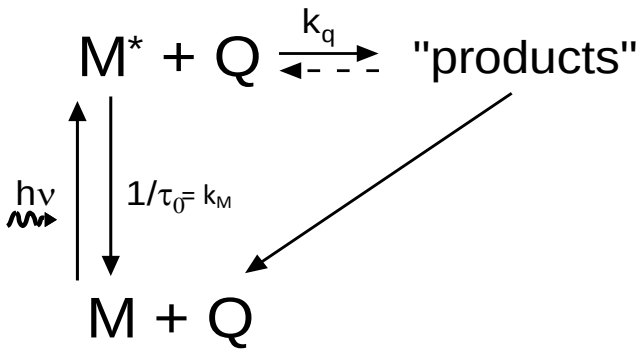

Fig.1.3- Simplified diagram illustrating the bimolecular process between the luminescent molecule, *M, and an external molecule - *quencher*, *Q*, adapted from [27].**

Quenching mechanisms are photophysical, *i.e*., after all the deactivation processes the fluorophore returns to the ground-state unaltered, *M*. Depending on the type of interaction between the *quencher* and the luminescent molecule it is possible to establish different models to better understand the kinetics of these processes. In fact, the analysis of this phenomena gives important quantitative information on the surroundings of a fluorescent molecule (if a kinetic analysis is possible in the sequence of a kinetic competitive model), or at least qualitative information [27].

1.2.1. Dynamic Quenching

Quenching occurs when an excited fluorophore reacts with a *quencher* molecule. In order for these two molecules to react it is necessary for them to meet. These diffusion controlled reactions are time dependent. Indeed, when the excited fluorophores, *M**, are at a shorter distance from a *quencher*, Q, the decay to the ground state, on average, occurs at shorter times than those that are more distant. These transient effects are not significant for moderate concentrations of quenchers in fluid solvents but they are quite relevant in viscous media.

This diffusion controlled mechanism affects the beginning of the fluorescence decay curves. In steady-state experiments, for example, it is responsible for deviations from the well known and widely used Stern–Volmer equation.

$$\frac{I_0}{I} = 1 + K_{SV}[Q] \qquad \text{(Equation 1.1)}$$

where K_{SV} is the Stern-Volmer constant, I_0 and I are the steady-state fluorescence intensities in the absence and in the presence of a quencher, respectively. Generally the ratio I_0 /I are plotted against the quencher concentration (Stern-Volmer plot). If the variation is found to be linear, the slope gives the Stern-Volmer constant [26].

1.2.2. Static Quenching

Static quenching is not dependent from the diffusion processes and occurs in two different situations: when there the formation of a sphere of effective quenching or when the formation of a ground-state non-fluorescence complex occurs.

The quenching mechanism that passes through the formation of an sphere of effective quenching was proposed by Perrin in 1924 [28]. The model describes the quencher as being inside a sphere around the fluorophore, and its effect on the dye is only when the *quencher* is inside this sphere. Additionally it is proposed that both M^* and Q cannot change their positions in space, relative to one another, during the excited-state lifetime of M^*. An example of this is when the quenching occurs in viscous media or rigid matrixes. In this sense, it is necessary to introduce some changes in the Stern-Volmer equation for it to properly represent the phenomena that is occurring is these cases.

$$\frac{I_0}{I} = \exp\left(V_q N_a [Q]\right) \qquad \text{(Equation 1.2)}$$

where N_a is the Avogadro's number and V_q represent the volume of the sphere. In contrast to the linear trend found in Equation 1.1, the static quenching by the

formation of a sphere plot can have an upward curvature when the *quencher* concentration is high or a linear trend for low *quencher* concentrations.

On the other hand the static quenching can also occur through the formation of a ground-state non-fluorescent complex. The formation of this non-fluorescent complex leads to the typical decay in the fluorescence intensity, however in this case, the excited-state lifetime of the uncomplexed fluorophore is not affected. Considering that the Stern-Volmer Equation shows a linear dependence between the fluorescence intensities and the quencher concentration, this equation is valid for this static quenching mechanism [26].

1.3. Sensing Applications of Cdots

1.3.1. Chemical and Bioanalytical sensing

Ever since the appearance of nanoparticles the interest in producing specific nanosensors has not stopped and, as such, there are actually numerous applications of different nanoparticles [29]. But the question remains: “Why the interest in nanoparticles for specific sensing?”. This question can be answered with two different answers: (i) There are now available numerous possibilities to functionalize different nanoparticles [30-33], which makes it possible to turn them into a specific sensor to a given analyte. (ii) The use of nanoparticles allows the miniaturization of the complex sensing systems, thereby it is possible to produce the so called – lab-on-a-chip [34]. This seemed futuristic a couple of years ago, however due to the development to the informatics technology and the incorporation of nanosensors, this is now a reality. In fact, there are some of these new miniaturized sensing systems already in the market.

Despite the simple explanation of the functionalization of the nanoparticle to become sensitive to a given target, in practice this is not easy to accomplish. There are several drawbacks that need to be overcome in order to say that the nanosensor is actually useful in comparison to others already in the market. First it is necessary to choose a molecule that is sensitive to a given analyte in order to functionalize the nanoparticle with it. Then some precautions must be made in the soft chemistry of functionalization so it will not affect the ability of the molecule to be sensitive to the analyte. If all this turns up well, there is still necessary that when the surface molecule interacts with the analyte it does so in a way that the fluorescence properties of the

nanoparticle changes (Emission shift, Lifetime and Fluorescence intensity decrease/increase). After all these steps are overcome it reaches the tricky part of the specific sensing, that is: functionalized nanoparticles must only interact with the desired analyte, therefore it must become inert to all other possible interferents. This is not easy to perform, since generally the chemical mechanism of interaction is trough affinity and there are some analyte that share the same affinity. One example of this is mercury sensing. It is quite difficult to get a Hg(II) sensor that does not react with Cu(II), therefore Cu(II) is a common interferent on mercury sensing [35].

Here it will be discussed some of the sensing applications were Sidots and Cdots have demonstrated an outstanding performance. Researchers in biomedicine area have been paying much attention to nanosensing and, as such, they are responsible for developing some sensors for important biomedical substances, like for example: dopamine and glucose. Developing sensors for *in vivo* and *in vitro* sensing it quite difficult, since, among other characteristics, these sensors need to be non-toxic, biocompatible and there are a number of parameters that can act as interferents.

1.3.2. Sensors based on Cdots

The use of Cdots is fairly recent, nevertheless there are some sensors developed based on these carbon nanomaterials. One example of a Cdots-based sensing is the Hg(II) sensor based on Cdots functionalized with Polyethylenoglicol 200 (PEG_{200}) and N-acetyl-L-cysteine (NAC) [35]. This sensor was used in a suspension form and also immobilized into different solid matrixes. In every case it showed a good response to Hg(II) and also the solution pH. Even though this Cdots-based sensor was tested in solution and after immobilization it was found that in all cases the main interferent for the system was Cu(II). The immobilized sensor showed a good reversibility. Additionally when the sensor was immobilized with poly(ethyleneimine), using the layer-by-layer technique, the sensitivity also increased, thereby allowing the detection of Hg(II) in a concentration range of $(0.01–2.69)\times10^{-6}$M.

Another sensor based on Cdots functionalized with PEG_{200} and tetraethylenepentamine pentahydrochloride (TEPA) is for Fe(II). This sensor when in presence of a concentration range of $(5.00x10^{-7}\text{-}1.00x10^{-4})$M of Fe(II) suffers a decrease in fluorescence (quenching) of about 55%. Additionally from all the known interferents of this type of sensor, only Fe(III) and Cu(II) had a measurable effect (50% and 35%).

1.3.3. *In-vivo* sensing and *Tags* using Cdots

Nowadays there are numerous organic dyes used for *in vivo* sensing and as fluorescence tags. Most of these molecules are synthetic mimics of natural occurring proteins that are involved in a process of interest. However these fluorescent dyes present some disadvantages, such as, photobleaching, blinking, short fluorescence lifetime, among others, that lead researchers to search for new alternatives.

Cdots are the new class of nanoparticles that present themselves as alternatives to the traditional organic dyes. These nanoparticles overcome the major drawbacks of the organic dyes and present the advantage of functionalization of specific targeting, are non-toxic and have a higher quantum yield and photostability. As such, it is without surprise the number of imaging applications that are now using these nanoparticles.

The number of assays in bioimaging using Cdots has been increasing, mainly due to three factors: (i) their non-toxicity nature, (ii) the easiness of functionalization for specific targeting and, (iii) their competitive fluorescence properties.

One of the main areas that is currently being explored is the specific targeting to cancer cells. Nevertheless before studying its internalization process and specific targeting of interesting biomolecules it is necessary to better understand how they act without any functionalization. In this sense studies like the one performed by Ray S.C. *et al.* in 2009 [36] is important. They determined that when Cdots are incubated with cells they are internalized by natural occurring mechanisms even without functionalization. This means that it is possible to track this nanoparticles using a conventional fluorescence microscope.

When the objective is specific targeting the functionalization is required. One interesting work of this matter is the one performed by Li Q. *et al.,* in 2010 [37]. This research groups focused on the study of the internalization process and the specific targeting of Cdots functionalized initially with polyethylene glycol (PEG) chains, polyethylenimide-*co*-polyethyleneglycol-*co*-polyethylenimide copolymer, and 4-armed PEG molecules and, then with human transferring (Tf). Tf has been used before in targeting assays, since it was proven that cancer cell membranes over express the TF receptors. Therefore the use of this glycoprotein on the Cdots surface should be a guarantee of specific targeting. Lin Q. *et al.,* found that Cdots functionalized with polyethylenimide-*co*-polyethyleneglycol-*co*-polyethylenimide copolymer and Tf had a higher passive cellular uptake when compared to the other functionalized and non-

functionalized Cdots. The authors indicate that this may be due to the charge on the Cdots surface, that in the case of this Cdots is positive, thereby allowing a higher binding ability with the cell membrane through electrostatic interactions.

When the fluorescence intensity is not adequate for the study or even if the excitation wavelength is too low, it is also possible to functionalize the Cdots with a shell of ZnO or ZnS. A study on these functionalized nanoparticles using bioimaging was performed by Yang S-T in 2009 [20]. The main conclusions of this work were: (i) despite the place where the Cdots were injected into the mouse, they remained strongly fluorescence throughout the experimental assay, (ii) upon the 3h of the intravenous injection of 440 μg in 200 μL, the urine exhibit strong fluorescence, thereby indicating that the pathway of excretion of these nanoparticles is through urine.

However when the particle size is critical, it may not be possible to use a shell just to increase the fluorescence intensity or to change the excitation wavelength, then it is necessary to use a new imaging technique: Two-Photon Excitation technique (TPE). In fact, ever since its appearance their application on Cdots has grown. The TPE technique allows the possibility of exciting the nanoparticle with two photons and, as such, it is possible to use a fluorophore that absorbs (is excited) in the UV with two photons of NIR. What happens is that it is possible to excite a fluorophore that typically is excited in the UV (i.e., 400 nm) with two photons of NIR (800 nm). By doing this the main advantage is to excite the fluorophore with a non-harmful energy for cells at the same time that emission wavelength remains the same. This system has two main advantages: it allows the possibility of studying cellular phenomena for longer times (since the cells will not be exposed to damaging wavelengths) and a higher penetration depth when compared to the traditional Single-Photon Excitation technique (SPE), since NIR is less absorbed by the tissue (Fig. 1.4).

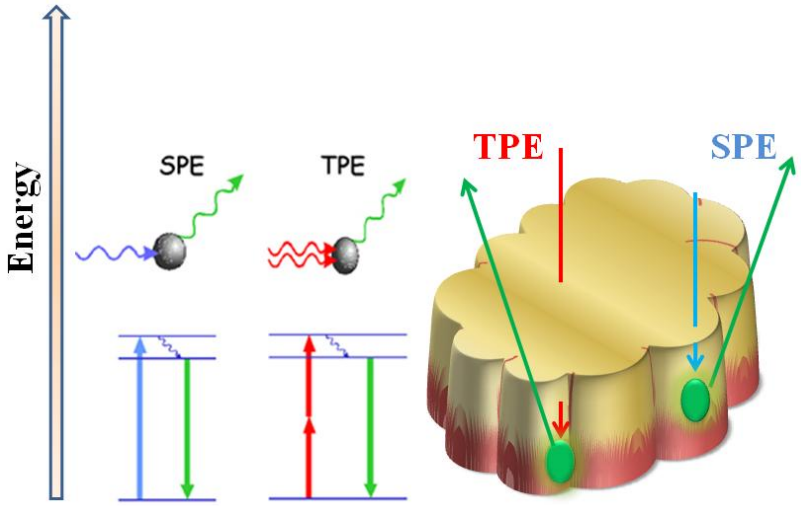

Fig. 1.4. – Schematic representation the penetration depth of Two-Photon Excitation (TPE) vs. Single-Photon Excitation (SPE) [18].

1.4. Toxicity assays of Cdots

Due to the interest that these nanoparticles raise in the *in vitro* and *in vivo* area the need for toxicity assays was imperious. The traditional Cadmium-based QDs were a landmark in nanochemistry and they found numerous applications in bioimaging due to their outstanding fluorescence properties. However the inherent toxicity of using such materials rise and was proven by several studies [38,39]. There are two main toxicity issues in QDs: (i) their heavy metal core, that upon contact with cells are known to produce ROS that will eventually lead to cell death, and (ii) the fact that they suffer bioaccumulation, i.e., on lymphatic nodules. Some solutions have been proposed to deal with this problem, namely the use of a shell that completely covers the QDs surface. This shell can even be though in such a way that it increases the fluorescence intensity or shifts the emission wavelength to a more desirable one. However this solution only deals with the problem of exposing cells to the heavy metal-based core. In order to try to resolve the bioaccumulation problem it has been proposed the functionalization of the QDs with biocompatible molecules (i.e., PEG) that are recognized by the cell as innocuous, thereby allowing the cell to dispose the QDs using its natural methods [40,41]. This in fact can avoid tissue inflammation due to recognition of a foreign material, nevertheless the possibility of bioaccumulation of heavy metals is still a issue to be concerned.

In order to overcome this toxicity issues the search for new nanomaterials that have the same outstanding fluorescence properties of QDs but are biocompatible and

non-toxic, lead to the appearance of Sidots and Cdots. Cdots have been presented as the non-toxic alternative to traditional Cadmium-based QDs. This is only possible due to the toxicity assays that have been performed so far by different investigation groups [4, 42].

One of the first toxicological assays performed in Cdots was the one presented by Yang S.T. in 2009 [20]. In this assay they intended to see if the presence of a ZnS shell on the Cdots surface had a toxicological difference from the raw Cdots (non-functionalized). The mice were injected subcutaneously with a solution of Cdots functionalized with PEG_{1500N} (30μg carbon-core equivalent in 30μL) or a solution of Cdots/ZnS with PEG_{1500N} (65μg in 30μL) (Fig.1.5). It was found that after 24h the fluorescence was only residual. Additionally after the 24h pos-injection the axillary lymph nodes were harvested and dissected and it was observed no fluorescence. This results is quite important since nanoparticles, like carbon nanotubes, have a tendency to suffer bioaccumulation, which is readily seen in the lymph nodes.

On another set of experiences this investigation group injected a Cdots solution of 440μg in 200μL intravenously. After 4h of the injection the organs were harvested and dissected to detect fluorescence. It was observed that only the kidneys and the liver presented a fluorescence intensity compatible to the Cdots, however this intensity was larger in the case of the kidneys. These results suggest not only that the main way of excretion of the nanoparticles is the urine, but also that they do not suffer bioaccumulation. Additionally the fluorescence detected in the liver is consistent to the results observed for other nanoparticles, nonetheless the presence of Cdots was in a lower concentration of the other nanoparticles. The authors suggest that this result may be related to the PEG functionalization that reduced the protein affinity and made the Cdots stealthy with respect to hepatic uptake.

Another interesting toxicity assay was performed by Li Q. *et al.,* in 2010 [37] that points out an interesting feature, the relationship between the nanoparticle size and the degradation/excretion process. Indeed it is difficult for the organism to excrete trough the kidneys nanoparticles larger them 10nm. Additionally particles over this size are hardly degraded by normal biological mechanisms, which can then lead to bioaccumulation. The study performed by Li Q. *et al.,* resorted the use of Cdots in a size range of 1.5-3nm. These Cdots were functionalized with polyethylene glycol (PEG) chains, polyethylenimide-*co*-polyethyleneglycol-*co*-polyethylenimide copolymer, and 4-armed PEG molecules, thereby producing CD2, 3 and 4, respectively. These Cdots were further functionalized with human transferrin and exposed to HeLa cell cultures. Their cytotoxicity was evaluated using twice the concentration necessary for imaging

studies. The results clearly demonstrate that the Cdots present low cytotoxicity when compared to the traditional imaging agents.

In order to safely use the nanoparticles in biological media for applications like drug delivery systems, pharmaceuticals, among others, it is necessary to completely understand the biological path and responses that these nanoparticles produce once in contact with live biological organelles and tissues. Despite the toxicity assays already performed, mechanism beneath the cytotoxicity mechanism and the inflammatory response is still to be uncovered, as such, it is still necessary to perform additional studies focusing of these subjects.

1.5. Conclusions and Future Perspectives

The Era of the nanoparticles is upon us and their application in almost all areas of science is a clear evidence of this. One can say that this nanoparticle revolution had as star participants the traditional Cadmium-based QDs. These nanoparticle present outstanding optical properties that has lead to their success in micro-electronics, fluorescence sensors for a wide analyte application, bioimaging, among others. One of the most interesting features of QDs was precisely the imaging ability, without blinking and photobleaching problems that are common to the imaging agents mostly used – organic dyes. However, despite this clear advantages, there is a major problem in the use of QDs for *in vivo* and *in vitro* applications: the inherent toxicity due to the heavy metal core.

In order to overcome this drawback of QDs the rush for other imaging agents began. Sidots and Cdots appeared in this context. Nowadays it was already proven that not only they have a contrast imaging ability competitive with QDs, but also the non-toxicity feature that was so necessary.

Since their appearance the interest in Sidots and Cdots has grown and, as such, now they can be produced by several synthetic pathways. Additionally, and by using soft chemistry, it is possible to functionalize them with different molecules in order to increase their fluorescence, change the emission wavelength and also for targeting applications. In this sense these nanoparticles have found numerous applications in sensing/biosensing of specific analytes. However all these steps must be considered carefully for the intended application, since their toxicity can increase due to the presence of certain functional groups on the dots surface.

The toxicity of the nanoparticles is a current line of investigation, mainly due to the possibility of applying them into live organisms for *in vivo* imaging and as advanced drug delivery systems. From the studies performed so far it was found that both Sidots and Cdots have a toxicity level lower than the traditional QDs. Additionally it was found that the use of PEG as a functionalization molecule helps to reduce their toxicity. Nevertheless it is still necessary to perform more studies in order to completely understand the mechanism beneath their toxicity.

1.6. References

[1] Wang X., Cao L., Lu F., Meziani M.J., Li H., Qi G., Zhou B., Harruff B.A., Kermarrec F., Sun Y.-P. **2009**. Photoinduced electron transfers with carbon dots. Chem. Commun. pp. 3774- 3776.

[2] Wang F., Chen Y.-H., Liu C.Y., Ma D.-G. **2011**. White light-emitting devices based on carbon dots' electroluminescence. Chem. Commun. 47, pp.3502-3504.

[3] Li H., He X., Kang Z., Huang H., Liu Y., Liu J., Lian S., Tsang C.H.A., Yang X. D,

Lee S.-T. **2010**. Water-Soluble Fluorescent Carbon Quantum Dots and Photocatalyst Design. Angew. Chem. Inter. Ed. 49 (26) pp. 4430–4434.

[4] Yang S.T., Cao L., Luo P.G., Lu F., Wang X., Wang H., Meziani M.J., Liu G., Qi G., Sun Y.P. **2009**. "Carbon Dots for Optical Imaging in Vivo". J. Am. Chem. Soc. 131 pp.11308-11309.

[5] Ryman-Rasmussen JP. **2007**. Surface coatings determine cytotoxicity and irritation potential of quantum dot nanoparticles in epidermal keratinocytes**.** J. Invest. Dermatol. 127, pp.143-153.

[6] Higuchi Y. **2008**. Mannosylated semiconductor quantum dots for the labeling of macrophages. J. Control. Release. 125, pp.131-136.

[7] Baker S.N., Baker G.A. **2010**. "Luminescent Carbon Nanodots: Emergent Nanolights, Angew. Chem. Int. Ed. 49, pp. 6726-6744.

[8] Xu X.Y., Ray R., Gu Y.L., Ploehn H.J., Gearheart L., Raker K., Scrivens W.A. **2004**. "Electrophoretic Analysis and Purification of Fluorescent Single-Walled Carbon Nanotube Fragments". J. Am. Chem. Soc. 126, pp. 12736-12737.

[9] Bourlinos A.B., Stassinopoulos A., Anglos, D. Zboril R., Karakassides M., Giannelis E.P., **2008**. "Surface Functionalized Carbogenic Quantum Dots". Small **4**, pp. 455-458.

[10] Cao L., Wang X., Meziani M.J., Lu F., Wang H., Luo P.G., Lin Y., Harruff B.A., Veca L.M., Murray D., Xie S.Y., Sun Y.P. **2007**. "Carbon Dots for Multiphoton Bioimaging". J. Am. Chem. Soc. 129, pp.11318-11319.

[11] Zhou J.G., Booker C., Li R.Y., Zhou X.T., Sham T.K., Sun X.L., Ding Z.F. **2007**. "An Electrochemical Avenue to Blue Luminescent Nanocrystals from Multiwalled Carbon Nanotubes (MWCNTs)". J. Am. Chem. Soc. 129, pp.744-745.

[12] Zheng L., Chi Y., Dong Y., Lin J., Wang B. **2009**. "Electrochemiluminescence of Water-Soluble Carbon Nanocrystals Released Electrochemically from Graphite" J. Am. Chem. Soc. **131**, pp.4564-4565.

[13] Liu H., Ye T., Mao C. **2007**. "Fluorescent Carbon Nanoparticles Derived from Candle Soot"**.** Angew. Chem. Int. Ed. 46, pp. 6473-6475.

[14] Bourlinos A.B., Stassinopoulos A., Anglos D., Zboril R., Georgakilas V., Giannelis E.P. **2008**. "Photoluminescent Carbogenic Dots". Chem. Mater. 20, pp. 4539-4541.

[15] Peng H., Travas-Sejdic J. **2009**. "Simple Aqueous Solution Route to Luminescent Carbogenic Dots from Carbohydrates". Chem. Mater. 21, pp. 5563-5565.

[16] Zhu H., Wang X., Li Y., Wang Z., Yang F., Yang X. **2009**. "Microwave synthesis of fluorescent carbon nanoparticles with electrochemiluminescence properties" Chem. Commun. 34, pp. 5118-5120.

[17] Li H., He X., Liu Y., Huang H., Lian S., Lee S.T., Kang Z. **2011**. "One-step ultrasonic synthesis of water-soluble carbon nanoparticles with excellent photoluminescent properties". Carbon 49, pp. 605-609.

[18] Esteves da Silva, J.C.G., Gonçalves H. **2012**. "Analytical and bioanalytical Applications of Carbon Dots". Trends Anal. Chem. 30, pp. 1327-1336.

[19] Zhou J., Sheng Z., Han H., Zou M., Li C. **2012**. "Facile synthesis of fluorescent carbondots using watermelon peel as a carbon source". Mat. Lett. 66 (1), pp.222-224.

[20] Y.-P. Sun, X. Wang, F. Lu, L. Cao, M. J. Meziani, P.G. Luo, L. Gu, L.M. Veca. **2008**. "Doped Carbon Nanoparticles as a New Platform for Highly Photoluminescent Dots". J Phys Chem C Nanomater Interfaces. 112 (47), pp.18295-18298.

[21] Klimov V.I. **2004**. "Semiconductor and metal nanocrystals: synthesis and electronic and optical properties". Marcel Dekker Inc.

[22] Krishna M.V.R., Friesner R.A. **1991**. "Quantum confinement effects in semiconductor clusters". J. Chem. Phys. 95, pp.8309-8315.

[23] Nirmal M., Brus L. **1999**. "Luminescence photophysics in semiconductor nanocrystals". Acc. Chem. Res. 32, pp.407-414.

[24] Gonçalves H.M.R., Esteves da Silva J.C.G. 2012. " A New Insight on Silicon Dots". Curr. Anal. Chem. 8, pp.67-77.

[25] A. Puzder, A.J. Williamson, J.C. Grossman, G. Galli. **2003**. "Computational Studies of the Optical Emission of Silicon Nanocrystals" J. Am. Chem. Soc. 9 (125), pp.2786-2791.

[26] Lakowicz J.R., **1999**. "*Principles of Fluorescence Spectroscopy"*. Chapter 1, Kluwer-Plenum, New York.

[27] Valeur B. **2001**. "Molecular Fluorescence Principles and Applications", Chapter 1, Wiley-VCH, New York.

[28] Chattopadhyay A. **1990**. "Depth profiling in membranes by fluorescence quenching". *J. Biosci*. 15 (3), pp.143–144.

[29] Mohanraj V.J., Chen Y. **2006**. "Nanoparticles – A Review". Tropical Journal of Pharmaceutical Research, 5 (1) pp. 561-573.

[30] Hua F.J., Swihart M.T., Ruckenstein E. **2005**. "Efficient surface grafting of luminescent silicon quantum dots by photoinitiated hydrosilylation". Langmuir 21, pp.6054-6062.

[31] Nelles, J.; Sendor, D.; Ebbers, A.; Petrat, F.M.; Wiggers, H.; Schulz, C.; Simon, U. **2007**. "Functionalization of silicon nanoparticles via hydrosilylation with 1-alkenes". Colloid Polymer Sci. 285, pp.729-736.

[32] Rogozhina E., Belomoin G., Smith A., Abuhassan L., Barry N., Akcakir O., Braun P.V., Nayfeh M.H. **2001**. "Si–N linkage in ultrabright, ultrasmall Si nanoparticles". Appl. Phys. Lett. 78, pp.3711-3713.

[33] Hernández-Padrón G., Rodríguez R., Castañro V. **2005**. "In-Situ Thiol-Modified Silica Nanoparticles". The Internet Journal of Nanotechnology. 1 (2) DOI: 10.5580/1f10. Available online in: http://www.ispub.com/journal/the-internet-journal-of-nanotechnology/volume-1-number-2/in-situ-thiol-modified-silica-nanoparticles.html, consulted in June 2012.

[34] Teste B., Malloggi F., Gassner A.-L, Georgelin T., Siaugue J.-M., Varenne A., Girault H., Descroix.S. **2011**. "Magnetic core shell nanoparticles trapping in a microdevice generating high magnetic gradient". Lab Chip. 11, pp.833-840.

[35] Gonçalves H., Jorge P., Fernandes J.R.A., Esteves da Silva J.C.G. **2010**. "Hg(II) sensing based on functionalized carbon dots obtained by direct laser ablation". Sensors and Actuators: B Chemistry 145, pp. 702-707.

[36] Ray S.C., Saha A., Jana N.R., Sarkar R. **2009**. "Fluorescent Carbon Nanoparticles: Synthesis, Characterization, and Bioimaging Application". J. Phys. Chem. C 113, p. 18546-18551.

[37] Qin L., Ohulchanskyy, T.Y.; Ruili L.; Kaloian K.; Dongqing W., Andreas B., Rajiv K., Adela B.; Prasad, P.N. **2010**. "Photoluminescent Carbon Dots as Biocompatible

Nanoprobes for Targeting Cancer Cells in Vitro". J. Phys. Chem. C. 114 (28), pp.12062–12068.

[38] M. Bottrill, M. Green. **2011**. "Some aspects of quantum dot toxicity". Chem. Commun. 47, pp.7039-7050.

[39] Hardman R. **2006**. "A toxicologic review of quantum dots: toxicity depends on physicochemical and environmental factos". Environ Health Perspect. 114 (2), pp.165-172.

[40] Higuchi Y. **2008**. "Mannosylated semiconductor quantum dots for the labeling of macrophages". J. Control. Release 125, pp.131-136.

[41] Faure, A.C., Dufort S, Josserand V, Perriat P, Coll J.L., Roux S, Tillement O. **2009**. "Control of the in vivo Biodistribution of Hybrid Nanoparticles with Different Poly(ethylene glycol) Coatings". Small 5 (22), pp.2565-2575.

[42] Yang S.T., Wang X., Wang H., Lu F., Luo P.G., Cao L., Meziani M.J., Liu J.H., Liu Y., Chen M., Huang Y., Sun Y.P. **2009**. **"**Carbon Dots as Nontoxic and High-Performance Fluorescence Imaging Agents". J. Phys. Chem. C 113, pp.18110-18114.

Chapter 2 – A New Insigth on Silicon Dots

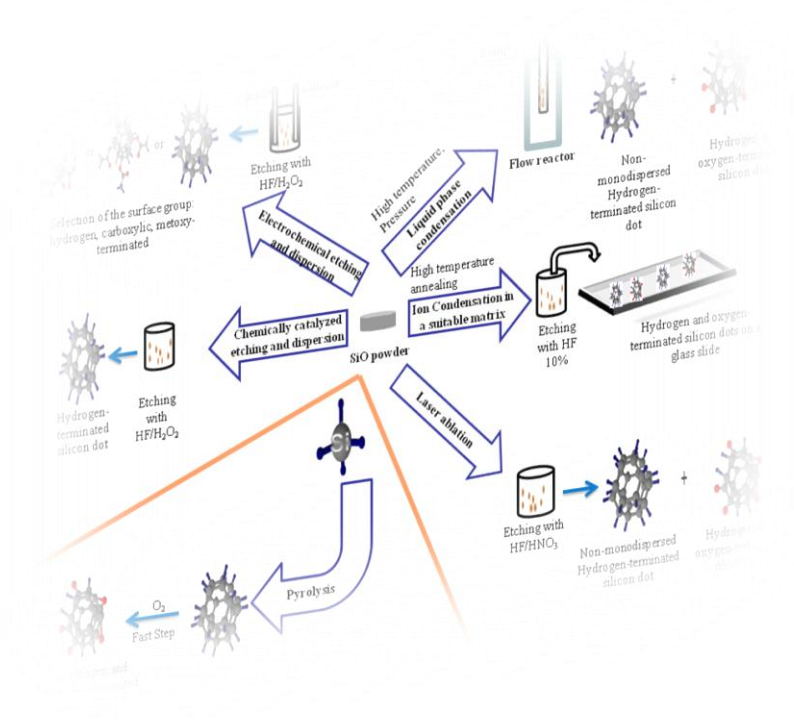

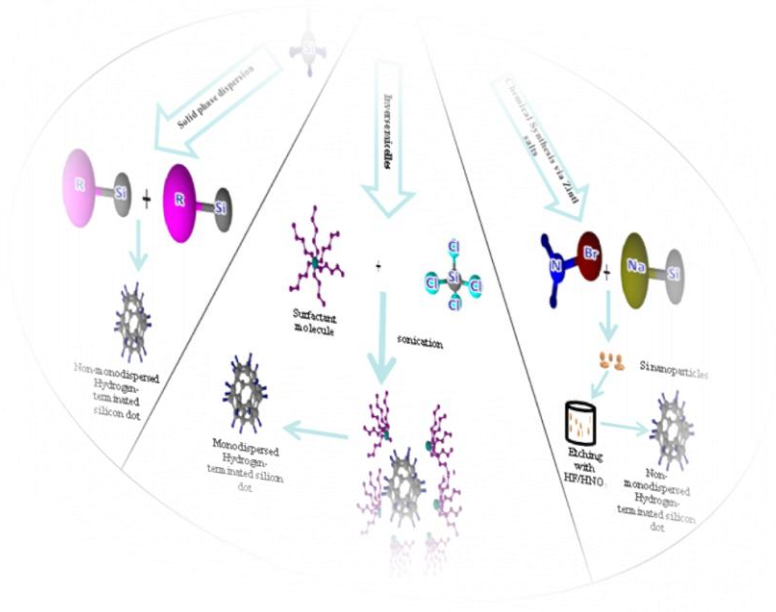

2.1. State of the Art

Silicon porous nanoparticles were first prepared in the 1950s by electrochemical etching in hydrofluoric acid and ultraviolet irradiation [1], however its red luminescence was only discovered by Canham in 1990 [2]. This red shift was considered quite interesting, but porous silicon is very fragile and highly reactive, which limits their applications. Silicon Dots were the solution to this problem and ever since then their application range has grown. Nowadays they can be found in electronics (as low power nanomemory and transistors) [3], photonics (photodetectors in the UV), photovoltaic and lighting technologies (solar cells and light emitting diodes) [4], substance sensors (e.g., glucose, dopamine and Anthrax®) [5], catalyst and fuel cells [6], biomedical fluorescent tags (has an alternative to the highly toxic cadmium based QDs), cosmetics that can penetrate skin [7], integration in the silicon industry as Green Technology [8], among others.

A key issue to control their photo-physical properties is to control their size, and this has been a great challenge over the years. In order to overcome this question numerous synthetic pathways have appeared but the solution was still not achieved [9].

2.2. References

[1] Parkhutik V., Timashev S. **2000**. "Kinetics of porous silicon growth studied using flicker-noise spectroscopy". J. Appl. Phys. 87, pp.7558-7560.

[2] Canham, L.T. **1990**. "Silicon quantum wire array fabrication by electrochemical and chemical dissolution of wafers". Appl. Phys. Lett. 57, pp.1046-1048

[3] Tiwari S., Rana F., Hanafi H., Hartstein A., Crabbe E.F., Chan K. **1996**. "A silicon nanocrystals based memory". Appl. Phys. Lett. 68 (10), pp.1377-1379.

[4] Ng W.L., Lourenço M.A., Gwilliam R.M., Ledain S., Shao G., Homewood K. P. **2001**. "An efficient room-temperature silicon-based light-emitting diode". Nature 410, pp.192-194.

[5] C.Yu, F.Zeng, M. Luo, S. Wu. **2012**. "A silica nanoparticle-based sensor for selective fluorescent detection of homocysteine via interaction differences between thiols and particle-surface-bound polymers"**.** *Nanotechnology* 23, doi:10.1088/0957-4484/23/30/305503.

[6] Choi Y., Wang G., Nayfeh M.H., Yau S.-T. **2008**. "Electro-oxidation of organic fuels catalyzed by ultrasmall silicon nanoparticles". Appl. Phis. Lett. 93, pp.164103-164106.

[7] Online report, available in: http://www.cosmeticsdesign-asia.com/Formulation-Science/Silica-nanoparticles-can-enhance-delivery-of-active-ingredients, consulted in June **2012**.

[8] Intartaglia R., Barchanski A., Bagga K., Genovese A., Das G., Wagener P., Di Fabrizio E., Diaspro A., Brandi F., Barcikowski S. **2012**. "Bioconjugated silicon quantum dots from one-step green synthesis". Nanoscale. 4 (4), pp.1271-1274.

[9] Gonçalves H.M.R., Esteves da Silva J.C.G. 2012. " A New Insight on Silicon Dots". Curr. Anal. Chem. 8, pp.67-77.

2.3. Personal Contribution to this Paper

My personal contribution to this work includes the following: the complete research on the Silicon Dots topic in order to ascertain the state of the art. After the complete overview on the most innovative synthesis and purification methods, along with the most recent applications, it was necessary to write a review on the subject for publication in an international scientific research journal. Additionally, it was necessary to create images that correctly reflected and simplified the text, so it would allow, a new researcher on the topic, to have a resume of the necessary data. After the submission of the paper it was required some adjustments to comply with the reviewers suggestions.

A New Insight on Silicon Dots

Helena M.R. Gonçalves and Joaquim C.G. Esteves da Silva*

Centro de Investigação em Química (CIQ-UP), Department of Chemistry and Biochemistry, Faculty of Sciences, Universidade do Porto, Rua do Campo Alegre 687, 4169-007 Porto, Portugal

Abstract: Fluorescent silicon nanoparticles (silicon dots) are low-toxicity nanomaterials of utmost interest to analytical and bioanalytical chemistry. Silicon dots have proved to be excellent fluorescent tags for sensor development applications. This review focuses on silicon dots and their fluorescent properties and applications. Silicon dots can be produced *via* nine basic synthetic methods and their fluorescent properties differ considerably, according to how they are produced and functionalized. The photoluminescent mechanism depends on the particle size, surface defects and functionalization molecules. This review presents a synopsis of the most important recent analytical and bioanalytical applications, along with the toxicity assays performed with silicon dots.

Keywords: Silicon dots, Synthesis methodologies, Functionalization, Fluorescence mechanisms, Bioanalytical applications, Bioimaging, Toxicity assays.

1. INTRODUCTION

The era of nanoparticles is installed and the continuous search for new and improved particles is unstoppable. At the end of the 1980s nanochemistry blossomed when quantum dots made their appearance (QDs) [1]. QDs are nanoparticles of semiconductor material (typically between 1 and 12 nm in diameter). Quantum confinement endows these materials with unique light emitting properties that are proving to be a powerful tool for labeling biological systems. In fact their nanoscale size range is compatible with most of the metabolic and internalization processes observed in cells and, unlike other nanoparticle-based optical imaging probes, QDs do not exceed the proteins' size, which makes them very useful for biological applications [2-5]. However, the most useful QDs in analytical/bioanalytical chemistry are based on a highly toxic metal core that has in fact proved to be toxic in biological systems [6].

Another highly fluorescent nanomaterial that has been the subject of intense investigation is silicon dots. These nanoparticles have fluorescence characteristics similar to those of the traditional QDs, but their toxicity is very low [7, 8]. Porous silicon nanoparticles were first prepared in the 1950s by electrochemical etching in hydrofluoric acid and ultraviolet irradiation [9] but their red luminescence was only discovered in 1990, by Canham [10]. Further studies revealed that the photoluminescence (PL) emission was red shifted as particle size increased [11]. This red shift in the visible spectral range meant that the silicon particles could be used for optoelectronic devices, but since porous silicon is very fragile and highly reactive the possibilities of new applications were limited. Silicon dots were suggested as a way of overcoming these limitations. Over the years they have been known as silicon quantum dots, silicon nanoparticles, silicon nanocrystals and, recently, silicon dots. In this review they are called silicon dots. Silicon dots are silicon-based nanoparticles, typically with a diameter of 1-10 nm, that can be produced by either top-down or bottom-up approaches.

Several methods have been proposed for their synthesis: gas-phase pyrolysis of silanes [12-14]; ultrasonic dispersion of porous silicon in organic solvents [15]; evaporation and laser ablation of silicon in an inert atmosphere [16, 17]; through high pressure, high temperature solution phase methods [18], and by chemical etching of silicon powder [19]. The objective is to produce silicon dots with high quantum yield, emission wavelength red-shift and narrow size dispersion. Their biocompatibility, high photoluminescence quantum efficiency, stability against photobleaching, and the non-blinking behavior, size-tunable emission and the possibility of functionalization with several molecules to render them sensitive to an analyte are properties that have made these dots highly useful for biological applications. Furthermore, they can be excited by single photon (UV: 330-400 nm) and two-photon (near infrared: 720-850 nm) absorption, which is considered biologically friendly. Despite all the good qualities irreversible bleaching does occur [20].

The silicon dots' range of applications is far wider than just bioimaging. They are used in electronics (as low power nanomemory and transistors), photonics (photodetectors in the UV), photovoltaic and lighting technologies (solar cells and light emitting diodes), substance sensors (e.g., glucose, dopamine and Anthrax®), catalyst and fuel cells, biomedical fluorescent tags (as an alternative to the highly toxic cadmium-based QDs), cosmetics that can penetrate skin, integration in the silicon industry as green technology, to mention some of their applications. A number of studies have been undertaken so as to better understand and control their optical properties. This review discusses methods of synthesizing silicon dots, their bioanalytical applications and toxicology assays, and their fluorescence mechanism.

*Address correspondence to this author at the Centro de Investigação em Química (CIQ-UP), Department of Chemistry and Biochemistry, Faculty of Sciences, Universidade do Porto, Rua do Campo Alegre 687, 4169-007 Porto, Portugal; Tel: +351220402569; Fax: +351220402659;
E-mail: jcsilva@fc.up.pt

1573-4110/12 $58.00+.00

2. SYNTHETIC METHODS

The silicon dots used in biomedical and optoelectronic applications must have high stability, a substantial photoluminescence quantum yield in the visible wavelength range and be soluble in aqueous media. The need to achieve these parameters was taken into account when developing the various synthetic methods. Nowadays there are nine main ways of producing the silicon dots as schematically shown in Fig. (**1**).

(1) **Gas Phase Condensation (Pyrolysis):** In this method a suitable molecule containing silicon (e.g., SiH_4) is dissociated and the silicon dots are produced after a nucleation process. Several techniques use this procedure, namely, combustion, thermal decomposition, microwave plasma, gas-evaporation and chemical vapor deposition. The use of these techniques usually makes it very difficult to collect the particles, which leads to a low yield. In addition, the silicon dots produced by these techniques are non-monodispersed and require capping to protect their surface [21, 22].

(2) **Ion Condensation in a Suitable Matrix:** Here, SiO powders are annealed at 1000°C in an ambient atmosphere and etched with HF at 10%. The resulting atoms are allowed to condense into glass. Silicon dots produced this way are polydispersed (5.1 ± 1.9 nm) and still have a significant amount of oxygen on their surface. The main advantage of this method is its relatively low cost [23, 24].

(3) **Liquid Phase Condensation:** This method is based on the pyrolysis of organosilanes in solvents heated

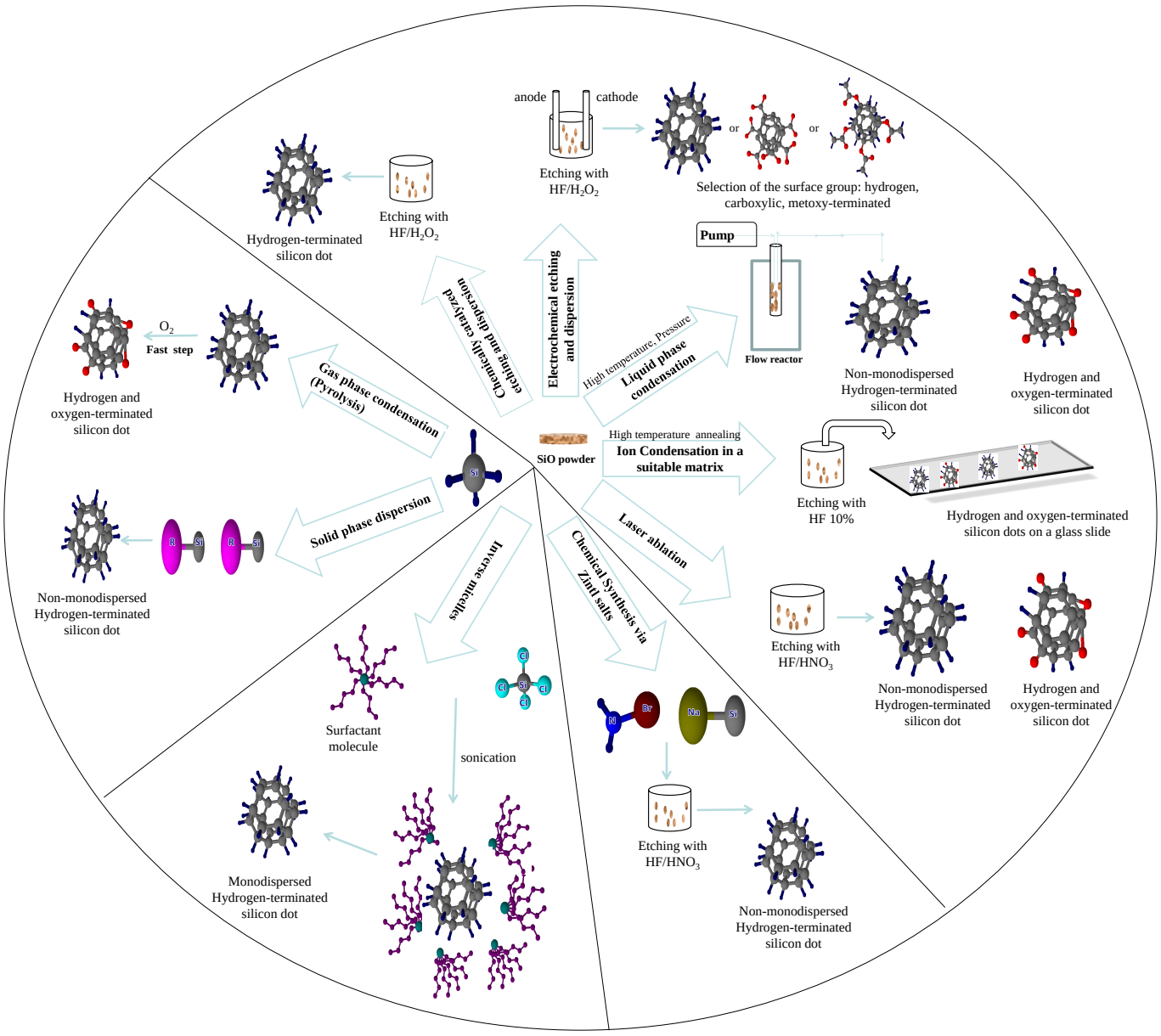

Fig. (1). Methods for silicon dot production.

and pressurized above their critical points [25, 26]. The nucleation takes place in a continuous flow reactor, in octanol at 500 ºC and approximately 250 bar [27]. The silicon dots obtained are non-monodispersed. The chemical decomposition is not easily controlled since about 50% of the nanoparticles obtained are alkoxy-terminated [22]. Organic capping is required to achieve some degree of control over the particle size during the synthesis step. The same synthetic approach can be employed to produce Si nanowires [28, 29].

(4) **Solid Phase Dispersion:** Over the years Kauzlarich and co-workers [31] have studied several oxidation-reduction reactions in order to produce silicon dots. The method is based on combining Si-containing precursors in solution under atmospheric conditions [32]. Several different routes were investigated (Fig. **2**). The size of Si nanoparticles can be changed by adjusting the balance between growth and nucleation speeds through the control of factors such as reaction temperature, concentration of precursors and surface ligands. The main advantage of these methods is definitely their versatility since they can also be employed to produce doped Si nanoparticles (with Mn [32] or P [33]) or mixed Si-Ge nanoparticles [34]. Also, silicon dots with halogen termination (Cl, Br) can be obtained (allowing further functionalization) using, for example, alkyllithium (R-Li) compounds [30, 35] and alkoxy groups - *via* reaction with alcohols [36, 37] - or hydrogen atoms by reduction with $LiAlH_4$ [38]. This method has been claimed to actually allow partial control over the silicon dots' shape, particularly when using sodium naphthalenide [39]. However, the silicon dots obtained by this method are polydispersed and need extensive purification, and there is the further disadvantage that the reactions are very time consuming (~72 h per reaction).

(5) **Laser Ablation:** (Microscopic explosions) In this method silicon wafers are torn to form nanoparticles. Swihart and co-workers [40], for example, used a CO_2 laser beam with a H_2/He gas to confine the reaction zone in the laser beam and to further increase the temperature. Particle nucleation occurs after 850ºC and by controlling the flow rates and the laser power they have some control over the nanoparticle sizes. The nanoparticles can also be etched with HF/HNO_3 in order to reduce their size. The silicon dots obtained by this method exhibit a mixture of hydrogen and oxygen termination. The main disadvantages are: difficulty in recovering the nanoparticles; they are polydispersed, need capping for protection and stabilization and the laser efficiency is hard to control, which makes it difficult to have real control over nanoparticle size.

(6) **Electrochemical Etching and Dispersion:** Rogozhina and co-workers [41] used an electrochemical dispersion of crystalline Si wafers to produce carboxylic- and methylester-terminated

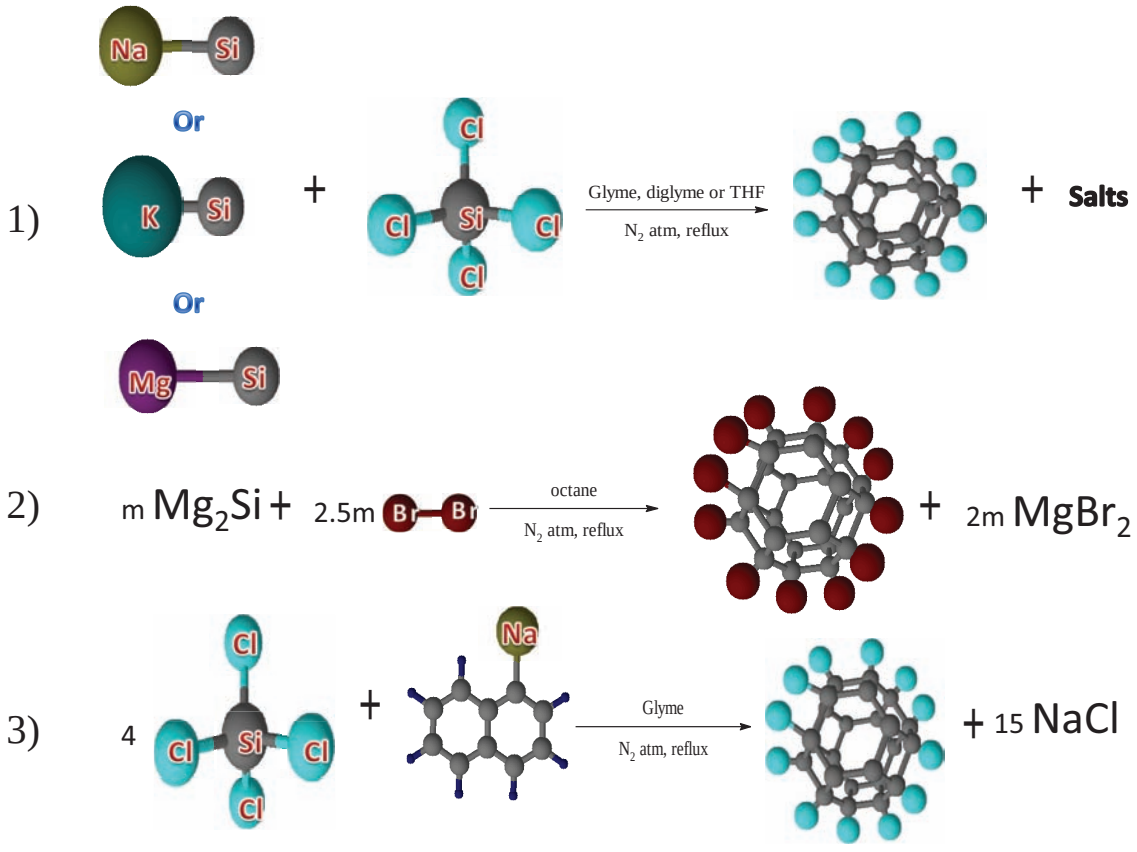

Fig. (2). Chemical routes for obtaining halogen-terminated silicon dots using solid phase dispersion.

silicon dots with diameters between 1 nm and 1.5 nm. Hydrogen-terminated silicon dots were formed through HF/H_2O_2 anodization and ultrasonic fractionation of crystalline Si wafers.

(7) **Chemically Catalyzed Etching and Dispersion:** The production of silicon dots by HF etching is a self-limiting process since HF does two things: it reduces the nanoparticles' size and introduces hydrogen passivation on the dots surface. This process usually leads to low yields and high size dispersion. The incorporation of a catalyst, like H_2O_2 or HNO_3, helps to further oxidize silicon while HF vigorously dissolves the oxide [42]. The combined effect of the two chemicals leaves no oxygen and also results in hydrogen passivation. Catalysis by H_2O_2 has other advantages over HNO_3, since the hydrogen passivation in this case is more complete (only allowing mono-hydride termination), and of better quality. The presence of H_2O_2 also eliminates hydrocarbons and other organic impurities, leading to "more stable" sizes and configurations. This method yields sizes ranging from 1nm (blue) to 3.7 nm (red) [43].

(8) **Chemical Synthesis *via* Zintl Salts:** This method is an aqueous route to obtaining significant amounts of hydrogen-terminated silicon dots from non-hazardous materials. But the yields of silicon dots are often low and frequently require HF etching treatment to acquire photoluminescence. The silicon dots are synthesized by a "metathesis" reaction of NaSi and NH_4Br. The nanoparticles can then undergo hydrosilylation to form Si-C bonds and be further functionalized with an adequate amphiphilic polymer to retain high quantum yield along with water solubility [44].

(9) **Inverse Micelles:** The basis of this method is the dissolution of an anhydrous compound (e.g. SiX_4; X = Cl, Br or I) in the hydrophilic interior of micelles. As such, the nucleation and growth of silicon dots are restricted to the micelle interior. This method has the clear advantage of size control, by varying micelle size, intermicellar interactions and reaction chemistry [45, 46]. The reaction occurs under inert atmosphere to prevent the oxidation of the silicon dots. Although the surface chemistry of dots obtained directly from the reaction of $SiCl_4$ with $LiAlH_4$ has not yet been described, the reactivity of these silicon dots suggests hydride surface termination [47].

After the raw silicon dots are produced their surface can be functionalized with a number of molecules according to the desired application. The functionalization process is quite important since it is responsible for giving a higher stability against oxidation and Ostwald ripening (the growth of larger nanoparticles by merging smaller, poorly passivated ones), and for reducing defect states on the silicon dots' surfaces caused by dangling bonds [48]. The nanoparticle surface can be modified by removing hydrogen terminations and replacing them with a mono-linker or bi-linker, without compromising

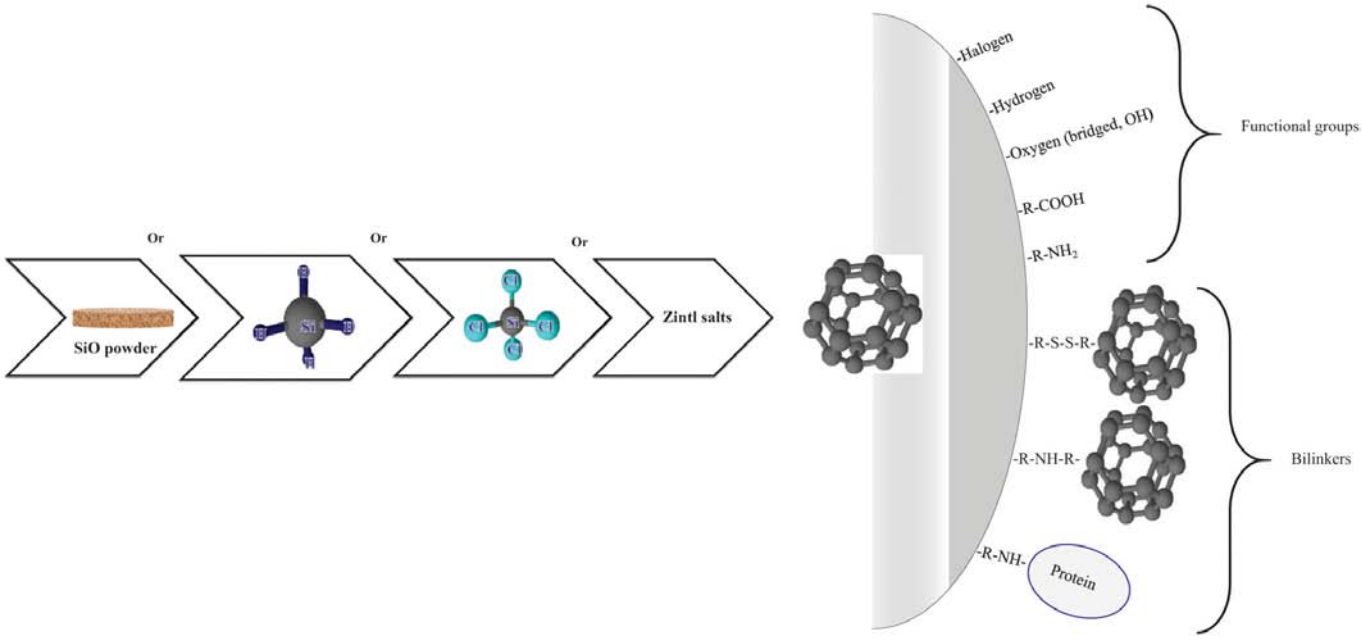

Fig. (3). Silicon dots' surface changes: introducing functional groups or bi-linkers.

the optical activity of the particles, using soft chemistry. It is thus possible to introduce different functional groups onto the silicon dots surface (Fig. **3**).

When functionalizing silicon dots there is a major factor to take into account, which is that this process should occur without breaking any Si-Si bond, since silicon dots are nanoparticles that have only 100-200 atoms. As such, any path leading to Si-Si bond cleavage will have an adverse impact on the dots' optical properties and could potentially dissolve the nanoparticles completely [41]. This effect was mainly observed in two circumstances: (i) in the reaction with alcohols, where the alkoxylation results in the cleavage of Si-Si bonds and the formation of Si-H and Si-O-C species [49]; (ii) in the alkylation with Grignard or alkyl lithium reagents, where there is a nucleophilic attack by a carbanion on an electron-deficient Si atom, thereby cleaving Si-Si bonds to form Si-C bonds and silyl anion (Si^-) species [50, 51]. With this in mind it was necessary to further investigate alternative paths for silicon dots functionalization. The solution may be hydrosilylation reactions. These are usually performed by halogen- or hydrogen- terminated silicon dots' reacting with alkyl-lithium salts [35] or terminal alkenes [31], and the result is very stable Si-C linkages. The reaction with terminal alkenes is performed by using light, [52] heat, [41] or a variety of platinum [47] and triphenylcarbenium-based catalysts [53].

The methods described above give a very broad range of compounds that can be used to functionalize the silicon dots for the intended purpose. It has been demonstrated that replacing the hydrogen terminations by –COOH [41] or $–NH_2$ groups [47, 54] makes the silicon dots water soluble. The carboxylation results in highly luminescent nanoparticles that are very stable in water, relatively easy to separate by electrophoresis [55**]** and, since carboxyl is quite a versatile bi-linker (Fig. **3**), this functionalization is a good option for many researchers [41]. However it has the disadvantage of side products like free radical cross-linking. Amines are also versatile bi-linkers - their use has proved helpful in attaching proteins such as *Streptavidin* [54] onto the silicon dots surface (Fig. **3**). Thiolation (introduction of a –SH group) has also proved useful to attach a molecule (e.g. a protein) or two silicon dots with an alkyl chain as spacer, through an S-S bond.

On the other hand the use of non-polar groups such as alkyl chains makes them soluble in non-polar solvents. It has been reported that silicon dots functionalized with non-polar dienes, for example, exhibit a higher energy emission than those capped with polar groups like epoxides, diols and amines [56]. This is interesting since not only the emission wavelength can be controlled by the particle size but it is also related to the polarity of the functionalization group.

Purification must be performed before starting any analytical test. The silicon dots may be purified before and after functionalization to achieve homogeneous size dispersion, regardless of the synthesis process. The number of papers reporting separation of the nanoparticles by size and/or zeta potential has been growing in recent years [57, 58]. Capillary electromigration separation techniques have been used to separate nanoparticles and nanoparticles functionalized with biomolecules. These may be valid methods to purify silicon dots.

All the optical changes described so far have helped the understanding of the fluorescence mechanism of these nanoparticles.

3. FLUORESCENCE MECHANISM

The fluorescence mechanism of nanoparticles has been explained by several theories [59]. The aspect common to all of them is the attempt to correlate the difference between the fluorescence properties of the bulk and nanomaterials with their size. The theory that is now most widely accepted is that of quantum confinement [60]. This states that there is a finite number of quantum states available to the valence electrons in nanoparticles. The smaller the particles, the larger the energy gap between the highest occupied molecular orbital (HOMO) and the lowest unoccupied molecular orbital (LUMO). Therefore electrons in the HOMO level need more energy to be excited to the LUMO level. After excitation the electrons relax to the lowest energy level of the first excited state and finally back to their ground state with the emission of light, i.e. photoluminescence (PL) [60, 61]. The wavelength of the emitted light is determined by the energy gap of the nanoparticles (Fig. **4**).

For smaller silicon nanoparticles, however, the percentage of surface atoms may predominate and so surface imperfections become predominant in the overall nanomaterial properties. Indeed, the termination of the lattice periodicity on the surface of the smaller nanoparticles creates a potential boundary and the coordination number of the surface atoms is reduced (dangling bonds), which gives rise to electronic defect states on the silicon dots [62-64]. Therefore the optical properties of semiconductor nanoparticles can only be fully understood by considering surface effects.

The PL mechanism for silicon nanoparticles has yet to be determined, although there have been several attempts using both experimental results and theoretical calculations [56, 65]. Almost all these attempts relate either to the theory of quantum confinement or surface state effects. With respect to the quantum confinement theory for silicon dots it can be said that there is a shift of the band gap (HOMO-LUMO gap) from 1.1 eV in bulk Si to 3.0 eV for 2 nm structures [22, 66]. On the other hand, the surface state mechanism claims that surface localized states, such as, an Si-oxide or Si-hydrogen interface are likely to serve as radiative recombination centers.

Gole *et al.* [67], for example, proposed a model which suggested that the PL of silicon dots was due to a silanone (Si=O) group on the particle surface, and Wolkin *et al.* [66], suggested that the quantum confinement effect and surface states contribute simultaneously to the Si PL. However, they both used porous silicon nanoparticles and careful consideration is required when extrapolating these results to silicon dots. Brus *et al.* [68] synthesized surface-oxidized silicon nanoparticles to investigate the origin of PL for silicon dots. Their silicon dots have hydroxyl and oxide groups on the surface, as indicated by IR spectroscopy, but they simply attribute PL to the quantum size effect. Yang *et al.* [69, 70], prepared silicon dots with surface groups terminated with organic alkyl groups, such as, methyl, ethyl, n-butyl, and n-octil. Their results suggest that the observed UV-blue PL

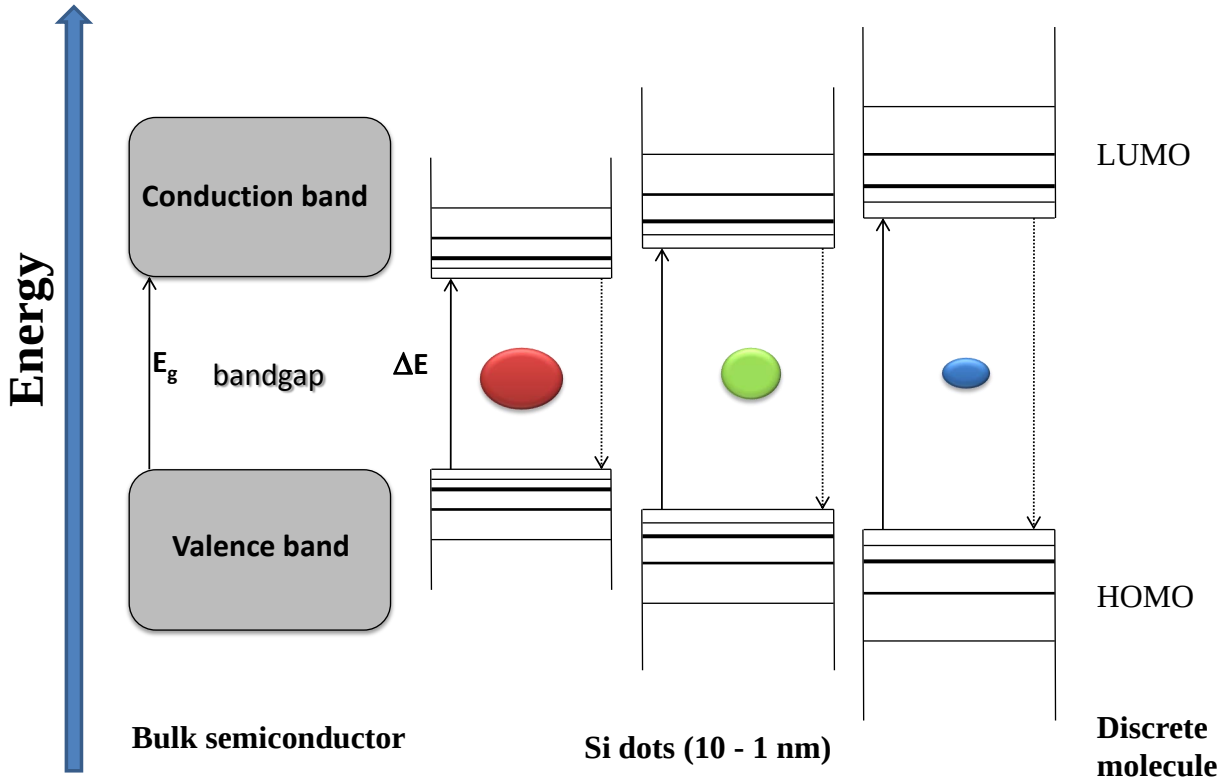

Fig. (4). Comparing the electronic energy states of a bulk semiconductor, silicon dots and a single molecule.

emission is consistent with optical transitions in quantum-confined silicon nanoparticles. They prepared larger nanoparticles by annealing of the smaller particles at different temperatures [70]. This resulted in surface changes, as revealed by the FT-IR spectrum, but they were not accounted for the explanation of the PL mechanism. It is now clear that the chemical processes used determine the surface groups of the silicon dots and are responsible for changing the internal electronic structure. These methods therefore play an important role in the fluorescence properties of the nanoparticles, i.e. the emission wavelength and radiative lifetime, and they ultimately define the solubility. Indirect band gap materials such as silicon generally have slow recombination rates with PL lifetimes ranging from tens of microseconds to milliseconds [71]. Direct band gap materials, however, such as the traditional QDs, have fast recombination rates with PL lifetimes of the order of 1–10 ns [72]. Taking this into account and considering that it was found that silicon dots with a hydrogen or carbon surface passivation display rapid recombination rates (1–10 ns), it is possible to say that this offers strong evidence that the observed emission results from electric-dipole-allowed direct band gap transitions [73, 45]. Alternatively, silicon dots with an oxide surface group typically display a dipole-forbidden yellow-red emission with radiative lifetimes of 10^3–10^6 ns [73, 65]. This slow recombination rate is a limitation to their use in biological imaging.

Nevertheless the PL mechanism of the silicon dots, prepared by any of the existing methods, cannot be complete if we consider only one or two of these factors. The theory developed by A. Putzer *et al.* [65] is the most complete up to now. According to this model the PL mechanism can be explained using these effects: quantum size, surface states, and/or defects on the surface. Their theory is based on computational studies which have led them to conclude that ionic rearrangements and electronic relaxations occurring upon absorption and emission, and the resulting Stokes shift, are extremely sensitive to the presence of surface passivants such as oxygen and to their bonding configuration. For example, a 1 nm cluster has a Stokes shift sensitivity of ± 0.9 eV, depending on the surface oxygen configuration - double bonded or bridged. In fact they have determined that nanoclusters with oxygen double bonded on the surface display the largest Stokes shifts and that a cluster with bridged oxygen on the surface, or reconstructed hydrogenated surfaces, exhibits the smallest Stokes shifts. This theory is also supported by experimental data [56, 74]. J. H. Warner *et al.* [74], for example, showed that the optical properties of silicon dots with identical size distributions are remarkably different. This indicates that it is not just the functional groups present on the surface that affect the PL, but also their configuration and ultimately the silicon dots' size.

4. ANALYTICAL APPLICATIONS

Several technological applications are known for silicon dots and many others are under investigation. The major applications within analytical chemistry are described below, and Fig. (**5**) shows the major areas of research and development.

4.1. Chemical and Bioanalytical Sensing

In general, we can say that sensors/biosensors consist of two major components: a highly specific recognition element,

Fig. (5). Analytical chemistry applications of silicon dots.

and a transducer that converts the molecular recognition event into a quantifiable signal [75]. Due to their unique characteristics, silicon dots have been used in several applications. The chemical and bioanalytical applications are discussed in this section. Good examples of chemical sensors are those for important biomedical substances, like dopamine, hydrogen peroxide, and glucose. Gang Wang *et al.* [76], for example, demonstrated the exclusive detection of glucose in the presence of interfering species, within the physiological concentration ranges of these substances. Their amperometric sensor based on silicon dots showed high reversibility, which is an indication that there was no electrode poisoning due to adsorption of reaction intermediates. Comparing this electrode with an immobilized glucose oxidase one [74], it is possible to say that the silicon dots sensor has an enhanced amperometric response. Their results revealed that the use of silicon dots offers great advantages as an inexpensive material in bioelectronics, including effective signal transduction and energy harvest and device miniaturization [78, 79].

In terms of biosensing, the use of silicon dots together with iron oxide has been reported to be a proficient tracking and drug delivery system [80]. Here the use of luminescent non-toxic nanoparticles with supermagnetic abilities means they can be visualized and manipulated externally through a magnetic field. It has also been shown that silicon dots are efficient photosensitizers of singlet oxygen [81]. This characteristic was used by researchers to suppress the division of cancer cells. Analysis of the DNA cells shows that they die through the apoptosis (programmed cell death) mechanism [82] after irradiation in the presence of silicon dots with a concentration of more than 0.1–0.5 g. V.Y. Timoshenko *et al.* [81] suggest that the death of the cancer cells occurs is probably due to the action of photosensitized active oxygen, in particular to the oxidation of cell material by singlet oxygen. In addition, the effect of other active forms of oxygen is also possible, e.g., superoxide ions (O_2^-), whose formation was observed by M. Fujii *et al*. [83]. The mechanism by which the active oxygen species are formed needs further study, but silicon dots appear promising for use in the photodynamic therapy of cancer.

4.2. *In vivo* Sensing

Silicon dots have been used more and more in bioanalytical applications over the years, and today applications ranging from devices for *in vivo* drug delivery systems [80], labs-on-chips [78, 79], bioanalysis [76-79] and new catalytic materials [84] are widespread. In all these applications the silicon dots' surface properties need to be tailored and controlled. Regarding the sensing applications, there is a need to introduce specificity through the functionalization with recognition elements. For molecular electronics, it is necessary to introduce molecules with specific electronic properties in such a way that it is fluid or open to electrons and electronic information. This reasoning is valid for all applications, and the possibility of tailoring the surface of the silicon dots, and thus their fluorescence and solubility properties, is one of the most appealing characteristics of these nanomaterials.

4.2.1. Bioimaging

Fluorescence tags and biosensors are of the utmost importance in areas like medicine and biology. Today they are used in everything from HIV tests to cell imaging. The molecular fluorescent dyes available have some serious drawbacks, however, these range from periodical dimming (blinking) to the absence of photostability and are responsible for introducing uncertainty in measurements [44]. The ambitious goal of developing treatment procedures that only need a minimal number of cells from living patients and smart drug delivery systems requires the development of a new generation of greatly improved fluorescent markers. The appearance of semiconductor QDs was revolutionary in this respect. However, the traditional QDs have toxicity issues that are difficult to surmount so that broader applications are possible, such as *in vivo* bioimaging and drug delivery systems [6]. The use of silicon dots has been gaining more and more support given their low toxicity and, since these nanoparticles do not require coating to achieve low toxicity it is possible to use even smaller nanoparticles than when using QDs. In fact it has been reported that silicon dots are better than the traditional QDs for *in vivo* applications [31, 85]. Also, silicon dots can be excited using two-photon excitation and this makes it possible to detect a single particle in a focal volume of 1 pcm^3 [83]. It has been proved that the efficiency under two-photon excitation is about three times higher than fluorescein. This intrinsic characteristic paves the way for their use in bioimaging and several studies have been performed relating to this aspect.

Silicon dots functionalized with carboxyl groups [86], allylamine [56] and poly(acrylic acid) (PAAc) [85] have been reported as efficient staining labels in both cancer and healthy cells, and three-dimensional sectioning has demonstrated that

the nanoparticles do indeed penetrate into cells. The PAAc capped silicon dots were used as fluorescent labels in Chinese hamster ovary cells (CHO) and their efficiency was compared with that of organic dyes, viz. Alexa 488, Cy5, fluorescein isothiocyanate (FITC), and laser dye styryl (LDS751). It was found that the cells with silicon dots remained fluorescent and no loss of intensity was observed during the measurement period (2h), which indicates high PL stability. This PL stability was further assessed under 24 h of UV exposure and it was observed that the nanoparticles kept 95% of their initial PL. On the other hand, all the organic dyes tested lost their PL completely after 30 min UV exposure. This clearly demonstrates that silicon dots can compete with organic dyes, and have much higher photostability [85].

4.2.2. Toxicity Assays

Hand in hand with the increasing interest in nanomaterials and their applications there has been an increase in the number of studies on the adverse biological responses to them [87-89]. Nevertheless, many questions remain unanswered and further studies are needed. They should focus particularly on cytotoxicity and the inflammatory responses of cells when exposed to nanoparticles, and on a correlation between their chemical constitution and the cells' responses. For example, it has been proved that different surface modifications can induce different levels of toxicity and there are some toxicity studies on various capping molecules, but no correlation has yet been established between these results and the inflammatory responses [90]. When talking about silicon dots it is also necessary to stress the difference between toxicity assays performed on porous silicon and silicon dots. Porous silicon can entrap particles within it and the functionalization may not be concentrated just on the nanoparticle surface, but in its interior, too. These processes cannot happen with silicon dots, and since the surface and its functionalizations seems to exhibit different toxicity indexes, the extrapolation should not be made that since porous silicon has been proved non-toxic the same will be true for silicon dots. A study on the variation of toxicity according to the capping molecules was performed by [56]. Here, the silicon dots obtained by the inverse micelles route were either epoxy- or diol-terminated. The toxicity was evaluated in two cell lines: Human skin fibroblasts (WS1) and lung epithelial cells (A549). It was found that cytotoxicity for the epoxide-terminated silicon dots appears at a concentration of 112 μg/mL and for the diol-terminated silicon dots it appears at 448 μg/mL. These authors suggest that this toxicity difference between silicon dots may be related to the fact that the epoxide group is a highly reactive specie and known to have oxidative toxicity [89]. As shown earlier, the effect of the surface chemistry on the silicon dots is very important, and so it is possible to say that different functional groups may have different toxicity values. The study by K. Fujioka *et al.* bears this out [90]. They used passive-oxidized silicon dots and evaluated their cytotoxicity response. In this assay the silicon dots were incubated with human cervical carcinoma cells (HeLa). The silicon dots' toxicity was not observed at 112 μg/ml. Furthermore, these authors prove that the passive-oxidized silicon dots are less toxic than CdSe QDs at high concentration, in both mitochondrial and lactate dehydrogenase (LDH) assays. This is particularly true under UV exposure, where silicon dots are more than ten times safer than CdSe QDs [92].

It is known that macrophages play an important role in the inflammatory process as a result of the presence of nanoparticles [91, 92] and that nanoparticle size is of the utmost importance. J. Choi *et al*. [89], studied cultured murine macrophages' (RAW 264.7) biological response to silicon dots of 3 nm and 100-3000 nm diameter. The silicon dots were exposed to macrophages with and without addition of endotoxin lipopolysaccharide (LPS), which is a positive inducer of NO and cytokines. It is known that in the presence of LPS particles may exhibit a synergistic or additive effect on the production of NO, tumor necrosis factor-alpha (TNF-*a*), interleukin 6 (IL-6), and NO. The cytotoxicity was assayed using the dye exclusion and the 3-(4,5-Dimethylthiazol-2-yl)-2,5-diphenyltetrazolium bromide reduction (MTT) assays. It was found that 3–5 nm diameter endotoxin-free silicon dots can reduce cell survival and cell viability in RAW 264.7 macrophages when incubated at concentrations above 20 mg/mL. No inflammatory response was found, however, i.e. production of NO, TNF-***a*** and IL-6, in macrophages incubated at 200 mg/ml. These authors suggest that the difference between the inflammatory responses of the two particle size distributions may be related to a higher molar concentration and relative surface area, as well as enhanced intracellular access. All these factors combined may have resulted in the macrophages' failure to identify the bigger silicon dots as "foreign" materials. The effect of the silicon dots' size and exposure time was also tested on human lung epithelial cells (A30) and on mouse fibroblasts (L929). The toxicity was evaluated after 6 and 24 h exposure and the nanoparticle size ranged from 200 to 367 nm. It was found that longer exposure time and larger the nanoparticle size affect the reduction of the toxicity level.

Regardless of the overall effect, toxicity or non-toxicity, there is still much to learn about the kinetics and intracellular localization of the silicon dots. A better understanding of these processes may be the well key to unlocking the mystery of the cytotoxicity mechanism and inflammatory process of the nanoparticles. The result will be the greater and safer use of nanoparticles in biological applications.

5. CONCLUSIONS AND PROSPECTS

Silicon dots can be produced by a number of methods and, depending on the one used, it is possible to achieve some degree of control over the nanoparticle size and surface defects. This control is very important since it has been proved that these two factors, together with the surface functionalization, are responsible for the fluorescence properties of the silicon dots. Moreover, the functionalization needs to be carefully designed for the intended purpose, because it is responsible for given the silicon dot a specific sensitivity and also a certain degree of toxicity.

In the past few years a number of toxicity assays have been performed and the cells' viability has been assessed and, even though the silicon dots exhibit a toxicity level below that of the traditional QDs, further studies are needed in order to understand the toxicity mechanism. The studies reviewed here have found that the functional groups have different potential

toxicity. However, these studies are only a small number of the papers published on silicon dots, and there are other molecules that should be studied, too, such as polyethylene glycol (PEG), which is relatively inert in biological media and can act, for example, as a good spacer between the dots' surface and a protein of interest.

REFERENCES

[1] Bimberg, D.; Grundmann, M.; Ledentsov, N.N. *Quantum Dots Heterostrutures*, Wiley: New York, **1999**.

[2] Gerion, D.; Pinaud, F.; Williams, S.C.; Parak, W.J.; Zanchet, D.; Weiss, S.; Alivisatos, A.P. Synthesis and properties of biocompatible water-soluble silica-coated cdse/zns semiconductor quantum dots. *J. Phys. Chem. B*, **2001**, *105*, 8861-8871.

[3] Rogach, A.N.; Nagesha, D.; Ostrander, J.W.; Giersig, M.; Kotov, N.A. "Raisin Bun"-type composite spheres of silica and semiconductor nanocrystals. *Chem. Mater*., **2000**, *12*, 2676-2685.

[4] Williams, Y.; Sukhanova, A.; Nowostawska, M.; Davies, A.M.; Mitchell, S.; Oleinikov, V.; Gun'ko, Y.; Nabiev, I.; Kelleher, D.; Volkov, Y. Probing cell-type-specific intracellular nanoscale barriers using size-tuned quantum dots. *Small*, **2009**, *5*, 2581-2588.

[5] Murcia, M.J.; Shaw, D.L.; Long, E.C.; Naumann, C.A. Fluorescence correlation spectroscopy of CdSe/ZnS quantum dot optical bioimaging probes with ultra-thin biocompatible coatings. *Opt. Commun*., **2008**, *28*, 1771-1780.

[6] Lovric, J.; Bazzi, H.S.; Cuie, Y.; Fortin, G.R.A.; Winnik, F.M.; Maysinger, D. Differences in subcellular distribution and toxicity of green and red emitting CdTe quantum dots. *J. Mol. Med*., **2005**, *83*, 377-385.

[7] Yang, S.T.; Wang, X.; Wang, H.; Lu, F.; Luo, P.G.; Cao, L.; Meziani, M.J.; Liu, J.H.; Liu, Y.; Chen, M.; Huang, Y.; Sun, Y.P. Carbon dots as nontoxic and high-performance fluorescence imaging agents. *J. Phys. Chem. C*, **2009**, *113*, 18110-18114.

[8] Yang, S.T.; Cao, L.; Luo, P.G.; Lu, F.; Wang, X.; Wang, H.; Mezian, M.J.; Liu, G.; Qi, G.; Sun, Y.P. Carbon dots for optical imaging *in vivo*. *J. Am. Chem. Soc*., **2009**, *131*, 11308-11309.

[9] Parkhutik, V.; Timashev, S. Kinetics of porous silicon growth studied using flicker-noise spectroscopy. *J. Appl. Phys*., **2000**, *87*, 7558-7560.

[10] Canham, L.T. Silicon quantum wire array fabrication by electrochemical and chemical dissolution of wafers. *Appl. Phys. Lett*., **1990**, *57*, 1046-1048.

[11] Canham, L.T. Lewis acid mediated hydrosilylation on porous silicon surfaces. *J. Am. Chem. Soc*., **1999**, *121*, 11491-11492.

[12] Wu, J.J.; Flagan, R.C. Onset of runaway nucleation in aerosol. Reactors. *J. Appl. Phys*., **1987**, *61*, 1365-1371.

[13] Schuppler, S.; Friedman, S.L.; Marcus, M.A.; Alder, D.L.; Xie, Y.H.; Ross, F.M.; Chabal, Y.J.; Harris, T.D.; Brus, L.E. Size, shape, and composition of luminescent species in oxidized Si nanocrystals and H-passivated porous Si. *Phys. Rev. B*, **1995**, *52*, 4910-4921.

[14] Wilson, W.L.; Szajowski, P.F.; Brus, L.E. Quantum confinement in size-selected, surface-oxidized silicon nanocrystals. *Science*, **1993**, *262*, 1242-1246.

[15] Bley, R.A.; Kauzlarich, S.M.; Lee, H.W.H.; Davis, J.E. Characterization of silicon nanoparticles prepared from porous silicon. *Mat. Res. Soc. Sym. Proc*., **1994**, *351*, 275-280.

[16] Hayashi, S.; Tanimoto, K.; Yamamoto, K.J. Analysis of surface oxides of gas-evaporated Si small particles with infrared spectroscopy, high-resolution electron microscopy, and x-ray photoemission spectroscopy. *Appl. Phys*., **1990**, *68*, 5300-5308.

[17] Okada, R.; Iijima, S. Oxidation property of silicon small particles. *Appl. Phys. Lett*., **1991**, *58*, 1662-1663.

[18] Heath, J.R. A liquid-solution-phase synthesis of crystalline silicon. *Science*, **1992**, *258*, 1131-1133.

[19] Keisuke, S.; Hiroaki, T.; Kenji, H.; Naoki, F.; Yusuke, Y. Controlled chemical etching for silicon nanocrystals with wavelength-tunable photoluminescence. *Chem. Commun*., **2009**, *25*, 3759-3761.

[20] Douglas, S.E.; Lindsay, E.P.; Zhonghua, Y.; Paul, F.B.; Brian, A.K. Size tunable visible luminescence from individual organic monolayer stabilized silicon nanocrystal quantum dots. *Nano Lett.*, **2002**, *2*, 681-685.

[21] Kumar, S.D.; Rauthan, P.N.; Parashar, C.M.S. Effect of power on the growth of nanocrystalline silicon films. *J. Phys.: Condens. Matter*, **2008**, *20*, 335215-335222.

[22] Holmes, J.D.; Ziegler, K.J.; Doty, R.C.; Pell, L.E.; Johnston, K.P.; Korgel, B.A. Highly luminescent silicon nanocrystals with discrete optical transitions. *J. Am. Chem. Soc*., **2001**, *123*, 3743-3744.

[23] Liu, S.; Sato, S.; Kimura, K. Synthesis of luminescent silicon nanopowders redispersible to various solvents. *Langmuir*, **2005**, *21*, 6324-6329.

[24] Liu, S.; Yang, Y.; Sato, S.; Kimura, K. Enhanced photoluminescence from Si nano-organosols by functionalization with alkenes and their size evolution. *Chem. Mater*., **2006**, *18*, 637-642.

[25] Shah, P.S.; Hanrath, T.; Johnston, K.P.; Korgel, B.A. Nanocrystal and nanowire synthesis and dispersibility in supercritical fluids. *J. Phys. Chem. B*, **2004**, *108*, 9574-9587.

[26] Ding, Z.F.; Quinn, B.M.; Haram, S.K.; Pell, L.E.; Korgel, B.A.; Bard, A.J. Electrochemistry and electrogenerated chemiluminescence from silicon nanocrystal quantum dots. *Science*, **2002**, *296*, 1293-1297.

[27] Holmes, J.D.; Ziegler, K.J.; Doty, R.C.; Pell, L.E.; Johnston, K.P.; Korgel, B.A. Highly luminescent silicon nanocrystals with discrete optical transitions. *J. Am. Chem. Soc*., **2001**, *123*, 3743-3744.

[28] Lee, D.C.; Hanrath, T.; Korgel, B.A. Role of precursor decomposition kinetics in silicon nanowire synthesis in organic solvents. *Angew. Chem. Int. Ed*., **2005**, *44*, 3573-3577.

[29] Holmes, J.D.; Johnston, K.P.; Doty, R.C.; Korgel, B.A. Control of thickness and orientation of solution-grown silicon nanowires. *Science*, **2000**, *287*, 1471-1473.

[30] Mayeri, D.; Phillips, B.L.; Augustine, M.P.; Kauzlarich, S.M. NMR Study of the synthesis of alkyl-terminated silicon nanoparticles from the reaction of $SiCl_4$ with the Zintl salt, NaSi. *Chem. Mater*., **2001**, *13*, 765-770.

[31] Veinot, J.G.C. Synthesis, surface functionalization, and properties of freestanding silicon nanocrystals. *Chem. Commun*., **2006**, 4160-4168.

[32] Zhang, X.; Brynda, M.; Britt, R.D.; Carroll, E.C.; Larsen, D.S.; Louie, A.Y.; Kauzarich, S.M. Synthesis and characterization of manganese-doped silicon nanoparticles: bifunctional paramagnetic-optical nanomaterial. *J. Am. Chem. Soc*., **2007**, *129*, 10668-10669.

[33] Baldwin, R.K.; Zou, J.; Pettigrew, K.A.; Yeagle, G.J.; Britt, R.D.; Kauzlarich, S.M. The preparation of a phosphorus doped silicon film from phosphorus containing silicon nanoparticles. *Chem. Commun*., **2006**, *6*, 658-660.

[34] Yang, C.S.; Kauzlarich, S.M.; Wang, Y.C. Synthesis and characterization of germanium/Si−alkyl and germanium/silica core−shell quantum dots. *Chem. Mater*., **1999**, *11*, 3666-3670.

[35] Pettigrew, K.A.; Liu, Q.; Power, P.P.; Kauzlarich, S.M. Solution synthesis of alkyl- and alkyl/alkoxy-capped silicon nanoparticles *via* oxidation of Mg_2Si. *Chem. Mater*., **2003**, *15*, 4005-4011.

[36] Baldwin, R.K.; Pettigrew, K.A.; Ratai, E.; Augustine, M.P.; Kauzlarich, S.M. Solution reduction synthesis of surface stabilized silicon nanoparticles. *Chem. Commun*., **2002**, *17*, 1822-1823.

[37] Zou, J.; Baldwin, R.K.; Pettigrew, K.A.; Kauzlarich, S.M. Solution synthesis of ultrastable luminescent siloxane-coated silicon nanoparticles. *Nano Lett*., **2004**, *4*, 1181-1186.

[38] Liu, Q.; Kauzlarich, S.M. A new synthetic route for the synthesis of hydrogen terminated silicon nanoparticles. *Mater. Sci. Eng. B*, **2002**, *96*, 72-75.

[39] Baldwin, R.K.; Pettigrew, K.A.; Garno, J.C.; Power, P.P.; Liu, G.Y.; Kauzlarich, S.M. Room temperature solution synthesis of alkyl-capped tetrahedral shaped silicon nanocrystals. *J. Am. Chem. Soc*., **2002**, *124*, 1150-1151.

[40] Li, X.G.; He, Y.Q.; Talukdar, S.S.; Swihart, M.T. Process for preparing macroscopic quantities of brightly photoluminescent silicon nanoparticles with emission spanning the visible spectrum. *Langmuir*, **2003**, *19*, 8490-8496.

[41] Rogozhina, E.V.; Eckhoff, D.A.; Gratton, E.; Braun, P.V. Carboxyl functionalization of ultrasmall luminescent silicon nanoparticles through thermal hydrosilylation. *J. Mat. Chem*., **2006**, *16*, 1421-1430.

[42] Nayfeh, M.H.; Rogozhina, E.V.; Mitas, L. In: *Synthesis, Functionalization and Surface Treatment of Nanoparticles*, M.-I. Baraton.; Ed.; American Scientific Publishers; USA, **2003**, pp.173-231.

[43] Nielsen, D.; Abuhassan, L.H.; Alchihabi, M.; Al-Muhanna, A.; Host, J.; Nayfeh, M.H. Current-less anodization of intrinsic silicon powder grains: formation of fluorescent Si nanoparticles. *J. Appl. Phys*., **2007**, *101*, 114302-114305.

[44] Zhang, X.; Neiner, D.; Wang, S.; Louie, A.Y.; Kauzlarich, S.M. A new solution route to hydrogen-terminated silicon nanoparticles: synthesis, functionalization and water stability. *Nanotechnology*, **2007**, *18*, 095601-095607.

[45] Wilcoxon, J.P.; Samara, G.A.; Provencio, P.N. Optical and electronic properties of Si nanoclusters synthesized in inverse micelles. *Phys. Rev. B*, **1999**, *60*, 2704-2714.

[46] Wilcoxon, J.P.; Samara, G.A. Tailorable, visible light emission from silicon nanocrystals. *Appl. Phys. Lett*., **1999**, *74*, 3164-3166.

[47] Warner, J.H.; Hoshino, A.; Yamamoto, K.; Tilley, R.D. Water-soluble photoluminescent silicon quantum dots. *Angew. Chem. Int. Ed*., **2005**, *44*, 4550-4554.

[48] Heintz, A.S.; Fink, M.J.; Mitchell, B.S. Mechanochemical synthesis of alkyl/alkenyl-passivated silicon nanoparticles. *Adv. Mater*., **2007**, *19*, 3984-3988.

[49] Sweryda-Krawiec, B.; Cassagneau, T.; Fendler, J.H. Surface modification of silicon nanocrystallites by alcohols. *J. Phys.Chem. B*, **1999**, *103*, 9524-9529.

[50] Buriak, J.M. Silicon carbon bonds on porous silicon surfaces: one step closer to device applications. *Adv. Mat*., **1999**, *11*, 265-267.

[51] Stewart, M.P.; Buriak, J.M. New approaches towards the formation of silicon-carbon bonds on porous silicon. *Comm. Inorg. Chem*., **2002**, *23*, 179-203.

[52] Hua, F.J.; Swihart, M.T.; Ruckenstein, E. Efficient surface grafting of luminescent silicon quantum dots by photoinitiated hydrosilylation. *Langmuir*, **2005**, *21*, 6054-6062.

[53] Nelles, J.; Sendor, D.; Ebbers, A.; Petrat, F.M.; Wiggers, H.; Schulz, C.; Simon, U. Functionalization of silicon nanoparticles *via* hydrosilylation with 1-alkenes. *Colloid Polym. Sci.*, **2007**, *285*, 729-736.

[54] Rogozhina, E.; Belomoin, G.; Smith, A.; Abuhassan, L.; Barry, N.; Akcakir, O.; Braun, P.V.; Nayfeh, M.H. Si–N linkage in ultrabright, ultrasmall Si nanoparticles. *Appl. Phys. Lett*., **2001**, *78*, 3711-3713.

[55] Eckhoff, D.A.; Jeffrey, N.S.; Sutin, J.D.B.; Sweedler, J.V.; Gratton, E. Capillary electrophoresis of ultrasmall carboxylate functionalized silicon nanoparticles. *J. Chem. Phys*., **2006**, *125*, 081103-081107.

[56] Shiohara, A.; Hanada, S.; Prabakar, S.; Fujioka, K.; Lim, T.H.; Yamamoto, K.; Northcote, P.T.; Tilley, R.D. Chemical reactions on surface molecules attached to silicon quantum dots. *J. Am. Chem. Soc.*, **2010**, *132*, 248-249.

[57] Surugau, N.; Urban. P.L. Electrophoretic methods for separation of nanoparticles. *J. Sep. Sci*., **2009**, *32*, 1889-1906.

[58] Pyell, U. Characterization of nanoparticles by capillary electromigration separation techniques. *Electrophoresis*, **2010**, *31*, 814-831.

[59] Klimov, V.I. *Semiconductor and Metal Nanocrystals: Synthesis and Electronic and Optical Properties*, Marcel Dekker Inc., New York: **2004**.

[60] Nirmal, M.; Brus, L. Luminescence photophysics in semi-conductor nanocrystals. *Acc. Chem. Res*., **1999**, *32*, 407-414.

[61] Krishna, M.V.R.; Friesner, R.A. Quantum confinement effects in semiconductor clusters. *J. Chem. Phys*., **1991**, *95*, 8309-8315.

[62] Gao, F. A chemical bond theory of quantum size effects of semiconductor clusters. *Inorg. Chem.*, **2010**, *49*, 10409-10414.

[63] Minati, L.; Speranza, G.; Bernagozzi, I.; Torrengo, S.; Toniutti, L.; Rossi, B.; Ferrari, M.; Chiasera, A. Investigation on the electronic and optical properties of short oxidized multiwalled carbon nanotubes. *J. Phys. Chem. C*, **2010**, *114*, 11068-11073.

[64] Majetich, S.A.; Carter, A.C. Surface effects on the optical properties of cadmium selenide quantum dots. *J. Phys. Chem*., **1993**, *97*, 8727-8731.

[65] Puzder, A.; Williamson, A.J.; Grossman, J.C.; Galli, G. Computational studies of the optical emission of silicon nanocrystals. *J. Am. Chem. Soc*., **2003**, *125*, 2786-2787.

[66] Wolkin, M.V.; Jorne, J.; Fauchet, P.M.; Allan, G.; Delerue, C. Electronic states and luminescence in porous silicon quantum dots: the role of oxygen. *Phys. Rev. Lett.*, **1999**, *82*, 197-200.

[67] Gole, J.L.; Prokes, S.M. Resonantly excited photoluminescence from porous silicon and the question of bulk phonon replicates. *Phys. Rev. B*, **1998**, *58*, 4761-4762.

[68] Littau, K.A.; Szajowski, P.J.; Muller, A.J.; Kortan, A.P.; Brus, L.E. A luminescent silicon nanocrystal colloid *via* a high-temperature aerosol reaction. *J. Phys. Chem*., **1993**, *97*, 1224-1230.

[69] Yang, C.S.; Bley, R.A.; Kauzlarich, S.M.; Lee, H.W.H.; Delgado, G.R. Synthesis of alkyl-terminated silicon nanoclusters by a solution route. *J. Am. Chem. Soc*., **1999**, *121*, 5191-5192.

[70] Yang, C.S.; Kauzlarich, S.M.; Wang, Y.C.; Lee, H.W.H. Photoluminescence as a function of aggregated size from n-butyl-terminated silicon nanoclusters. *J. Clust. Sci*., **2000**, *11*, 423-431.

[71] Takagahara, T.; Takeda, K. Theory of the quantum confinement effect on excitons in quantum dots of indirect-gap materials. *Phys. Rev. B*, **1995**, *46*, 15578-15581.

[72] Warner, J.H.; Thomsen, E.; Watt, A.R.; Heckenberg, N.R.; Rubinsztein-Dunlop, H. Time-resolved photoluminescence spectroscopy of ligand-capped PbS nanocrystals. *Nanotechnology*, **2005**, *16*, 175-179.

[73] Zhou, Z.; Brus, L.; Friesner, R. Electronic structure and luminescence of 1.1-and 1.4-nm silicon nanocrystals: oxide shell *versus* hydrogen passivation. *Nano Lett*., **2003**, *3*, 163-167.

[74] Warner, J.H.; Rubinsztein-Dunlop, H.; Tilley, R.D. Surface morphology dependent photoluminescence from colloidal silicon nanocrystals. *J. Phys. Chem. B*, **2005**, *109*, 9064-9067.

[75] Mayne, A.H.; Bayliss, S.C.; Barr, P.; Tobin, M.; Buckberry, L.D. Biologically interfaced porous silicon devices. *Phys. Stat. Sol*., **2000**, *182*, 505-513.

[76] Wang, G.; Mantey, K.; Nayfeh, M.H., Yau, S-T. Enhanced amperometric detection of glucose using Si_{29} particles. *Appl. Phys. Lett.*, **2006**, *89*, 43901-43902.

[77] Wang, G.; Yau, S.-T. Enzyme-immobilized SiO_2–Si electrode: Fast interfacial electron transfer with preserved enzymatic activity. *Appl. Phys. Lett*., **2005**, *87*, 253901-25904.

[78] Piechotta, G.; Albers, J.; Hintsche, R. Novel micromachined silicon sensor for continuous glucose monitoring. *Biosens. Bioelect*., **2005**, *21*, 802-808.

[79] Wang, X.; Chen, Y.; Gibney, K.A.; Erramilli, S.; Mohanty, P. Silicon-based nanochannel glucose sensor. *Appl. Phys. Lett*., **2008**, *92*, 013902-013905.

[80] Gu, L.; Park, J-H; Duong, K.H.; Ruoslahti, E.; Sailor, M.J. Magnetic luminescent porous silicon microparticles for localized delivery of molecular drug payloads. *Small*, **2010**, *6*, 2546-2552.

[81] Timoshenko, V.Y.; Kudryavtsev, A.A.; Osminkina, L.A.; Vorontsov, A.S.; Ryabchikov, Y.V.; Belogorokhov, I.A.; Kovalev, D.; Kashkarov, P.K. Silicon nanocrystals as photosensitizers of active oxygen for biomedical applications. *JETP Lett*., **2006**, *83*, 423-426.

[82] Steller, H. Mechanisms and genes of cellular suicide. *Science*, **1995**, *267*, 1445-1449.

[83] Fujii, M.; Kovalev, D.; Goller, B.; Minobe, S.; Hayashi, S.; Timoshenko, V.Y. Time-resolved photoluminescence studies of the energy transfer from excitons confined in Si nanocrystals to oxygen molecules. *Phys. Rev. B*, **2005**, *72*, 165321-165329.

[84] Scriba, M.R.; Britton, D.T.; Härting, M. Electrically active, doped monocrystalline silicon nanoparticles produced by hot wire thermal catalytic pyrolysis. *Thin Solid Films*, **2010**, *14*, 4491-4494.

[85] Li, Z.F.; Ruckenstein, E. Water-soluble poly(acrylic acid) grafted luminescent silicon nanoparticles and their use as fluorescent biological staining labels. *Nano Lett*., **2004**, *4*, 1463-1467.

[86] Akcakir, O.; Therrien, J.; Belomoin, G.; Barry, N.; Muller, J.D.; Gratton, E.; Nayfeh, M. Detection of luminescent single ultrasmall silicon nanoparticles using fluctuation correlation spectroscopy. *Appl. Phys. Lett*., **2000**, *76*, 1857-1859.

[87] Hardman, R. A Toxicologic review of quantum dots: toxicity depends on physicochemical and environmental factors. *Environ. Health Persp*., **2006**, *114*, 165-172.

[88] Lewinski, N.; Colvin, V.; Drezek, R. Cytotoxicity of nanoparticles. *Small*, **2008**, *4*, 26-49.

[89] Choi, J.; Zhang, Q.; Reipa, V.; Wang, N.S.; Stratmeyer, M.E.; Hitchins, V.M.; Goering, P.L. Comparison of cytotoxic and inflammatory responses of photoluminescent silicon nanoparticles with silicon micron-sized particles in RAW 264.7 macrophages. *J. Appl. Toxicol*., **2009**, *29*, 52-60.

[90] Fujioka, K.; Hiruoka, M.; Sato, K.; Manabe, N.; Miyasaka, R.; Hanada, S.; Hoshino, A.; Tilley, R.D; Manome, Y.; Hirakuri, K.; Yamamoto, K. Luminescent passive-oxidized silicon quantum dots as biological staining labels and their cytotoxicity effects at high concentration. *Nanotechnology*, **2008**, *19*, 415102-415108.

[91] Mitchell, L.A.; Gao, J.; Vander, W.R.; Gigliotti, A.; Burchiel, S.W.; McDonald, J.D. Pulmonary and systemic immune response to inhaled multiwalled carbon nanotubes. *Toxicol. Sci*., **2007**, *100*, 203-214.

[92] Lucarelli, M.; Gatti, A.M.; Savarino, G.; Quattroni, P.; Martinelli, L.; Monari, E.; Boraschi, D. Innate defense functions of macrophages can be biased by nano-sized ceramic and metallic particles. *Eur. Cytokine Netw.*, **2004**, *15*, 339-346.

Received: June 13, 2011 Revised: July 22, 2011 Accepted: August 03, 2011

Chapter 3 – Hg(II) Sensing Based on Carbon Dots Obtained by Direct Laser Ablation

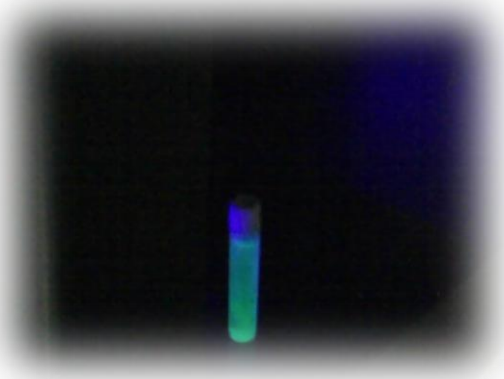

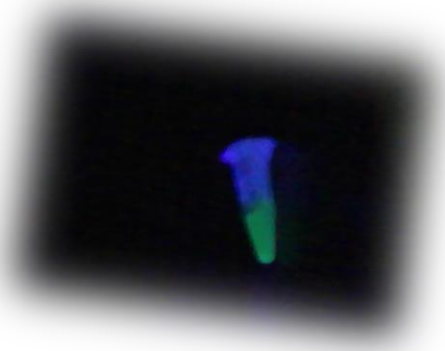

Chapter 3 – Hg(II) Sensing Based on Carbon Dots Obtained by Direct Laser Ablation

3.1. State of the Art

Mercury occurs naturally, predominantly in the form of cinnabar ore – HgS. It is present in minerals, rocks and fossil fuels in low concentrations and, as such, it causes no problem to human health. However one of the main ways that the industrialized world has to create energy is through the combustion of fossil fuels [1].

Ever since its discovery and insight on its properties the use of mercury grew. Over the years its toxicological effects on human and animal life were known and there has been an attempt to replace this element for something less harmful. Indeed mercury can be applied in numerous activities, some of the most known are: thermometers, light bulbs and gold mining. The use of mercury in thermometers is limited and in most countries it has been discontinued. A big campaign on recycling mercury containing bulbs is going worldwide, however the most problematic seems to be the gold extraction. Gold is a highly valuable metal and its price is increasing continually over the past years. One of the methods for extracting gold from its natural sources is by adding mercury. This element forms amalgam with gold that when exposed to high temperatures leads to the evaporation of mercury and the separation of gold from the debris of the mining procedure. This process is illegal in countries like Indonesia and United States [2], however in the Brazilian Amazon it is limited but allowed and it is estimated that the number of miners now surpasses the 200 thousand people [3]. Indeed this is an alarming number that can account for the growing contamination of the air and water in areas, such as, the Brazilian Amazon. The limit accepted for mercury in fishes for human consumption is 0.4ppm, however studies like the one published by Lembo, (1999) [4] reports values two hundred times higher than the legal value. This is quite troubling since it presents a huge health risk, not only for the local citizens but also to the entire world.

The most common anthropogenic causes for mercury release into the atmosphere are gold mining, power plants, combustion of municipal and medical waste and smelting plants. Nevertheless it is important to say that industries are not responsible for creating mercury, in fact their contribute to the increase of this element

pollution is mainly through combustion. Upon their release they enter the somewhat known and commonly accepted mercury cycle. A simple representation of this complex mercury cycle can be seen in Fig.3.1.

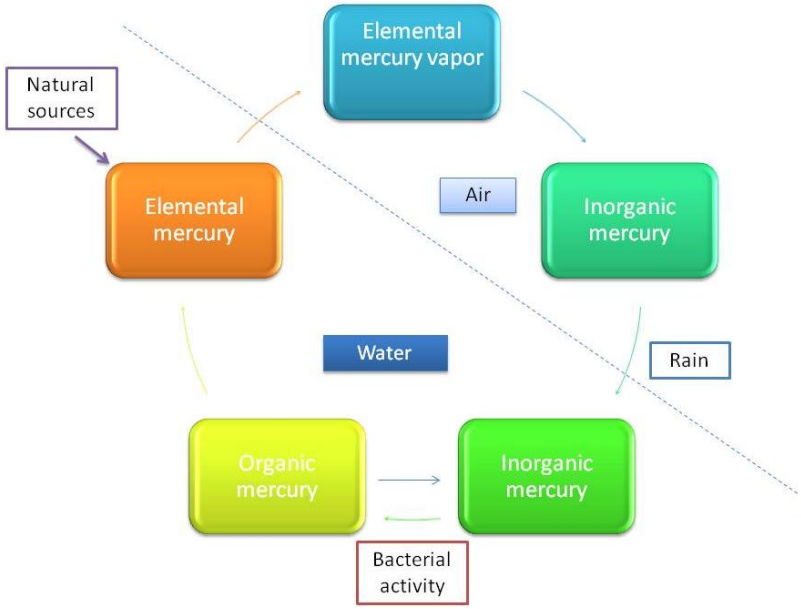

Fig.3.1. – Representation of the mercury cycle upon its release into the atmosphere

Upon the mercury released into the atmosphere, regardless of the process that lead there, it is scattered over large distances due to air currents. Eventually these particles fall, most often in rain drops, and are deposited in soils, oceans, lakes and rivers. Despite the place where the mercury fall it is only very problematic when it suffers chemical changes, because until then it just forms different layers that do not present a problem to human health. Problems seem to arise when mercury is deposited in water, where due to microbial activity it can be converted into methyl mercury. This is quite problematic since the conversion to methyl mercury is the way that mercury enters the food chain. Methyl mercury is a fat-soluble molecule and, as such, it is prone to bioaccumulation. The path until mercury reaches humans is quite simple. Mercury enters the food chain initially through plankton, making its way through little and big fishes, until it reaches larger organisms, such as, humans. This way it is possible to say that methyl mercury never leaves the body, it is accumulated in fatty tissue upon the ingestion of contaminated food [3].

Indeed, mercury has quite adverse effects on human and animal life, which has lead some countries like the United States to issue regulatory limits for fish consumption. In fact, even though the United States did not report any cases of mass

poisoning due to the ingestion of contaminated fish, in 1999 forty one states had issued advisories limits [5]. In this sense the states of Pennsylvania and New Jersey, in an attempt to decrease the industrial contaminations, implemented a strict Maximum Achievable Control Technologies (MACT), that requires mercury-emitting plants to meet the highest level of emissions control that is presently available in the market. This measure has lead to a considerable decrease in mercury emission from power plants in both states, however the energy demand has increased and states like Illinois and Detroit (Michigan) have increased significantly the mercury emission. In fact, in this last state, it was determined that the mercury level in rain is sixty five times higher that the safety limit for humans. This increase in pollution is carried to the Pennsylvania and New Jersey states by the prevailing winds, therefore making their attempt to limit the mercury release unsuccessful.

Recent studies have estimated the annual global mercury in the atmosphere to be 5000 tons and the mercury in water as high as 10800 tons. According to the pre-industrial data, the global mercury in atmosphere was 1600 tons and in water 3600 tons. This leads to the conclusion that ever since the begging of industrialization, the level of mercury is about three times higher in both media [6].

Despite the fact that human activities represent the largest share of mercury pollution this is not the only way. Indeed mercury can be released from its naturally occurring sources, by phenomena, such as, erosion and volcanoes. However the increase of mercury concentrations is mainly assigned to the industrialized world. In fact, some researchers of the Canadian Government have proven that total annual mercury emissions have increased two to five times over the last century. Moreover in remote areas where the industry world has not yet arrived, such as, Alaskan Arctic, the difference between mercury concentration in the pre-industrial and present day layers in core samples of lake sediment, is almost irrelevant [7].

The human risk of mercury exposure has been extensively studied over the years, particularly since one of the biggest mercury disasters known to Men: the Minamata Bay-Japan. This disaster was caused by an acetaldehyde factory that between the years of 1932 to 1968 dumped approximately twenty seven tons of mercury compounds into the Minamata Bay. The Bay was the main source of food for thousands of fisherman’s and farmers that lived in its vicinity. It was only in 1956 that the first human case of methyl mercury poisoning was described and ever since then the number grew. Methyl mercury mostly affects the nervous system, so symptoms like numbness of limbs and lips, slurred speech, constricted vision and involuntary movements, began to occur. The effect of mercury poisoning appeared not only on

humans but also on wild life. Indeed birds were actually falling from the sky and cats were “committing suicide”. In 1997 a complete study was performed and it was estimated that at least 10 353 people were directly or indirectly affected by mercury poisoning [8]. This disaster was so severe that the methyl mercury poisoning was known as “Minamata disease”.

The effects that elemental mercury, mercuric chloride and methyl mercury have on biological systems has been studied, as it is possible to see from the analysis of Fig.3.2.

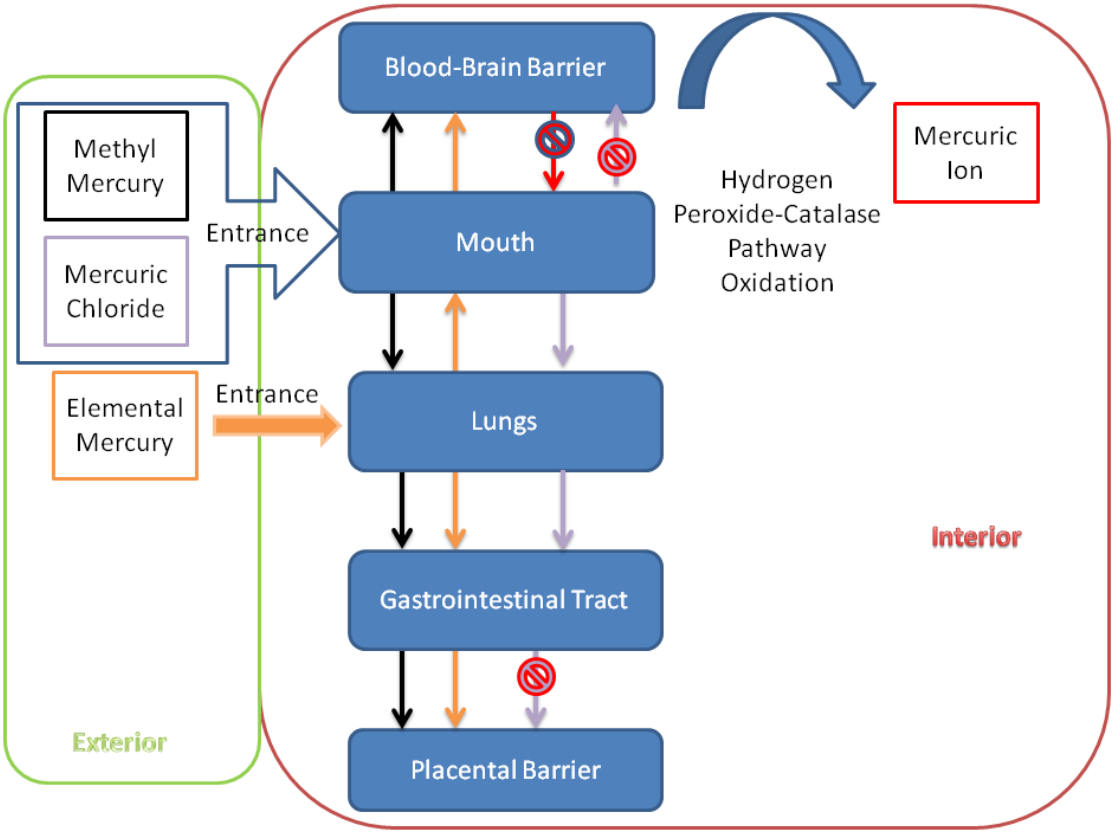

Fig.3.2. – Biological pathways of elemental mercury, mercuric chloride and methyl mercury.

Elemental mercury in the vapour form is rapidly absorbed by the lungs and readily distributed throughout the body. It can pass membrane barriers like the placenta and blood-brain, thereby affecting unborn children. Once inside the tissues the elemental mercury is oxidized by hydrogen peroxide-catalase pathway to mercuric ion, which is good since this specie cannot pass through barriers thereby limiting its distribution. However the same is true once elemental mercury pass the barriers and become oxidize afterwards. This can lead to the retention of mercury in brain tissue.

On the other hand mercuric chloride is mainly absorbed in the gastrointestinal tract, due to an electrostatic interaction with the brush border membrane and limited passive diffusion. Furthermore, this absorption can be increased by the intestinal pH that is dependent on the person diet and cause corrosion. However on the contrary to elemental mercury, mercuric chloride has a limited capacity to pass through placental or blood-brain barriers. There has been some cases describing the oral ingestion of mercury chloride, however since it is poorly absorbed, the majority is excreted through the faeces.

The other predominant form of mercury poisoning is methyl mercury. This specie is readily absorbed in the gastrointestinal tract and, in a similar manner of the elemental mercury, it can pass through barriers. The transport of this molecule in the human body seems to be mediated by cysteine residues, in fact it was described the formation of methyl mercury-cysteine complexes in both humans and animals. This mercury specie is quite stable in biological media and it has a relatively long half-life. Three human studies were performed in order to attempt to establish a relationship between this methyl mercury and cancer, however the results are limited by the small population in the study. There has also some limited evidence of carcinogenicity in animal studies. For example, male ICR and B6C3F1 mice were orally exposed to methyl mercury and the results showed that these mice had an increase of renal adenomas, adenocarcinomas and carcinomas. When the concentration of methyl mercury was increased into extreme values, renal epithelial cell hyperplasia and tumours appeared. Additionally some studies in mammalian germ cells have lead to the conclusion that the presence of methyl mercury can be responsible for chromosomal aberrations, as such, it seems that this mercury specie can be clastogenic, but it is not a potent mutagen. The main effect of methyl mercury is on the nervous system and since it passes through the placental barrier, and even though the mother has no poisoning symptoms, developing fetus may exhibit delayed onset of walking and talking, cerebral palsy, altered muscle tone and deep tendon reflexes, and reduced neurological test scores.

The importance of mercury in biological media has lead to the development of new and specific sensing systems. One example are the two acridine derivatives described by Lee H.N. *et al.* (2008) [9]. These sensors were successfully tested in mammalian cells and the major interferent was cadmium. Despite these good results there are two main disadvantages of this system for *in vivo* sensing: the disadvantages inherent to organic dyes, namely blinking, photobleaching, among others, and the excitation/emission wavelength, that is approximately 356 and 450nm, respectively.

Another example for Hg(II) sensing is the system developed by Guo L. *et al.* (2009) [10] based on a oligodeoxyribonucleotide-fluorescein. This sensing system has a detection limit of 20nM and is quite selective. However fluorescein is a known organic dye with its inherent drawbacks. Nevertheless upon the addition of Hg(II) the fluorescence of the system was quenched and a red shift was observed with and excitation/emission wavelength of 496 to 501 and 519 to 527, respectively. These excitation and emission values seem more promising for *in vivo* applications than the system described by Lee H.N. *et al.* (2008) [9].

Indeed the development of sensing systems for *in vivo* Hg(II) tracking and evaluation of its bioaccumulation in different tissues is an actual theme. As such, this worked focused on the development of a new nanosensing system for Hg(II) for a possible *in vivo* application. Herein it will be described the synthesis of a new Carbon Dots (Cdots) based system. In order to make these nanoparticles sensitive to Hg(II) it was necessary to adapt its surface, as such, the following molecules were chosen: poliethileneglycol 200 (PEG_{200}) and N-acetyl-L-cysteine (NAC). The use of NAC as a functionalization agent is due to its biological action. NAC is a metabolite of the sulphur-containing amino acid, cysteine and is produced within the human body. Its function, among others, is the detoxification and removal of metals, such as, lead, mercury and arsenic from the body [12]. Therefore it is expected that the functionalized Cdots should have some heavy metal sensitivity.

3.2. References

[1] EPA. **1997**. Mercury Study Report to Congress: Health Effects of Mercury and Mercury Compounds, Vol. 5.

[2] Report available online: http://www.msnbc.msn.com/id/28596948/ns/world_news-world_environment/t/mercury-gold-mining-poses-toxic-threat/, consulted in August of 2012.

[3] Report available online: http://www.google.pt/url?sa=t&rct=j&q=&esrc=s&frm=1&source=web&cd=3&ved=0CCwQFjAC&url=http%3A%2F%2Fwww.colegioacademia.com.br%2Fadmin%2Fprofessores%2Farquivos_upl%2F28_recursos-minerais-e-meio-ambiente.pdf&ei=DJtLULDaO8TF0QXT0YCoBg&usg=AFQjCNGKtSErLwdrtxaZ0B14DmcBDRJsUg&sig2=4lE2f9CrO3HN19JqX59TQQ, consulted in August of 2012.

[4] Lembo, A. **1999**. Química, realidade e contexto. São Paulo, Ática.

[5] EPA. 2012. Available online: http://www.epa.gov/hg/advisories.htm, consulted in August 2012.

[6] Barbalace R.C. **2005**. Mercury Pollution: increase attributed to industrial activities. Available online: http://environmentalchemistry.com/yogi/environmental/mercurypollution2005.html, consulted in August 2012.

[7] Braune B.M., Outridge P.M., Fisk A.T., Muir D.C.G., Helm P.A., Hobbs K., Hoekstra P.F., Kuzyk Z.A., Kwan M., Letcher R.J., Lockhart W.L., Norstrom R.J., Stern G.A., Stirling I. **2005**. "Persistent organic pollutants and mercury in marine biota of the Canadian Arctic: An overview of spatial and temporal trends". Science Total Environment 351, pp. 4– 56.

[8] Report available online: http://www1.american.edu/ted/MINAMATA.HTM, consulted in August 2012.

[9] Lee H.N., Kim H.N., Swamy K.M.K., Park M.S., Kim J., Lee H., Lee K-H., Park S., Yoon J. **2008**. "New acridine derivatives bearing immobilized azacrown or azathiacrown ligand as fluorescent chemosensors for Hg^{2+} and Cd^{2+}. Tetrahedron Letters 49, pp.1261–1265.

[10] Guo L., Hu H., Sun R., Chen G. **2009**. "Highly sensitive fluorescent sensor for mercury ion based on photoinduced charge transfer between fluorophore and stacked T–Hg(II)–T base pairs. Talanta 79, pp. 775-779.

[11] Faure' AC, Dufort S, Josserand V, Perriat P, Coll JL, Roux S, Tillement O. **2009**. "Control of the in vivo Biodistribution of Hybrid Nanoparticles with Different Poly(ethylene glycol) Coatings". Small 22, pp.2565-2575.

[12] Raspanti E., Cacciola S.O., Gotor C., Romero L.C., García I. **2009**. "Implications of cysteine metabolism in the heavy metal response in Trichoderma harzianum and in three Fusarium species". Chemosphere 76, pp. 48-54.

3.3. Personal Contribution to this Paper

My personal contribution to this work includes the following: establishment of an initial objective and all the necessary research to ascertain the molecule that presented be best option for Hg(II) sensing. It was then required the suiting of this knowledge to the material and equipment available. Once this was determined all the procedures for the synthesis, functionalization and purification of all the nanoparticles were performed. Subsequently, it was studied the structural and chemical properties of the produced nanoparticles and with this knowledge some tests were performed, namely: pH, metal ion sensitivity, among others. The results were interpreted and compared to the existing data provided by other research groups. Once all the data were collected it was necessary to repeat all the functionalization, purification and sensitivity towards different parameters in order to ascertain if the results were reproducible. When all these procedures were repeated and the data were considered reproducible it was necessary to write a manuscript with all the necessary data for publication in an international scientific research journal and perform the required adjustments to comply with the reviewers suggestions.

Sensors and Actuators B 145 (2010) 702–707

Contents lists available at ScienceDirect

Sensors and Actuators B: Chemical

journal homepage: www.elsevier.com/locate/snb

Hg(II) sensing based on functionalized carbon dots obtained by direct laser ablation

Helena Gonçalves[a], Pedro A.S. Jorge[b], J.R.A. Fernandes[b,c], Joaquim C.G. Esteves da Silva[a,*]

[a] Centro de Investigação em Química, Departamento de Química, Faculdade de Ciências da Universidade do Porto, R. Campo Alegre 687, 4169-007 Porto, Portugal
[b] Optoelectronics Unit, INESC Porto, R. Campo Alegre 687, 4169-007 Porto, Portugal
[c] Universidade de Trás-os-Montes e Alto Douro, Apartado 1013, 5001-801 Vila Real, Portugal

ARTICLE INFO

Article history:
Received 9 December 2009
Received in revised form 13 January 2010
Accepted 15 January 2010
Available online 25 January 2010

Keywords:
Carbon nanoparticles
Carbon dots
Laser ablation
Functionalization
N-acetyl-L-cysteine
Mercury(II) sensing

ABSTRACT

The synthesis of carbon nanoparticles obtained by direct laser ablation [UV pulsed laser irradiation (248 nm, KrF)] of carbon targets immersed in water is described. Laser ablation features were optimized to produce carbon nanoparticles with dimensions up to about 100 nm. After functionalization with NH_2–polyethylene-glycol (PEG_{200}) and N-acetyl-L-cysteine (NAC) the carbon nanoparticles become fluorescent with excitation and emission wavelengths at 340 and 450 nm, respectively. The fluorescence decay time was complex and a three-component decay time model originated a good fit ($\chi = 1.09$) with the following lifetimes: $\tau_1 = 0.35$ ns; $\tau_2 = 1.8$ ns; and $\tau_3 = 4.39$ ns. The fluorescence of the carbon dots is sensitive to pH with an apparent $pK_a = 4.2$. The carbon dots were characterized by ^{1}H NMR and HSQC and the results show an interaction between PEG_{200} and the carbon surface as well as a dependence of the chemical shift with the reaction time. The fluorescence intensity of the nanoparticles is quenched by the presence of Hg(II) and Cu(II) ions with a Stern–Volmer constant (pH = 6.8) of 1.3×10^5 and 5.6×10^4 M^{-1}, respectively. As such the synthesis and application of a novel biocompatible nanosensor for measuring Hg(II) is presented.

1. Introduction

Quantum dots (QDs) are nanoparticles (typically between 1 and 12 nm in diameter) of semi-conducting material. Due to the quantum confinement effects, these materials possess unique light emitting properties, like a broad excitation spectra and a sharp emission wavelength that can be tuned by controlling the reaction time. In the last decade they have revealed to be a powerful tool for labeling biological systems since their nanoscale size range is compatible to most of the metabolic and internalization processes observed in cells [1–3] and, unlike other nanoparticle-based optical imaging probes, QDs do not exceed the protein's size [4], which makes them highly interesting for biological applications. Carbon dots, show some common properties to QDs, but are carbon nanoparticles that through functionalization acquire strong photoluminescence in both solution and solid state. In general, the photoluminescence has been attributed to the presence of surface energy traps, likely related to the abundant surface defect sites that become emissive upon functionalization. In addition, the surface emissive sites of the carbon dots are likely quantum confined in the sense that a large surface-to-volume ratio is required for the strong photoluminescence [5–8]. With emission properties similar to those described for the traditional cadmium based QDs, these carbon dots represent a possibility of performing *in vivo* measurements in a non-invasive and non-toxic manner. Moreover, carbon dots are able to emit visible light after two-photon excitation using near infrared light which makes them particularly interesting material for the development of *in vivo* imaging applications [9,10]. Since they can be functionalized with several molecules in a number of layers accordingly with the desirable application [11], these nanoparticles show great potential for *in vivo* fluorescence sensing applications.

Herein we report a straightforward synthesis of carbon dots by laser ablation (UV pulsed laser irradiation) of carbon targets immersed in water and their functionalization with NH_2–polyethylene-glycol (PEG_{200}) and N-acetyl-L-cysteine (NAC). It was recently shown that using QDs capped with PEG_{200} in cultured keratinocytes significantly inhibited cytotoxicity and immune responses when compared with QDs without this capping [12]. These results suggest that PEG coating is an effective approach for the safe use of QDs for *in vivo* applications [13,14]. On the other hand NAC is a metabolite of the sulfur-containing amino acid, cysteine and is produced within the human body. Metals like lead, mercury and arsenic are detoxified and removed from the body by NAC [15]; therefore we tested the sensitivity of the synthesized carbon dots towards metal ions.

* Corresponding author. Tel.: +351 220 402 569; fax: +351 220 402 659.
E-mail address: jcsilva@fc.up.pt (J.C.G. Esteves da Silva).

0925-4005/$ – see front matter © 2010 Elsevier B.V. All rights reserved.
doi:10.1016/j.snb.2010.01.031

2. Experimental

2.1. Synthesis and functionalization of CNP

All chemicals were purchased from Sigma–Aldrich and were used without further purification. The ablation process was implemented using UV pulsed laser irradiation (248 nm, KrF) of carbon targets immersed in water.

The functionalization process was adapted from [16] and it is constituted by three steps:

(i) *Activation of carbon nanoparticles* – 20 mL of the water solution with the nanoparticles dispersed plus 20 mL of HNO_3 (0.1 M) were refluxed for 12 h.
(ii) *Functionalization with PEG*$_{200}$ – solution from (i) plus 20 mL of PEG_{200} were refluxed for 28 h.
(iii) *Functionalization with N-acetyl-L-cysteine (NAC)* – solution from (ii) plus 2.984 g of NAC were refluxed for 31 h. The solution goes from colorless to yellow-brown.

The obtained carbon dots solution was extracted six times with ethyl acetate in order to eliminate unreacted reagents. 1 mL of this purified solution was diluted in a 100 mL flask which constituted the sensing solution used throughout the work. For the ^{1}H NMR and HSQC analyses the carbon dots were dried in vacuum for 1 h before dilution with deuterated water.

2.2. pH and metal ion titrations

The pH of the sensing solution was adjusted to 5.0 ± 0.1, 6.8 ± 0.1 and 8.0 ± 0.1 using phosphate buffer solutions and the addition of micromolar quantities of all metal ions did not change this value.

Standard aqueous solutions of $Hg(NO_3)_2$, $Pb(NO_3)_2$, $CdCl_2$, $Cu(NO_3)_2$, $NiCl_2$, $CoCl_2$ and $Zn(NO_3)_2{\cdot}4H_2O$ from Merck, were prepared in water with concentrations of 5.00×10^{-4} M. Aliquots of these standard solutions were added to 20 mL of carbon dots solution at pH 6.8 – 25 mL of the solution A and 25 mL of phosphate buffer solution at pH 6.8 – in order to obtain the following metal ions concentrations: 1.00×10^{-7}, 5.99×10^{-7}, 1.30×10^{-6}, 1.99×10^{-6}, 1.30×10^{-6}, 2.69×10^{-6} M. Hg(II) was subjected to a detailed analysis and a series of solutions in the range up to 3.60×10^{-6} M were prepared.

2.3. Instrumentation

Excitation emission matrices of fluorescence (EEM) [excitation between 199.4 and 672.8 nm and emission between 349.7 and 719.7 nm] were obtained with a Spex 3D luminescence spectrophotometer equipped with a Xenon pulse discharge lamp (75 W) and a CCD detector, 0.25 mm slits and 1 s integration time were used. Lifetime measurements were recorded with a Horiba Jovin Yvon Fluoromax 4 TCSPC using the following instrumental settings: 368 nm NanoLED; time range, 200 ns; peak preset 10,000 counts; repetition rate at 1 MHz; synchronous delay of 50 ns; emission detection of 550 nm. Quartz cuvettes were used.

Scanning electron microscopy (SEM) and X-ray analysis of the three purified carbon dots were done on a FEI Quanta 400FEG/EDAX Genesis X4M High Resolution Scanning Electronic Microscope.

NMR characterization was performed in D_2O for both ^{1}H NMR (500.13 MHz) and HSQC, on a Bruker-AMX500 spectrometer at 298 K. PEG_{200}, NAC and the synthesized carbon dots were characterized by ^{1}H NMR spectrometry (500 MHz, D_2O): PEG_{200}: δ = 3.66–3.68 (m, 36H), 3.740–3.742 (m, 110H); NAC: δ = 1.99 (s, 3H), 2.89–2.91 (m, 2H), 4.53–4.56 (t, 1H); carbon nanoparticles + PEG_{200}: δ = 2.91–3.02 (m, 92H), 3.51 (m, 2H), 4.61 (s, 1H); carbon nanoparticles + PEG_{200} + NAC 1 h: δ = 1.82–1.88 (m, 7H), 3.38–3.55 (m, 264H), 3.95–4.11 (m, 11H); carbon nanoparticles + PEG_{200} + NAC 31 h: δ = 1.82–1.88 (m, 15H), 2.73 (s, 5H), 3.38–3.55 (m, 376H), 3.95–4.10 (m, 15H), 4.37–4.40 (m, 4H), 8.00 (s, 1H).

The size distribution of carbon dots in water was determined by dynamic light scattering analysis using a Malvern Instruments (Malvern, UK) Zeta Sizer Nano ZS, using disposable polystyrene cells from Sigma.

2.4. Data analysis

Lifetime deconvolution analysis was done using Decay Analysis Software v6.4.1 (Horiba Jovin Yvon). Fluorescence decays were interpreted in terms of a multiexponential model:

$$I(t) = A + \sum B_i \exp\left(-\frac{t}{\tau_i}\right)$$

where B_i are the pre-exponential factors and τ_i the decay times. The fraction contribution (percentage of photons) of each decay time component is represented by B_i.

Although carbon dots show a polyelectrolyte behavior the variation of its fluorescence intensity resulting from the ionization reaction can be linearized using a Henderson–Hasselbach type equation which allows the calculation of an apparent pK_a.

$$\mathrm{pH} = \mathrm{p}K_a + n \log\left[\frac{I_{max} - I}{I - I_{min}}\right]$$

where I_{max} and I_{min} are respectively the maximum and minimum of the fluorescence intensity of the acid or conjugated base species and I is the fluorescence intensity as function of the pH. For a polyelectrolyte the slope of the plot of pH as function of $\log[(I_{max} - I)/(I - I_{min})]$, n, is an empirical parameter usually greater than unity [17].

In this study static quenching of fluorescence by metal ions [M(II)] was described using the Stern–Volmer equation:

$$\frac{I_o}{I} = 1 + K_{SV}[\mathrm{M(II)}]$$

where I_o is the fluorescence intensity without metal ion, I is the fluorescence intensity observed in the presence of a metal ion and K_{SV} is the static (conditional stability constant) Stern–Volmer constant [18].

3. Results and discussion

3.1. Synthesis and morphological characterization

The synthesis of the carbon nanoparticles was performed in deionized water using a similar but simplified strategy to one previously described [16]. The carbon targets were irradiated for 1 min and no support method to expedite the movement of the generated nanoparticles was used. Literature described synthesis of carbon nanoparticles used ultrasounds and the carbon targets were irradiated for several hours using a system apparatus far more complex than the one used in this work [16,19].

A pulsed UV laser (Lambda Physik LPX 300i – 248 nm KrF) was used to irradiate the carbon targets and a positive lens of +50 cm of focal distance was used to change the area illuminated by the laser. In all experiments the same energy (400 mJ) and repetition rate (10 Hz) were used. It was also maintained the same distance between the carbon target and the water surface and all experiments occurred at room temperature.

To optimize the laser ablation procedure, the area of the irradiated carbon target was changed and the size dispersion of the resulting nanoparticles was evaluated by SEM. When the distance between the focusing lens and the carbon target was 107 cm, the incidence area of the laser was of 348 mm^2 resulting in a fluence of

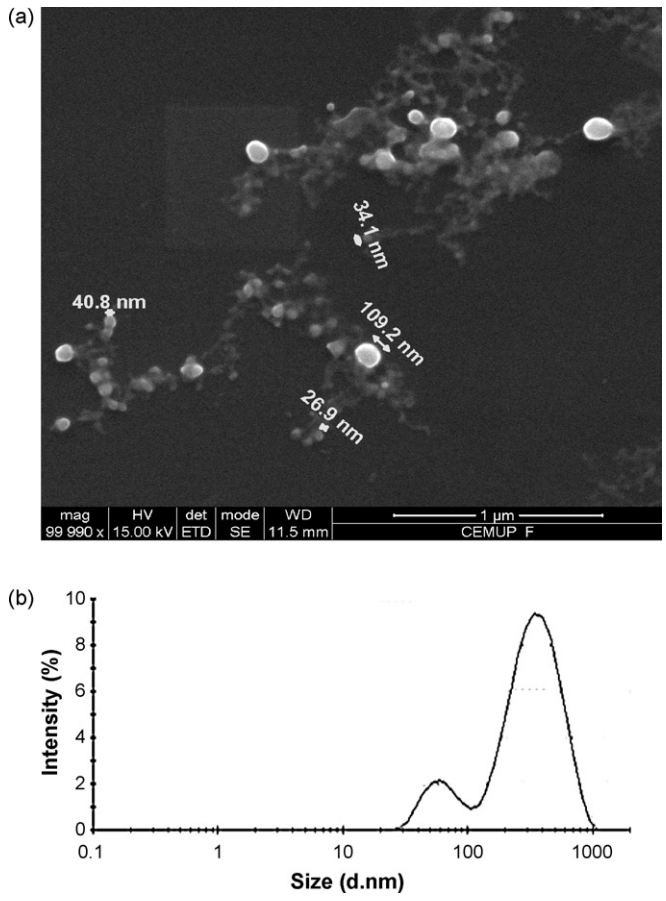

Fig. 1. (a) SEM image in a TEM grid and (b) DLS size dispersion of the carbon particles produced by laser ablation.

115 mJ/cm^2. In these conditions, the carbon particles obtained have wide size dispersion – however, the most predominant are in the hundred nanometers range. On the other hand, when the distance between the focusing lens and the carbon target was set to 85 cm, the laser area of incidence was 139 mm^2 resulting in a fluence of 288 mJ/cm^2, smaller particles were produced with dimensions down to about 27 nm (Fig. 1a). Fig. 1b shows the DLS of the nanoparticles obtained by direct laser ablation which shows two major average size dispersions centred at values of 63 and 373 nm – the smaller particles were probably obtained from laser ablation of the bigger particles. Since the objective is to synthesize nanosensors these conditions were used for further studies.

The carbon nanoparticles obtained by laser ablation are not fluorescent. In order to make them fluorescent it was necessary first to activate the carbon surface by refluxing the carbon nanoparticles in nitric acid for 12 h and, afterwards, add PEG_{200}. After 1 h reaction with PEG_{200} the carbon dots exhibited a pale yellow color and fluorescence with an emission wavelength of 565 nm. After 28 h reaction, NAC was added to the reaction mixture and samples of the reaction medium were taken over time in order to control the wavelength and intensity variation. The samples taken during the functionalization reaction showed an emission wavelength variation of 20 nm towards the red and an increase in fluorescence. The reaction ended after 31 h when the fluorescence intensity started to decrease which corresponded to the maximum nanoparticle size and quantum confinement.

The resulting solution contains carbon dots functionalized with PEG_{200} and NAC and could not be dried, limiting the possibility of electron microscopy analysis. Alternatively, carbon dots were characterized by NMR.

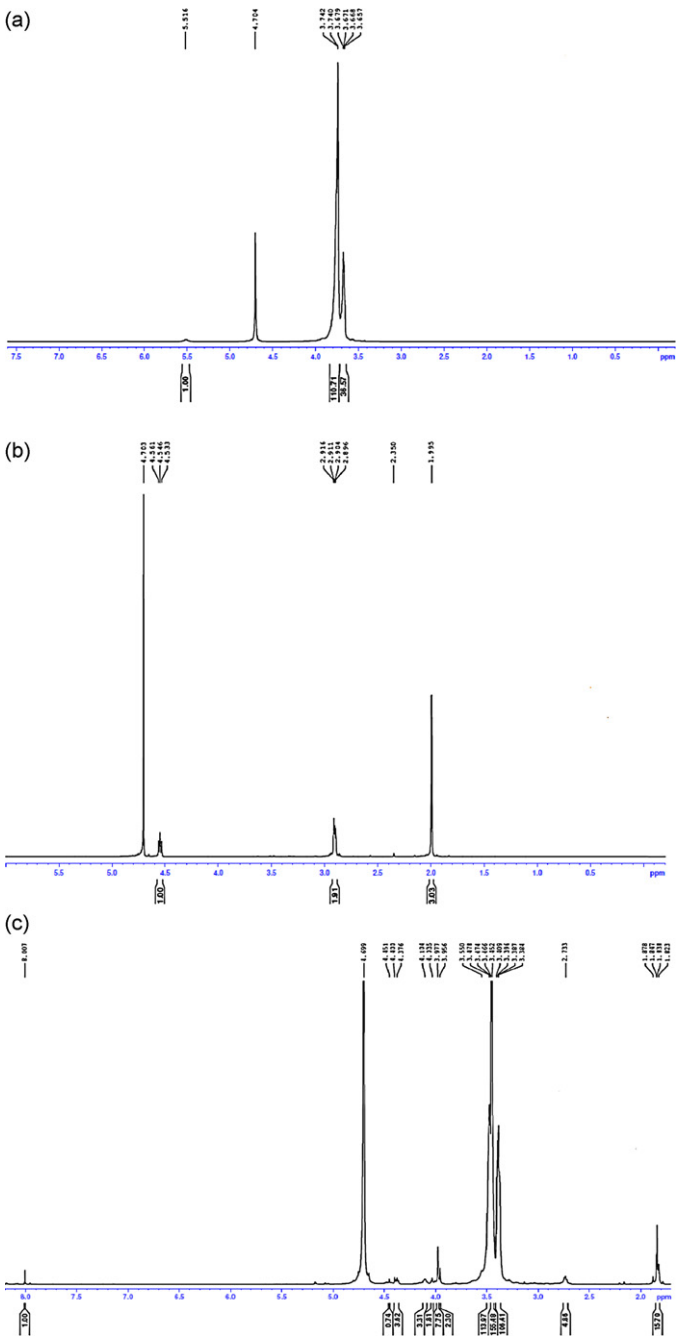

Fig. 2. ^{1}H NMR spectra of (a) PEG_{200}, (b) NAC and (c) carbon nanoparticles + PEG_{200} + NAC 31 h reaction time in D_2O.

3.2. NMR analysis

NMR analysis of the carbon dots were performed in D_2O. In order to follow the reaction samples of PEG_{200}, NAC and samples of carbon nanoparticles + PEG_{200} 1 h reaction, carbon nanoparticles + PEG_{200} + NAC 1 h reaction, and carbon nanoparticles + PEG_{200} + NAC 31 h reaction were analyzed by ^{1}H NMR (Fig. 2 and Supplementary material) and HSQC (Supplementary material). The analysis of the evolution of the chemical shifts, and respective multiplicity, due to PEG_{200} and NAC during the reaction time in the presence of the carbon nanoparticles suggests the formation of covalent bonds among all the species.

The analysis of the NMR spectra of carbon nanoparticles with PEG_{200} sample after 1 h reaction shows a chemical shift to lower

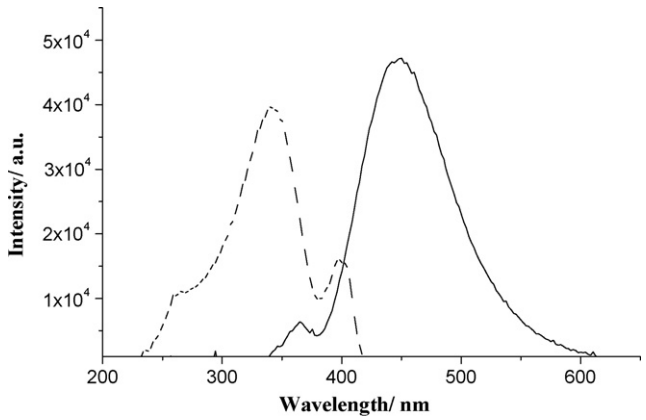

Fig. 3. Fluorescence excitation (– – –) and emission (—) spectra of the carbon dots.

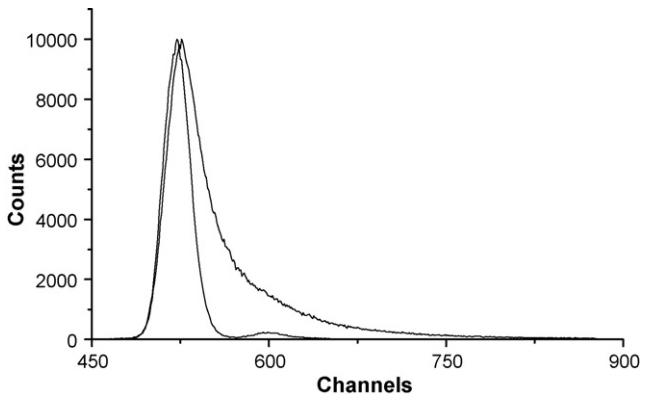

Fig. 4. Fluorescence decay of aqueous carbon dots.

values of all the signals attributed to PEG protons. This evolution of the chemical shift indicates a stabilization of the molecule, probably due to the interaction between the carbon dots surface and the PEG residue. Also the multiplet that in pure PEG (Fig. 2) appeared well defined at 3.7 ppm is now being split into two probably due to the proximity effect of several PEG molecules on the carbon dots surface.

Upon addition of NAC and after 1 h reaction the signal from the PEG and NAC protons shifted to higher values. This evolution of the chemical shift indicates an interaction between the PEG and NAC residues. This hypothesis is supported by the analysis of the signal at 1.8 ppm from the R-$COCH_3$ that typically is a singlet but, due to the presence of other non-equivalent protons, becomes a multiplet (Fig. 2). After 31 h reaction it is still possible to see PEG protons that remained at 3.9 ppm, indicating that the PEG_{200} was in excess but also that the residues that are interacting with the dots surface are probably more stable, therefore appearing at lower chemical shifts. The analysis of the HSQC data (Supplementary material) supported the observations of ^{1}H NMR.

3.3. Fluorescent properties of the carbon dots

The excitation and emission spectra of the synthesized carbon dots functionalized with PEG_{200} and NAC are shown in Fig. 3. The maximum excitation and emission are located at 340 and 450 nm, respectively, with a Stokes shift of about 110 nm.

This Stokes shift is superior than the one previously reported [13] of 70 nm (excitation maximum at 420 nm and emission at 490 nm) for the carbon dots functionalized only with PEG_{200} indicating not only that the reaction time is important to obtain higher emission and Stokes shifts values; but also that the presence of two different molecules (NAC and PEG_{200}) on the nanoparticles surface affects the quantum yield and quantum confinement. These variations on the emission wavelength with the reaction time suggest that the carbon dots are increasing their size and that the two functionalization molecules interact with their surface affecting the quantum confinement [20,21].

A typical fluorescence decay time profile of the carbon dots is shown in Fig. 4. The preliminary analysis of the decay time indicates that it is complex as it shows the presence of several lifetime ranges. Indeed, only a three-component decay time model originated a good fit ($\chi = 1.09$) with the following lifetimes: $\tau_1 = 0.35$ ns; $\tau_2 = 1.8$ ns; and $\tau_3 = 4.39$ ns (Table 1).

3.4. Effect of the pH and metal ions on the fluorescence of CNP

After functionalization with PEG_{200} and NAC it was observed that the fluorescence of the carbon dots was sensitive to pH (Fig. 5).

Table 1
Lifetime intensity decays of carbon dots in water[a].

N	τ_i (ns)	α_i	f_i	
1	0.35(0.02)	0.0958(0.0006)	30.6%	
2	1.8(0.1)	0.0263(0.0002)	42.2%	
3	4.39(0.05)	0.00673(0.00005)	27.1%	$\chi = 1.09$

[a] Standard deviation in parenthesis.

This sensitivity is marked by a decrease of the fluorescence intensity as the pH increases and, by fitting the fluorescence intensities with the Henderson–Hasselbach equation, it was found an apparent pK_a of 4.2 ± 0.1 and a slope of 2.5. This pH behavior is reversible. Also, as the slope is higher than unity it suggests that the carbon dots follow a polyelectrolyte ionization.

This variation is due to the ionization of the acid groups of the NAC residue of the carbon dots which may influence the confinement energy of the nanoparticles resulting in a variation of the fluorescence. Since the carbon dots presented sensitivity towards the pH, when we passed on to the quenching assays it was necessary to perform a preliminary study in order to determine the appropriate pH to do such studies. For these assays it was studied the quenching effect of Hg(II) on the synthesized carbon dots at pH 5.0, 6.8 and 8.0. At pH 5.0 a white precipitate was found which eliminated this pH for further studies. At pH 8.0 the intensity signal was better than at pH 6.8, however the quenching effect on the carbon dots was negligible, when compared to the signal observed at pH 6.8. Accordingly to these results the quenching effect of the metal ions was performed in a buffered phosphate solution at pH 6.8. This pH quenching dependence is due to the hydrolysis of the mercury

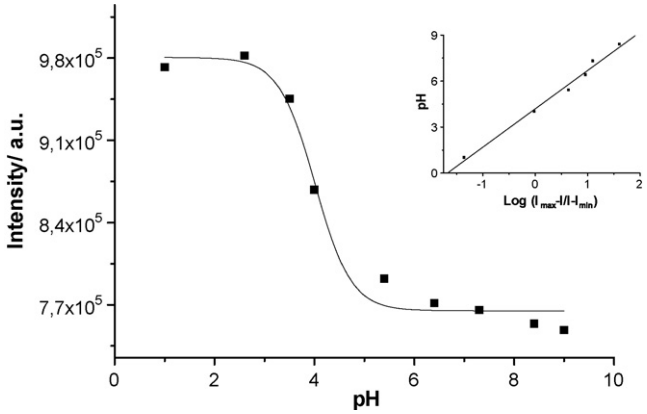

Fig. 5. Variation of the fluorescence intensity of aqueous carbon dots as a function of the pH.

Table 2
Stern–Volmer parameters for the quenching of carbon dots by Hg(II) and Cu(II) ions[a].

Ion	K_{SV} (M^{-1})	Intercept	R	Points	Concentration range (M)
Hg(II)	$1.3(0.4) \times 10^5$	0.97(0.01)	0.9719	17	1.00×10^{-7}–2.69×10^{-6}
Cu(II)	$5.6(0.8) \times 10^4$	1.0(0.2)	0.9607	6	1.00×10^{-7}–2.69×10^{-6}

[a] Averages and standard deviation (in parenthesis) of three independent experiences. R, correlation coefficient.

ions [22]. Indeed, although the total mercury concentration is quite low, at pH 8.0 the $Hg(OH)_2$ species is quantitatively formed and the NAC is not able to complex the mercury. At pH 6.8, the $[Hg(OH)]^+$ species is probably the main mercury species in aqueous solution and it is available to be complexed by the carbon dots.

Since the carbon dots were functionalized with NAC, it is expected that their fluorescence properties would change when they react with metal ions. Several metal ions [Hg(II), Cu(II), Cd(II), Ni(II), Zn(II) and Ca(II)] were tested to check if they affect the fluorescence properties of the carbon dots.

As shown in Fig. 6 the carbon dots fluorescence is affected by Hg(II), where it is possible to observe a marked quenching effect – the fluorescence signal decreases 25% upon addition of micromolar concentration of Hg(II) (2.69×10^{-6} M). The addition of Cu(II) also provokes quenching of the fluorescence of the carbon dots but in less extent than with Hg(II) – about 13% decrease is observed. The other metal ions analyzed, namely Cd(II), Ni(II), Zn(II) and Ca(II), show no measurable effect on the fluorescence of the carbon dots.

The quenching provoked by Hg(II) is described as a typical Stern–Volmer plot (Fig. 7). Table 2 presents the parameters of the linear fitting of the quenching provoked by Hg(II) and Cu(II). The analysis of the Stern–Volmer plots show that they follow a linear trend with $K_{SV} = 1.3(4) \times 10^5$ and $5.6(8) \times 10^4$ for Hg(II) and Cu(II), respectively. This order of magnitude is compatible with the formation of a quite stable complexes (static quenching) between the NAC residues on the surface of the carbon dots and Hg(II) and Cu(II) ions.

In order to access if the quenching effect is due to the NAC or the PEG residue, a study was performed using the nanoparticles functionalized only with PEG (Supplementary material) and it was found that there is no significant fluorescence emission or intensity variations upon addition of the same micromolar concentration of Hg(II). As such, and as expected, the sensitivity towards Hg(II) (soft donor) is due to the NAC residue (namely the sulfur atom – soft acceptor) of the carbon dots.

A variety of analytical tools are commonly employed to detect mercury in biological samples [23–27]. However while traditional

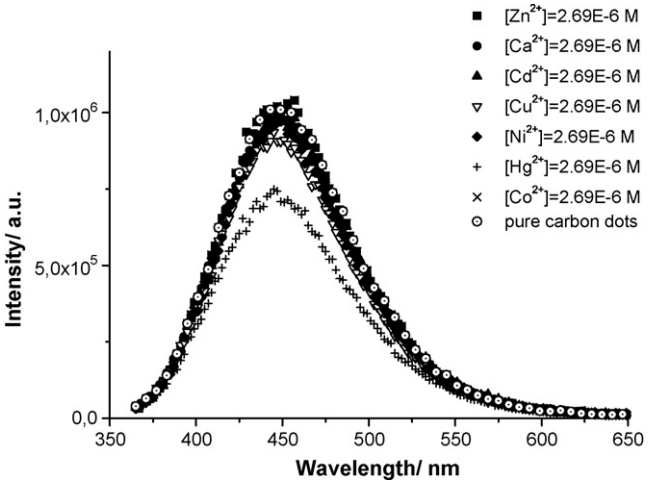

Fig. 6. Fluorescence quenching of the synthesized carbon dots in aqueous solution by 2.69×10^{-6} M of all metal ions.

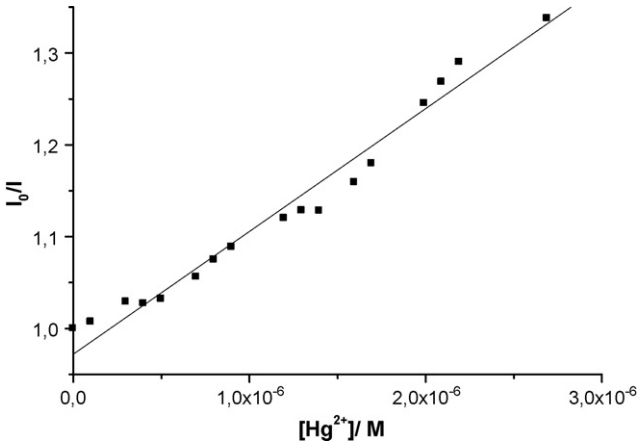

Fig. 7. Stern–Volmer plot of the fluorescence quenching of carbon dots in aqueous solution by Hg(II).

analytical detection methods allow detection limits in the nanomolar range [28–30], they commonly do not allow time-dependent or location-specific *in vivo* measurements. As the uptake and distribution of this heavy metal are not understood, highly sensitive and non-invasive methods are needed for its detection in a living organism.

Herein these carbon dots are of great importance due not only to their nanometer size and fluorescence properties but also because they can be specifically targeted in order to perform *in vivo* measurements in a non-invasive way, thereby representing a novel non-toxic nanoanalytical tool.

4. Conclusions

The use of direct laser ablation to produce carbon nanoparticles in water rendered a wide variety of sizes accordingly with the laser fluence. As such, by controlling the energy and incidence area it is possible to produce particles in tens of nanometer range. These nanoparticles can easily be functionalized using more than one molecule and remain stable in an aqueous solution. Due to this stability it is also possible to immobilize them in the optical fiber devices using the sol–gel technique, which would render a specific optical nanoanalytical sensor. The functionalization using PEG_{200} and NAC allowed us to synthesize a nanosensor sensitive to micromolar concentrations of Hg(II) and Cu(II) as well as the solution pH. Since these carbon dots are biologically inert they are a promising solution for *in vivo* measurements of the mercury uptake dynamics. However, for the *in vivo* analysis of metal ions further research is needed to study the effect of biological molecules on the speciation of the metal ions (cysteine residuals, water soluble proteins, other anionic cellular components, etc.) in the presence of the carbon dots.

Acknowledgements

Financial support from Fundação para a Ciência e Tecnologia (Lisboa) (FSE-FEDER) (Project PTDC/QUI/71001/2006) is acknowledged. A PhD grant to Helena Gonçalves SFRH/BD/46406/2008 is acknowledged to Fundação para a Ciência e Tecnologia (Lisboa).

Appendix A. Supplementary data

Supplementary data associated with this article can be found, in the online version, at doi:10.1016/j.snb.2010.01.031.

References

[1] D. Gerion, F. Pinaud, S.C. Williams, W.J. Parak, D. Zanchet, S. Weiss, A.P. Alivisatos, Synthesis and properties of biocompatible water-soluble silica-coated CdSe/ZnS semiconductor quantum dots, J. Phys. Chem. B 105 (2001) 8861–8871.

[2] A.N. Rogach, D. Nagesha, J.W. Ostrander, M. Giersig, N.A. Kotov, "Raisin Bun"-type composite spheres of silica and semiconductor nanocrystals, Chem. Mater. 12 (2000) 2676–2685.

[3] Y. Williams, A. Sukhanova, M. Nowostawska, A.M. Davies, S. Mitchell, V. Oleinikov, Y. Gun'ko, I. Nabiev, D. Kelleher, Y. Volkov, Probing cell-type-specific intracellular nanoscale barriers using size-tuned quantum dots, Small 5 (2009) 2581–2588.

[4] M.J. Murcia, D.L. Shaw, E.C. Long, C.A. Naumann, Fluorescence correlation spectroscopy of CdSe/ZnS quantum dot optical bioimaging probes with ultra-thin biocompatible coatings, Opt. Commun. 281 (2008) 1771–1780.

[5] P. Juzenas, W. Chen, Y.-P. Sun, M.A.N. Coelho, R. Generalov, N. Generalova, I.L. Christensen, Quantum dots and nanoparticles for photodynamic and radiation therapies of cancer, Adv. Drug Deliv. Rev. 60 (2008) 1600–1614.

[6] J. Lia, D. Baoa, X. Honga, D. Li, J. Li, Y. Baia, T. Lia, Luminescent CdTe quantum dots and nanorods as metal ion probes, Colloids Surf. A: Physicochem. Eng. Aspects 257–258 (2005) 267–271.

[7] C. Sun, B. Liu, J. Li, Sensitized chemiluminescence of CdTe quantum-dots on Ce(IV)-sulfite and its analytical applications, Talanta 75 (2008) 447–454.

[8] Z. Wang, J. Li, B. Liu, J. Li, CdTe nanocrystals sensitized chemiluminescence and the analytical application, Talanta 77 (2009) 1050–1056.

[9] P.T.C. So, Two-photon fluorescence light microscopy, in: Encyclopedia of Life Sciences, Macmillan Publishers Ltd, Nature Publishing Group, 2002, www.els.net.

[10] S.-T. Yang, X. Wang, H. Wang, F. Lu, P.G. Luo, L. Cao, M.J. Meziani, J.-H. Liu, Y. Liu, M. Chen, Y. Huang, Y.-P. Sun, J. Phys. Chem. C (2009), doi:10.1021/jp9085969.

[11] A.M. Smith, H. Duan, A.M. Mohs, S. Nie, Bioconjugated quantum dots for in vivo molecular and cellular imaging, Adv. Drug Deliv. Rev. 60 (2008) 1226–1240.

[12] J.P. Ryman-Rasmussen, Surface coatings determine cytotoxicity and irritation potential of quantum dot nanoparticles in epidermal keratinocytes, J. Invest. Dermatol. 127 (2007) 143–153.

[13] Y. Higuchi, Mannosylated semiconductor quantum dots for the labeling of macrophages, J. Control. Rel. 125 (2008) 131–136.

[14] A.C. Faure, S. Dufort, V. Josserand, P. Perriat, J.L. Coll, S. Roux, O. Tillement, Control of the in vivo biodistribution of hybrid nanoparticles with different poly(ethylene glycol) coatings, Small 5 (2009) 2565–2575.

[15] E. Raspanti, S.O. Cacciola, C. Gotor, L.C. Romero, I. García, Implications of cysteine metabolism in the heavy metal response in *Trichoderma harzianum* and in three *Fusarium* species, Chemosphere 76 (2009) 48–54.

[16] S.-L. Hu, K.-Y. Niu, J. Sun, J. Yang, N.-Q. Zhao, X.-W. Du, One-step synthesis of fluorescent carbon nanoparticles by laser irradiation, J. Mater. Chem. 19 (2009) 484–488.

[17] Q.Z. Wang, X.G. Chen, N. Liu, S.X. Wang, C.S. Liu, X.H. Meng, C.G. Liu, Protonation constants of chitosan with different molecular weight and degree of deacetylation, Carbohydrate Polym. 65 (2006) 194–201.

[18] J.R. Lakowicz, Principles of Fluorescence Spectroscopy, Kluwer-Plenum, New York, 1999 (Chapter 8).

[19] Y.-P. Sun, B. Zhou, Y. Lin, W. Wang, K.A.S. Fernando, P. Pathak, M.J. Meziani, B.A. Harruf, X. Wang, H. Wang, P.G. Luo, H. Yang, M.E. Kose, B. Chen, M. Veca, S.-Y. Xie, Quantum-sized carbon dots for bright and colorful photoluminescence, J. Am. Chem. Soc. 128 (2006) 7756–7757.

[20] C. Maule, H. Gonçalves, C. Mendonça, P. Sampaio, J.C.G. Esteves da Silva, P. Jorge, Wavelength encoded analytical imaging and fiber optic sensing with pH sensitive CdTe quantum dots, Talanta (2009), doi:10.1016/j.talanta.2009.10.048.

[21] J.M.M. Leitão, H. Gonçalves, C. Mendonça, J.C.G. Esteves da Silva, Multiway chemometric decomposition of EEM of fluorescence of CdTe quantum dots obtained as function of pH, Anal. Chim. Acta 628 (2008) 143–154.

[22] M.F. McComish, J.H. Ong, Trace metals, in: I. Bodek, W.J. Luman, W.F. Reehl, D.H. Rosenblatt (Eds.), Environmental Inorganic Chemistry, Pergamon Press, New York, 1988 (Chapter 7).

[23] R.R. Chapleau, R. Blomberg, P.C. Ford, M. Sagermann, Design of a highly specific and noninvasive biosensor suitable for real-time in vivo imaging of mercury (II) uptake, Protein Sci. 17 (2008) 614–622.

[24] L. Geiselhart, M. Osgood, D.S. Holmes, Construction and evaluation of a self-luminescent biosensor, Ann. N.Y. Acad. Sci. 646 (1991) 53–60.

[25] O. Selifonova, R. Burlage, T. Barkay, Bioluminescent sensors for detection of bioavailable Hg(II) in the environment, Appl. Environ. Microbiol. 59 (1993) 3083–3090.

[26] H. Yu, D. Mukhopadhyay, T.K. Misra, Purification and characterization of a novel organometallic receptor protein regulating the expression of the broad spectrum mercury-resistant operon of plasmid pDU1358, J. Biol. Chem. 269 (1994) 15697–15702.

[27] O.K. Lyngberg, D.J. Stemke, J.L. Schottel, M.C. Flickinger, A single-use luciferase-based mercury biosensor using *Escherichia coli* HB101 immobilized in a latex copolymer film, J. Ind. Microbiol. Biotechnol. 23 (1999) 668–676.

[28] H.N. Lee, H.N. Kim, K.M.K. Swamy, M.S. Park, J. Kim, H. Lee, K.-H. Lee, S. Park, J. Yoon, New acridine derivatives bearing immobilized azacrown or azathiocrown ligand as fluorescent chemosensors for Hg^{2+} and Cd^{2+}, Tetrahedron Lett. 49 (2008) 1261–1265.

[29] L. Guo, H. Hu, R. Sun, G. Chen, Highly sensitive fluorescent sensor for mercury ion based on photoinduced charge transfer between fluorophore and π-stacked T-Hg(II)–T base pairs, Talanta 79 (2009) 775–779.

[30] S Yoon, A.E. Alberts, A.P. Wong, C.J. Chang, Screening mercury levels in fish with a selective fluorescent chemosensor, J. Am. Chem. Soc. 127 (2005) 16030–16031.

Biographies

Helena Gonçalves obtained his B.Sc. and M.Sc. in chemistry from the Faculty of Sciences of the University of Porto (FCUP), Portugal, where she worked on the development of new bioanalytical sensors based new ruthenium and osmium complexes and CdTe quantum dots. Currently, she has a Ph.D. grant to work on the development of new bioconjugated and functionalized quantum and carbon dots.

Pedro A.S. Jorge graduated in applied physics (optics and lasers) from the University of Minho in 1996. He received his M.Sc. in optoelectronics and lasers from the physics department of the University of Porto in 2000. In 2006, he concluded his Ph.D. program at Porto University in collaboration with the department of physics and optical sciences at the University of Charlotte, North Carolina, USA, with work developed in luminescence based optical fiber. He is currently a senior researcher at INESC Porto, where he leads a small team in the development of biochemical sensors for environmental and medical applications.

J.R.A. Fernandes is a professor in the physics department of Universidade de Trás-os-Montes e Alto Douro and senior researcher at Optoelectronics Group of INESC Porto. He received his Ph.D. from Porto University. His research interests are in laser ablation of inorganic materials area for the production of thin films or for the production of nanoparticles to be used in sensors.

Joaquim C.G. Esteves da Silva obtained his B.Sc., M.Sc. and Ph.D. in chemistry from the Faculty of Sciences of the University of Porto (FCUP), Portugal, where he worked on chemometric methodologies to environmental inorganic systems. Currently, he is an associate professor in the chemistry and biochemistry department of the FCUP where he teaches inorganic, environment, forensic, bioanalytical and chemometric courses. His current main research interests are the development of fluorescent nanomaterials and enzymatic bioanalytical methods for biochemical, environmental and technological applications.

CHAPTER 4 – CDOTS FOR IODINE SENSING

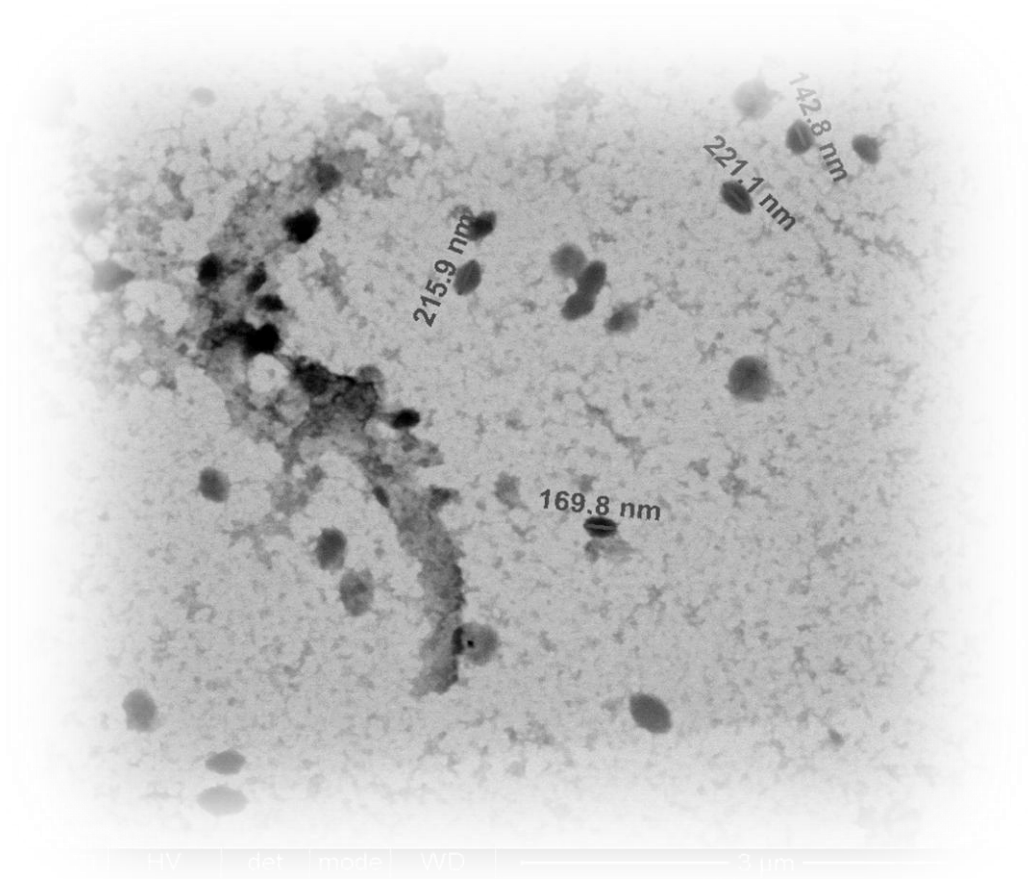

4.1. State of the Art

The element known as iodine was first discovered in 1811 by Bernard Courtois. At the time France was at war and there was a great demand for sodium carbonate, necessary for the saltpetre production. The purification of sodium carbonate was through the addition of sulphuric acid. One time Courtois added an excessive amount of sulphuric acid and noticed that a purple cloud appeared. The vapour crystallized when in contact with cold surfaces and dark crystals precipitated – iodine. Unfortunately he did not have enough funding to try to determine what was this substance, therefore he gave small samples to some of his researchers friends, Charles Bernard Desormes, Nicolas Clément, Joseph Louis Gay-Lussac and André-Marie Ampère. Ampère gave a small sample to Humphry Davy that also performed some experiments on this new element. Later Davy and Gay-Lussac argued for the acknowledgment of being the first to identify iodine, nevertheless both agreed that the first to isolate and discover the element was Courtois [1].

Nowadays the knowledge of iodine properties is far developed. There are 37 known isotopes of iodine, however the most stable is ^{127}I. The iodine isotopes that are more commonly used are ^{125}I, ^{123}I and ^{131}I. Its different applications are mainly related with their relative half-life. ^{125}I has a half-life of 59 days and is used as “tag” due to its gamma emitting pattern, for proteins in biological assays. Additionally it is also used in some medicine imaging tests and in brachytherapy, where iodine is in implanted capsules that are put in contact with tumours, sensitive to local short-range gamma radiation. ^{123}I is the isotope most used in nuclear medicine for the thyroid gland, that naturally accumulates all iodine isotopes. The choice of this isotope for medicine imaging is due to its relative low half-life (13h). Another isotope used in medicine is ^{131}I. This isotope has a half-life of 8 days and it is beta emitting. This characteristic is useful in nuclear fission and in aggressive thyroid cancer therapies, where it is administered in very high dosages. Indeed, it use in therapies is quite peculiar, since it was proven that in low doses it is a powerful thyroid carcinogenic, however in high dosages it is less harmful and it helps to destroy cancer cells without a dramatic damage on healthy tissue. The use of ^{127}I is performed in a preventative manner, since it is used for saturating the thyroid gland of this isotope, thereby preventing future toxicity from ^{131}I generated by nuclear fission accidents, such as Chernobyl and Fukushima, as well as, the nuclear fallout from nuclear weapons [2].

Iodine is, beyond tungsten, the heaviest element essential in biological media. It is not a very abundant element, nonetheless its annual production from natural sources is about 19 000 tons [3]. Iodide salts are quite soluble in water, so it is not surprising that the higher concentration of this element is found in seawater and brine, as such, some algae are very rich in iodine. Indeed, the brown algae *Laminaria* and *Fucus* that can be found in temperate zones of the Northern Hemisphere can contain about 0.028–0.454 of dry weight of iodine. Additionally, it can also be found in rocks, such as caliche - a mineral common in Chile - and on iodine-containing brines of gas and oil fields mainly in Japan and United States of America.

When iodide is in water, and in resemble to what happens to mercury, the activity of microorganisms is responsible for the production of the so called organoiodine compounds. One of the most abundant organoiodine compounds is methyl iodide. In fact, its annual production is about 214 kilotonnes. Methyl iodide is volatile and, as such, upon its production it is released into the atmosphere, thereby entering the global iodine cycle. Over the years there has been several attempts to describe the iodine global environment cycle. The first one was by Kocher in 1981 [4], followed by Whitehead in 1984 [5] and a revision by White and Smith in 1984 [6].

Iodine has important biological roles, namely it helps to regulate the metabolic rate, growth and development, promotes bone and protein synthesis and one of the most known is the production of thyroxin, an important hormone produced by the thyroid gland. Since its relative importance has been defined, some dietary limits where established for daily ingestion. These values change with the person age and it can go from 90 (1-3 years) to 290μg (lactation women from 19-50). Additionally there are also upper limits for iodine consumption per day, that are also age dependent. Nevertheless the higher value permitted is 1100 μg [7].

It is not easy to manage the amount of iodine ingested per day, particularly because the population is not aware of the complications that may arise from a iodine imbalance. In order to better control the iodine in the dietary it is necessary to take into account that the major natural food sources for iodine can be found in food grown in or near coastal seas and in seafood. Two simple examples of this are: the iodine content on ¼ of a teaspoon table salt (100μg) and cooked spinach (5μg).

The control over the ingestion of iodine is quite relevant. Indeed, it has determined that a iodine deficiency is a big risk factor for gastric, mammalian and thyroid cancer [8-10]. Moreover, some recent work has reported that an unbalance in this element may represent not only a risk factor for gastric cancer but also of atrophic

gastritis [11]. Its action mechanism is through antagonizing several iodine inhibitors, such as, nitrates, thiocyanates and salts that are well known risk factors for gastric carcinogenesis. Despite the carcinogenic effect, a low biological concentration of iodine can lead to hypothyroidism due to the decrease in hormones production and subsequent release to the body. On the other hand an increase of iodine can be responsible for hyperthyroidism. This is particularly critical in children since it can cause intellectual disability and abnormal growth.

Iodine vital role in biological processes is the main responsible for the pressing need for rapid, sensitive and selective iodine sensors in food, pharmaceutical products and biological samples, such as, urine and blood [12]. Nowadays there are numerous methods for iodine detection, namely gas chromatography with mass spectrometry detection [13], electrostatic ion chromatography [14], capillary electrophoresis [15], indirect atomic absorption spectrometry [16] and, fluorescence spectroscopy[17]. Nevertheless many of these methods require specialized personnel, multistep sample preparation and sophisticated instrumentation. Moreover, since the most common sample for iodine detection in biological sample is urine, which is a complex mixture of compounds, the sample preparation can be quite complex. The combination of all these factors is responsible for the complexity if iodine sensing.

The use of fluorescence for iodine sensing has become quite interesting due to the sensitivity and simplicity of the technique [18]. Fluorescence sensors for iodine can be “turn-on” or probes “turn-off”. “Turn-on” sensors are based on fluorescence enhancement and “turn-off” on fluorescence quenching. “Turn-on” fluorescence sensors are quite difficult to obtain, since iodine is an intrinsic *quencher* due to its heavy atom effect [19]. This is indeed the main reason why the iodine sensors are mainly based on fluorescence quenching. In fact there are only a few examples of iodine “turn-on” sensors in the literature [12, 20-21]. An example is the sensor based on p-[(dimethylamino)benzylidene]thiosemicarbazide of Huang *et al*. [21], that has a detection limit of 450nm. Its two-step mechanism of action is quite peculiar since p-[(dimethylamino)benzylidene]thiosemicarbazide is sensitive to mercury(II) and rapidly binds to this ion with a subsequent decrease in the fluorescence. When iodine is added to this complex, it binds to mercury and the initial fluorescence of the organic dye is recovered. Another “turn-on” sensor for iodine is described by Wang *et al.*, [12] and is based on thymine-anthracene. Its action mechanism is similar to the one described by *Huang et al*., where initially the fluorescence is quenched due to the formation of a mercury(II) complex with the organic dye and a recovery of the fluorescence occurs after the addition of iodine. However it is not easy to synthesize and purify organic dyes

that are sensitive to iodine through fluorescence enhancement. Moreover, since there is a great demand for iodine sensors for biological fluids, these organic dyes should be soluble in complex aqueous systems. Indeed this two-step iodine sensing is complex and hard to perform.

On the other hand it is simpler to develop a iodine sensor based on fluorescence quenching – "turn-off". Some examples of these sensors are the bis-imidazolium and benzimidazole derivatives [23-24], conjugated polymers [25] and, functionalized Quantum Dots [26].

Here it will be reported a new "turn-off" iodine sensor based on Carbon Dots (Cdots). These carbon based nanoparticles will be functionalized with poliethileneglycol 200 (PEG_{200}) and mercaptosuccinic acid (MSS) and tested for pH and iodine sensing. This work was published in the Journal of Fluorescence, 20 (2010), pp. 1023.

4.2. References

[1] http://www.mnwelldir.org/docs/history/iodine.htm, consulted in September **2012**.

[2] U.S NRC report, available online in: http://www.nrc.gov/materials/miau/med-use-toolkit/seed-localization.html, consulted in September **2012**.

[3] Christiansen J.V., Carlsen L. **1989**. "Iodine in the environment revisited: an evaluation of the chemical- and physico chemical processes possibly controlling the migration behaviour of iodine in the terrestrial environment. Available online in: www.risoe.dtu.dk/rispubl/reports_INIS/RISOM2791.pdf, consulted in September 2012.

[4] Kocher, D.C. **1981**. "A Dynamic Model of the Global Iodine Cycle and Estimation of Dose to the World Population from Releases of Iodine-129 to the Environment." Environ. Int. 5, pp.15.

[5] Whitehead D.C. **1984**. "The Distribution and Transformation of Iodine in the Environment". Environ. Inter. 10, pp 321-339.

[6] White L.F., Smith C.M. **1984**. "Management modes for Iodine-129". Euratom Report 9267 CEC. Luxenburg.

[7]http://www.aurorahealthcare.org/yourhealth/healthgate/getcontent.asp?URLhealthgate=%2225139.html%22, consulted in September **2012**.

[8] Venturi S, Donati FM, Venturi A, Venturi M, Grossi L, Guidi A. **2000**. "Role of iodine in evolution and carcinogenesis of thyroid, breast and stomach". Adv Clin Path. 4 (1), pp.11-17.

[9] Versloot PM, Schröder-van der Elst JP, van der Heide D, Boogerd L. **1997**. "Effects of marginal iodine deficiency during pregnancy: iodide uptake by the maternal and fetal thyroid". Am J Physiol. 273 (6), pp.E1121-6.

[10] Venturi S. **2001**. "Is there a role for iodine in breast diseases?". Breast. 10 (5), pp.379-382.

[11] Venturi S., Venturi M. **1999**. "Iodide, thyroid and stomach carcinogenesis: evolutionary story of a primitive antioxidant?" European Journal of Endocrinology 140**,** pp.371–372.

[12] Boling M., Fang Z., Fangyuan Z., Shuizhu W. **2011**. "A Fluorescence Turn-on Sensor for Iodide Based on a Thymine–HgII–Thymine Complex" Chem. Eur. J. 17, pp.14844 – 14850.

[13] Bichsel Y., Von-Gunten U. **1999**. “Determination of iodide and iodate by ion chromatography with postcol-umn reaction and UV/visible detection”. Anal. Chem. 71, pp.34–38.

[14] Hu W., Yang P.J., Hasebe K., Haddad P.R., Tanaka K. **2002**. “Rapid and direct determination of iodide in seawater by electrostatic ion chromatography”. J. Chromatogr. A 956, pp.103–107.

[15] Ito K., Ichihara T., Zhuo H., Kumamoto K., Timerbaev A. R., Hirokawa T. **2003**. “Determination of trace iodide in seawater by capillary electrophoresis following transient isotachophoretic preconcentration - Comparison with ion chromatography”. Anal. Chim. Acta. 497, pp.67–74.

[16] Bermejo-Barrera P., Fernandez-Sanchez L.M., Aboal-Somoza M., Anllo-Sendin R. M., Bermejo-Barrera A. **2001**. “Indirect atomic absorption spectrometry (IAAS) as a tool for the determination of iodide in infant formulas by precipitation of AgI and redissolution with cyanide”. Microchem. J. 69, pp.205–211.

[17] Gonçalves H.M.R., Esteves da Silva J.C.G. **2010**. “Fluorescent Carbon Dots Capped with PEG_{200} and Mercaptosuccinic Acid”. J. Fluorescence, 20 pp.1023-1028.

[18] Wang X.-H., Peng H.-S., Shang H., Chang Z., Hou L.-L., You F.-Y., Song H.-W., Dong B. **2012**. “Synthesis of ratiometric fluorescent nanoparticles for sensing oxygen”. Microchimica Acta. 178, pp 147-152.

[19] Martínez-Máñez R., Sancenon F. **2003**. “Fluorogenic and Chromogenic Chemosensors and Reagents for Anions”. Chem. Rev. 103, pp.4419–4476.

[20] Li H., Han C., Zhang L. **2008**. “Synthesis of cadmium selenide quantum dots modified with thiourea type ligands as fluorescent probes for iodide ions”. J. Mater. Chem. 18, pp.4543–4548.

[21] Lin L.R., Fang W., Yu Y., Huang R.B., Zheng L.S. **2007**. “Selective recognition iodide in aqueous solution based on fluorescence enhancement chemosensor”. Spectrochim. Acta, Part A. 67, 1403 – 1406.

[22] Kim H., Kang J. **2005**. “Bromide selective fluorescent anion receptor with glycoluril molecular scaffold”. Tetrahedron Lett. 46, pp.5443–5445.

[23] Singh N., Jang D.O. **2007**. “Benzimidazole-Based Tripodal Receptor: Highly Selective Fluorescent Chemosensor for Iodide in Aqueous Solution”. Org. Lett. 9, pp.1991–1994.

[24] Lee D.Y., Singh N., Kim M.J., Jang D.O. **2011**. “Chromogenic and Fluorescent Recognition of Iodide with a Benzimidazole-Based Tripodal Receptor”. Org. Lett. 13, pp. 3024–3027.

[25] Ho H.A., Leclerc M. **2003**. “New colorimetric and fluorometric chemosensor based on a cationic polythiophene derivative for iodide-specific detection”. J. Am. Chem. Soc. 125, pp.4412–4413.

[26] Li H., Han C., Zhang L. **2008**. “Synthesis of cadmium selenide quantum dots modified with thiourea type ligands as fluorescent probes for iodide ions”. J. Mater. Chem. 18, pp.4543–4548.

4.3. Personal Contribution to this Paper

My personal contribution to this work includes the following: establishment of an initial objective and all the necessary research to ascertain the state of the art for the Cdots synthesis and functionalization. It was then required the suiting of this knowledge to the material and equipment available. Once this was determined all the procedures for the synthesis, functionalization and purification of all the nanoparticles produced by laser ablation were performed. Afterwards, it was necessary to choose the nanoparticles that had the best fluorescent properties regarding to the primarily objective. Subsequently, it was studied the structural and chemical properties of the produced nanoparticles and with this knowledge some tests were performed, namely: solvents effect, pH, metal ion sensitivity, among others. The results were interpreted and compared to the existing data provided by other research groups. Once all the data were collected it was necessary to repeat all the functionalization, purification and sensitivity towards different parameters in order to ascertain if the results were reproducible. When all these procedures were repeated and the data were considered reproducible it was required the write a manuscript with all the necessary data for publication in an international scientific research journal and perform the necessary adjustments to comply with the reviewers suggestions.

J Fluoresc (2010) 20:1023–1028
DOI 10.1007/s10895-010-0652-y

ORIGINAL PAPER

Fluorescent Carbon Dots Capped with PEG_{200} and Mercaptosuccinic Acid

Helena Gonçalves · Joaquim C. G. Esteves da Silva

Received: 5 January 2010 / Accepted: 24 March 2010 / Published online: 30 March 2010

Abstract The synthesis and functionalization of carbon nanoparticles with PEG_{200} and mercaptosuccinic acid, rendering fluorescent carbon dots, is described. Fluorescent carbon dots (maximum excitation and emission at 320 and 430 nm, respectively) with average dimension 267 nm were obtained. The lifetime decay of the functionalized carbon dots is complex and a three component decay time model originated a good fit with the following lifetimes: τ_1= 2.71 ns; τ_2=7.36 ns; τ_3=0.38 ns. The fluorescence intensity of the carbon dots is affected by the solvent, pH (apparent pK_a of 7.4±0.2) and iodide (Stern-Volmer constant of 78± 2 M^{-1}).

Keywords Carbon nanoparticles · Carbon dots · Fluorescence · Functionalization · PEG_{200} and mercaptosuccinic acid

Introduction

Carbon dots are a new class of fluorescent nanoparticles with a carbon based core. These carbon dots possess high stability over time, exceptional resistance to photo and chemical degradation, tunable fluorescence emission and excitation, high quantum yields, large Stokes shifts and since their synthesis is performed in water they are water soluble. Although this new class of quantum dots (QDs) was recently discover they are gaining a lot of attention since they enable fluorescence imaging with both one-and two-photon excitations on the same platform [1, 2]. They are imaging agents with a performance competitive to the traditional CdSe/ZnS quantum dots [2]. Furthermore, these carbon dots have proved to be a valuable tool to overcome the toxicity issues arising from the use of cadmium core based quantum dots. A toxicity assay of these new nanoparticles was performed very recently [2, 3] and it was proved that unlike the traditional cadmium based quantum dots and nanotubes their accumulation level in the liver was very low.

So far, carbon dots have been produced from multi-walled carbon nanotubes with electrochemical methods [4], from candle soot, through thermal oxidation of suitable molecular precursors [5, 6], from commercial lampblack, which is a primary material of Chinese ink [7], and by laser ablation of graphite and subsequent surface oxidation with nitric acid [8]. Despite the different ways of obtaining carbon dots, they have only been functionalized with NH_2-polyethylene-glycol of different molecular weights. This may be due to the fact that it was recently shown that using QDs capped with PEG_{200} in cultured keratinocytes significantly inhibited cytotoxicity and immune responses when compared with QDs without this capping [9], thereby suggesting that PEG coating is an effective approach for the safe use of QDs for in vivo applications [10, 11]. However it is known that quantum dots can be capped with selected molecules according to the intended application, as such, and due to the possibility that carbon dots can overcome the toxicity limitation of the cadmium based quantum dots for biological applications, it is important to develop and analyze the stability of new nanosensors by further functionalization of these PEG coated carbon dots.

Here we report the synthesis and characterization of carbon nanoparticles obtained by direct laser ablation of

H. Gonçalves · J. C. G. Esteves da Silva (✉)
Centro de Investigação em Química, Departamento de Química e Bioquímica, Faculdade de Ciências da Universidade do Porto, R. Campo Alegre 687,
4169-007 Porto, Portugal
e-mail: jcsilva@fc.up.pt

carbon targets immersed in water and the carbon dots that these nanoparticles originate after functionalization with PEG_{200} and mercaptosuccinic acid (MSS).

Experimental section

Functionalization of the carbon dots

All chemicals were purchased from Sigma Aldrich and were used without further purification.

The synthesis of the carbon nanoparticles was performed by laser ablation [UV pulsed laser irradiation (248 nm, KrF)] of carbon targets immersed in deonized water [12]. The carbon nanoparticles obtained by laser ablation are not fluorescent and the following activation/functionalization process is necessary to render them fluorescence [13]: (i) 20 mL of the water solution with the carbon nanoparticles dispersed plus 20 mL of HNO_3 (0.1 M) was refluxed for 12 h in order to activate the carbon nanoparticles surface; (ii) afterwards it was added 20 mL of PEG_{200} and the mixture continue refluxing for 28 h; (iii) after 28 h it was added 2.650 g of mercaptosuccinic acid (MSS) and left refluxing for more 31 h. The color of the solution evolves from colorless to light brown. The obtained carbon dots solution was extracted six times with ethyl acetate in order to eliminate unreacted reagents. 1 mL of this purified solution was diluted to 100 mL water which constituted the sensing solution used throughout the work. For the solvent analyses the carbon dots were dried in vacuum for 2 h resulting in a viscous light brown liquid.

pH and ion titrations

The pH response was obtained through an acid-base titration of the sensing solution with HCl 0.1 M and NaOH 0.1 M. For testing the carbon dots sensitivity towards heavy metals the pH of the sensing solution was adjusted to 6.4± 0.1 using a phosphate buffer solution and the addition of micromolar quantities of all metal ions did not change this value.

Standard aqueous solutions of $Hg(NO_3)_2$, $Pb(NO_3)_2$, $CdCl_2$, $Cu(NO_3)_2$, $NiCl_2$, $CoCl_2$, KI and $Zn(NO_3)_2{\cdot}4H_2O$ from Merck, were prepared in water with concentrations of 5.00×10^{-4} M. Aliquots of these standard solutions were added to 20 mL of a carbon dots solution at pH 6.4–25 mL of the sensing solution and 25 mL of phosphate buffer solution at pH 6.4. For all ion solutions, except iodide, the range of concentrations were between 1.00×10^{-7} and 2.69×10^{-6} M. Iodide concentrations were: 9.70×10^{-4}, 2.90×10^{-3}, 4.83×10^{-3}, 6.75×10^{-3}, 8.66×10^{-3}, 1.06×10^{-2}, 1.15×10^{-2}, 1.34×10^{-2}, 1.53×10^{-2}, 1.72×10^{-2} and 1.90×10^{-2} M.

To perform the dynamic light scattering (DLS) analysis the solutions of carbon dots was diluted in water and passed through two continuous 0.2 μm Fischer Scientific RC filters.

Instrumentation

Fluorescence excitation emission matrices (EEM) [excitation between 300 to 600 nm and emission between 350 to 700 nm] were recorded with a Horiba Jovin Yvon Fluoromax 4 TCSPC using an integration time of 0.1 s and a slit of 5 nm. The emission fluorescence measurements were acquired using the Horiba Jovin Yvon Fluoromax 4 TCSPC using an excitation of 330 nm and an emission range of 300–650 nm, with an integration time of 0.1 s and a slit of 5 nm.

Lifetime measurements were recorded with a Horiba Jovin Yvon Fluoromax 4 TCSPC using the following instrumental settings: 368 nm NanoLED; time range, 200 ns; peak preset 10,000 counts; repetition rate at 1 MHz; synchronous delay of 50 ns. Quartz cells were used.

The size distribution of carbon dots in water was determined by dynamic light scattering analysis using a Malvern Instruments (Malvern, UK) Zeta Sizer Nano ZS, using disposable polystyrene cells from Sigma.

Data analysis

Lifetime deconvolution analysis was done using Decay Analysis Software v6.4.1 (Horiba Jovin Yvon). Fluorescence decays were interpreted in terms of a multiexponential model:

$$I(\mathrm{t}) = \mathrm{A} + \Sigma\,\mathrm{B_i}\,\exp(-t/\tau_i)$$

where B_i are the pre-exponential factors and τ_i the decay times. The fraction contribution (percentage of photons) of each decay time component is represented by P_i.

The variations in the fluorescence intensity of the carbon dots resulting from the ionization reaction can be linearized using a Henderson-Hasselbalch type equation which allows the calculation of the pK_a.

$$\mathrm{pH} = \mathrm{p}K_\mathrm{a} + \log[(I_{\max.} - I)/(I - I_{\min.})]$$

where $I_{max.}$ and $I_{min.}$ are respectively the maximum and minimum of the fluorescence intensity of the acid or conjugated base species and I the fluorescence intensity as function of the pH.

In this study quenching of fluorescence by ions [E(II)] was described using the Stern-Volmer equation:

$$I_\mathrm{o}/I = 1 + K_{SV}[\mathrm{E(II)}]$$

where I_o is the fluorescence intensity without ion, I is the fluorescence intensity observed in the presence of an ion

and K_{SV} is the (conditional stability constant) Stern-Volmer constant [14].

Results and discussion

Functionalization and DLS characterization

The effect of functionalization was studied by taking samples overtime. After 1 and 31 h reaction the maximum fluorescence emission remained almost constant at about 430 nm. The resulting solution obtained at 31 h reaction time contains fluorescent carbon dots functionalized with PEG_{200} and MSS. Due to the physical characteristics of PEG_{200}, electron microscopy analysis could not be performed because the sample could not be dried. Alternatively, the size dispersion of the carbon dots was characterized by DLS.

Figure 1 shows the size dispersion of the nanoparticles as a function of the reaction time. The nanoparticles obtained by direct laser ablation (Fig. 1a) have two major size dispersions at average values of 63 and 373 nm. Accordingly to the laser ablation method used (without dispersing the nanoparticles) this size dispersion feature may be due to two factors: (i) the formation of clusters in an initial phase of the ablation and the subsequent ablation of these clusters, thereby leading to two size dispersions; (ii) the particles of 373 nm may be impurities since after functionalization these particles were no longer detected.

After activation and functionalization the size distribution becomes unimodal (Fig. 2b and c). Also, the analysis of the DLS shows that the carbon dots size grows up

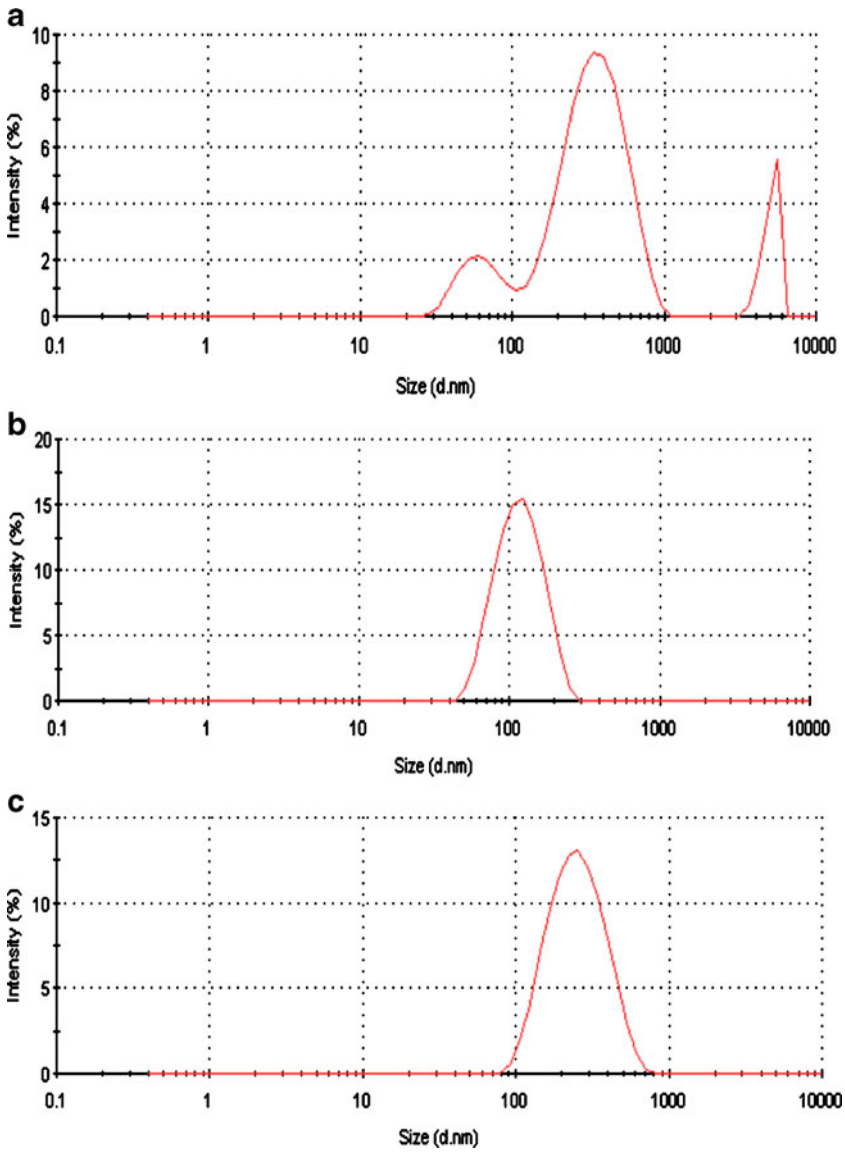

Fig. 1 DLS size dispersion of the **a** carbon nanoparticles obtained by direct laser ablation, **b** carbon dots functionalized with PEG_{200} at 31 h reaction time and, **c** carbon dots functionalized with PEG_{200} and MSS at 31 h reaction time

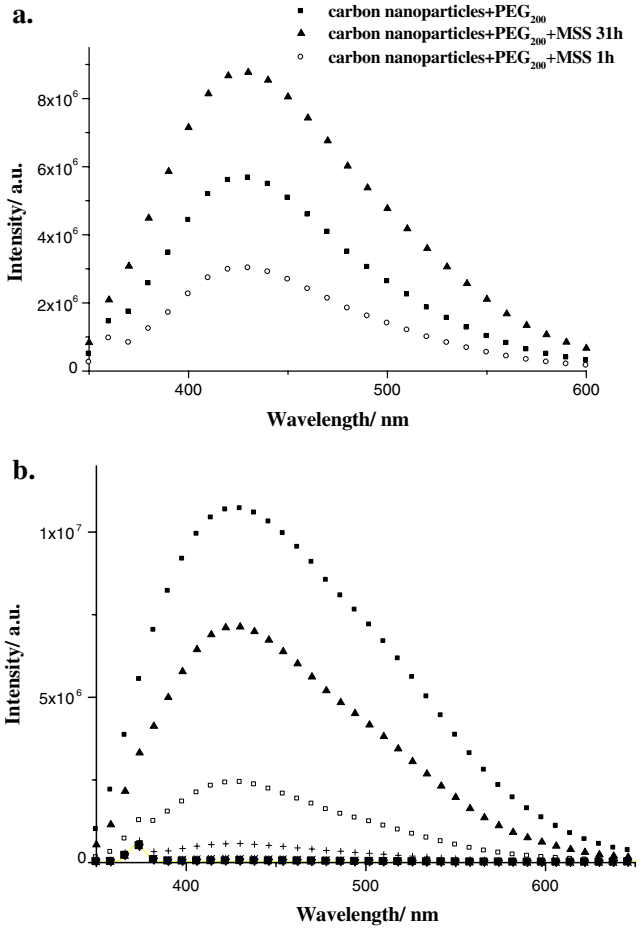

Fig. 2 **a** Fluorescence emission spectra of carbon dots functionalized with PEG_{200} at 31 h reaction, with PEG_{200} and MSS at 1 h reaction and with PEG_{200} and MSS at 31 h reaction time (excitation: 320 nm). **b** Variation of the fluorescence emission spectrum as function of the dilution of the aqueous carbon dots

accordingly with the reaction time: carbon dots + PEG_{200} 31 h - 122 nm (Fig. 1b); carbon dots + PEG_{200} + MSS 1 h - 193 nm; and, carbon dots + PEG_{200} + MSS 31 h - 267 nm (Fig. 1c).

Fluorescent properties

The emission spectra at maximum excitation (320 nm) of the synthesized carbon dots functionalized with PEG_{200} and MSS are shown in Fig. 2a. The fluorescence intensity increased with the reaction time but the maximum emission wavelength remained approximately the same at about 430 nm, which is an indication of a little variation of the quantum confinement. When the fluorescence intensity started to decrease with the reaction time, it was considered that the maximum particle size and quantum confinement was reached for that ligand and as such the reaction was stopped. The emission bands are relatively broad and the full with half maximum increases with the reaction time, namely: 87, 89 and 122 nm, respectively. Figure 2b shows that the decrease of the carbon dots concentration provokes a linear decrease of the fluorescence intensity without changing the emission wavelength.

The preliminary analysis of the decay time indicates that it is complex as it shows the presence of several lifetime ranges. Indeed, as shown in Table 1, only a three component decay time model originated a good fit for carbon dots functionalized with PEG_{200} (χ=1.08), and for carbon dots with PEG_{200} and MSS (χ=1.25) with the following lifetimes, respectively: τ_1=2.76 ns; τ_2=0.33 ns; τ_3=6.59 ns and τ_1=2.71 ns; τ_2=7.36 ns; τ_3=0.38 ns. These results show that the fluorescence lifetimes of the carbon dots were not affected after MSS functionalization. The results here obtained for carbon dots with PEG_{200} are comparable with the data reported by Sun et al. [7] for PEG_{1500}, indicating that the lifetime is also not affected by the length of the polymer in the dot surface.

Solvent, pH and ions effect on the carbon dots fluorescence

Figure 3 shows the effect of the solvent on the fluorescence properties of the carbon dots. As observed only the fluorescence intensity and not the emission wavelength is affected by solvents. This result shows that the solvent do not affect the quantum confinement of the carbon dots and only provokes the quenching of the fluorescence.

After functionalization with PEG_{200} and MSS it was possible to see a marked sensitivity of the fluorescence intensity as a function of the pH. Since both MSS and PEG_{200} are sensitive to the surrounding environmental pH, the sigmoid curve represented in Fig. 4 is broad. When we applied the Henderson-Hasselbalch equation, it was found an apparent pK_a of 7.4±0.2 and a slope of 2.1. This pH behavior is reversible. Also, as the slope is higher than 1 showing that a polyelectrolyte ionization is occurring.

However, the variation with the pH of the fluorescence intensity of the carbon dots was only observed when the titration of the sensing solution was performed with strong

Table 1 Lifetime intensity decays of carbon dots functionalized with PEG_{200} and MSS in water

Sample	N	τ_i (ns)	α_i	f_i	
Carbon dots with PEG_{200} 31 h	1	2.76(9)	0.0227(1)	42.9%	
	2	0.33(2)	0.0921(5)	20.7%	
	3	6.59(6)	0.00812(4)	36.4%	χ= 1.08
Carbon dots with PEG_{200} + MSS 31 h	1	2.71(8)	0.0227(1)	43.6%	
	2	7.36(9)	0.00634(4)	33.0%	
	3	0.38(1)	0.0870(5)	23.4%	χ= 1.25

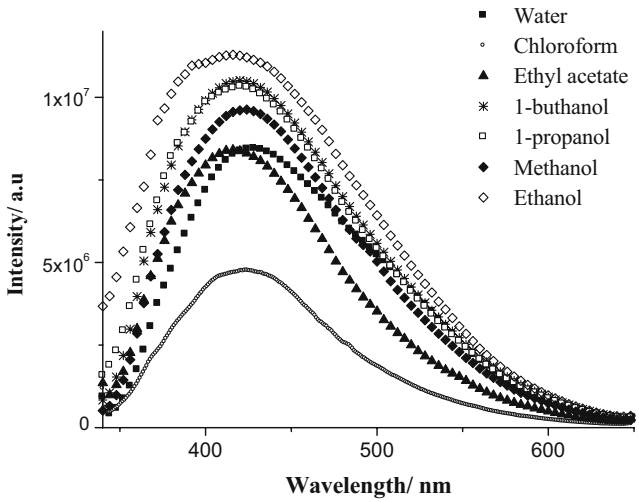

Fig. 3 Fluorescence emission spectra (excitation: 320 nm) of carbon dots functionalized with PEG_{200} and MSS at 31 h reaction time in different solvents

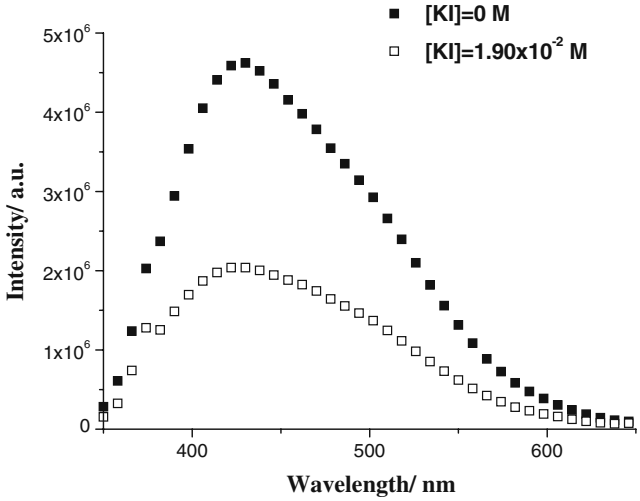

Fig. 5 Fluorescence emission spectrum (excitation: 320 nm) quenching of the carbon nanoparticles + PEG_{200} + MSS 31 h reaction time by iodide

acid and/or base. Indeed, when the same total phosphate buffer solutions with different pH values were used the fluorescence intensity did not change. This observation may be due to a stabilization effect on the dots surface charge promoted by the buffer solution.

In order to access if these carbon dots were sensitive to ions, several ion solutions of Hg(II), Cu(II), Cd(II), Ni(II), Zn(II), Ca(II) and iodide were tested.

Figure 5 shows the effect of iodide at milimolar concentration levels on the carbon dots fluorescence and it is possible to observe a marked quenching—the fluorescence signal decreases 55% upon addition of relatively high concentration of iodide (1.90×10^{-2} M). The analysis of typical Stern-Volmer plot of the I^- quenching on the carbon dots fluorescence shows that they follow a linear trend with $K_{sv}=78\pm2$ M^{-1} (Intercept = 0.92; $r=0.996$ with 12 points).

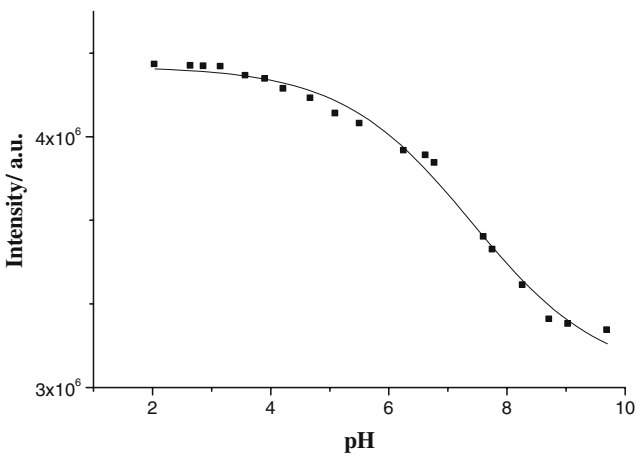

Fig. 4 Variation of the fluorescence intensity (excitation: 320 nm; emission: 430 nm) of aqueous carbon dots as function of the pH

This order of magnitude is compatible with a dynamic quenching mechanism.

The other metal ions analyzed, namely, Hg(II), Cu(II), Cd(II), Ni(II), Zn(II) and Ca(II) at micromolar concentration range show no measurable effect on the fluorescence of the carbon dots. The fact that these carbon dots remained stable in aqueous solutions and that they their fluorescence properties were not affected by the common interfering metals is an important step for the development of a non-toxic and stable nanosensor for bioimaging applications.

Conclusions

Fluorescent carbon nanoparticles (carbon dots) (with excitation at 320 and emission at 430 nm) with 267 nm dimension were easily synthesized in water and functionalized with PEG_{200} and MSS. The fluorescence intensity of the functionalized carbon dots remain stable in water and are solvent and pH sensitive. The lifetime decay of the carbon dots is complex and it is not affected by the size of the PEG chain as well as the presence of other capping agents. The fluorescence intensity of the carbon dots are not affected by the presence of micromolar quantities of metal ions but quenched (dynamic quenching) by the presence of the milimolar quantities of iodide.

Acknowledgments Financial support from Fundação para a Ciência e Tecnologia (Lisboa, Portugal) (FSE-FEDER) (Project PTDC/QUI/71001/2006) and (Project PTDC/QUI/71336/2006) is acknowledged. A PhD grant to Helena Gonçalves SFRH/BD/46406/2008 is acknowledged to Fundação para a Ciência e Tecnologia (Lisboa). P.A.S. Jorge and J.R.A. Fernandes are acknowledging for assisting the laser ablation experiments.

References

1. Cao L, Wang X, Meziani MJ, Lu F, Wang H, Luo PG, Lin Y, Harruff BA, Veca LM, Murray D, Xie SY, Sun YP (2007) Carbon dots for multiphoton bioimaging. J Am Chem Soc 129:11318
2. Yang ST, Wang X, Wang H, Lu F, Luo PG, Cao L, Meziani MJ, Liu JH, Liu Y, Chen M, Huang Y, Sun YP (2009) Carbon dots as nontoxic and high-performance fluorescence imaging agents. J Phys Chem C 113:18110
3. Yang ST, Cao L, Luo PG, Lu F, Wang X, Wang H, Mezian MJ, Liu G, Qi G, Sun YP (2009) Carbon dots for optical imaging in vivo. J Am Chem Soc 131:11308
4. Liu HP, Ye T, Mao CD (2007) Fluorescent carbon nanoparticles derived from candle soot. Angew Chem Int Ed 46:6473–6475
5. Bourlinos AB, Stassinopoulos A, Anglos D, Zboril R, Karakassides M, Giannelis EP (2008) Surface functionalized carbogenic quantum dots. Small 4:455
6. Bourlinos AB, Stassinopoulos A, Anglos D, Zboril R, Georgakilas V, Giannelis EP (2008) Photoluminescent carbogenic dots. Chem Mater 20:4539
7. Mao XJ, Zheng HZ, Long YJ, Du J, Hao JY, Wang LL, Zhou DB (2009) Study on the fluorescence characteristics of carbon dots. Spectrochimica Acta A. doi:10.1016/j.saa.2009.11.015
8. Sun YP, Zhou B, Lin Y, Wang W, Fernando KAS, Pathak P, Meziani MJ, Harruff BA, Wang X, Wang HF, Luo PG, Yang H, Kose ME, Chen B, Veca LM, Xie SY (2006) Quantum-sized carbon dots for bright and colorful photoluminescence. J Am Chem Soc 128:7756–7757
9. Ryman-Rasmussen JP (2007) Surface coatings determine cytotoxicity and irritation potential of quantum dot nanoparticles in epidermal keratinocytes. J Invest Dermatol 127:143
10. Higuchi Y (2008) Mannosylated semiconductor quantum dots for the labeling of macrophages. J Control Release 125:131
11. Faure AC, Dufort S, Josserand V, Perriat P, Coll JL, Roux S, Tillement O (2009) Control of the in vivo biodistribution of hybrid nanoparticles with different poly(ethylene glycol) coatings. Small 5:2565–2575
12. Gonçalves H, Jorge PAS, Fernandes JRA, Esteves da Silva JCGES (2010) Hg(II) sensing based on functionalized carbon dots obtained by direct laser ablation. Sens Actuactors B 145:702–707
13. Hu SL, Niu KY, Sun J, Yang J, Zhao NQ, Du XW (2009) One-step synthesis of fluorescent carbon nanoparticles by laser irradiation. J Mat Chem 19:484
14. Lakowicz JR (1999) Principles of fluorescence spectroscopy. Kluwer-Plenum, New York, Ch. 8

Chapter 5 – Optical Fiber Sensor for Hg(II) Based on Carbon Dots

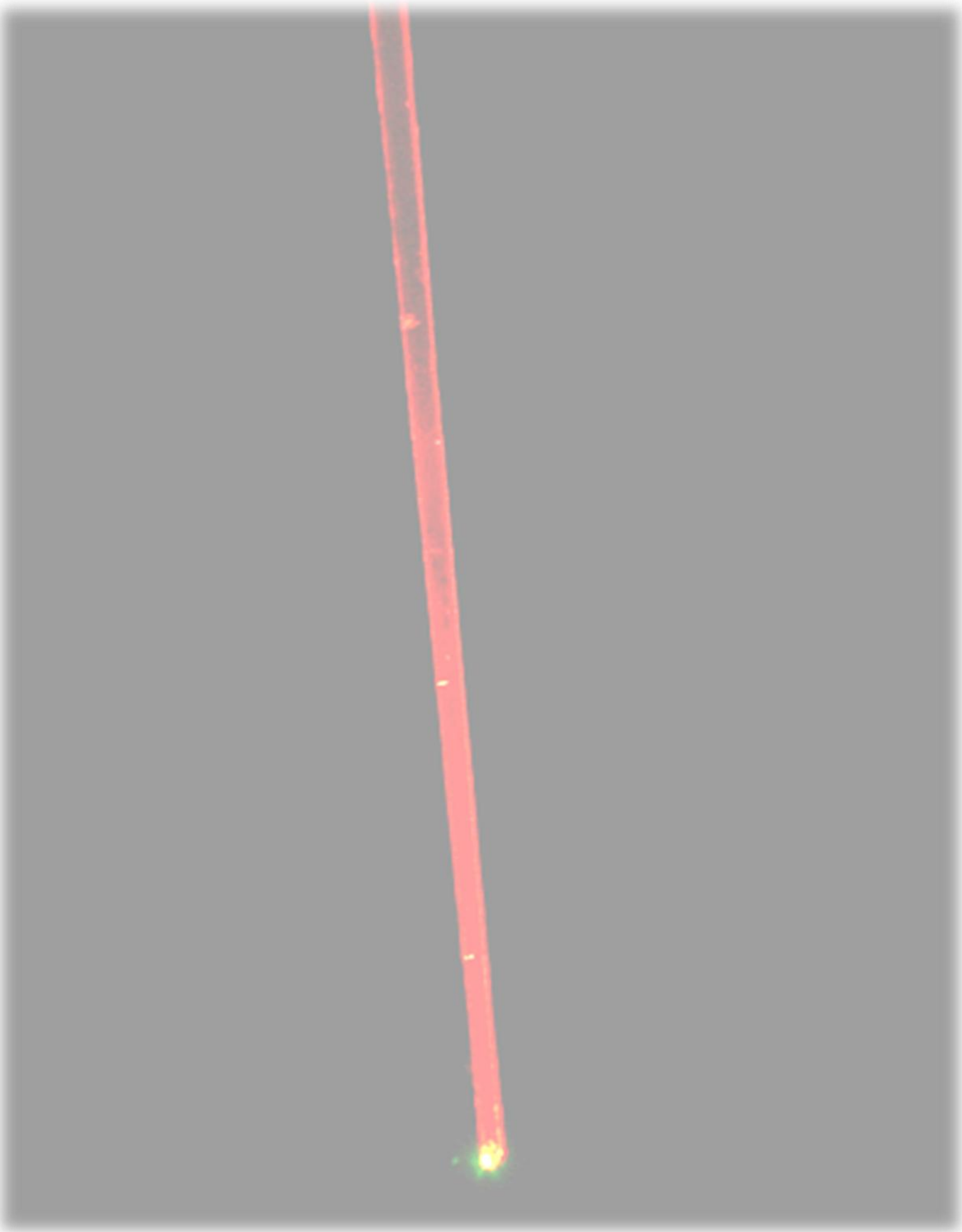

Chapter 5 – Optical Fiber Sensor for Hg(II) Based on Carbon Dots

5.1. State of the Art

Carbon dots can be targeted to a specific analyte according to the molecules on its surface. There are numerous applications for Cdots [1-3], one of which has been described in Chapter 3 – sensing of Hg(II) ion. The sensing ability described is due to its surface functionalization with N-acetyl-L-Cysteine (NAC). This residue has the biological function of capturing heavy metals, thereby helping the organism to deal with this potential threat.

Nowadays there are some good fluorescence sensors based on organic dyes that has a low detection limit. Moon *et al.,* [4] prepared a Hg(II) fluorescence sensor based upon 8-hydroxyquinoline with the detection limit of 5.00×10^{-6}M. Youn *et al.,* [5] prepared a Hg(II) fluorescent sensor based in Dimethylcyclam that proved to have a detection limit of 1.45×10^{-6} M for Hg(II).

One of the common problems for Hg(II) sensing is the possibility of other metal ion interference, namely Cu(II) and Cd(II).

In this work functionalized Cdots, that have already proven useful for Hg(II) sensing when suspended in water, will be immobilized using the sol-gel technique.

The sol-gel method is a well described process that has gathered a great number of followers over the years. The interest in this technology began in the mid-1800s with Ebelman [6] and Grahams' [7] studies on silica gels. These early investigators observed that the hydrolysis of tetraethyl ortosilicate (TEOS), $Si(OC_2H_5)_4$, under acidic conditions yielded SiO_2 in the form of a "glass-like material" [6]. This material could be coupled to optical fibers to give rise to monolithic optical lenses [8] or composites. However, extremely long drying times of one year or more were necessary to avoid the silica gels fracturing into a fine powder and, consequently, there was little technological interest [9]. Over the years the sol-gel process was investigated by several noted chemists, like Ostwald [10] and Lord Rayleigh [11] and the technique was improved.

Nowadays there are three main approaches to successfully produce sol-gel monoliths. Method 1: Gelation of a solution of colloidal powders; Method 2: Hydrolysis

and polycondensation of alkoxide or nitrate precursors followed by hypercritical drying of gels and Method 3: Hydrolysis and polycondensation of alkoxide or nitrate precursors followed by aging and drying under ambient precursor [12].

Despite the production method, in order to successfully create a sol-gel matrix with adequate polarity and porosity it is quite important to control two variables: the solution pH and the drying conditions. This can be explained by the reaction that occur throughout the chemistry of the sol-gel process:

Methods 2 and 3 both require liquid precursor such as $Si(OR)_4$, where R is CH_3, C_2H_5 or C_3H_7 and as such it passes through these three main stages: hydrolysis, condensation and polymerization.

A. Hydrolysis

In this stage the liquid precursor is hydrolyzed by mixing it with water according to the following chemical reaction:

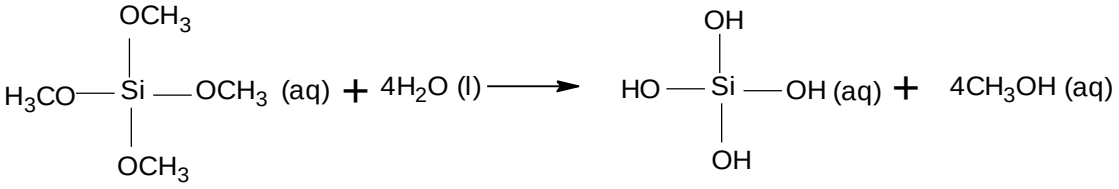

B. Condensation

The silica hydroxide suffers a condensation reaction given rise to a dimmer:

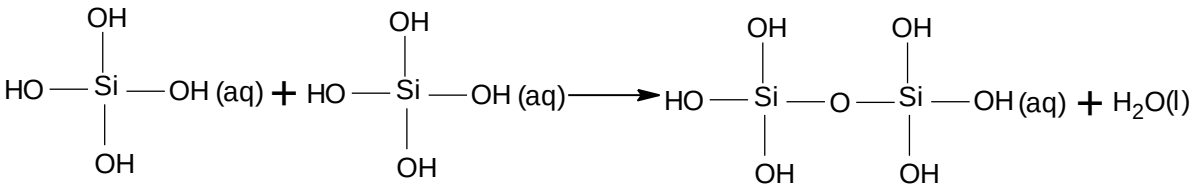

C. Polymerization

The condensation reaction continues and eventually results in a SiO_2 network, polymer.

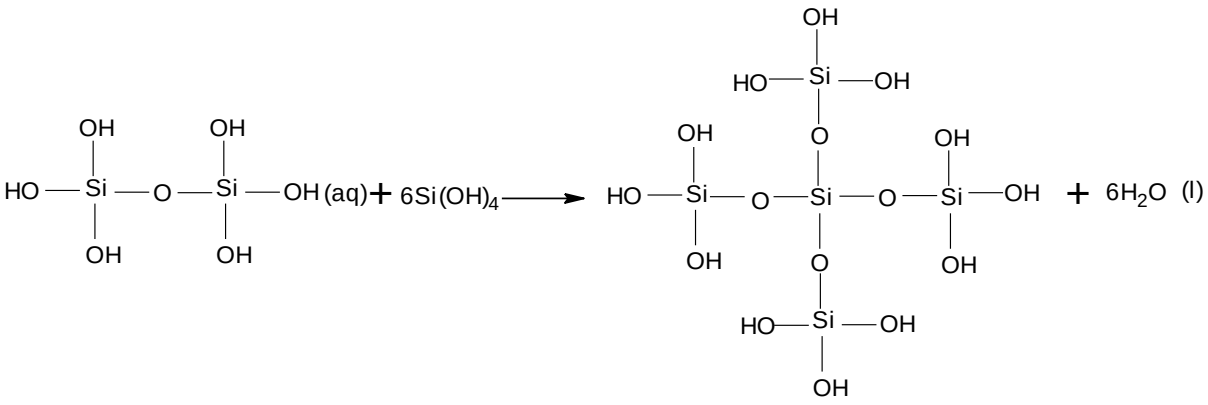

The side products, water and methanol, remain in the network pores. The size of the sol-gel particles and the cross-linking within the particles depend upon the pH and the R ratio (R= $[H_2O]$/ $[Si(OR)_4]$. Usually the pH is acid, because it is generally more simple and allows the formation of a thin transparent film [9]. Additionally, one of the most used precursors is TEOS due to its commercial availability. TEOS based materials are normally hydrophilic which enables the immobilization of a soluble sensor without chemically altering it. There are other precursors and an impressive number of combinations so that the pore size and the chemical environment/inertness inside the solid matrix is adapted to a given sensor. Indeed there are numerous factors to take into account before selecting the adequate precursors for the sol-gel entrapment. One that can be considered the first factor is the intended application of the film. In this sense if the sensor inside the matrix is a gas sensor, the film should be permeable to the gas and normally hydrophobic. It is necessary to ensure that the matrix does not interact/ forms physical bonds with the sensor, but at the same time it should retain the sensor for long periods of time. This seems to be the simplest case within the complexity of the sol-gel technique. On the other hand if the sensor reacts to species in solution it is quite more difficult to obtain a good sol-gel matrix. In this case the pore size is dramatically relevant, since the film will be immersed in a given solvent at it is possible that the sensor is removed into the solvent. Moreover the porosity adjustment needs also to take into account the size of the analyte, since it is necessary that it can penetrate the matrix completely to interact with the sensor, otherwise the decrease in the signal could be so significant that it will be hard to distinguish between the signal and the background noise of the measurement equipment. Additionally, these matrixes will suffer several hydration and drying cycles that could be responsible for cracking the film. This can be overcome by adjusting the water/ethanol ratios. On top of all the matrix needs also to be inert towards the sensor, the analyte and all the other possible species present in the analyte solution.

Taking into account all these factors it seems that the sol-gel technique is not very appealing, however this is what makes the technique interesting. Indeed it is not possible to research for a sol-gel film used successfully with a sensor and try it with a new sensor, since it requires adjustments, nonetheless this is what makes each application unique and a step further into future applications.

5.2. References

[1] Y.-P. Sun, X. Wang, F. Lu, L. Cao, M. J. Meziani, P.G. Luo, L. Gu, L.M. Veca. **2008**. "Doped Carbon Nanoparticles as a New Platform for Highly Photoluminescent Dots". J Phys Chem C Nanomater Interfaces. 112 (47), pp.18295-18298.

[2] Ray S.C., Saha A., Jana N.R., Sarkar R. **2009**. "Fluorescent Carbon Nanoparticles: Synthesis, Characterization, and Bioimaging Application". J. Phys. Chem. C 113, p. 18546-18551.

[3] Qin L., Ohulchanskyy, T.Y.; Ruili L.; Kaloian K.; Dongqing W., Andreas B., Rajiv K., Adela B.; Prasad, P.N. **2010**. "Photoluminescent Carbon Dots as Biocompatible Nanoprobes for Targeting Cancer Cells in Vitro". J. Phys. Chem. C. 114 (28), pp.12062–12068.

[4] Moon S.Y., N.R. Cha, Y.H. Kim, S.-K. Chang. **2004**. "New Hg^{2+}-Selective Chromo- and Fluoroionophore Based upon 8-Hydroxyquinoline". *J. Org. Chem.* 69 (1), pp 181–183.

[5] Youn N.J., Chang S.K. **2005**. "Dimethylcyclam based fluoroionophore having Hg^{2+} and Cd^{2+} selective signalin behaviors". *Tetrahedron Lett.* 46, pp.125–129.

[6] Ebelman M. **1846**. "Untersuchungen uber die Verbindung der Borsaure und Kieselsaure mit Aether. *Ann. Chimie Phys.* 16, pp.129.

[7] Graham T. **1864**. "On the properties of silicic acid and other analogous colloidal substances" *J. Chem. Soc.* 17, pp.318.

[8] Ebelman M. **1847**. "Sur l'hyalite artificielle et l'hydrphane". *C.R. Acad. Sci.* 25, pp.854-856.

[9] Hench L.L., West J.K. **1990**. "The sol-gel Process". *Chem. Rev.* 90, pp.33-72.

[10] Ostwald W.Z.. **1897**. "Studies on formation and transformation of solid materials". *Phys. Chem.* 27, pp.365.

[11] Iler R.K. **1955**. *"The Chemistry of Silica"*, Wiley, New York.

[12] Iler R.K. **1979**. *"The Chemistry of Silica"*, Wiley, New York.

5.3. Personal Contribution

My personal contribution to this work includes the following: establishment of an initial objective and all the necessary research to ascertain the state of the art for the sol-gel immobilization. It was then required the suiting of this knowledge to the material and equipment available. Once this was determined all the procedures for the adjustment in precursors, ratios, fiber preparation and immobilization of the sensor on the tip of the optical fiber were performed. It was also necessary to perform numerous tests on the photostability and the stability against cracking by the drying and hydration cycles. Considering the results obtained the best protocol for the sol-gel film was selected. Afterwards, it was required the preparation of the fibers by chemically etching them. The solution was then applied and the stability of the film over time before the first water immersion was studied. The fibers were then tested over more than three months towards pH and metal ion sensing. Additionally physical tests were selected and performed to better ascertain the film homogeneity and thickness. The results were interpreted and compared to the existing data provided by other research groups. Once all the data were collected it was necessary to repeat all procedures in order to ascertain if the results were reproducible. When all these procedures were repeated and the data were considered reproducible it was necessary to write a manuscript with all the necessary data for publication in an international scientific research journal and perform the necessary adjustments to comply with the reviewers suggestions.

Biosensors and Bioelectronics 26 (2010) 1302–1306

Contents lists available at ScienceDirect

Biosensors and Bioelectronics

journal homepage: www.elsevier.com/locate/bios

Optical fiber sensor for Hg(II) based on carbon dots

Helena M.R. Gonçalves [a], Abel J. Duarte [b], Joaquim C.G. Esteves da Silva [a,*]

[a] Centro de Investigação em Química, Departamento de Química e Bioquímica, Faculdade de Ciências da Universidade do Porto, Rua Campo Alegre 687, 4169-007 Porto, Portugal
[b] REQUIMTE, Instituto Superior de Engenharia do Porto, R. António Bernardino Almeida 431, 4200-072 Porto, Portugal

ARTICLE INFO

Article history:
Received 15 April 2010
Received in revised form 21 June 2010
Accepted 6 July 2010
Available online 13 July 2010

Keywords:
Carbon dots
Fiber optics
Sol–gel immobilization
Mercury(II) sensing

ABSTRACT

An optical fiber sensor for Hg(II) in aqueous solution based on sol–gel immobilized carbon dots nanoparticles functionalized with PEG_{200} and N-acetyl-L-cysteine is described. This sol–gel method generated a thin (about 750 nm), homogenous and smooth (roughness of 2.7 ± 0.7 Å) film that immobilizes the carbon dots and allows reversible sensing of Hg(II) in aqueous solution. A fast (less than 10 s), reversible and stable (the fluorescence intensity measurements oscillate less than 1% after several calibration cycles) sensor system was obtained. The sensor allow the detection of submicron molar concentrations of Hg(II) in aqueous solution. The fluorescence intensity of the immobilized carbon dots is quenched by the presence of Hg(II) with a Stern-Volmer constant (pH = 6.8) of $5.3 \times 10^5\ M^{-1}$.

1. Introduction

Carbon dots are the newest member of the quantum dot series. They are a new class of fluorescent nanoparticles that are gaining a great interest since they were first presented by Sun et al. (2006). The possibility of using the exceptional properties of the traditional quantum dots without the toxicity issues that arises from the use of a heavy metal core is of the most interest. As such, several studies have been made in this past years covering the possible functionalizations/applications (Mao et al., 2009; Yang et al., 2009a; Gonçalves et al., 2010; Gonçalves and Esteves da Silva, 2010) and the toxicity/bioaccumulation (Yang et al., 2009b) of carbon dots. So far the results have demonstrated that they enable fluorescence imaging with both one-and two-photon excitations on the same platform (Cao et al., 2007) and possess high stability over time, exceptional resistance to photo and chemical degradation, tunable fluorescence emission and excitation, high quantum yields, large Stokes shifts and they are soluble in water (Liu et al., 2007). Furthermore, carbon dots have proved to be imaging agents with a performance competitive to the traditional CdSe/ZnS quantum dots (Yang et al., 2009a).

The coupling of carbon dots with optical fibers to produce a specific and cheap nanosensor is highly interesting. The main issue to overcome in order to make this task possible is the immobilization of the carbon dots in a suitable matrix in a way that it retains all the properties that it had before and the matrix must avoid leaching of the sensor and be permeable to water and analytes. Various immobilization techniques have been applied to fiber optics, including adsorption to solid supports, covalent attachment and entrapment in polymers, but the most promising one is the sol–gel technique (Besanger and Brennan, 2006; Gupta and Chaudhury, 2007; Wang et al., 2001). Due to the porous nature of the sol–gel network, entrapped species remains accessible and can interact with external chemical species or analytes (Flora and Brennan, 2001). Sol–gel based sensors also suffer from some disadvantages, e.g., entrapment in sol–gel glass may change chemical and biological properties of the entrapped species, due to reduced degrees of freedom and interactions with the inner surface of the pores (Zink et al., 1994; Lin and Brown, 1997). Nevertheless this problem may be overcome by using a sol–gel derived matrix accordingly to the sensor under investigation. Sol–gel derived thin films are desired because of the basic requirement of short diffusion path for quick interaction and detection of the analyte molecule (MacCraith et al., 1995; Lev et al., 1995; Malins et al., 2000).

This paper presents, for the first time, the immobilization of the fluorescent nanomaterials carbon dots in a sol–gel matrix in the tip of a fiber optic. When immobilized in the optimized sol–gel membrane the carbon dots kept their photophysical and chemical properties. Indeed, the fiber optic system (sensing head) described in this paper allows reversible sensing of Hg(II) in the submicron molar concentration range in aqueous solution and remains stable after six months of use.

* Corresponding author. Tel.: +351 220 402 569; fax: +351 220 402 659.
E-mail address: jcsilva@fc.up.pt (J.C.G. Esteves da Silva).

0956-5663/$ – see front matter © 2010 Elsevier B.V. All rights reserved.
doi:10.1016/j.bios.2010.07.018

2. Experimental

2.1. Synthesis and functionalization of the carbon dots

All chemicals were purchased from Sigma Aldrich and were used without further purification. The ablation process was implemented using UV pulsed laser irradiation (248 nm, KrF) of carbon targets immersed in water.

The functionalization process was the same used by (Gonçalves et al., 2010) without further changes. The synthesis of the carbon nanoparticles was performed by laser ablation [UV pulsed laser irradiation (248 nm, KrF)] of carbon targets immersed in deonized water. The carbon nanoparticles obtained by laser ablation are not fluorescent and the following activation/functionalization process was necessary to render them fluorescence: (i) 20 mL of the water solution with the carbon nanoparticles dispersed plus 20 mL of HNO_3 (0.1 M) was refluxed for 12 h in order to activate the carbon nanoparticles surface; (ii) afterwards it was added 20 mL of PEG_{200} and the mixture continue refluxing for 28 h; (iii) after 28 h it was added 2.984 g of N-acetyl-L-cysteine (NAC) and left refluxing for more 31 h. The obtained carbon dots solution was extracted six times with ethyl acetate in order to eliminate unreacted reagents. 1 mL of this purified solution was diluted to 100 mL water which constituted the sensing solution used throughout the work.

2.2. Preparation of optical fibers

Silica optical fibers with core/cladding diameters of 600 μm were purchased from Thorlabs. The fiber tips were carefully polished and their protective coating removed with acetone followed by rinsing with deionised water. To enhance the efficiencies of excitation and collection of luminescence the fiber tips were reshaped by chemical etching (Jorge et al., 2004). By slow and controlled immersion of the tip in 40% HF a tapered probe with conical shape was obtained (in a 2-cm fiber length the diameter is reduced from 600 to approximately 200 μm) (Gonçalves et al., 2008).

2.3. Preparation of sol–gel films and sensing heads

The sol–gel matrix was prepared by the addition of 400 μL of tetraethyl orthosilicate (TEOS), 20 μL of triethoxy(octyl)silane (Oc-TriEOS), 250 μL of ethanol, 40 μL of HCl (0.1 M) and 60 μL of Triton-X. The as prepared matrix was left stirring for 45 min. Immediately after this process 400 μL of the sensing solution containing carbon dots functionalized with poly(ethylene glycol) with a molecular weight of 190–210 g/mol (PEG_{200}) and N-acetyl-L-cysteine was added to the sol–gel solution and stirred for 3 min.

Sensing fibers were prepared by immersing the prepared fiber tips in the resulting sol–gel and matrix fibers were prepared using the sol–gel preparation without sensor. All fibers were left to dry for one day, immersed in water two days and left to dry for one day previously to the beginning of the experiment. All the immobilization and drying procedures were performed at 25 °C.

2.4. Metal ion titrations

Standard aqueous solutions of $Hg(NO_3)_2$, $Pb(NO_3)_2$, $CdCl_2$, $Cu(NO_3)_2$, $NiCl_2$, $CoCl_2$, $Zn(NO_3)_2{\cdot}4H_2O$ and N-acetyl-L-cysteine from Merck, were prepared in a buffer phosphate solution (pH = 6.8), in a concentration range of 1.00×10^{-7}, 7.99×10^{-7}, 1.30×10^{-6}, 1.99×10^{-6} and 2.69×10^{-6} M.

2.5. Instrumentation

Fluorescence measurements were performed with an homemade equipment containing a stabilized light source constituted of 360 nm LEDs from Roithner Lasertechnik (Ref. NS360L-3RLQ); a CCD detector from Ocean Optics (USB4000); a 1.0 mm glass fiber optic was used to guide the light from the source to the sampling compartment; this was a black optimized compartment with a sampler were the different solutions could be put in contact with the sensing fibers; the sensing fibers also served as light guides to the detector. The integration time used was 4 s and the time series experiments were performed using a maximum emission wavelength of 498 nm. This system, schematically shown in Supplementary Fig. A, was developed in order to minimize light losses (Duarte and Esteves da Silva, 2010).

Scanning electron microscopy (SEM) and of the two sensing fibers and one matrix were done on a FEI Quanta 400FEG/EDAX Genesis X4 M High Resolution Scanning Electronic Microscope. Atomic Force Microscopy (AFM) was performed on two sensing fibers and one matrix on a Veeco Metrology Multimode/Nanoscope on a tipping mode with a RTESP-Veeco cantilever.

2.6. Quenching data analysis

The quenching of fluorescence by metal ions [M(II)] was described using the Stern-Volmer equation:

$$\frac{Io}{I} = 1 + K_{sv}[M(II)]$$

where *Io* is the fluorescence intensity without metal ion, *I* is the fluorescence intensity observed in the presence of a metal ion and Ksv is the static Stern-Volmer constant (Lakowicz, 1999).

3. Results and discussion

3.1. Carbon dots immobilization on the optical fiber

Several factors need to be accounted for in the functionalized carbon dots [Hg(II) sensor] immobilization on the optical fibers (Gupta and Chaudhury, 2007), namely: stability of the film overtime; uniformity and thickness of film; adhesion to the substrate and resistance to cracking; and, designing of stable internal environment and minimizing the potential of leaching of entrapped species.

In order to adjust the stability of the film, its uniformity, thickness and the design of a stable internal environment and to minimize the leaching of entrapped species the ratio between the precursors and ethanol was adjusted. The most promising volumetric ratios were (6.7:1:4.2:1.3), (6.7:0.33:3.7:0.67) and (6.7:0.33:4.2:0.67) of TEOS, Oc-TriEos, ethanol and HCl (0.1 M), respectively. It was still necessary to study the film resistance to cracking and different amounts of the surfactant Triton-X were added – the volumetric ratios between Triton-X and ethanol that were studied were (3.7:1), (4.2:2) and (4.2:1). The different films obtained by these mixtures were immersed in water and dried at room temperature in order to evaluate the stability and resistance to cracking. The final volumetric ratio used for film sensing was (6.7:0.33:4.2:0.67:1) of TEOS, Oc-TriEos, ethanol, HCl (0.1 M) and Triton-X, respectively. The volumetric ratio between the precursors and the sensor solution was always the same (6.7:0.33:4.2:0.67:1:6.7), however the concentration of the sensor used in the mixtures was adjusted to obtain the highest intensity signal but, at the same time, avoid inner filter effects. The sensor solutions tested in these mixtures correspond to the following dilutions in water of the concentrated sensor: (1:100), (5:100) and (25:100) – the film that yields the best results was the one with a dilution of (5:100).

The aging process of the sol–gel was also analyzed and all the parameters were tested over six months using different fibers. The aging process was analyzed in two different ways:

(i) Firstly, it was tested the aging of the sol–gel matrix before the addition of the film, in order to allow a more complete hydrolysis, and as such, smaller pore sizes, in the absence on the sensor. Before the addition of the sensor the matrix was left to stabilize in a time range between 30 min and 24 h. According to this procedure it was observed that the best stabilization time was 45 min – otherwise, sensor leaching was observed. The films were left to dry for another day and them immersed in water. This aging process was evaluated by measuring the fluorescence intensity of the water solution where the films were immersed.

(ii) Secondly, the aging influence of the film containing the sensor was also tested. Some fibers were prepared under similar conditions in the same day but their first immersion on water was performed in different following days corresponding to different film aging times. Aging times ranging from 2 h to two days were tested and it was observed that one day the optimum aging period. These parameters were evaluated by microscope observation.

The morphology and analytical properties of the optimized sensing head are described in the following sections.

3.2. Morphology analysis of the sensing film in the optical fiber

SEM analysis of the tip of the fiber optic showed a highly homogenous sensing film (Fig. 1a) with some nanometer dust particles deposited on the fibers. The analysis of a broken section of the optical fiber showed that the film thickness above the fiber optic glass was about 750 nm (Fig. 1b).

To better access the topography of the film it was performed an AFM analysis (Fig. 2). The analysis of Fig. 2a shows that the fiber optic matrix film is quite homogenous and the insertion of the sensor on the sol–gel matrix (Fig. 2b) did not change it – although the film with carbon dots become fluorescent and their fluorescence properties changes in contact with Hg(II) aqueous solutions. The roughness of both films is about 2.7 ± 0.7 å. The homogeneity of the film was only possible after the chemical etching of the optical fiber that resulted in an optimized tip (in terms of optical transmission) and smooth.

The morphology analysis of the sensing head shows that the sol–gel method generated a thin, homogenous and smooth film that should contain the immobilized sensor. The analytical performance and reversibility of this sensing head towards Hg(II) in aqueous solution will be discussed in the following section.

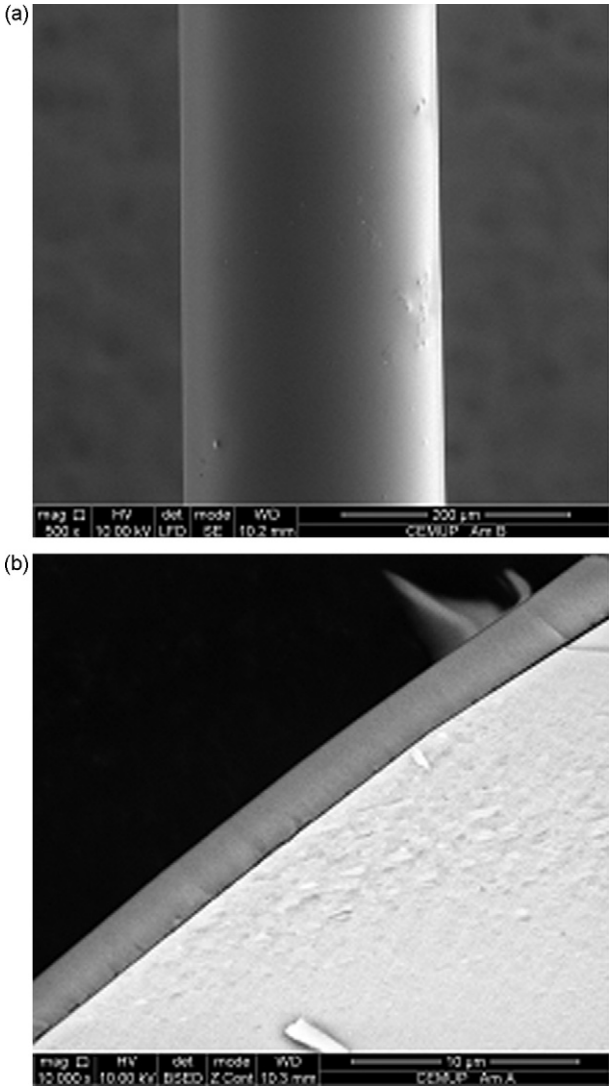

Fig. 1. SEM images of the fiber optic with the sensing film (a) and of a cross-section of a broken tip (b).

3.3. Analytical performance

Previously it has been shown that the fluorescence of carbon dots functionalized with N-acetyl-L-cysteine is quenched by Hg(II) (Gonçalves et al., 2010). Consequently, the analytical performance of the sensing head previously described towards Hg(II) in aqueous solutions was assessed at constant pH = 6.8 (phosphate buffer).

In water the maximum excitation and emission wavelengths of the carbon dots are located at 340 and 450 nm, respectively (Gonçalves et al., 2010). When immobilized in sol–gel the maximum of the emission wavelength shows a red shift to 495 nm. Similar wavelength shifts have already been observed after sol–gel immobilization of quantum dots nanoparticles probably due to the reduction of the confinement potential of the immobilized nanoparticles (Maule et al., 2010).

Fig. 3a shows the dynamic response of the fluorescence intensity of the fiber probe when dry and subjected to three cycles between six different concentrations of Hg(II) (between 0 and 2.69 μM). The analysis of this figure shows that the response time is fast and less than 10 s but a slightly fluorescence intensity decrease is detected when the fiber probe is in contact with an aqueous solution. Although each step of Fig. 3a shows a noisy response, the relative standard deviation is quite small and always less than 0.5% – for example, typical values for the zero Hg(II) concentration the average and standard deviation of the fluorescence intensity are: 9689 ± 28, 9671 ± 48 and 9739 ± 17; and, for the highest Hg(II) concentration the following typical values are observed: 8210 ± 36, 8235 ± 34 and 8122 ± 31. Taking this result into consideration the criteria for signal measurement was the average of the fluorescence intensity readings for a 90 s interval after the sensing head being immersed in the aqueous analyte solution. The analysis of the two first steps of Fig. 3a shows that the hydration of the sensing sol–gel film provokes a slight decrease of the fluorescence intensity.

The analysis of Fig. 3a also shows that the fluorescence intensity of the immobilized carbon dots is a function of the Hg(II) concentration when the tip of the optical fiber is immersed in aqueous solution and that the responses are quite reproducible and reversible. Indeed, the relative standard deviation of the average fluorescence intensities for each Hg(II) concentration for a set of several cycles is always less than 1% – for example, the average and standard deviation of three fluorescence intensities independent measurements are 9670 ± 35, 8798 ± 67 and 8189 ± 59, respectively for Hg(II) concentration of zero, 1.30×10^{-6} and 2.69×10^{-6} M. This feature was invariant for at least six months suggesting that the immobilized sensor (carbon dots) was not being leached from the membrane.

Table 1
Stern-Volmer parameters for the quenching of carbon dots sol–gel immobilized in the fiber optic by Hg(II) and Cu(II) ions[a].

Ion	K_{SV}[a] M^{-1}	Intercept[a]	R	Points	Concentration range M
Hg(II)	$(5.3 \pm 0.3) \times 10^5$	1.0 ± 0.2	0.9770	6	1.00×10^{-7}–2.69×10^{-6}
Cu(II)	$(6.3 \pm 0.3) \times 10^4$	0.99 ± 0.02	0.9750	6	1.00×10^{-7}–2.69×10^{-6}

[a] Averages and standard deviation (under parenthesis) of six independent experiences on three different fibers. R – correlation coefficient.

The quenching provoked by the Hg(II) in the sol–gel immobilized carbon dots fluorescence is described by a typical Stern-Volmer plot (Fig. 3b). The analysis of the Stern-Volmer plots show that they follow a linear trend with a $K_{sv} = 5.2(3) \times 10^5\ M^{-1}$ (Table 1). This constant is somewhat higher to that observed for these carbon dots in aqueous solution [$K_{sv} = 1.3(4) \times 10^5\ M^{-1}$] (Gonçalves et al., 2010). This result is compatible with the formation of a quite stable complexes between the carbon dots and Hg(II) inside the hydrated sol–gel matrix.

In order to check for possible interferent species on the sensing head response some common interferents were tested (Fig. 4). The analysis of Fig. 4 shows that only Cu(II) ion has a measurable quenching effect on the fluorescence intensity of the immobilized carbon dots (Table 1) which agrees with the behavior of these nanomaterials when in solution (Gonçalves et al., 2010). Consequently, the sensing probe also responds to Cu(II) but it is about ten time less sensible to this ion than to Hg(II). The analysis of the Stern-Volmer plots for the Cu(II) quenching show that they follow a linear trend with a $K_{sv} = 6.3(3) \times 10^4\ M^{-1}$ (Table 1) which similar to that observed in aqueous solution [$K_{sv} = 5.6(8) \times 10^4 M^{-1}$] (Gonçalves et al., 2010).

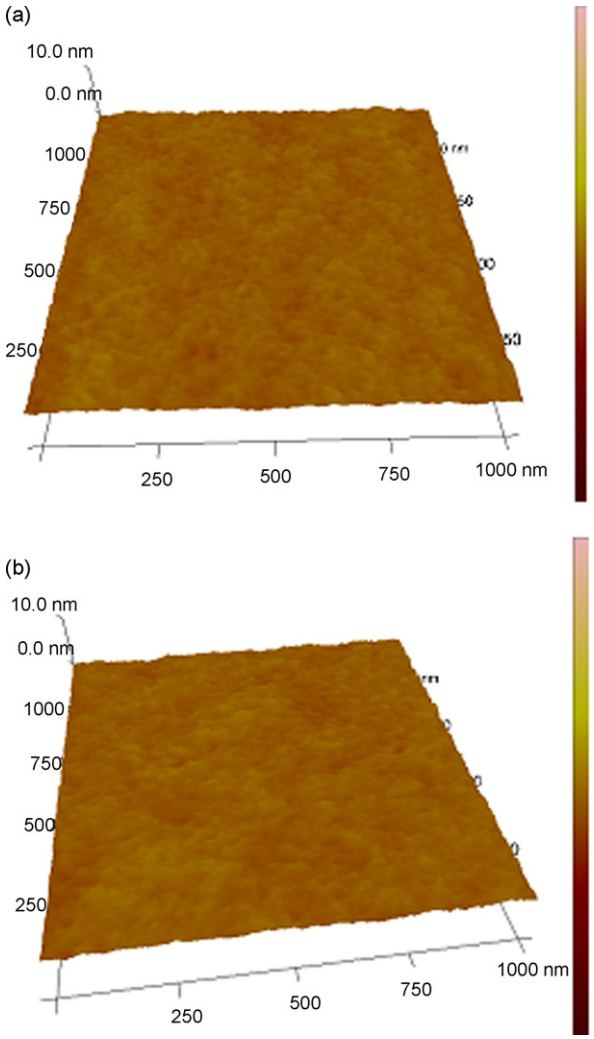

Fig. 2. Three-dimensional amplification of the AFM image of the optical fiber without (a) and with the sensing film (b).

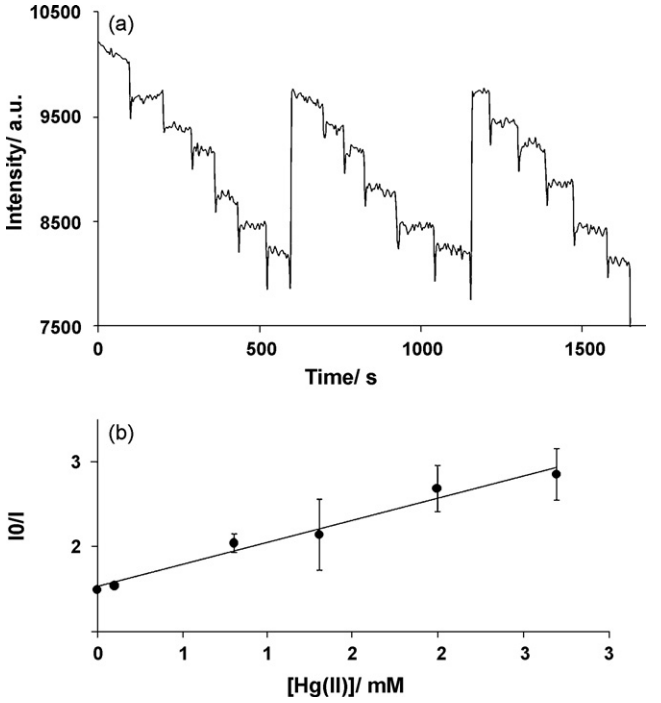

Fig. 3. (a) Steady-state fluorescence measurements (excitation 360 nm and emission 498 nm) of the dry optic fiber sensing head followed by three cycles of Hg(II) aqueous solutions with the following concentrations: 0, 0.1, 0.799, 1.30, 1.99 and 2.69 μM. (b) Stern-Volmer plot of the quenching of the fluorescence of the sol–gel immobilized carbon dots by Hg(II) ion.

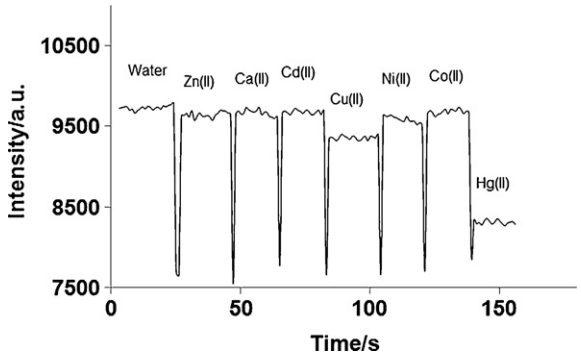

Fig. 4. Steady-state fluorescence quenching (excitation 360 nm and emission 498 nm) of the optic sensing head with different interfering ions at 2.69 μM.

4. Conclusions

An optical fiber sensor for Hg(II) in water based on carbon dots immobilized on an optimized sol–gel matrix was obtained. The sensor is reversible and stable with a fast response time. The sol–gel matrix was successfully optimized allowing the immobilization of

carbon dot based sensor without affecting its physico-chemical properties.

With the homemade instrumental setup used in this work to assess the analytical potential of the carbon dots based fiber optical sensor, a submicron molar concentrations detection of Hg(II) in aqueous solution was achieved. Probably lower Hg(II) aqueous concentrations can be detected if a higher system sensitivity is obtained by using more powerful light sources and more sensible detectors.

This fiber optic sensor system has a quite interesting analytical potential because the carbon dots nanoparticles are non-toxic and biocompatible and fiber optics are highly flexible analytical support tool.

Acknowledgements

Financial support from Fundação para a Ciência e Tecnologia (Lisboa) (FSE-FEDER) (Project PTDC/QUI/71001/2006) is acknowledged. A PhD grant to Helena Gonçalves SFRH/BD/46406/2008 is acknowledged to Fundação para a Ciência e Tecnologia (Lisboa). P.A.S. Jorge and J.R.A. Fernandes are acknowledged for assisting the laser ablation experiments.

Appendix A. Supplementary data

Supplementary data associated with this article can be found, in the online version, at doi:10.1016/j.bios.2010.07.018.

References

Besanger, T.R., Brennan, J.D., 2006. Journal of Sol–Gel Science and Technology 40 (2–3), 209–225.
Cao, L., Wang, X., Meziani, M.J., Lu, F., Wang, H., Luo, P.G., Lin, Y., Harruff, B.A., Veca, L.M., Murray, D., Xie, S.Y., Sun, Y.P., 2007. Journal of American Chemical Society 129 (37), 11318–11319.
Duarte, A.J., Esteves da Silva, J.C.G., 2010. Sensors 10 (3), 1661–1669.
Flora, K.K., Brennan, J.D., 2001. Chemistry of Materials 13 (11), 4170–4179.
Gonçalves, H., Esteves da Silva, J.C.G., 2010. Journal of Fluorescence, doi:10.1007/s10895-010-0652-y.
Gonçalves, H., Jorge, P.A.S., Fernandes, J.R.A., Esteves da Silva, J.C.G., 2010. Sensors and Actuators B 145 (2), 702–707.
Gonçalves, H.M.R., Maule, C.D., Jorge, P.A.S., Esteves da Silva, J.C.G., 2008. Analytica Chimica Acta 626 (1), 62–70.
Gupta, R., Chaudhury, N.K., 2007. Biosensors and Bioelectronics 22 (11), 2387–2399.
Jorge, P.A.S., Caldas, P., Rosa, C.C., Oliva, A.G., Santos, J.L., 2004. Sensors and Actuators B 103 (1–2), 290–299.
Lakowicz, J.R., 1999. Principles of Fluorescence Spectroscopy. Kluwer-Plenum, New York (Chapter 8).
Lin, J., Brown, C.W., 1997. Trends Analytical Chemistry 16 (4), 200–211.
Liu, H.P., Ye, T., Mao, C.D., 2007. Angewandte Chemie International Edition 46 (34), 6473–6475.
MacCraith, B.D., McDonagh, C.M., O'Keeffe, G., McEvoy, A.K., Butler, T., Sheridan, F.R., 1995. Sensors and Actuators B 29 (1–3), 51–57.
Malins, C., Glever, H.G., Keyes, T.E., Vos, J.G., Dressick, W.J., MacCraith, B.D., 2000. Sensors and Actuators B 67 (1–2), 89–95.
Mao, X.J., Zheng, H.Z., Long, Y.J., Du, J., Hao, J.Y., Wang, L.L., Zhou, D.B., 2009. Spectrochimica Acta A 75 (2), 553–557.
Maule, C., Gonçalves, H., Mendonça, C., Sampaio, P., Esteves da Silva, J.C.G., Jorge, P., 2010. Talanta 80 (5), 1932–1938.
Sun, Y.P., Zhou, B., Lin, Y., Wang, W., Fernando, K.A.S., Pathak, P., Meziani, M.J., Harruff, B.A., Wang, X., Wang, H.F., Luo, P.G., Yang, H., Kose, M.E., Chen, B., Veca, L.M., Xie, S.Y., 2006. Journal of American Chemical Society 128 (24), 7756–7757.
Yang, S.T., Cao, L., Luo, P.G., Lu, F., Wang, X., Wang, H., Mezian, M.J., Liu, G., Qi, G., Sun, Y.P., 2009a. Journal of American Chemical Society 131 (32), 11308–11309.
Yang, S.T., Wang, X., Wang, H., Lu, F., Luo, P.G., Cao, L., Meziani, M.J., Liu, J.H., Liu, Y., Chen, M., Huang, Y., Sun, Y.P., 2009b. Journal of Physical Chemistry C 113 (42), 18110–18114.
Wang, P., Dai, S., Waezsada, S.D., Tsao, A.Y., Davison, B.H., 2001. Biotechnology and Bioengineering 74 (3), 249–255.
Zink, J.I., Valentine, J.S., Dunn, B., 1994. New Journal of Chemistry 18 (10), 1109–1115.

Chapter 6 – Layer-by-Layer Immobilization of Carbon Dots Fluorescent Nanomaterials on Single Optical Fiber

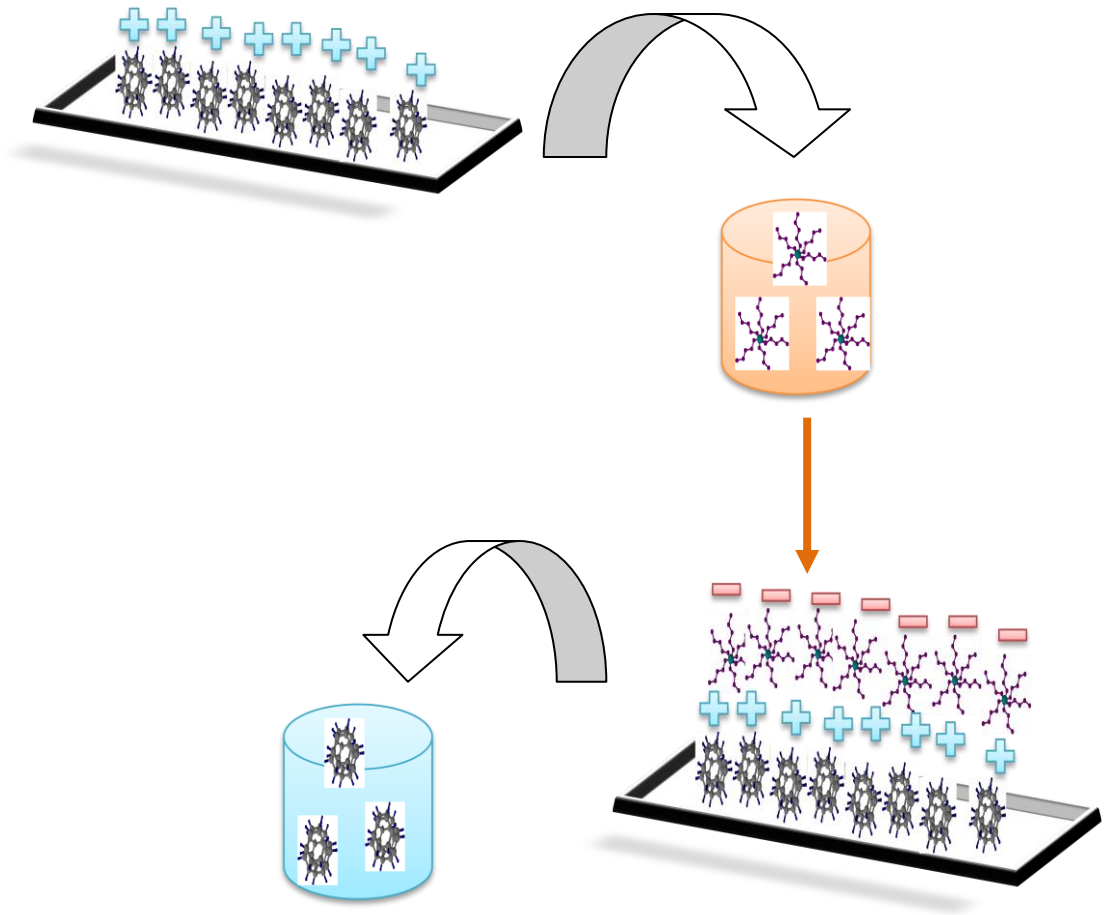

Chapter 6 – Layer by Layer Immobilization of Carbon Dots Fluorescent Nanomaterials on Single Optical Fiber

6.1. State of the Art

The layer-by-layer technique has been used extensively over the last few years for the deposition of discrete layers of multiple compounds. It was first introduced by Iler in 1966 [1] and ever since then it has been gathering numerous supporters. Biomedical research has taken this technique as a very good alternative to all existing immobilization techniques. In this sense polyelectrolyte multilayer films (PEM) have been described for applications, such as, implantable device coatings, drug delivery systems, gene therapy and 3D biomimetic cell/biomaterial constructs [2-5].

The popularity of this technique is associated with its simplicity and versatility. Indeed, the concept that lies beneath this deposition method makes it possible to apply it to several biomolecules and nanoparticles. This technique is based on charge interactions, therefore it only requires that the nanoparticles have an electric charge. The nanoparticles are deposited in discrete layers that are spaced with an adequate polymer with an electric charge opposite to the nanoparticle, as it is possible to see in Fig. 6.1. The basic process involves dipping a charged substrate into a dilute aqueous solution of a polyelectrolyte (A) and allowing it to be adsorbed and reverse the charge of the substrate. When this process is finished the substrate with the polyelectrolyte (A) is carefully washed several times and then immersed in another polyelectrolyte solution (B). It is left there for a controlled amount of time, in order to allow the polyelectrolyte B, with an opposite charge of A, to adsorb. The overall charge is changed again and this process can be repeated numerous times to obtain discrete layers of the nanoparticles interspaced with an polyelectrolyte.

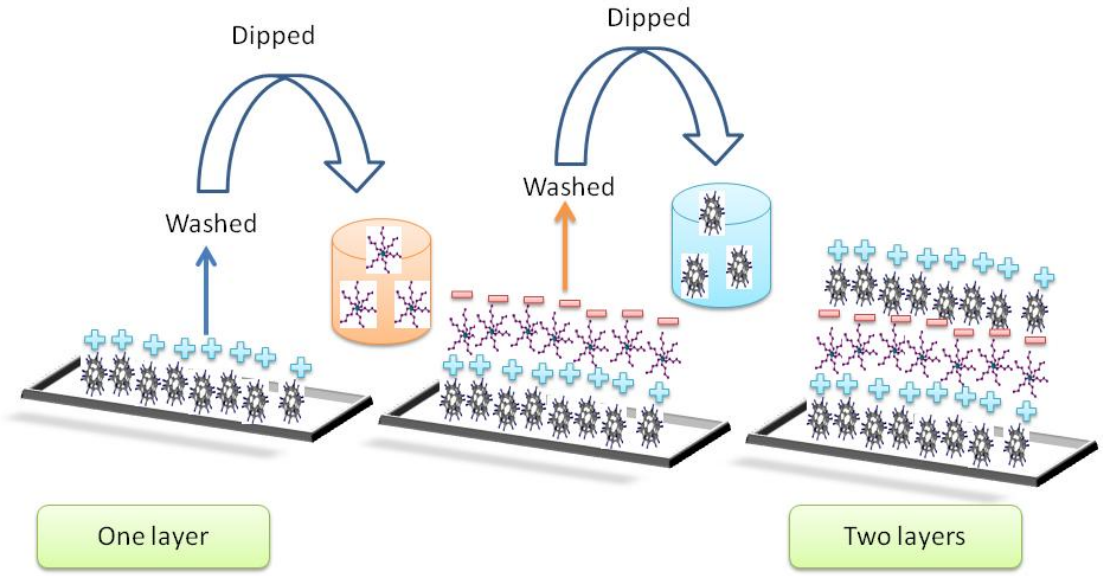

Fig.6.1– Scheme representing the layer-by-layer deposition method with all the steps required in order to obtain a good and homogenous film of discrete sensor layers.

The layer-by-layer unique characteristics make it quite appealing. Features, such as, robustness and minimal setup, along with the potential to modulate surface chemical, physical and structural properties at the nanoscale by adjusting, for example, the solution composition, pH, ionic strength, number of deposited layers, dipping and rinsing times, film post-treatment and the relative manufacture low cost. Additionally it is also possible to introduce a large panoply of molecules into the multilayer in a programmed sequence thereby adding new functionalities [6].

This technique present some important advantages over others that are now popular in the multilayered immobilization area. Indeed, for example, the advantage of spontaneous adsorption allows its application independently of size, shape, topography or topology of the molecule/nanoparticle that needs to be immobilized. Furthermore since the process occurs by adsorption there it no need to develop complex reactions with accurate stoichiometric control to assure a good deposition [7].

The layer-by-layer technique is still in the crib stage, there is a pressing need for the development of new polyelectrolytes with controlled features that are essential to this deposition method. Properties, such as, controlled charge density, charge location and functionality are very important and necessary to further develop this methodology. Moreover the development of polyelectrolytes that enable the adsorption from nonaqueous solutions, competitive adsorptions to prepare mixed layers and chemical reaction of adsorbed layers, are possible directions that only require advances in the polyelectrolytes synthesis [8].

The possibility of depositing thin layers of a given sensor (molecule/nanoparticle), without the need to adjust several parameters to avoid our sensor to lose its sensing properties is quite appealing. This was one of the reasons that pushed the following work forward.

6.2. References

[1] Iler R. K. **1966**. “Multilayers of colloidal particles”. *J. Colloid Interface Sci. 21*, pp.569−594.

[2] Bertrand P., Jonas A., Laschewsky A., Legras R. **2000**. “Ultrathin polymer coatings by complexation of polyelectrolytes at interfaces: suitable materials, structure and properties”. *Macromol. Rapid Commun. 21*, pp.319−348.

[3] Boudou T., Crouzier T., Ren K.F., Blin G., Picart C. **2010**. “Multiple functionalities of polyelectrolyte multilayer films: new biomedical applications”. *Adv. Mater. 22*, pp.441−467.

[4] Schlenoff J.B. **2009**. “Retrospective on the future of polyelectrolyte multilayers”. *Langmuir. 25*, pp.14007−14010.

[5] Ariga K., Hill J.P., Ji Q.M. **2007**. “Layer-by-layer assembly as a versatile bottom-up nanofabrication technique for exploratory research and realistic application”. *Phys. Chem. Chem. Phys. 9*, pp.2319−2340.

[6] He L.Z., Dexter A.F., Middelberg A.P.J. **2006**. “Biomolecular engineering at interfaces”. *Chem. Eng. Sci. 61*, pp.989−1003.

[7] Chen W., McCarthy T.J. **1997**. “Layer-by-Layer Deposition: A Tool for Polymer Surface Modification”. Macromolecules. 30, pp. 78-86.

[8] Dias A.J., McCarthy T.J. **1987** “Introduction of carboxylic acid, aldehyde, and alcohol functional groups onto the surface of poly(chlorotrifluoroethylene)” Macromolecules. 20, pp. 2068-2076.

6.3. Personal Contribution

My personal contribution to this work includes the following: establishment of an initial objective and all the necessary research to ascertain the state of the art on the layer-by-layer technique. Afterwards it was necessary to prepare the fibers by chemical etching and prepare more Cdots functionalized and purified to send to Scotland, where Dr. Frank Davis performed the immobilization. It was then necessary to perform some initial analysis on the fibers and adjust the protocols in order to increase the fluorescence intensity signal and adapt our sensing system to correctly measure the Cdots fluorescence through fibers. Some new fibers and Cdots samples were sent and immobilized. Subsequently, the fibers were tested against photostability and leaching. When all these procedures produced acceptable results the fibers were tested towards pH and metal ion sensitivity over some months. The results were interpreted and compared to the existing data provided by other research groups. When all these procedures resulted in a reproducible method it was necessary to write a manuscript with all the necessary data for publication in an international scientific research journal and perform the necessary adjustments to comply with the reviewers suggestions.

Analytica Chimica Acta 735 (2012) 90–95

Contents lists available at SciVerse ScienceDirect

Analytica Chimica Acta

journal homepage: www.elsevier.com/locate/aca

Layer-by-layer immobilization of carbon dots fluorescent nanomaterials on single optical fiber

Helena M.R. Gonçalves[a], Abel J. Duarte[b], Frank Davis[c], Seamus P.J. Higson[c], Joaquim C.G. Esteves da Silva[a,*]

[a] Centro de Investigação em Química, Departamento de Química, Faculdade de Ciências da Universidade do Porto, R. Campo Alegre 687, 4169-007 Porto, Portugal
[b] REQUIMTE, Instituto Superior de Engenharia do Porto, R. António Bernardino Almeida 431, 4200-072 Porto, Portugal
[c] Cranfield Health, Cranfield University, Bedford MK43 0AL, UK

HIGHLIGHTS

- Fluorescent single fiber optic sensor.
- Carbon dots fluorescent nanoparticles.
- Fiber optic carbon dot based Hg(II) sensor.
- Sensor immobilized by the layer-by-layer technique.

GRAPHICAL ABSTRACT

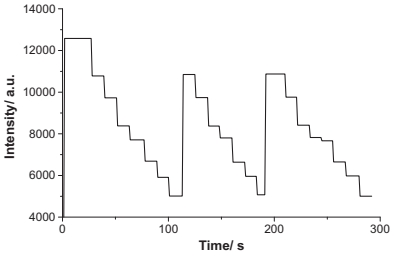

ARTICLE INFO

Article history:
Received 1 February 2012
Received in revised form 11 May 2012
Accepted 13 May 2012
Available online 22 May 2012

Keywords:
Carbon dots
Nanoparticles
Layer-by-layer immobilization
Single optical fiber
Mercury sensor

ABSTRACT

We report within this paper the development of a fiber-optic based sensor for Hg(II) ions. Fluorescent carbon nanoparticles were synthesized by laser ablation and functionalized with PEG_{200} and N-acetyl-L-cysteine so they can be anionic in nature. This characteristic facilitated their deposition by the layer-by-layer assembly method into thin alternating films along with a cationic polyelectrolyte, poly(ethyleneimine). Such films could be immobilized onto the tip of a glass optical fiber, allowing the construction of an optical fluorescence sensor. When immobilized on the fiber-optic tip, the resultant sensor was capable of selectively detecting sub-micromolar concentrations of Hg(II) with an increased sensitivity compared to carbon dot solutions. The fluorescence of the carbon dots was quenched by up to 44% by Hg(II) ions and interference from other metal ions was minimal.

1. Introduction

Carbon dots are recently discovered nontoxic fluorescent nanoparticles with high biocompatibility [1,2]. With fluorescence properties comparable with the traditional quantum dots they have been gathering much attention over the last five years [2–4]. One of the most interesting feature of this nanomaterial is the simplicity of functionalization procedures with several different molecules that can impart a specific functionality [5]. In this context these systems have found applications in bioimaging [2,6,7], white light emitting devices [8] and sensors [2,9–12].

The use of thin single optical fibers combined with immobilized fluorescence sensors is a challenging analytical chemistry area. Indeed, the fragile nature of the exposed fiber tip and the reduced surface area for sensor immobilization of the optical fiber are some of the problems responsible for optical fiber detection that have been reported so far. Some of these issues can be overcome if high quantum yield fluorescent sensors are used and carbon dot nanomaterials possess this characteristic. However, in order to obtain analytically useful fluorescent signals, the concentration of

* Corresponding author. Tel.: +351 220 402 569; fax: +351 220 402 659.
E-mail address: jcsilva@fc.up.pt (J.C.G. Esteves da Silva).

0003-2670/$ – see front matter © 2012 Elsevier B.V. All rights reserved.
http://dx.doi.org/10.1016/j.aca.2012.05.015

the sensor in the tip of the fiber optic should be relatively high – which can be achieved by a suitable immobilization procedure. The immobilized sensing film should moreover be physically stable and allow fast and reversible sensor responses.

Layer-by-layer immobilization procedures allow the construction of thin films of charged materials which are stable and can be constructed with precise control of thickness and constitution [13,14]. Basically a solid surface can be chemically modified in order to be electrostatically charged. Exposure to a solution of species with multiple opposite charges, such as, a polyelectrolyte or multiply charged particle leads to a spontaneous assembly of a monolayer of this species. Further treatment with a second opposing charged polyelectrolyte causes the deposition of a second layer on top of the first. This process can be repeated to form multilayers containing a precise number of layer upon almost any substrate [13,14]. Many uses for these films are being investigated, and in this context for example they can be used in the construction of biosensors [15] or to build up lattices of semiconducting nanoparticles [16].

The layer-by-layer technique [13,14] has been used for a number of applications, such as, the construction of biosensors [15] and inorganic lattices of semiconductor nanoparticles such as CdS or ZnS [16]. However the use of this technique to produce optical fiber sensors based on carbon dots has never been performed.

In this paper we report the Hg(II) sensing performed by carbon dots immobilized in the tip of an optical fiber using the layer-by-layer deposition method. The previously described sol–gel technique [11] requires that the matrix is adapted to each fluorophore characteristics, since it needs to take into account the pore size and the affinity toward water, among other factors. Additionally the sol–gel film requires more care in fabrication in order to guarantee that the film does not break. With this technique it is possible to immobilize the sensing film on any substrate, regardless of its size. It is also an advantage that since the analyte is not required to pass through any matrix before interacting with the carbon dots, this allows an increase in the sensor availability, which is reflected in an increase in the sensor sensitivity. Also, since it should not be dependent on the diffusion of the analyte across a solid matrix, it also allows a more rapid time response.

2. Experimental

2.1. Synthesis of the carbon dots

The carbon dots were synthesized by laser ablation of a carbon target immersed in water. They were then functionalized and purified according to the procedure previously described [9] to and the solution thereby obtained used for the immobilization procedures.

2.2. Preparation of optical fibers

Silica optical fibers with core/cladding diameters of 600 μm were purchased from Thorlabs. The fiber tips were carefully polished and their protective coating removed with acetone followed by rinsing with deionized water. To enhance the excitation and collection of luminescence efficiencies the fiber tips were reshaped by chemical etching. By slow and controlled immersion of the tip in 40% HF for two hours a tapered probe with conical shape was obtained (in a 2-cm fiber length the diameter is reduced from 600 to approximately 200 μm) [17].

2.3. Immobilization of the carbon dots on the optical fiber

Immediately before immobilization, the fibers were immersed for 30 min in a 1:1:4 mixture of 25% ammonia solution, 30% hydrogen peroxide solution and water, thereby further cleaning and leaving the surface covered with Si—OH groups, rendering it relatively anionic in nature. After rinsing with water they were then placed in a 2 mg mL^{-1} solution of poly(ethyleneimine) (Sigma, MW = 50,000) for 30 min to deposit a layer of the polycation. The fibers were then rinsed in water and immersed into a concentrated solution of carbon dots [9] for 30 min to allow deposition of a layer of the nanoparticles. This process could be repeated to give alternating polymer/nanoparticles multilayers containing 1–6 layers of carbon dots. Finally the samples were dried and stored at room temperature until analysis.

2.4. pH and metal ion titrations

Standard aqueous solutions of $Hg(NO_3)_2$, $Pb(NO_3)_2$, $CdCl_2$, $Cu(NO_3)_2$, $NiCl_2$, $CoCl_2$, $Zn(NO_3)_2{\cdot}4H_2O$ and N-acetyl-L-cysteine (NAC) from Merck, were prepared in phosphate buffer (pH = 6.8) with concentrations of 0.0100, 0.0500, 0.100, 0.799, 1.99 and 2.69 μM. For the pH measurements the fibers were immersed in phosphate buffers in a pH range of 2.0–8.0. The fibers were exposed initially to a pH buffer solution of 2.0, then immersed in deionized water before exposition to another pH buffer solution. This procedure was performed in cycles where each cycle represents the fibers response to the complete pH range.

The metal ion titrations where performed in a similar way as reported for pH measurements. The dry fibers were initially measured to access their fluorescence intensity. They were then left in water for 5 min to allow a good hydration of the film – this was found to be the optimal time for this step. Afterwards the fibers were exposed to increasing metal sensing solutions and, in between each metal solution they were immersed in water to remove any analyte from the fiber surface. When an entire cycle was performed (from dry up to metal concentrations of 2.69 μM) the fiber was used consecutively for other cycles.

2.5. Instrumentation

Fluorescence measurements were performed using homemade equipment containing a stabilized light source constituted of 380 nm LEDs from Roithner Lasertechnik (Ref. LED360-01); a cut-off filter of 400 nm; a CCD detector from Ocean Optics (USB4000); a 1.0 mm glass fiber optic to guide the light from the source to the sampling compartment; this was a black optimized compartment with a sampler were the different solutions could be put in contact with the sensing fibers; the sensing fibers also served as guides until the detector. The integration time used was 1 s and the time series experiments were performed using a maximum emission wavelength of 500 nm. This system was developed in order to minimize light losses.

The carbon dots were characterized by SEM on a FEI Quanta 400FEG/EDAX Genesis X4M High Resolution Scanning Electronic Microscope and by TEM on a Leica LEO 906E microscope. Optical fibers were characterized by Atomic Force Microscopy (AFM) on a Veeco Metrology Multimode/Nanoscope on a tipping mode with a RTESP-Veeco cantilever. The size distribution of carbon dots in water was determined by dynamic light scattering (DLS) analysis using a Malvern Instruments (Malvern, UK) Zeta Sizer Nano ZS, using disposable polystyrene cells from Sigma.

2.6. Calculation

In this study static quenching of fluorescence by metal ions [M(II)] was described using the Stern–Volmer equation:

$$\frac{I_0}{I} = 1 + K_{SV}[\mathrm{M(II)}]$$

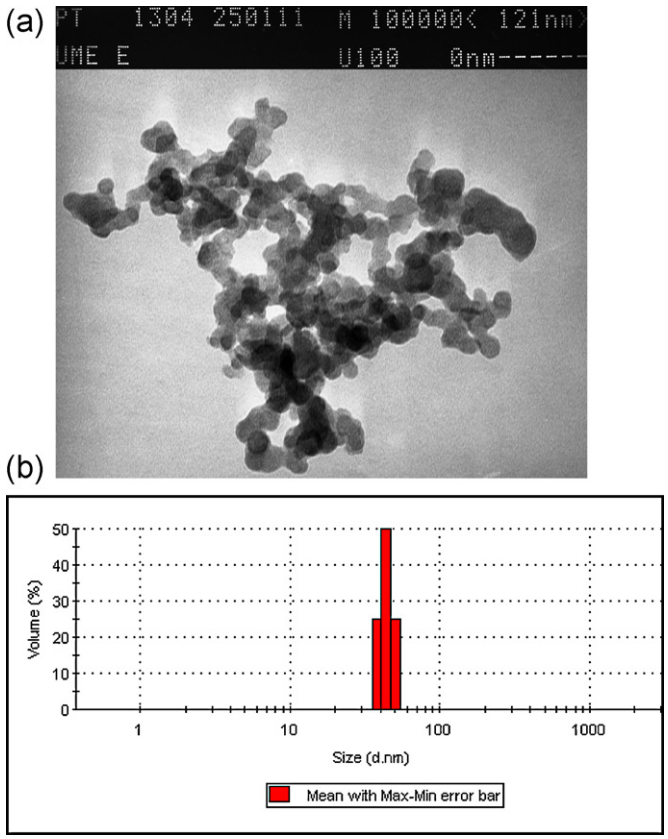

Fig. 1. TEM image of the raw carbon dots produced by laser ablation (a) and DLS representation of the functionalized carbon dots (b).

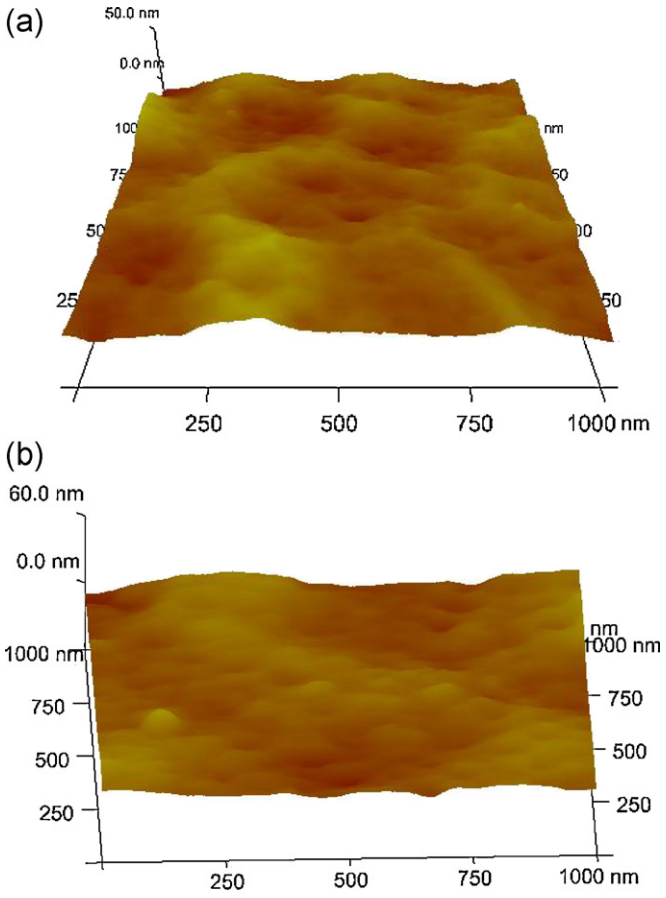

Fig. 2. Three dimensional representation of the AFM image of the optical fiber without the sensing film (a) and six layers (b).

where I_o is the fluorescence intensity without metal ion, I is the fluorescence intensity observed in the presence of a metal ion and K_{SV} is the static (conditional stability constant) Stern–Volmer constant [18].

The variations in the fluorescence intensity of carbon dots with the solution pH can be linearized using a Henderson–Hasselbalch type equation which allows the calculation of an apparent p*K*a.

$$\frac{I_o}{I} = 1 + K_{SV}[\mathrm{M(II)}]$$

where I_{max} and I_{min} are respectively, the maximum and minimum of the fluorescence intensity of the acid or conjugated base species and I is the fluorescence intensity as a function of the pH.

3. Results and discussion

3.1. Sensor morphological characterization

The raw carbon dots (obtained directly from the laser ablation, before any functionalization procedures) were characterized by SEM and TEM (Fig. 1a) where it was found that the smaller particles had diameters up to about 20 nm. After functionalization the carbon dots were analyzed by TEM [12] and DLS and their diameter was estimated (Fig. 1b) to be 44 nm.

The carbon dots solutions (concentrated and diluted) were deposited on the tip of several optical fibers activated using poly(ethyleneimine) as described above. On each fiber a different number of sensor layers from 1 to 6, were deposited and their response was evaluated over time. All fibers were prepared with concentrated solutions of carbon dots.

The fibers with and without the sensor were characterized by AFM analysis. In this analysis it was possible to observe points of depression on the fibers without (Fig. 2a) and with (Fig. 2b) the sensor. These points are defects on the fibers most likely due to their pre-treatment with HF and even though all fibers were prepared at the same time using the same etching solution it is not possible to guarantee that the defects are exactly the same. Since the particularity of each defect affects the efficiency of light transmission of the fiber it is possible to interpret the fluctuations of the maximum intensity (Table 1) not as an increase – due to the increase in carbon dots – but as a random behavior since these effects were not controlled. Also from the analysis of AFM it was possible to find a trend between the film roughness and the number of deposited layers. The roughness tends to decrease with the number of layers (7.39; 4.32; 4.09; 3.26; 2.25 nm for one, two, four and six layers, respectively). These results are consistent to the one observed previously with a sol–gel film [8]. Since the deposition by sol–gel was performed by dip coating and the film thickness was approximately 700 nm, the defects on the fiber were not detected, with the film being found to have a roughness of 2.7 ± 0.7 Å. Previous workers [13,14] have reported on the ability of films deposited by the layer-by-layer technique to bridge over or smooth out defects in the solid substrates onto which they have been deposited.

3.2. Fluorescence mechanism

The fluorescence mechanism of carbon dots has yet to be completely determined, however it is commonly accepted that it has a component due to surface defects and quantum confinement [19,20]. Carbon dots present several surface defects that can act as energy traps, that along with the confinement due to its size is responsible for its fluorescence. Upon functionalization with

Table 1
Quenching effect and Stern–Volmer parameters of the carbon dots functionalized with PEG_{200} and NAC, immobilized in the tip on an optical fiber, when exposed to Hg(II) aqueous solutions in the following concentrations: 0, 0.01, 0.05, 0.1, 0.799, 1.99 and 2.69 μM.[a]

Property	Immobilization method					
	Solution [9]	Sol–gel [11]	1 layer	2 layers	4 layers	6 layers
Max. Int./u.a.	–	–	13,319	8681	11,212	10,704
Min. Int./u.a.	–	–	10,853	6847	7602	6020
%Q[a]	(25 ± 1)	(15 ± 4)	(19 ± 3)	(21 ± 2)	(32 ± 2)	(44 ± 3)
K_{SV}[a]/(× 10^5) M^{-1} Hg(II)	(1.3 ± 0.4)	(5.3 ± 0.3)	(0.76 ± 0.09)	(0.89 ± 0.01)	(1.6 ± 0.1)	(2.6 ± 0.2)
Intercept[a]	(0.97 ± 0.01)	(1.0 ± 0.2)	(1.02 ± 0.01)	(1.04 ± 0.02)	(1.03 ± 0.02)	(1.1 ± 0.5)
R	0.9719	0.9770	0.9860	0.9833	0.9844	0.9786
K_{SV}[a]/(× 10^4) M^{-1} Cu(II)	(5.6 ± 0.8)	(6.3 ± 0.3)	(0.50 ± 0.07)	(0.69 ± 0.09)	(1.3 ± 0.2)	(2.8 ± 0.3)
Detection limit/(× 10^{-6}) M	0.1	0.1	0.1	0.07	0.05	0.01
Concentration range/(× 10^{-6}) M	(0.1–2.69)	(0.1–2.69)	(0.01–2.69)	(0.01–2.69)	(0.01–2.69)	(0.01–2.69)

[a] Averages and standard deviation (under parenthesis) of six independent experiences on three different fibers. R – correlation coefficient.

different molecules it was found that there is a shift in the emission wavelength along with an increase in the fluorescence intensity. When the carbon dots are exposed to different Hg(II) ion concentrations, its fluorescence is quenched. In order to better understand this effect, the carbon dots in the different phases of the carbon dots of functionalization were exposed to Hg(II). It was found that from, raw carbon dots, carbon dots functionalized with PEG_{200} and carbon dots functionalized with PEG_{200} and NAC only carbon dots functionalized with NAC were sensitive toward the Hg(II). As such, since NAC treatment leads to the carbon dots surface being coated with —SH groups it is possible to say that this sensitivity is due to an interaction between this groups and Hg(II) ions.

3.3. Analytical sensing characterization

Each fiber was tested over a period of two weeks and passed through a number of hydration and drying cycles. It was observed that despite the numerous drying and hydration cycles the fibers did not present a loss in signal and the solutions where they were immersed had no residual fluorescence. Again this corresponds with previous work [13,14] reporting the high physical and chemical stability of many of the different types of layer-by-layer films. The presence of surface defects on the optical fiber has a measurable influence on the background noise. Since it was established by AFM that an increasing number of layers led to a decrease in roughness it is unsurprising that the fiber with least background noise is that containing 6 layers of carbon dots. Fig. 3 represents an average of the results obtained over three independent cycles gathered over six days. In each cycle the fibers were exposed to different Hg(II) concentrations and in between each concentration the fiber was immersed in water to remove any Hg(II) excess from the fiber surface. The analysis of this figure can be performed in two ways: (i) within each cycle and (ii) across cycles. Upon analysis of the results obtained within the same cycle it is possible to say that the variation of the fluorescence intensity, for each analyte concentration is almost constant. In fact, the average fluorescence intensity and standard deviation, in the first cycle, e.g., for: 0, 0.01, 0.05, 0.1, 0.799, 1.99 and 2.69 μM of Hg(II), respectively, is: (14,580 ± 41), (12,777 ± 47), (11,728 ± 25), (10,379 ± 25), (9708 ± 82), (8685 ± 10), (7910 ± 17) and (7012 ± 13). The fibers were first immersed in water and then immersed in different concentrations of Hg(II), as we can see in Fig. 3. In point (1), the fiber was immersed in water and left to stabilize for a few seconds, afterwards the fiber was removed (point 2) and immersed in a Hg(II) sensing solution (point 3). The cycle continued by removing the fiber from the sensing solution and immersing it in another solution of higher concentration. When analyzing the data across the three consecutive cycles it becomes apparent that not only is the

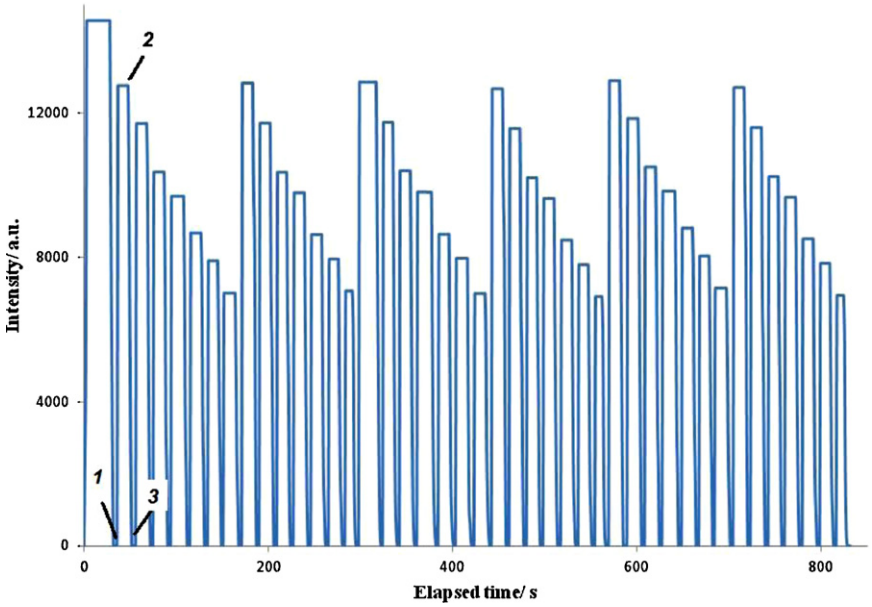

Fig. 3. Steady-state fluorescence measurements over time (excitation 380 nm and emission 500 nm) of the dry optical fiber with six layers, followed by three cycles of Hg(II) aqueous solutions with in the following concentrations: 0, 0.01, 0.05, 0.1, 0.799, 1.99 and 2.69 μM. (1) The fiber was immersed in water, (2) removed from water, and (3) immersed in Hg(II) 0.01 μM.

sensor is highly reversible – the average standard deviation for the same analyte concentration has a maximum of 30 and a minimum of 2 for Hg(II) concentrations of 0.1, 0.799 μM, respectively, while also demonstrating a rapid sensor response.

The use of carbon dots as fluorescent metal sensors represents an advantage over the use of organic dyes, since among other things they are more photostable. However it is not easy to design a sensor specific to Hg(II) in small concentrations since Cu(II) ions are common interferents in fluorescence measurements of mercury. The use of carbon dots immobilized by the layer-by-layer technique allowed a lower detection limit than the one previously demonstrated for these metals. For example, Moon et al. [21] prepared a fluorescence sensor based upon 8 hydroxyquinoline as a Hg(II) fluorescence sensor with the detection limit of 5×10^{-6} M. Youn and Chang [22] prepared a different Hg(II) fluorescent sensor that detected both Hg(II) and Cu(II), with a detection limit of 1.45×10^{-6} M for Hg(II).

The sensor was shown to display pH sensitivity probably due to the NAC groups introduced onto the carbon dots being ionized to different extents according to the media pH and influencing the confinement energy of the nanoparticles. A trend between the decrease in the fluorescence intensity as the pH increases was found for all fibers. In Fig. SI.1 is the representation of the Henderson–Hasselbach linearization of a fiber with one layer of carbon dots. Through the analysis of this figure, it was possible to obtain an apparent p*K*a of 4.4 ± 0.1 and a slope of 1.6, which is consistent with the results obtained for a carbon dots solution [9]. This slope is an indication that the carbon dots undergo a polyelectrolyte type of ionization behavior, and since there is only one layer of carbon dots, this is perhaps the closest we can get to understand the ionization behavior of a single carbon dot. As is was observed for the Hg(II) sensing the pH behavior is reversible. In fact, in both cases, the sensor response is only limited by the time acquisition of the setup used (1 s).

In Fig. 4 it is possible to see the difference between the Hg(II) quenching on the optical fiber with one (Fig. 4a) and six carbon dot layers (Fig. 4b). The results of the fluorescence steady-state measurements are summarized in Table 1.

From the observation of Table 1 it is possible to see an interesting trend of the quenching effect (*Q*) with the number of layers. In fact the quenching effect increases with the number of layers of carbon dots on the tip of the optical fiber. Also when comparing the results of the sensor immobilized layer-by-layer with the ones for solution and using the sol–gel technique, it is possible to observe that even with only one layer the fluorescence quenching by Hg(II) is more pronounced than previously reported [9,11]. This is probably a consequence of the availableness of the carbon dots to interact with the analyte when immobilized in discrete layers within such a thin film. Also these results demonstrate that quenching occurs throughout the multilayer, not just in the top layer and also that as the layer thickness increase, the quenching actually becomes more pronounced thereby indicating the formation of a more regular structure with increasing thickness and more reproducible behavior for the carbon dots. These results thereby demonstrate that this immobilization method allows three different things:

(i) The number of layers allows to overcome the irregularity of the surface fibers upon the necessary etching procedure.
(ii) A remarkable improvement of the sensor time response.
(iii) An increase in the sensitivity, since it led to a decrease in the detection limit, from 0.1 μM (in solution/sol–gel) to 0.01 μM (layer-by-layer deposition). Furthermore the fiber with six layers of carbon dots has the highest response to analyte and represents an increase in quenching effect of 29% when compared to the solution [9].

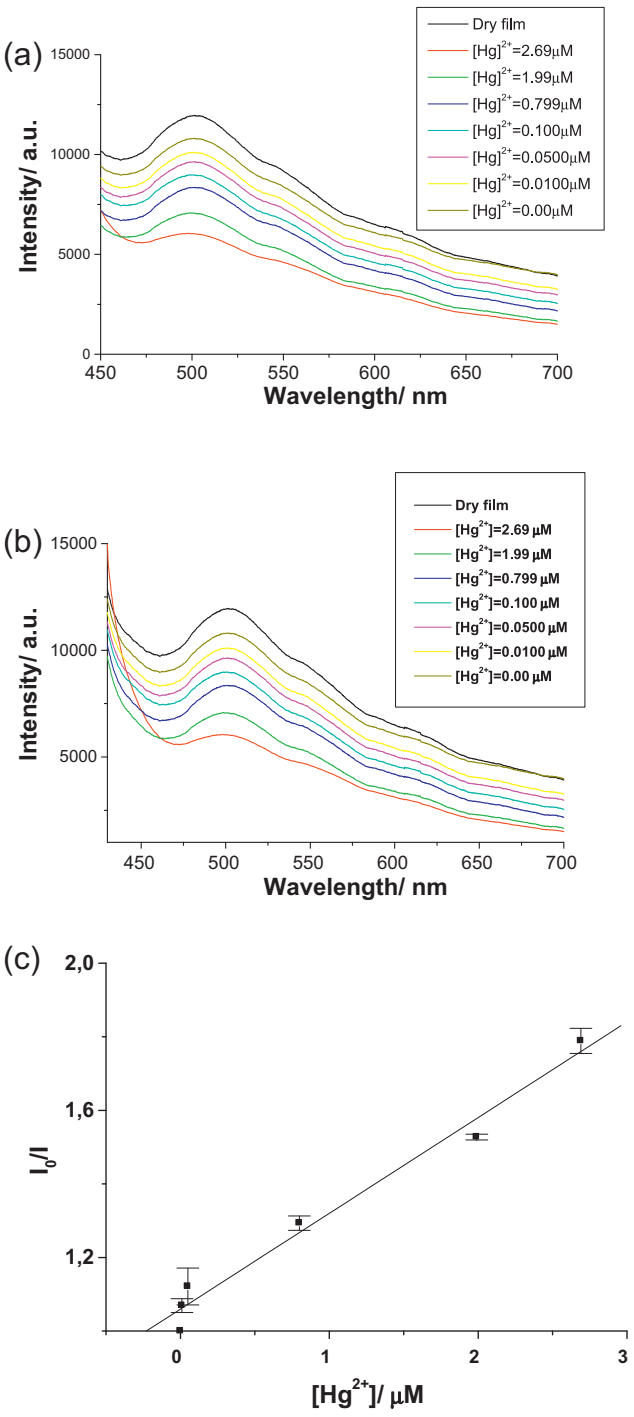

Fig. 4. Steady-state fluorescence measurements (excitation 380 nm and emission 500 nm) of the dry optical fiber and with Hg(II) aqueous solutions in the following concentrations: 0, 0.01, 0.05, 0.1, 0.799, 1.99 and 2.69 μM with (a) one layer and (b) six layers. (c) Stern–Volmer plot of the fluorescence quenching of the carbon dots immobilized in the tip of the optical fiber with six layers by Hg(II).

Interference from other metal ions can be a major challenge for any metal ion sensor and therefore the fiber-optic sensor was exposed to solutions of a range of potential ionic interferents, the results of which are shown in Fig. SI.2.

As previously observed for both solution and upon immobilization in sol–gel, the major interferent is the Cu(II) ion. Nevertheless the quenching effect of this ion for the fiber with six layers, e.g. (*Q* = 12%) is much lower compared to the Hg(II) quenching (*Q* = 44%)

for the same fiber. These results suggest a high selectivity of these carbon dots toward Hg(II) ions.

4. Conclusions

In summary the Hg(II) optical sensor based on carbon dots described here, demonstrates a detection limit of 0.01 μM, a rapid response toward the analyte, as well as extremely high reproducibility and reversibility. The use of the layer-by-layer deposition method allowed the immobilization of an optimal number of layers which both minimized the background noise due to imperfections on the fiber surface, as well as, leading to an increase in sensor sensibility due to the availability of the carbon dots to interact with the analyte. Since this immobilization method does not require an adjustment of the matrix porosity but only that the carbon dots can become negatively charged, it is potentially possible to couple this Hg(II) sensor with another sensor of interest, that has an different emission profile, and thereby measure more than one parameter at the same time. In addition to this the potential availability of a wide range of organic compounds which could be used instead of N-acetyl-L-cysteine to stabilize the carbon dots allows the possibility of tailoring these nanoparticles to sense a wide range of analytes simply by changing the stabilizer.

Acknowledgements

Financial support from Fundação para a Ciência e a Tecnologia (FCT, Lisbon) (Programa Operacional Temático Factores de Competitividade (COMPETE) e comparticipado pelo Fundo Comunitário Europeu FEDER) (Project PTDC/QUI/71001/2006) is acknowledged. A PhD grant to Helena Gonçalves SFRH/BD/46406/2008 is acknowledged to Fundação para a Ciência e Tecnologia (Lisboa).

Appendix A. Supplementary data

Supplementary data associated with this article can be found, in the online version, at http://dx.doi.org/10.1016/j.aca.2012.05.015.

References

[1] Y.-P. Sun, B. Zhou, Y. Lin, W. Wang, K.A.S. Fernando, P. Pathak, M.J. Meziani, B.A. Harruf, X. Wang, H. Wang, P.G. Luo, H. Yang, M.E. Kose, B. Chen, M. Veca, Su-Yuan. Xie, J. Am. Chem. Soc. 128 (2006) 7756.
[2] J.C.G. Esteves da Silva, H. Gonçalves, Trends Anal. Chem. 30 (2011) 1327.
[3] S.T. Yang, L. Cao, P.G. Luo, F. Lu, X. Wang, H. Wang, M.J. Mezian, G. Liu, G. Qi, Y.P. Sun, J. Am. Chem. Soc. 131 (2009) 11308.
[4] S.T. Yang, X. Wang, H. Wang, F. Lu, P.G. Luo, L. Cao, M.J. Meziani, J.H. Liu, Y. Liu, M. Chen, Y. Huang, Y.P. Sun, J. Phys. Chem. C 113 (2009) 18110.
[5] H.P. Liu, T. Ye, C.D. Mao, Angew. Chem. Int. Ed. 46 (2007) 6473.
[6] L. Cao, X. Wang, M.J. Meziani, F. Lu, H. Wang, P.G. Luo, Y. Lin, B.A. Harruff, L.M. Veca, D. Murray, S.Y. Xie, Y.P. Sun, J. Am. Chem. Soc. 129 (2007) 11318.
[7] L. Cao, P. Anilkumar, X. Wang, J.-H. Liu, S. Sahu, M.J. Meziani, E. Myers, Y.-P. Sun, Can. J. Chem. 89 (2011) 104.
[8] F. Wang, Y.H. Chen, C.Y. Liu, D. Ma, Chem. Commun. 47 (2011) 3502.
[9] H. Gonçalves, P. Jorge, J.R.A. Fernandes, J.C.G. Esteves da Silva, Sens. Actuators B 145 (2010) 702.
[10] H. Gonçalves, J.C.G. Esteves da Silva, J. Fluoresc. 20 (2010) 1023.
[11] H.M.R. Gonçalves, A.J. Duarte, J.C.G. Esteves da Silva, Biosens. Bioelectron. 26 (2010) 1302.
[12] Y. Zhang, H. Gonçalves, J.C.G. Esteves da Silva, C.D. Geddes, Chem. Commun. 47 (2011) 5313.
[13] G. Decher, Science 277 (1997) 1232.
[14] M. Schonhoff, Curr. Opin. Colloid Interface Sci. 8 (2003) 86.
[15] F. Davis, S.P.J. Higson, Biosens. Bioelectron. 21 (2005) 1.
[16] A. Suryajaya, F. Nabok, A. Davis, S.P.J. Hassan, H.J. Evans-Freeman, Appl. Surf. Sci. 254 (2008) 4891.
[17] P.A.S. Jorge, P. Caldas, C.C. Rosa, A.G. Oliva, J.L. Santos, Sens. Actuators B 103 (2004) 290.
[18] J.R. Lakowicz, Principles of Fluorescence Spectroscopy, vol. 410, Kluwer-Plenum, New York, 1999 (Chapter 8).
[19] F. Gao, Inorg. Chem. 49 (2010) 10409.
[20] J. Fan, P.K. Chu, Small 6 (2010) 2080.
[21] S.Y. Moon, N.R. Cha, Y.H. Kim, S.K. Chang, J. Org. Chem. (2004) 181.
[22] N.J. Youn, S.K. Chang, Tetrahedron Lett. (2005) 125.

Chapter 7 – Parallel Factor Analysis of EEM of the Fluorescence of Carbon Dots Nanoparticles

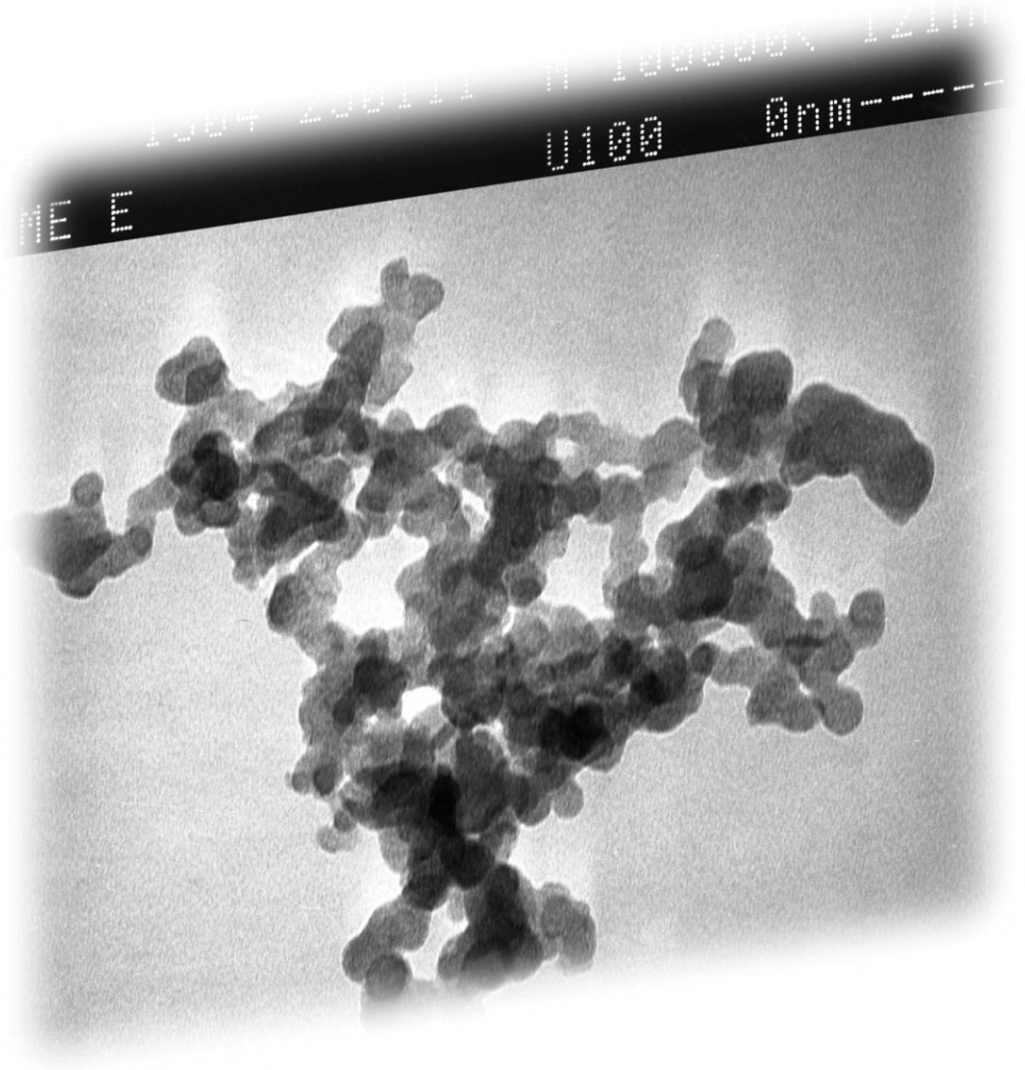

Chapter 7 – Parallel Factor Analysis of EEM of the Fluorescence of Carbon Dots Nanoparticles

7.1. State of the Art

In analytical chemistry analysis, as well as in other research areas, the number of data gathered from a given experiment can be quite large and it is necessary to analyse them in a consistent statistical manner in order to obtain all the possible information. This is possible due to chemometrics. Chemometrics can be described as the science of extracting information from chemical systems by data-driven means. It uses multivariate statistics and computational science to better understand systems in numerous areas, e.g., chemistry, biochemistry, medicine, biology, among others [1-3].

Chemometrics can be used to solve descriptive and predictive problems, according to the particularities of the system. In this sense the descriptive application is used to determine relationships and the structure of the chemical system. On the other hand the predictive application is required when it is intended the prediction of new properties or behaviors of the system.

This science is continuously being developed by research groups, indeed even though it is widely used in analytical chemistry industries, there is a need to further develop the chemometrics theory and methods in order to improve and overcome some of the drawbacks of the existing methods [4, 5].

The application of chemometrics in chemistry is relevant for many techniques, e.g., mass spectrometry, atomic emission/absorption, chromatography, fluorescence, UV/visible spectroscopy, among others, that are by nature multivariate. Thereby the application of this science allows to better extract the total amount of information that these chemical techniques provide.

7.2. References

[1] Mark H., Workman J.. 2007. “Chemometrics in spectroscopy”. Academic Press-Elsevier.

[2] Beebe K.R., Pell R.J., Seasholtz M.B. 1998. “Chemometrics: a practical guide” Wiley Ed.

[3] Leitão J.M.M., Gonçalves H.M.R., Mendonça C., Esteves da Silva J.C.G. 2008. “Multiway chemometric decomposition of EEM of fluorescence of CdTe quantum dots obtained as function of pH”. Anal. Chim. Acta. 628, pp.143-149.

[4] Gonçalves H.M.R., Mendonça C., Esteves da Silva J.C.G. 2008. “Analysis of the Quenching of EEM of Fluorescence of Glutathione Capped CdTe Quantum Dots by Pb(II)”. J. Fluorescence. 19, pp.141-154.

[5] Gemperline P.J. 2006. “Practical guide to chemometrics”. 2nd Edition, CRC Press.

7.3. Personal Contribution

My personal contribution to this work includes the following: establishment of an initial objective and all the necessary research to ascertain the state of the art for the Cdots synthesis and functionalization. It was then required the suiting of this knowledge to the material and equipment available. Once this was determined all the procedures for the synthesis, functionalization and purification of all the nanoparticles produced by laser ablation were performed. Afterwards, it was necessary to choose the nanoparticles that had the best fluorescent properties regarding to the primarily objective. Subsequently, it was required the revision of the manuscript before its submission to an international scientific research journal and perform the necessary adjustments to comply with the reviewers suggestions about the Cdots synthesis, functionalization, purification and other questions related to the experimental work.

Special Issue Article

JOURNAL OF CHEMOMETRICS

Received: 8 February 2010, Revised: 14 May 2010, Accepted: 19 May 2010, Published online 21 July 2010 in Wiley Online Library: 2010

(wileyonlinelibrary.com) DOI: 10.1002/cem.1327

Parallel factor analysis of EEM of the fluorescence of carbon dots nanoparticles

João M. M. Leitão[a], Helena Gonçalves[b] and Joaquim C. G. Esteves da Silva[b]*

The effect of experimental factors [pH and Hg(II)] on the fluorescence excitation emission matrices (EEMs) of nanosensor carbon dots (CDs) was analyzed by multiway decomposition methods based on parallel factor (PARAFAC) analysis. PARAFAC analysis of the EEM structures identifies three components corresponding to two different-sized CDs with the Hg(II) and pH profiles highly correlated plus a background. Parallel profiles with Linear Dependences (PARALIND) model with three components in the excitation–emission spectral modes and two components in the Hg(II) or pH mode gave similar results as PARAFAC, but is more useful from a theoretical point of view because PARALIND shows that the two different-sized CDs have similar chemical reactivity toward Hg(II) and pH. PARAFAC2 was used as a trilinear confirmatory test of the data structures under analysis. Copyright © 2010 John Wiley & Sons, Ltd.

Keywords: carbon dots; nanoparticles; EEM; PARAFAC; PARALIND

1. INTRODUCTION

Parallel factor (PARAFAC) analysis models are a generalization of principal component analysis (PCA) to a set of data matrices. PARAFAC model is particularly suitable for the analysis of trilinear (or multilinear) data structures and permits the decomposition of three-way (or multiway) data arrays in a unique manner, thereby allowing estimations in all modes—this property is known as the second-order advantage [1–3]. PARAFAC2 and parallel profiles with linear dependences (PARALIND) models, also based on a parallel factor analysis, were developed in order to deal with data structure specificities [4,5]. These models are a generalization of the PARAFAC model, and in some conditions, the uniqueness properties of the PARAFAC model are maintained with the two models. PARAFAC2 model deals with small deviations of trilinearity in one of the modes and with different rows (or columns) modes of the slabs in a three-way array [6,7]. PARALIND deals with linear dependences of the factors and consequently rank deficiency of the component matrices [8,9].

For the three models, the decomposition of the $\mathbf{X}_k$ ($I \times J$) slab of a three-dimensional structure $\mathbf{X}$ ($I \times J \times K$) with K slabs follows the mathematical formulation shown in Equation (1) for PARAFAC, Equation (2) for PARAFAC2, and Equation (3) for the PARALIND model. For all the equations, the matrix $\mathbf{E}_k$ holds the residuals

$$\mathbf{X}_k = \mathbf{A}\mathbf{D}_k\mathbf{B}^T + \mathbf{E}_k, k = 1, \ldots, K \quad (1)$$

In PARAFAC model (1), the matrix $\mathbf{A}$ ($I \times F$) is the first-mode loading and $\mathbf{B}$ ($J \times F$) is the loading matrix of the second mode, $\mathbf{D}_k$ is a diagonal matrix that holds the kth row of $\mathbf{C}$ matrix in its diagonal, and $\mathbf{C}$ ($K \times F$) is the third-mode loading.

$$\mathbf{X}_k = \mathbf{A}\mathbf{D}_k\mathbf{B}_k{}^T + \mathbf{E}_k = \mathbf{A}\mathbf{D}_k(\mathbf{P}_k\mathbf{H})^T + \mathbf{E}_k, k = 1, \ldots, K \quad (2)$$

In PARAFAC2 model (2), $\mathbf{A}$ ($I \times F$) is the first-mode loading, $\mathbf{B}_k$ ($J \times F$) is the kth loading matrix of the second mode, $\mathbf{D}_k$ is a diagonal matrix that holds the kth row of C in its diagonal, $\mathbf{C}$ ($K \times F$) is the third-mode loading, H is an $F \times F$ matrix, and $\mathbf{P}_k$ is a $J \times F$ orthogonal matrix (J may actually vary from *1* to K).

$$\mathbf{X}_k = \tilde{\mathbf{A}}\mathbf{D}_k\mathbf{B}^T + \mathbf{E}_k = \mathbf{A}\mathbf{H}\mathbf{D}_k\mathbf{B}^T + \mathbf{E}_k, k = 1, \ldots, K \quad (3)$$

In PARALIND model (3), $\tilde{\mathbf{A}}$ ($I \times S$) is the first-mode loading, $\mathbf{A}$ is an ($I \times R$) matrix, $\mathbf{B}$ ($J \times S$) is the loading matrix of the second mode, $\mathbf{D}_k$ is a diagonal matrix that holds the kth row of C ($K \times S$) in its diagonal, $\mathbf{C}$ ($K \times S$) is the third-mode loading, and $\mathbf{H}$ is an $R \times S$ interaction matrix defining the interactions between the R first mode loadings and the S loadings in $\mathbf{B}$ and $\mathbf{C}$.

Due to the inherent linearity of fluorescence data, PARAFAC is becoming a well-established method for the analysis of excitation emission matrices (EEMs) [10–22]. Even so, if any of the orders shows nonlinearity or some linear dependences among the factors, PARAFAC2 and PARALIND models are a good alternative to the PARAFAC model in the three-way data structure analysis. These two models are being increasingly incorporated in analytical chemistry methodologies, namely in the analysis of fluorescence data structures [7,8,13,16,20,21].

Carbon dots (CDs) are gaining a great scientific interest in biosensing applications [23] as well as bioanalytical labeling [24–27]. The reasons for this growing awareness are: their tunable luminescent optical properties (absorption and emission radiation),

* *Correspondence to: J. C. G. E. da Silva, Centro de Investigação em Química, Departamento de Química, Faculdade de Ciências da Universidade do Porto, Rua Campo Alegre 687, Porto 4169-007, Portugal*
E-mail: jcsilva@fc.up.pt

a *J. M. M. Leitão*
Laboratório de Métodos Instrumentais de Análise, Faculdade de Farmácia da Universidade de Coimbra, Centro de Estudos Farmacêuticos, Coimbra 3000-432, Portugal

b *H. Gonçalves, J. C. G. E. da Silva*
Centro de Investigação em Química, Departamento de Química, Faculdade de Ciências da Universidade do Porto, Rua Campo Alegre 687, Porto 4169-007, Portugal

high quantum yields, pronounced photostability, and good stability in water with a competitive performance as imaging agents when compared to the traditional CdSe/ZnS quantum dots (QDs) [26]. Their analytical interest results from the simple modification of the dot surface with hydrophilic capping ligands, which leads to selective analytical methodologies and the easy tunning of the fluorescent properties by increasing the size of the nanoparticles.

Nevertheless, in spite of their highly remarkable fluorescence properties, all the analytical applications involving CDs resume to a zero- or first-order instrument. Indeed, besides the high dimensional potential of fluorescence, CD applications are being developed using fluorescence intensities as function of the excitation and/or emission wavelengths. However, CDs, and fluorescent nanoparticles in general, are mixtures of different-sized materials that can show unequal fluorescent properties and sensibilities toward a particular substance. Consequently, unless mono-sized nanoparticles are being analyzed, the study of CDs or QDs can be classified as a mixture analyses problem. The intrinsic structure of the fluorescence EEMs of CDs has, up to the authors' knowledge, never been subject of analysis.

The objective of this paper is to analyze, for the first time, the intrinsic structure of EEM of CDs and evaluate the modeling performance of different parallel factor models in the study of EEM of CD nanoparticles. Parallel factor analysis by PARAFAC, PARAFAC2, and PARALIND models was used for the analysis of the pH effect and of quenching by Hg^{2+} and the performance of these models was assessed. Indeed, chemistry literature shows that there is increasing development of new fluorescent nanoparticles (nanosensors) and their analytical applications. The fields of application of these nanosensors are usually characterized by quite complex backgrounds like those found in biological systems, and a multivariate chemometric data analysis is required to fully explore the advantages of these new sensor nanomaterials.

2. EXPERIMENTAL SECTION

2.1. Synthesis of CDs

All chemicals were purchased from Sigma Aldrich and used without further purification. The synthesis of the carbon nanoparticles was performed by laser ablation [UV pulsed laser irradiation (248 nm, KrF)] of carbon targets immersed in deionized water. The carbon nanoparticles obtained by laser ablation are not fluorescent, and it is necessary to activate and functionalize them with NH_2-polyethylene glycol (PEG_{200}) and *N*-acetyl-L-cysteine to render fluorescence and sensibility to experimental factors [27].

2.2. Instrumentation

A Spex 3D Spectrofluorimeter with a 75 W xenon discharge lamp and a charge-coupled device (CCD) detector was used. EEMs were acquired in an excitation wavelength range from 200.5 to 675.1 nm and an emission wavelength range from 200.7 to 718.7 nm, with a resolution of 2 nm, slit of 0.05 mm, and integration of 3 s.

2.3. Multiway decomposition analysis

Three-way data sets of EEMs of the CDs structured as [excitation (nm) × emission (nm) × Hg concentration (M)] and [excitation (nm) × emission (nm) × pH] were analyzed using PARAFAC and PARAFAC2; three-way data structures [Hg concentration (M) × emission (nm) × excitation (nm)] and [pH × emission (nm) × excitation (nm)] were analyzed by the PARALIND model. The three-way data sets were structured changing the Hg concentration and pH. For the three-way data analysis, the raw EEMs were reduced to excitation and emission wavelength ranges of 276.6–390.8 nm (52 wavelengths) and 427.4–583.5 nm (76 wavelengths), respectively, in order to isolate the fluorescence band and eliminate the nonlinear first order Rayleigh scattering. Figure 1 shows typical experimental and analyzed EEMs.

Except for PARAFAC2 on the second mode, non-negativity constraints are applied in all the modes of the EEMs. Also for PARALIND, the dependence matrix is non-negativity constraint due to slightly better results obtained in the first mode.

PARAFAC, PARAFAC2, and PARALIND estimations are found by an iterative alternating least squares procedure. As convergence criteria, a value of 1×10^{-6} and a maximum number of 2500 iterations were used for PARAFAC; for PARAFAC2 and PARALIND a value of 1×10^{-7} and a maximum number of 2000 iterations

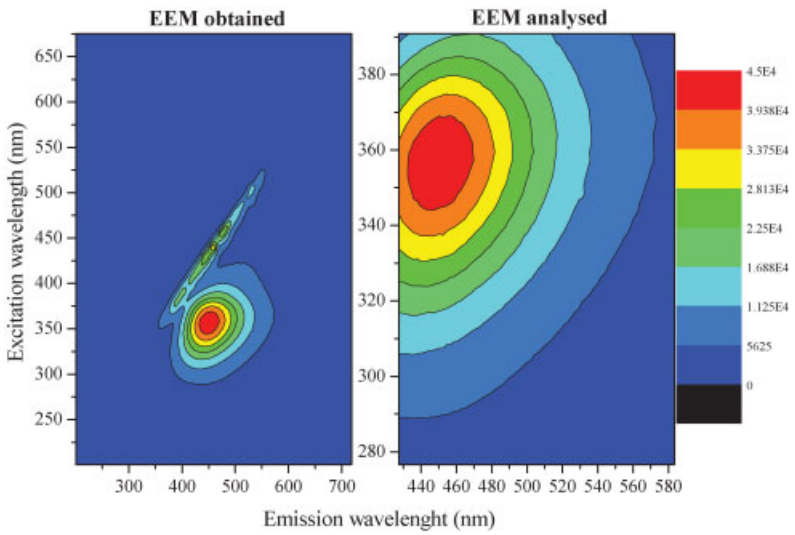

Figure 1. Typical obtained and analyzed EEMs of CDs.

were used as convergence criteria. The initial estimates used for the three models were the estimates of a model without constraints.

The results obtained from the PARAFAC, PARAFAC2, and PARALIND three-way data analysis were compared using the model fit [fit (%)]. The model fit (%) for PARAFAC, PARAFAC2, and PARALIND models is defined by Equation (4) [2,6].

$$\text{Fit}(\%) = 100 \times \left(1 - \sqrt{\frac{\sum_{i=1}^{I}\sum_{j=1}^{J}\sum_{k=1}^{K}\left(x_{ijk} - \hat{x}_{ijk}\right)^2}{\sum_{i=1}^{I}\sum_{j=1}^{J}\sum_{k=1}^{K}\left(x_{ijk}\right)^2}} \right) \quad (4)$$

In this equation, $\hat{x}_{ijk}$ is the *ijk* element of the estimated three-dimensional matrix and x_{ijk} is the *ijk* element of the experimental three-dimensional matrix.

Also, the results obtained with PARAFAC models were assessed using the Corcondia or core consistency test [Corcondia (%)] defined by Equation (5) [2,28].

$$\text{Corcondia}(\%) = 100 \times \left(1 - \frac{\sum_{d=1}^{N}\sum_{e=1}^{N}\sum_{f=1}^{N}\left(g_{def} - t_{def}\right)^2}{\sum_{d=1}^{N}\sum_{e=1}^{N}\sum_{f=1}^{N}\left(t_{def}\right)^2} \right) \quad (5)$$

In this equation, g_{efg} and t_{efg} represent the elements of the calculated core and of the intrinsic super-diagonal core, respectively, and *N* the number of components of the model. If they are equal, the core consistency is perfect and has a value of unity (100%). The appropriate number of components is assessed with the model with the highest number of components and a valid value of core consistency diagnostic test.

2.4. Software

The chemometric analysis was done in MATLAB® version 5.3 environment. The algorithms for implementation of PARAFAC, PARAFAC2, and PARALIND models were obtained from Bro available at http://www.models.kvl.dk/source/. All the graphs were drawn in Microcal Origin® version 7.5.

3. RESULTS AND DISCUSSION

3.1. PARAFAC analysis

CDs are carbon nanoparticles that, through functionalization, acquire strong photoluminescence with a typical EEM of fluorescence in aqueous solution as shown in Figure 1. Typical excitation and emission spectra obtained, respectively, at maximum emission and excitation wavelengths of the synthesized CDs are shown in Figure 2—maximum excitation and emission are located at 350 and 450 nm, respectively [27]. Figure 2 shows the effect of experimental factors on the fluorescence emission of the CDs and an increase in the Hg(II) concentration and the pH provokes a steady decrease in the fluorescence (quenching). These variations are a consequence of the change in the quantum confinement of the CDs [12,14,15,27].

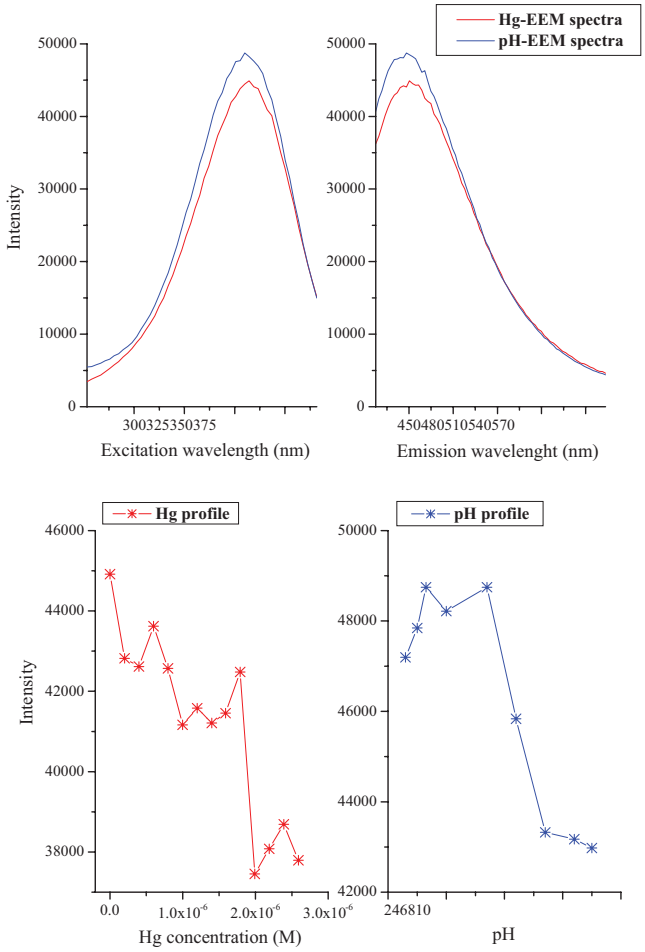

Figure 2. Experimental excitation and emission spectra at maximum fluorescence intensity and Hg and pH profile, respectively, of the Hg- and pH-EEMs.

Previous studies on the effect of the pH on the EEM of fluorescent nanoparticles constituted by cadmium/tellurium showed that the emission spectrum shifts as function of the pH, initiating a marked nonlinear behavior [16]. In order to

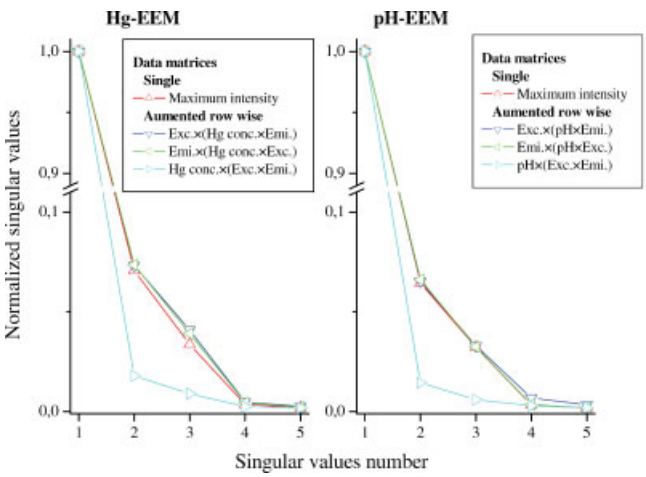

Figure 3. Singular value decomposition of the singular data matrices and row-wise augmented data matrices in the excitation, emission, and Hg or pH orders.

Table I. PARAFAC model evaluation in the analysis of the Hg^{2+} and pH EEMs three-way data structures[a]

Model evaluation	PARAFAC			
	Number of components			
	One	Two	Three	Four
	[Excitation spectra (nm) × Emission spectra (nm) × Hg^{2+} concentration (M)]			
Fit (%)	91.5	95.7	98.9	99.2
Number of Iterations	2	2	1192	1118
SSQr	1.1×10^{11}	2.7×10^{10}	1.7×10^{9}	1.0×10^{9}
Corcondia (%)	100.0	100.0	22.1	−2.9
	[Excitation spectra (nm) × Emission spectra (nm) × pH]			
Fit (%)	92.5	96.6	99.0	99.3
Number of Iterations	2	2	42	782
SSQr	6.3×10^{10}	1.3×10^{10}	1.2×10^{9}	6.1×10^{8}
Corcondia (%)	100.0	100.0	54.2	11.1

[a] SSQr—sum square of residuals.

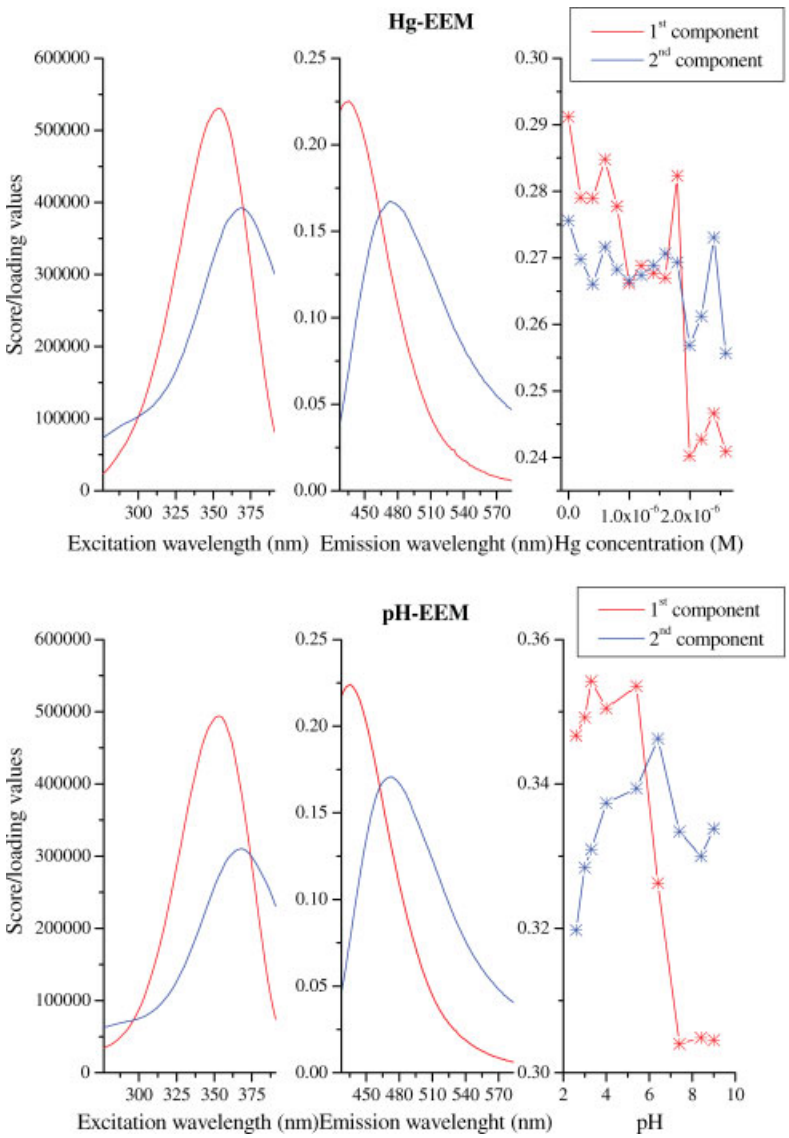

Figure 4. Excitation spectra, emission spectra and pH profile calculated with a PARAFAC two components non-negativity constraint model respectively in the analysis of the Hg- and pH-EEMs.

check for possible nonlinearity in the sets of CDs, EEM under Singular Value Decomposition (SVD) analysis of single and augmented row-wise matrices were performed. Figure 3 presents the normalized singular values for the single and augmented row-wise matrices and its analysis shows that the augmented row-wise matrices with Hg(II) concentration and pH as the common factors require less components than the others. This rank difference suggests the existence of collinearity (rank deficiency) in these orders.

In order to further analyze the structure and/or number of fluorescent components of the experimental EEM data acquired as function of the experimental factors, PARAFAC analysis was done using different component models (from one and up to four components). Indeed, PARAFAC analysis is a straightforward test of the trilinearity of a set of EEM, and allows good estimation of the concentration profiles because it uses all the EEM data instead of only one intensity point obtained at selected excitation and emission wavelengths. The analysis of the Corcondia tests for the studied models (Table I) shows that the intrinsic EEM models are constituted by at least two components. The three-component model has a Corcondia test value of 22% [Hg(II) experiment] or 54% (pH experiment). These Corcondia values suggest a possible valid third component, for example a background signal, or they may by a sign of trilinear deviation of the EEM structure. Indeed, for both experiments, only a three-component model allows a fit (%) of about 99%. Consequently, the two- and three-component models deserve further analysis.

Figure 4 shows typical results of the two-component model PARAFAC decomposition of sets of EEM data collected in the presence of increasing amounts of Hg(II) ion and varying pH. In both experiments, the analysis of the extracted excitation and

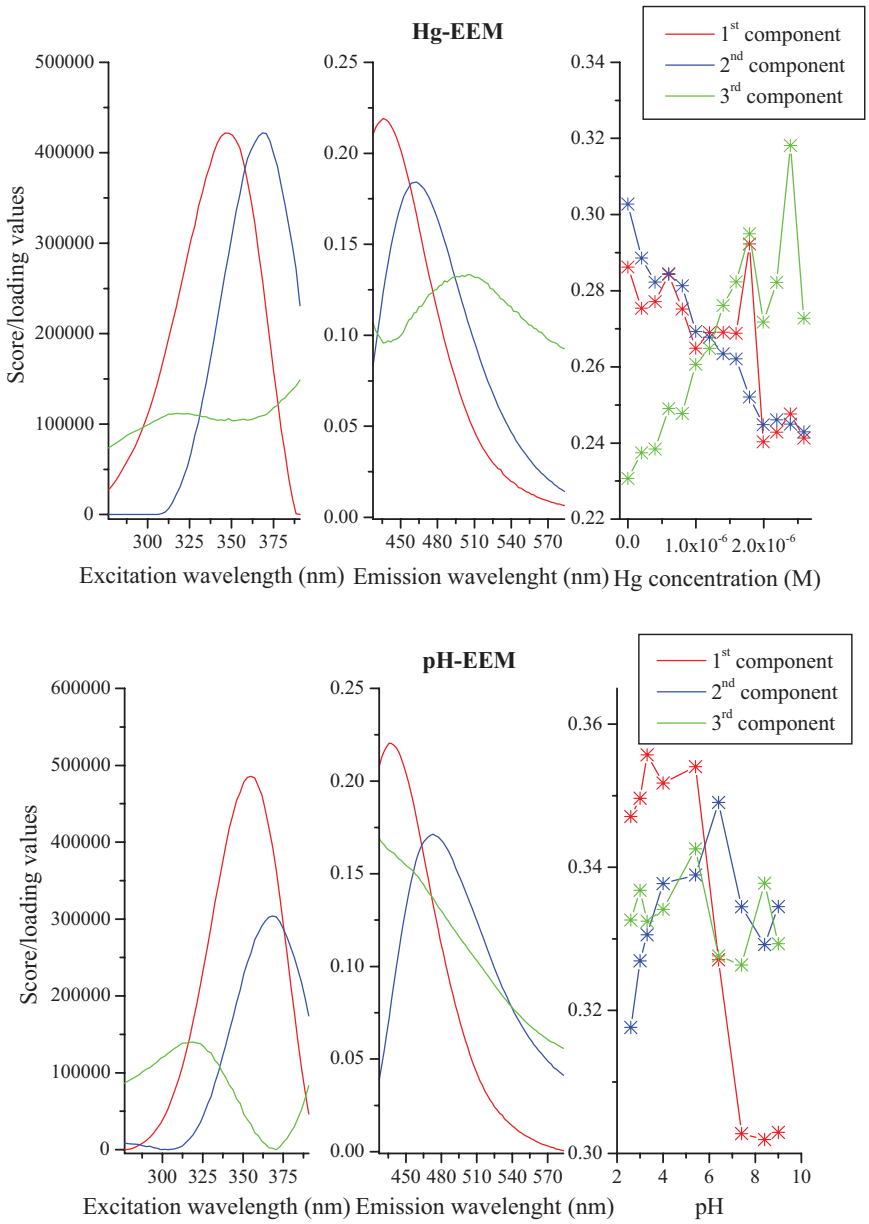

Figure 5. Excitation spectra, emission spectra and pH profile calculated with a PARAFAC three components non-negativity constraint model respectively in the analysis of the Hg- and pH-EEMs.

Table II. PARALIND model evaluation in the analysis of the Hg^{2+} and pH EEMs three-way data structures[a]

Model evaluation	PARALIND	
	Number of components	
	R—One; S—Two	R—Two; S—Three
	[Hg^{2+} concentration (M) × Emission spectra (nm) × Excitation spectra (nm)]	
Fit (%)	95.6	98.7
Number of Iterations	47	1333
SSQr	1.8×10^{10}	2.4×10^{9}
	[pH × Emission spectra (nm) × Excitation spectra (nm)]	
Fit (%)	96.3	98.9
Number of Iterations	42	374
SSQr	1.5×10^{10}	1.3×10^{9}

[a] R—number of components in the first mode; S—number of components in the second and third modes; SSQr—sum square of residuals.

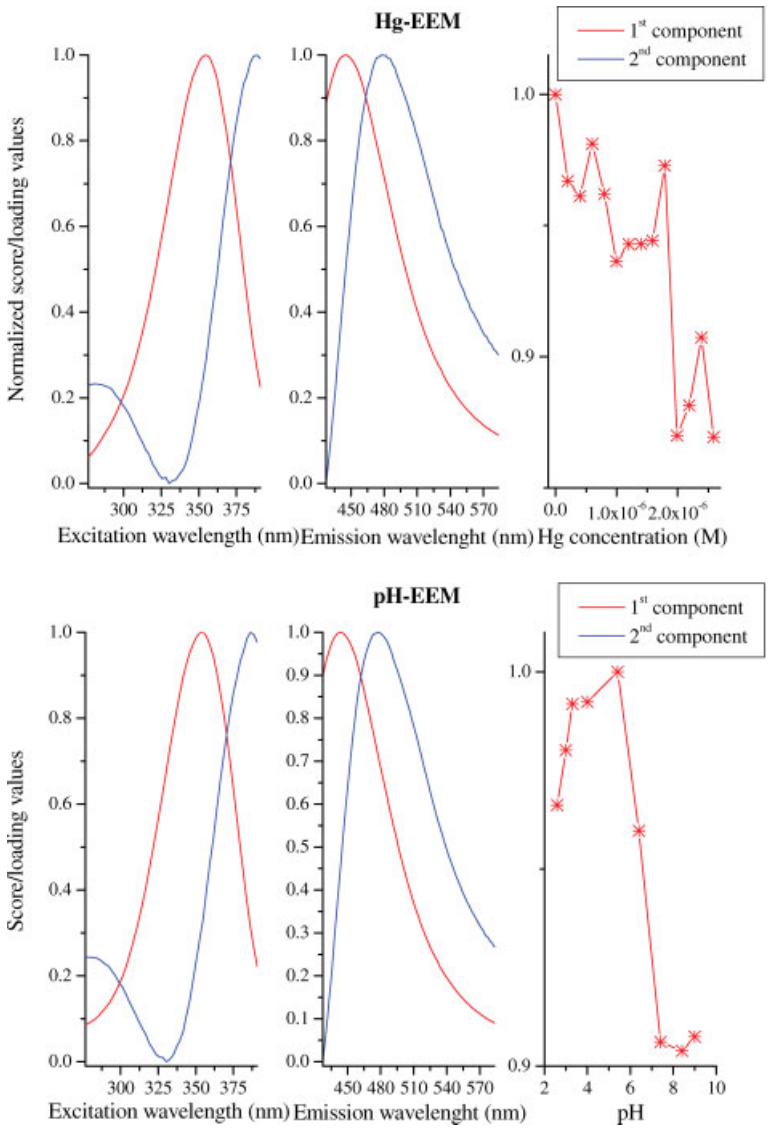

Figure 6. Excitation spectra, emission spectra and pH profile calculated with a PARALIND one component in the first mode and two components in the second and third modes non-negativity constraint model respectively in the analysis of the Hg and pH-EEMs.

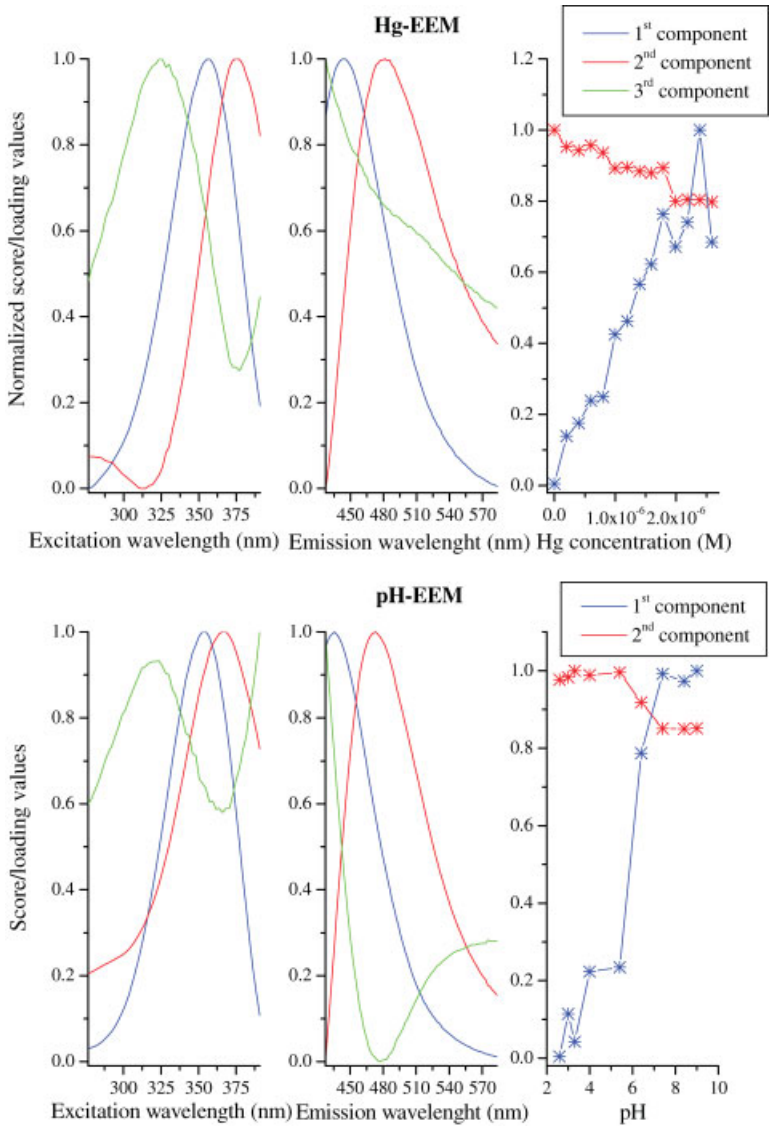

Figure 7. Excitation spectra, emission spectra and pH profile calculated with a PARALIND two components in the first mode and three components in the second and third modes non-negativity constraint model respectively in the analysis of the Hg- and pH-EEMs.

emission spectra shows the existence of two fluorophores that probably correspond to two classes of CDs. Taking into consideration that the laser ablation syntheses of CDs can originate different sizes of nanoparticles, these two components may correspond to two different-sized classes of CDs [27]. The excitation/emission wavelength pairs for these two classes are: smaller CDs 330/435 nm and bigger CDs 360/485 nm. The experimentally observed excitation/emission wavelengths (350/450 nm) correspond roughly to the average wavelengths of the two classes detected by PARAFAC.

Figure 5 shows typical results of the three-component model PARAFAC decomposition of sets of EEM data collected in the presence of increasing amounts of Hg(II) ion and varying pH. Two of the calculated components have similar excitation and emission spectra as well as the Hg(II) and pH profiles as the two components estimated using a two-component PARAFAC model. The third component of the Hg-EEM experiments now calculated corresponds to a background signal due to a weak fluorescence of unreacted PEG_{200} used to activate the CDs, and to scattering due to the existence of hydroxyl complexes of Hg(II) [27]. Supporting the existence of scattering is the corresponding increasing trend of the Hg(II) profile with the increase in the concentration. The third component of the pH-EEM experiments now calculated corresponds only to a background signal due to a weak fluorescence of unreacted PEG_{200}.

If the two components correspond to different classes of different-sized CDs, it is expected correlation among the Hg(II) and pH profiles because the classes of CDs respond similarly to the experimental factor with, probably, different sensibilities. Different sensibilities may result from the fact that bigger nanoparticles have higher number of functionalized molecules (sensor on the CD surface) than smaller nanoparticles. Indeed, the analysis of the intensity profiles in Figures 4 and 5 barely shows that smaller CDs (first component) have a relatively smaller variation than the second component that corresponds to bigger CDs.

PARAFAC analysis shows the existence of at least two detectable components corresponding to different-sized CDs with intensity

Table III. PARAFAC2 model evaluation in the analysis of the Hg^{2+} and pH EEMs three-way data structures[a]

Model evaluation	PARAFAC2			
	Number of components			
	One	Two	Three	Four
	[Excitation spectra (nm) × Emission spectra (nm) × Hg^{2+} concentration (M)]			
Fit (%)	91.6	95.8	99.1	99.3
Number of iterations	2	644	1689	2000
SSQr	1.0×10^{11}	2.6×10^{10}	1.3×10^{9}	8.0×10^{8}
	[Excitation spectra (nm) × Emission spectra (nm) × pH]			
Fit (%)	92.6	96.6	99.0	99.3
Number of iterations	2	46	2000	2000
SSQr	6.1×10^{10}	1.3×10^{10}	1.1×10^{9}	5.5×10^{8}

[a] SSQr—sum square of residuals.

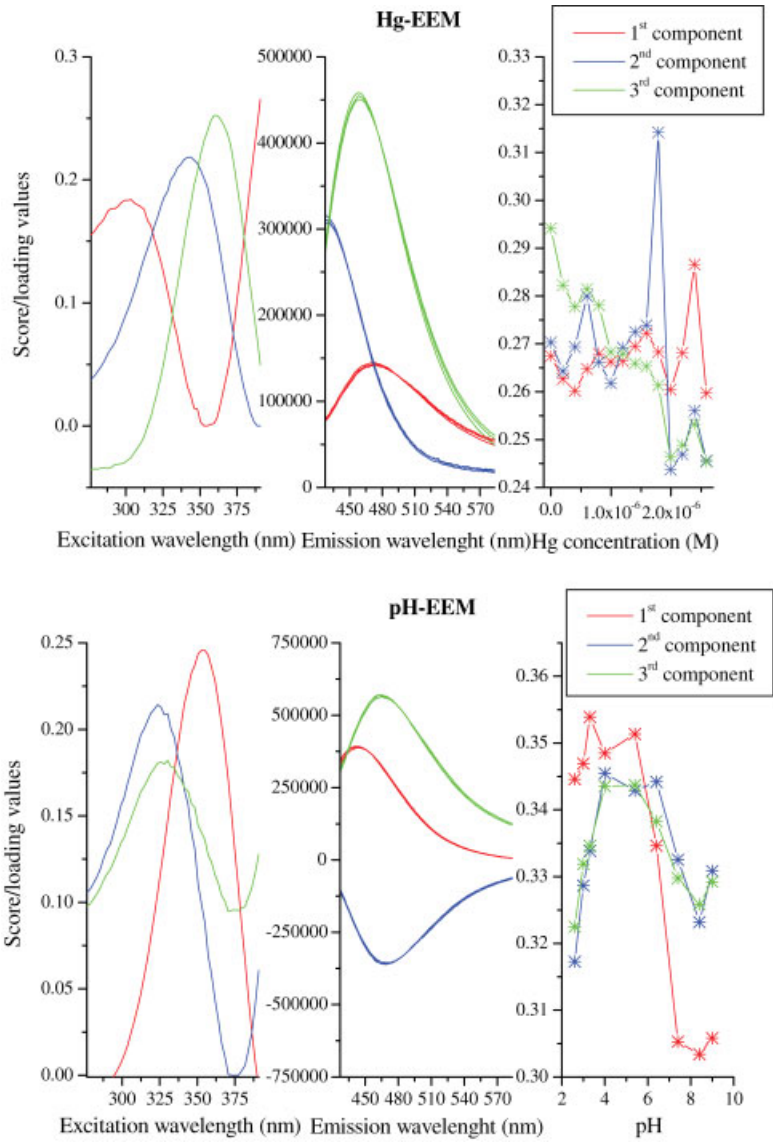

Figure 8. Excitation spectra, emission spectra and pH profile calculated with a PARAFAC2 three components non-negativity constraint model respectively in the analysis of the Hg- and pH-EEMs.

profiles highly correlated plus a measurable background. In order to assess how other PARAFAC analysis models deal with collinearity and nonlinearity problems in one of the orders, PARALIND and PARAFAC2 will be used as validation tools.

3.2. PARALIND analysis

As discussed above, the existence of similar Hg(II) or pH profiles in more than one component creates a rank-deficiency problem. PARALIND was developed to extend the use of PARAFAC to this type of problems where it eventually could fail to provide meaningful results [9]. According to the PARAFAC analysis, the CDs EEMs are constituted by three components, with two of them having the highly correlated Hg(II) concentration or pH profiles. Table II resumes the error parameters, and Figures 6 and 7 present the calculated spectra and profiles obtained with PARALIND using two models: one plus two components; two plus three components.

The analysis of Table II shows that a three-component model (two plus three) is enough to obtain a fit (%) of about 99%, which is similar to what was obtained with PARAFAC. However, the spectra estimated with a two-component model by PARALIND shown in Figure 6 are not similar to those calculated with PARAFAC. Indeed, the PARALIND solution was not able to resolve the spectra of the two classes of CDs because the spectra of one of the components correspond to the background.

The results obtained with PARAFAC and PARALIND with three components are similar (Figure 7). This result constitutes a validation test for the collinearity of the Hg(II) and pH profiles of two components of the EEMs of the CDs. Moreover, PARALIND results are, from a theoretical point of view, more interesting than those obtained with PARAFAC because they confirm the existence of different classes of CDs with similar reactivity toward the experimental factors under investigation.

3.3. PARAFAC2 analysis

Although a three-component PARAFAC and a two- plus three-component PARALIND model globally fit quite well the experimental data of CDs, PARAFAC2 was used as a diagnostic test for the existence of nonlinearity in the emission spectral order. Indeed, it has been reported that the position of the emission band of fluorescent nanoparticles is sensitive to some experimental factors, such as the pH [16]. Table III resumes the error parameters obtained with PARAFAC2 using two-, three-, and four-component models.

The analysis of Table III shows that a three-component model is enough to obtain a fit (%) of about 99%, which is similar to what was obtained with PARAFAC and PARALIND. Figure 8 shows the spectra and Hg(II) and pH profiles calculated with the three-component model.

The analysis of Figure 8 shows that the calculated spectra and Hg(II) and pH profiles are similar for one component and are not similar for the other two when compared with those estimated with PARAFAC and PARALIND. Indeed, there is some mixture of the estimated spectra, which probably results from the detected rank deficiency of the sets of EEMs. Nevertheless, the analysis of the calculated set of emission spectra shows that no shift either with the Hg(II) concentration or with the pH is detected (all the component spectra overlap). This result confirms that no nonlinear behavior is induced in the EEMs of CDs when the concentration of Hg(II) or the pH is varied.

4. CONCLUSIONS

A three-component PARAFAC model successfully described a CD nanoparticle fluorescent material and the effect of the Hg(II) concentration and pH on the EEMs. Indeed, as a consequence of the EEM three-way decomposition, it was possible to detect the existence of two different-sized classes of CDs as well as a background EEM. However, in order to validate the PARAFAC results, two confirmatory tests are proposed using PARALIND and PARAFAC2 three-way decomposition models.

PARALIND was used to confirm that the two different-sized classes of CDs show a similar reactivity toward Hg(II) concentration and pH, which corresponds to the existence of only one component common profile to both CDs. PARAFAC2 was used as a confirmatory test for the existence of wavelength shifts in the emission spectra.

Acknowledgements

Financial support from Fundação para a Ciência e Tecnologia (Lisboa, Portugal) (FSE-FEDER) (Project PTDC/QUI/71001/2006) and (Project PTDC/QUI/71336/2006) is acknowledged. A PhD grant to Helena Gonçalves SFRH/BD/46406/2008 is acknowledged to Fundação para a Ciência e Tecnologia.

REFERENCES

1. Harshman R. Foundations of the PARAFAC procedure: models and conditions for an "explanatory" multimodal factor analysis. *UCLA Work. Pap. Phon.* 1970; **16**: 1–84.
2. Bro R. PARAFAC. Tutorial and applications. *Chemom. Intell. Lab. Syst.* 1997; **38**: 149–171.
3. Booksh K, Kowalski B. Theory of analytical chemistry. *Anal. Chem.* 1994; **66**: 782A–791A.
4. Acar E, Yener B. Unsupervised multiway data analysis: a literature survey. *IEEE Trans. Knowl. Data Eng.* 2009; **21**: 6–20.
5. Escandar G, Faber N, Goicoechea H, de la Peña M, Olivieri C, Poppi R. Second- and third-order multivariate calibration: data, algorithms and applications. *Trends Analyt. Chem.* 2007; **26**: 752–765.
6. Kiers H, Berge J, Bro R. PARAFAC2—Part I: a direct fitting algorithm for the PARAFAC2 model. *J. Chemom.* 1999; **13**: 275–294.
7. Harshman R. PARAFA C2: mathematical and technical notes. *UCLA Work. Pap. Phon.* 1972; **22**: 30–44.
8. Bro R, Harshman R, Sidiropoulos N, Lundy M. Modeling multi-way with linearly dependent loadings. *J. Chemom.* 2009; **23**: 324–340.
9. Bahram M, Bro R. A novel strategy for solving matrix effect in three-way data using parallel profiles with linear dependencies. *Anal. Chim. Acta* 2007; **584**: 397–402.
10. Azofra R, Sarabia L, Ortiz M. Optimization of a solid-phase extraction procedure in the fluorimetric determination of sulphonamides in milk using the second-order advantage of PARAFAC and D-optimal design. *Anal. Bioanal. Chem.* 2010; **396**: 923–935.
11. Kowalczuk P, Cooper W, Durako M, Kahn A, Gonsior M, Young H. Characterization of dissolved organic matter fluorescence in the South Atlantic Bight with use of PARAFAC model: relationships between fluorescence and its components, absorption coefficients and organic carbon concentrations. *Mar. Chem.* 2010; **118**: 22–36.
12. Campos B, Algarra M, Alonso B, Casadoc C, Esteves da Silva J. Mercury(II) sensing based on the quenching of fluorescence of CdS–dendrimer nanocomposites. *Analyst* 2009; **134**, 2447–2452.
13. Valderrama P, Poppi R. Determination of propranolol enantiomers in plasma and urine by spectrofluorimetry and second-order standard addition method. *Anal. Chim. Acta* 2009; **651**: 31–35.
14. Gonçalves H, Mendonça C, Esteves da Silva J. PARAFAC analysis of the quenching of EEM of fluorescence of glutathione capped CdTe quantum dots by Pb(II). *J. Fluoresc.* 2009; **19**: 141–149.

15. Campos B, Algarra M, Esteves da Silva J. Fluorescent properties of a hybrid cadmium sulfide-dendrimer nanocomposite and its quenching with nitromethane. *J. Fluoresc.* 2010; **20**: 143–151.
16. Leitão J, Gonçalves H, Mendonça C, Esteves da Silva J. Multiway chemometric decomposition of EEM of fluorescence of CdTe quantum dots obtained as function of pH. *Anal. Chim. Acta* 2008; **628**: 143–154.
17. Valderrama P, Poppi R. Bilinear least squares (BLLS) and molecular fluorescence in the quantification of the propranolol enantiomers. *Anal. Chim. Acta* 2008; **623**: 38–45.
18. Bosco M, Larrechi M. Rapid and quantitative evaluation of the effect of process variables on the kinetics of photocatalytic degradation of phenol using experimental design techniques and parallel factor (PARAFAC) analysis. *Anal. Bioanal. Chem.* 2008; **390**: 1203–1207.
19. Ohno T, Wang Z, Bro R. PowerSlicing to determine fluorescence lifetimes of water-soluble organic matter derived from soils, plant biomass, and animal manures. *Anal. Bioanal. Chem.* 2008; **390**: 2189–2194.
20. Leitão J, Esteves da Silva J, Girón A, de la Peña A. Optimization of verapamil drug analysis by excitation-emission fluorescence in combination with second-order multivariate calibration. *J. Fluoresc.* 2008; **18**: 1065–1076.
21. Lozano V, Ibañez G, Olivieri A. A novel second-order standard addition analytical method based on data processing with multidimensional partial least-squares and residual bilinearization. *Anal. Chim. Acta* 2009; **651**: 165–172.
22. Bruun S, Holm J, Hansen S, Andersen C, Nørgaard L. A chemometric analysis of ligand-induced changes in intrinsic fluorescence of folate binding protein indicates a link between altered conformational structure and physico-chemical characteristics. *Appl. Spectrosc.* 2009; **63**: 1315–1442.
23. Cao L, Wang X, Meziani MJ, Lu F, Wang H, Luo PG, Lin Y, Harruff BA, Veca LM, Murray D, Xie SY, Sun YP. Carbon dots for multiphoton bioimaging. *J. Am. Chem. Soc.* 2007; **129**: 11318–11319.
24. Yang ST, Wang X, Wang H, Lu F, Luo PG, Cao L, Meziani MJ, Liu JH, Liu Y, Chen M, Huang Y, Sun YP. Carbon dots as nontoxic and high-performance fluorescence imaging agents. *J. Phys. Chem. C* 2009; **113**: 18110.
25. Yang ST, Cao L, Luo PG, Lu F, Wang X, Wang H, Mezian MJ, Liu G, Qi G, Sun YP. Carbon dots for optical imaging in vivo. *J. Am. Chem. Soc.* 2009; **131**: 11308–11309.
26. Liu HP, Ye T, Mao CD. Fluorescent carbon nanoparticles derived from candle soot. *Angew. Chem. Int. Ed. Engl.* 2007; **46**: 6473–6475.
27. Gonçalves H, Jorge PAS, Fernandes JRA, Esteves da Silva JCG. Hg(II) sensing based on functionalized carbon dots obtained by direct laser ablation. *Sens. Act. B* 2010; **145**: 702–707.
28. Bro R, Kiers HA. A new efficient method for determining the number of components in PARAFAC models. *J. Chemom.* 2003; **17**: 274–286.

CHAPTER 8 – METAL-ENHANCED PHOTOLUMINESCENCE FROM CARBON NANODOTS

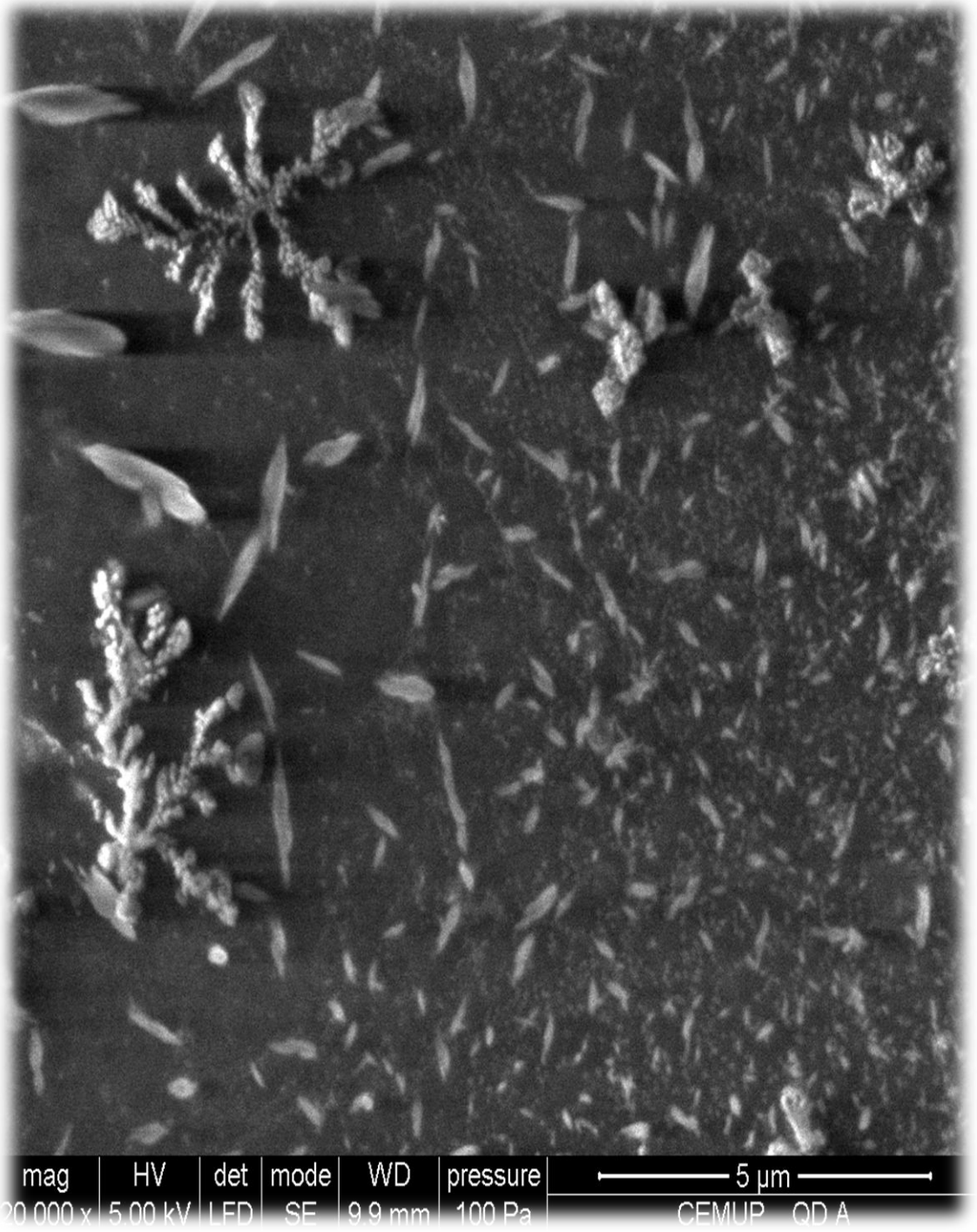

Chapter 8 – Metal Enhanced Photoluminescence from Carbon Nanodots

8.1. State of the Art

The research group lead by Guedes C.D. has been focusing their attention in the effect that silver nanoparticles have on fluorescence characteristics of different fluorophores [1]. The increase/enhancement of the fluorescence intensity is just one of the possibilities of putting fluorophores in contact with silver nanoparticles, as such, in order to ascertain if the shape of the nanoparticles is related to the effect, different silver formations has been tested, namely, silver Island films [1–4]; silver colloids films [5]; solution based silver colloids [6]; silver nanorods [7]; and fractal-like silver surfaces [8-10]. Indeed, different shapes can produce different effects, such as, increased quantum yields, decreased lifetimes, increased photostability and increased rates of energy transfer.

The differences produced by the proximity of the silver nanoparticles are due to the interactions of the excited-state fluorophores with the surface plasmon resonances on the surface of the metal [11-14]. Fluorescence enhancement, for example, is due to an increase in the radiative decay rate of the fluorophores, that are approximately between 50-200 Å of the metallic surface.

The fluorescence enhancement is an interesting feature, regardless of the application, since it will allow to use less expensive and complex systems for the fluorophore measurements. this is just one of the numerous advantages of a controlled increase in the fluorescence intensity.

8.2. References

[1] Malicka J., Gryczynski I., Geddes C.D., Lakowicz J.R. **2003**. "Metal-enhanced emission from Indocyanine Green: A new approach to in vivo imaging". J. Biomed. Opt. 8(3), pp.472–478.

[2] Lakowicz J.R., Shen Y., D'Auria S., Malicka J., Fang J., Gryczynski Z., Gryczynski I. **2002**. " Effects of silver island films on fluorescence intensity, lifetimes, and resonance energy transfer". Anal. Biochem. 301, pp.261–277.

[3] Pugh V.J., Szmacinski H., Moore W. E., Geddes C.D., Lakowicz J.R. **2003**. "Submicrometer spatial resolution of metal-enhanced fluorescence". Appl. Spectrosc. 57(12), pp.1592–1598.

[4] Lakowicz J.R., Malicka J., Gryczynski Z., Huang J., Geddes C.D., Gryczynski I. **2003**. "Increased sensitivity of fluorescence detection". Pharmagenomics 3(3), pp.38–46.

[5] Geddes C.D., Cao H., Gryczynski I., Gryczynski Z., Fang J., Lakowicz J.R. **2003**. "Metal-Enhanced Fluorescence (MEF) due to silver colloids on a planar surface: Potential applications of indocyanine green to in vivo imaging. J. Phys. Chem. A. 107, pp.3443–3449.

[6] Aslan K., Lakowicz J.R., Szmacinski H., Geddes C.D. **2004**. "Metal-enhanced fluorescence solution based Platform". J. Fluorescence. 14, pp.677–679.

[7] Geddes C.D., Cao H., Lakowicz J.R. **2003**. "Enhanced photostability of ICG in close proximity to Gold colloids". Spectrochemica Acta A. 59(11), pp.2611–2617.

[8] Geddes C.D., Parfenov A., Roll D., Gryczynski I., Malicka J., Lakowicz J. R. **2004**. "Roughened silver electrodes for use in metalenhanced fluorescence". Spectrochemica Acta A. 60, pp.1977–1983.

[9] Parfenov A., Gryczynski I., Malicka J., Geddes C.D., Lakowicz J. R. **2003**. "Enhanced fluorescence from fluorophores on fractal silver surfaces". J. Phys. Chem. B. 107(34), pp.8829–8833.

[10] Geddes C.D., Parfenov A., Roll D., Gryczynski I., Malicka J., Lakowicz J. R. **2003**. "Silver fractal-like structures for metalenhanced fluorescence: Enhanced fluorescence intensities and increased probe photostabilities". J. Fluorescence 13(3), pp.267–276.

[11] Lakowicz J.R. **2001**. "Radiative decay engineering: Biophysical and biomedical applications". Anal. Biochem. 298, pp.1–24.

[12] Lakowicz J.R., Malicka J., Gryczynski I., Gryczynski Z., Geddes C.D. **2003**. "Radiative decay engineering: The role of photonic mode density in biotechnology". J. Physics D. Appl. Phys. 38, pp.R240–249.

[13] Geddes C.D., Gryczynski I., Malicka J., Gryczynski Z., Lakowicz J.R. **2003**. "Metal-Enhanced fluorescence: Potential applications in HTS". Combinatorial Chemistry HTS. 6(2), pp.109–117.

[14] Geddes C.D., Lakowicz J.R. **2002**. "Metal-enhanced fluorescence". J. Fluorescence 12(2), 121–129.

8.3. Personal Contribution

My personal contribution to this work includes the following: the Cdots synthesis and functionalization and purification methods. Afterwards, it was necessary to choose the nanoparticles that had the best fluorescent properties regarding to the primarily objective and send it to Massachusetts. Subsequently, it was required the revision of the manuscript before its submission to an international scientific research journal and perform the necessary adjustments to comply with the reviewers suggestions about the Cdots synthesis, functionalization and purification methods.

ChemComm

Cite this: *Chem. Commun.*, 2011, **47**, 5313–5315

www.rsc.org/chemcomm

COMMUNICATION

Metal-enhanced photoluminescence from carbon nanodots

Yongxia Zhang,[a] Helena Gonçalves,[b] Joaquim C. G. Esteves da Silva[c] and Chris D. Geddes*[d]

Received 13th September 2010, Accepted 8th March 2011
DOI: 10.1039/c0cc03832f

In the last couple of years, carbon dots have emerged as a new novel luminescent particle for applications in fluorescence and microscopy in some ways analogous to quantum dots and silicon nanocrystals/particles. As with any fluorescent label or tag, absolute fluorescence intensity, brightness, and particle photostability are a primary concern. In this communication we subsequently show that similar to classical fluorophores, carbon dots located in the near-field, near to Plasmon supporting materials, show enhanced intensities and improved photostabilities.

In the last several years, there has been a growing literature on the synthesis and utility of carbon dots, also known as carbon nanoparticles.[1–3] Similar to the well-known and commercialized semiconductor quantum dots, the carbon nanoparticles display high quantum yields and photostability, but conversely have low cytoxicity and excellent biocompatibility. Subsequently, these new fluorescent labels have found use in biological imaging applications.[4] As with all the new luminescent particle embodiments reported to date, absolute brightness, photostability as well as optical tunability remain primary concerns. In this communication we subsequently show that Plasmon supporting materials, such as silver island films,[5] can further enhance carbon nanodot brightness, photostability and thus potentially detectability in biological imaging applications.

Over the last 10 years, metal-enhanced fluorescence (MEF) has emerged as a technology which directly complements fluorescent labels. In the near-field, within the wavelength of light, luminescent species can interact with metallic surface plasmons in ways which ultimately enhance particle/fluorophore brightness and reduce the excited "system" decay times, which invariably leads to enhanced photostability.

[a] *Institute of Fluorescence and Department of Chemistry and Biochemistry, University of Maryland Baltimore County, 701 East Pratt Street, Baltimore, MD 21202, USA*
[b] *Centro de Investigação em Química, Departamento de Química, Faculdade de Ciências da Universidade do Porto, R. Campo Alegre 687, 4169-007 Porto, Portugal*
[c] *Centro de Investigação em Química, Departamento de Química, Faculdade de Ciências da Universidade do Porto, R. Campo Alegre 687, 4169-007 Porto, Portugal*
[d] *Institute of Fluorescence and Department of Chemistry and Biochemistry, University of Maryland Baltimore County, 701 East Pratt Street, Baltimore, MD 21202, USA. E-mail: geddes@umbc.edu; Fax: +1 410-576-5722; Tel: +1 410-576-5720*

For a fluorescent species in the far-field condition, *i.e.* more than 1 wavelength of light away from either a surface or particle, the quantum yield of a fluorophore is given by:[6]

$$Q_0 = \frac{\Gamma}{\Gamma + K_{nr}} \quad (1)$$

where Γ is the fluorophores' radiative decay rate and K_{nr} are the nonradiative decay rates for excited state relaxation. In the presence of metal, *i.e.* near-field condition, Geddes and Lakowicz have shown that the *system quantum yield*, Q_m, can readily be defined by:[6]

$$Q_m = \frac{\Gamma + \Gamma_m}{\Gamma + \Gamma_m + K_{nr}} \quad (2)$$

where Γ_m is the system modified radiative rate. Similarly, both far- and near-field lifetimes are given by:

$$\tau = \frac{1}{\Gamma + K_{nr}} \quad (3)$$

$$\tau_m = \frac{1}{\Gamma + \Gamma_m + K_{nr}} \quad (4)$$

Interestingly, by increasing Γ_m in eqn (2) and (4), *i.e.* the near-field condition, MEF readily affords for increased *system quantum yields* and reduced decay times, *i.e.* enhanced photostabilites. This is in contrast to the far-field condition, where the lifetime and quantum yield change in unison. In these equations we do not account for metal-modified non-radiative rates, and while some authors have reported very-close proximity quenching, Geddes *et al.* have recently hypothesized that these reductions in close range luminescent intensities are in fact due to changes in the near-field electric field distributions, which are substrate specific.[7]

Polyethylene Glycol (PEG) terminated carbon dots were synthesized as previously reported.[1] Excitation of the carbon

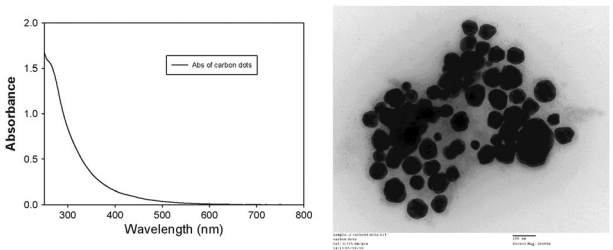

Fig. 1 TEM image (right) of carbon dots and absorbance spectrum (left).

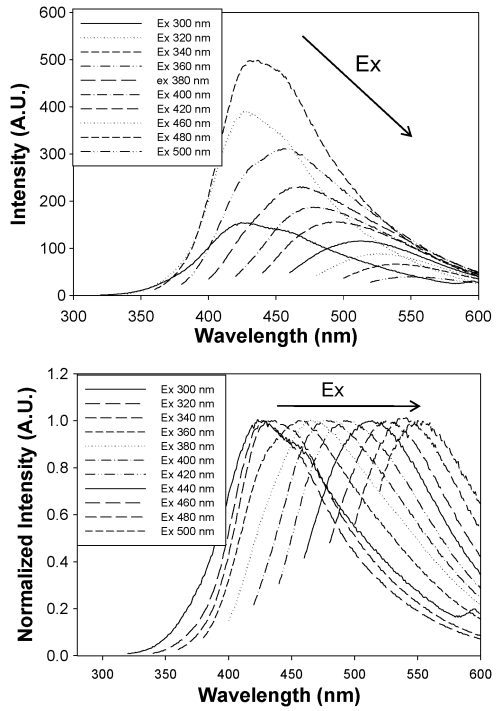

Fig. 2 Fluorescence emission spectra (top) and normalized emission spectra (bottom) of carbon dots for different excitation wavelengths.

dots was undertaken using a Spectrofluorometer Fluoromax 4 for excitation dependence studies, and using 405, 473 and 532 nm laser lines for the MEF studies, where an ocean optics HD 2000 + Spectrometer with a 600 μm fiber bundle was used for the collection of fluorescence emission. The preparation of SiFs has been reported previously.[8] Fluorescence lifetimes of the carbon dots from both SiFs surfaces and glass substrates (a control sample containing no silver) were undertaken using the Time-Correlated Single Photon Counting Technique (TCSPC) with a 400 nm laser for excitation and a TBX-4 module for detection. Deconvolution analysis of the respective luminescence decays was performed using DAS 6.0 software. The calculation of the mean τ and amplitude weighted lifetimes $\langle\tau\rangle$ has been reported previously.[8]

Fig. 1 (right) shows a typical TEM image of the carbon dots, where the size of the dots appears to be in the range of 60–80 nm. The optical absorption of the carbon nanodots is primarily in the UV and tails out beyond 500 nm, Fig. 1—left. Interestingly, the dots show an excitation wavelength and quantum yield dependence, Fig. 2, with the luminescence quite weak when excited beyond 500 nm. The spectral width of the emission is also very similar when normalized, Fig. 2 (bottom). The mechanism of photoluminescence from carbon dots was attributed to the presence of surface energy traps that become emissive upon stabilization as a result of the surface

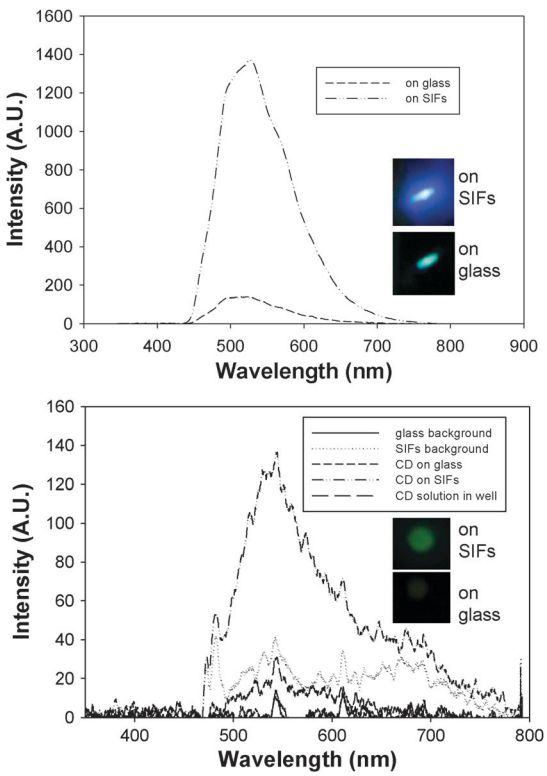

Fig. 3 (top) Fluorescence emission spectra of carbon dots with λ_{Ex} = 405 nm CW laser from both a SiFs surface and also from a glass control sample. (bottom) Fluorescence emission spectra of carbon dots with λ_{Ex} = 473 nm. Real color photographs were taken through a 473 nm razor edge filter.

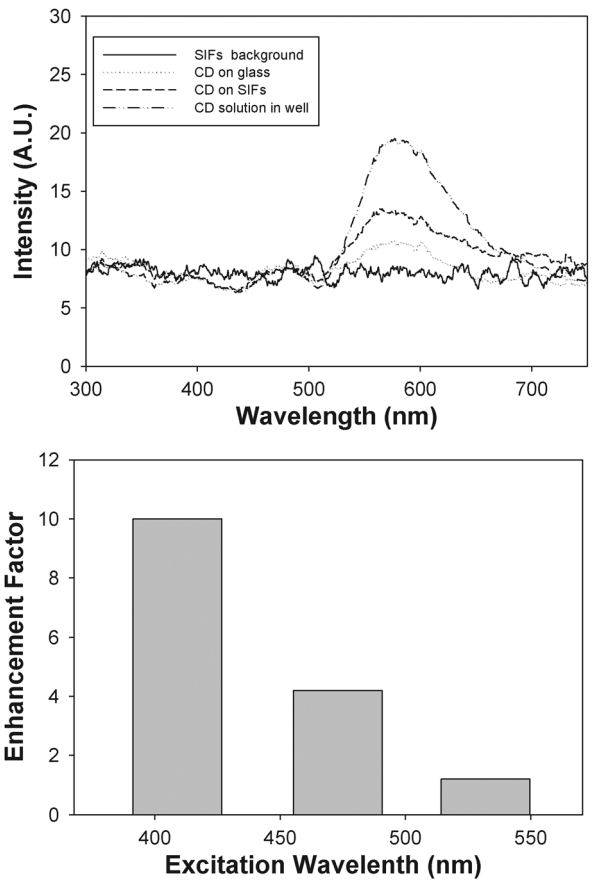

Fig. 4 (top) Fluorescence emission spectra of carbon dots with λ_{Ex} = 532 nm laser from both SiFs and a glass control sample. (bottom) Enhancement factor *vs.* excitation wavelength: 405 nm, 473 nm and 532 nm. Enhancement factor was calculated as the ratio between the emission from the SiFs substrate divided by that observed from an otherwise identical control sample (glass), containing no metal.

Table 1 Fluorescence intensity decay analysis. $\bar{\tau}$—mean lifetime, $\langle\tau\rangle$—amplitude-weighted lifetime. CD—carbon dots. Ex: 400 nm

	τ_1/ns	α_1 (%)	τ_2/ns	α_2 (%)	τ_3/ns	α_3 (%)	$\langle\tau\rangle$/ns	$\bar{\tau}$/ns	χ^2
CD in cuvette	1.23	23.49	0.19	50.94	6.67	25.57	5.65	2.09	1.24
CD glass/glass	0.12	76.64	0.55	21.32	5.14	2.04	0.31	1.94	1.17
CD glass/SIFs	0.14	81.83	0.56	16.81	5.81	1.36	0.26	1.53	1.30

passivation. These findings suggest that the spectral properties are dependent on not only the particle size but also a distribute of different emissive sites on each passivated carbon dots.[9]

When solutions of the nanodots were excited on SiFs (silver island films), significantly enhanced luminescence could be seen, Fig. 3—top, and photograph insets. At an excitation wavelength of 405 nm, over a 10-fold increase in luminescence could be observed as compared to an otherwise identical control sample, but which contained no silver. Fig. 3 (bottom) shows the emission from carbon dots on SiFs and control glass substrate (containing no silver nanoparticles) at the excitation wavelength of 473 nm. Over 4-fold increase in luminescence could be observed. Furthermore, Fig. 4 (top) shows a 1.5-fold enhancement factor of carbon dots on SiFs with excitation wavelength 532 nm. Similar to the free space condition, the emission intensity is reduced with increasing wavelength, with very little enhanced luminescence observed when excited at 532 nm, Fig. 4—bottom. Interestingly, in the MEF literature, some authors have suggested that the enhancement factors near to metals are proportional to the reciprocal of the free space quantum yield, *i.e.* E.F $\propto 1/Q_0$, where Dragon and Geddes conversely suggest that the MEF enhancement factor is underpinned by an excitation volumetric effect (EVE).[10] Given that we in fact do not see greater enhancements for longer wavelengths of excitation, then this enhancement trend follows the MEF EVE hypothesis postulated by Dragon and Geddes, where modulation in MEF efficiency is by far-field excitation power volume dependence. The near-field volume changes non-linearly with far-field power, in Fig. 4—bottom.

The time-resolved decay times for carbon dots in both the far and near-field conditions were measured as shown in Table 1. The lifetime of the dots is multiexponential in solution with mean and amplitude weighted lifetimes of 2.09 and 5.65 ns respectively. In the near field, *i.e.* on SiFs, these values significantly decrease to 1.53 and 0.26 ns, respectively, which is consistent with current MEF thinking and eqn (2) and (4). Subsequently, we have studied the photostability of carbon dots from both the control sample and the SiFs surface. On the SiFs surface one readily sees more emission *vs.* time, *i.e.* photon flux, which is proportional to the integrated area under the curve, Fig. 5. From the glass substrate we readily see significantly less luminescence, which photobleaches more rapidly than the adjusted SiFs substrate, Fig. 5. This increase in photostability from SiFs is consistent with the reduced lifetime on SiFs, Table 1 and eqn (4), where luminescent species in an excited state are less prone to excited state photophysics if the decay time is shorter.

In this communication we have shown that similar to regular organic fluorophores, carbon dots can also show enhanced emission intensities and photostabilities from Plasmon supporting substrates. Given the need for highly luminescent and photostable particles, which are both non-toxic and biocompatible, we foresee several approaches for carbon dots and MEF in imaging and multiplexed immunoassays. Work is currently underway in this regard and will be reported in due course.

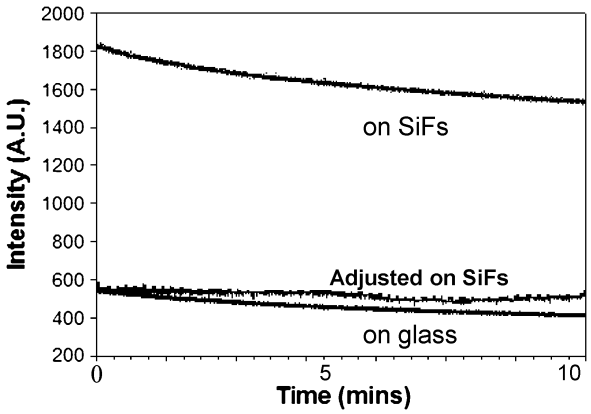

Fig. 5 Emission intensity *vs.* time, photostability of carbon dots on SiFs and glass and with the laser power adjusted to give the same initial steady-state fluorescence intensity as observed on glass (bottom traces). SiFs—silver island films.

The authors would like to thank the Mid Atlantic Regional Center of Excellent (MARCE), NAID, NIH, 2 U54 AIO57168-07, the Institute of Fluorescence, the Department of Chemistry and Biochemistry at the University of Maryland Baltimore County for financial support. Financial support from Fundação para a Ciência e Tecnologia (Lisboa, Portugal) (FSE-FEDER) (Project PTDC/QUI/71001/2006) and (Project PTDC/QUI/71336/2006) is acknowledged. A PhD grant to Helena Gonçalves SFRH/BD/46406/2008 is acknowledged to Fundação para a Ciência e Tecnologia (Lisboa).

References

1 Y. Sun, B. Zhou, Y. Lin and A. Xie, *J. Am. Chem. Soc.*, 2006, **128**, 7756–7757.
2 X. Xu, R. Ray, Y. Gu, H. J. Ploehn, L. Gearheart, K. Raker and W. A. Scrivens, *J. Am. Chem. Soc.*, 2004, **126**, 12736–12737.
3 Q. Li, T. Y. Ohulchanskyy, R. Liu, K. Koynov, D. Wu, A. Best, R. Kumar, A. Bonoiu and P. N. Prasad, *J. Phys. Chem. C*, 2010, **114**, 12062–12068.
4 S. K. Nune, P. Gunda, P. K. Thallapally, Y. Y. Lin, M. L. Forrest and C. J. Berkland, *Expert Opin. Drug Delivery*, 2009, **6**, 1175–1194.
5 R. Pribik, A. I. Dragan, Y. Zhang, C. Gaydos and C. D. Geddes, *Chem. Phys. Lett.*, 2009, **478**, 70–74.
6 C. D. Geddes and J. R. Lakowicz, *J. Fluoresc.*, 2002, **12**, 121–129.
7 K. Aslan, Z. Leonenko, J. R. Lakowicz and C. D. Geddes, *J. Fluoresc.*, 2005, **15**, 643–654.
8 Y. Zhang, A. Dragan and C. D. Geddes, *J. Phys. Chem. C*, 2009, **113**, 12095–12100.
9 H. Gonçalves and J. C. G. Esteves da Silva, *J. Fluoresc.*, 2010, **20**, 1023–1028.
10 A. Dragon and C. D. Geddes, *Phys. Chem. Chem. Phys.*, 2010, **13**, 3831–3838.

Chapter 9 – Conclusions

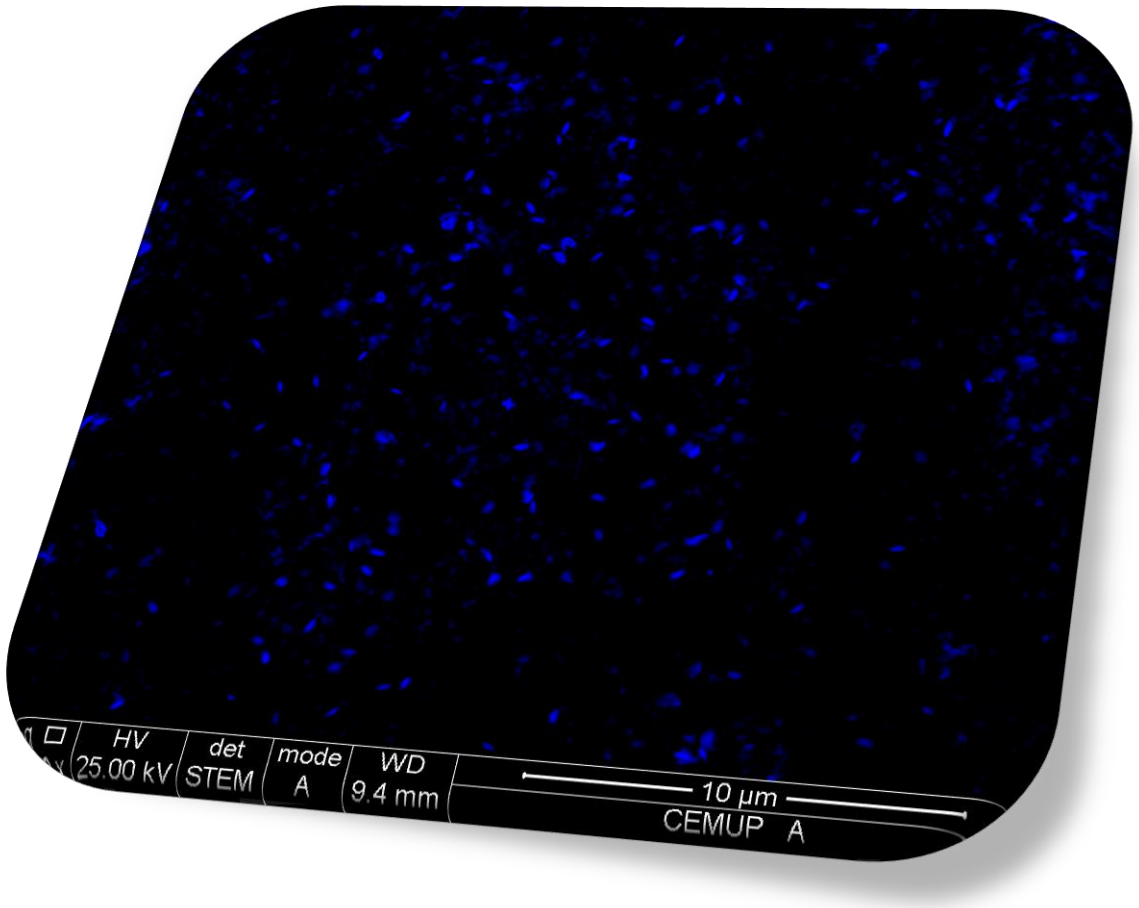

In this worked it was described the successful synthesis of Carbon dots (Cdots), carbon-based nanoparticles, by laser ablation of a carbon target immersed in water. The produced nanoparticles were activated in HNO_3 and further functionalized with adequate molecules according to their intended application.

Initially the Cdots were functionalized with PEG_{200} and mercaptosuccinic acid (MSS) and their fluorescence properties were accessed. It was determined that the maximum emission and excitation wavelengths of these Cdots are 430nm and 330nm, respectively. Furthermore it was accessed that the fluorescence intensity is the only optical property that changes upon the functionalization. Indeed, the lifetime and emission wavelength remained almost constant when the Cdots were functionalized with PEG_{200} and then with MSS. Additionally it was observed that the lifetime decay is complex, consistent with the data published by other research groups on Cdots.

In order to determine the solvents effect on the fluorescence properties these Cdots were exposed to different solvents and their characteristics were evaluated. It was determined that the solvent has indeed a measurable effect on the fluorescence intensity, as well as, in the maximum emission wavelength. Nevertheless this effect is more pronounced in the fluorescence intensity than in the emission wavelength. These Cdots were also studied for a possible pH and metal ion sensitivity. In this sense it was obtained an apparent pK_a of 7.4±0.2, which is consistent with mercaptocarboxilic acids. On another hand the Cdots were exposed to different concentrations of Hg(II), Cu(II), Cd(II), Ni(II), Zn(II), Ca(II) and it was determined that the presence of these metal ions had no effect on the fluorescence properties. However when the Cdots are in contact with micromolar concentrations of I^- the fluorescence intensity remarkably decreases by 55%. The Stern-Volmer equation allowed the determination of a Stern-Volmer constant of 78±2 M^{-1}, which is consistent with dynamic quenching.

On another study the Cdots obtained by laser ablation were functionalized with PEG_{200} and N-acetyl-L-cysteine (NAC). The functionalized Cdots proved to be quite sensitive towards the solution pH. Moreover, due to the NAC molecules on the Cdots surface, these Cdots can be used as an effective Hg(II) sensing system. Some common metal ion interferents were also tested and it was determined that only the presence of Cu(II) had some measurable effect on the fluorescence intensity of the Cdots. This sensing system is quite interesting and it was developed for *in vivo* sensing of Hg(II), however the excitation and emission wavelength of these nanoparticles are not adequate for this purpose. Nevertheless there is an urgent need for analytical tools that allow time-dependent or location-specific *in vivo* measurements in order to study the uptake and distribution of this heavy metal. The possibility of using an analytical

tool that is highly sensitive and non-invasive for Hg(II) detection in living organisms is quite appealing, however it is necessary to further study the production method, in order to develop Cdots with adequate fluorescence properties for *in vivo* sensing.

These Cdots functionalized with PEG_{200} and NAC were immobilized in the tip of an optical fiber by the sol-gel method and the layer-by-layer technique. All fibers were subjected to a pre-treatment with HF 40% in order to minimize the light losses, however this treatment caused some irregularities in the optical fiber surface. When the fibers were used for sol-gel immobilization the irregularities of the fibers were not noticed since the film had about 750nm thickness. However when the Cdots were deposited in discrete layers this presented a problem, since it lead to an increase in the background noise. Both immobilization methods were successful in the entrapment of the Cdots with a high reproducibility and reversibility. Nevertheless the fastest response time and the lowest background noise was obtained with the layer-by-layer method.

The fluorescence data obtained for the immobilized Cdots and the solution were compared and it was found an apparent p*Ka* of 4.4±0.1. Additionally it was determined that the immobilized Cdots present better results than in solution. Furthermore, the detection limit for Hg(II) decreased to $1.00x10^{-8}$M when the Cdots were immobilized in discrete layers. Moreover it was determined that the analyte interacted with the Cdots not only on the surface layer but also on the most inner ones. This result is quite interesting, since it allows the deposition of more than one fluorescence sensor, with a different emission profile, in the same sensing platform. In this sense it would allow the measurement of more than one parameter using the same optical fiber. This is not easy to obtain in the sol-gel method since the entrapment of each molecule/nanoparticle, is almost unique and requires adjustments on the matrix porosity and inner environment.

Additionally it was possible to use chemometrics analysis of the Excitation Emission Matrixes (EEM) of the Cdots functionalized with PEG_{200} and NAC. This chemometric analysis allowed to distinguish two different size populations in solution that responded to the pH and metal ions in the same manner. Indeed, the size characterization of these nanoparticles suggested that there were more than one size population, however it was not possible, at this time, to separate them. By using chemometrics it is possible to confirm the size characterization and to perfectly distinguish the effect that the different factors have on their fluorescence properties.

On another work, the produced Cdots were put in close contact to silver islands that are known for their plasmonic effect. These silver islands induced an interesting

fluorescence enhancement of about 10 times fold. These results are quite interesting, since most Cdots sensors are based on fluorescence quenching and, sometimes it may be difficult to distinguish between the fluorescence signal and the background noise, for high analyte concentrations. When taking advantage of this knowledge it is possible to increase the signals and go even further into more concentrated analyte solutions. This is also useful in immobilizations, since often when the Cdots and other fluorophores are immobilized there is a marked decrease in the fluorescence intensity.

The described procedures allowed the attainment of carbon-based nanoparticles that can be functionalized in order to obtain a selective nanosensor. Additionally it was also possible to successfully immobilize one of the sensors produced using two different methodologies and with it improve de detection limit and the time response of the sensing system.

Final Remarks

This work is focused on Carbon-based nanoparticles, known as Cdots. They represent an innovating theme that is very recent. Indeed, the first published work on these nanoparticles is from 2004, however their first application only appeared in 2006. Ever since then they have been proved non-toxic and competitive contrast agents for bioimaging when compared to the traditional heavy metal-based QDs.

In 2009 when this PhD started the number of synthetic pathways was limited and the development to new ones was quite pressing, particularly “green methods”. The idea of synthesizing Cdots from carbon targets was not easy to implement, mainly due to technical and equipment issues. When it was established a partnership with the physical department of this university to use the laser for the ablation of the nanoparticles, the work began. Initially it was necessary to develop a simplified laser ablation method that was simpler and less expensive than the one used previously by other research groups. After the initial tests successfully produced nanoparticles it was essential to further optimize the conditions in order to purify and separate the size populations in all samples. Additionally it was required the development of functionalization procedures to cover the surface of the Cdots with adequate molecules for advanced nanosensing systems. This was quite common for the QDs, however for the Cdots the only functionalization was PEG_{1500N} and no application was described besides bioimaging. It was not easy to adapt the functionalization procedure with the desired molecule and obtain specific sensors for different analytes so it was quite rewarding when it was successful. Afterwards there was the challenge to immobilize the Cdots nanosensors into adequate matrixes in order to establish a ground point for the development of advanced lab-on-a-chip systems. When the first immobilization method was successful, there was still some further challenge, to optimize this sensing system so it would be more efficient than the non-immobilized. This was accomplished by a partnership with the Cranfield University in the person of Dr. Frank Davis. He is a known specialist in the layer-by-layer immobilization technique and after an initial contact in a Biosensors conference he was quite willing to participate in this project. It was very rewarding when the system worked.

The work develop in these three years resulted in the publication of 8 papers in international peer-reviewed journals:

✓ ***Hg(II) sensing based on functionalized carbon dots obtained by direct laser ablation.*** Helena Gonçalves, Pedro A.S. Jorge, J.R.A. Fernandes, Joaquim C.G. Esteves da Silva. *Sensors and Actuators B*, 145 **(2010)** 70.

✓ ***Fluorescent Carbon Dots Capped with PEG_{200} and Mercaptosuccinic Acid.*** Helena Gonçalves, Joaquim C. G. Esteves da Silva. *J. Fluorescence, 20* ***(2010)*** *1023.*

✓ ***Optical fiber sensor for Hg(II) based on carbon dots.*** Helena M.R. Gonçalves, Abel J. Duarte, Joaquim C.G. Esteves da Silva. *Biosensors and Bioelectronics,* 26 **(2010)** 1302.

✓ ***Parallel factor analysis of EEM of the fluorescence of carbon dots nanoparticles.*** João M. M. Leitão, Helena Gonçalves, Joaquim C. G. Esteves da Silva. *J. Chemometrics,* 24 **(2010)** 655.

✓ ***Analytical and bioanalytical applications of carbon dots.*** Joaquim C. G. Esteves da Silva, Helena Gonçalves. *Trends in Analytical Chemistry* 30 **(2011)** 1327.

✓ ***Metal-Enhanced Photoluminescence from Carbon Nanodots.*** Yongxia Zhang, Helena Gonçalves, Joaquim C.G. Esteves da Silva, Chris D. Geddes. *Chemical Communications* 47**(2011)** 5313.

✓ ***A New Insight on Silicon Dots.*** Helena M.R. Gonçalves, Joaquim C.G. Esteves da Silva. *Current Analytical Chemistry,* 8 **(2012)** 67.

✓ ***Layer-by-layer immobilization of carbon dots fluorescent nanomaterials on single optical fiber.*** Helena Gonçalves, Abel Duarte Frank Davis, Seamus Higson, Joaquim C.G. Esteves da Silva. *Analytica Chimica Acta* **(2012)** : Vol. 26, 2010, page 1302

Additionally it resulted in the participation on two international conferences:

✓ ***Optical fiber nanosensor for Hg(II) based on carbon dots.*** Poster Presentation in Biosensors 2010. Helena M.R. Gonçalves, Joaquim C.G. Esteves da Silva.

✓ ***Silica dots vs. Carbon dots as fluorescence nanosensors.*** Poster Presentation in 10th National Meeting on Photochemistry/ENF2010 – SPQ. Helena Gonçalves, Joaquim C.G. Esteves da Silva.

✓ ***Synthesis of fluorescent nanomaterials as nanosensors.*** Oral Presentation in 10th National Meeting on Photochemistry/ENF2010 – SPQ. Joaquim C.G. Esteves da Silva, Helena Gonçalves, Abel Duarte.

Furthermore there are currently two manuscripts that are being reviewed for publication in international journals.

It was with great pleasure that I've worked on this theme and I hope this could be considered useful for other colleagues investigating in this area, along with enterprises that are willing to invest in the state of the art sensors.